Spring 5-5-2018

Determinants of multi-scale patterning in growth plate cartilage

Alek Erickson
University of Nebraska Medical Center

DETERMINANTS OF MULTI-SCALE PATTERNING IN GROWTH PLATE CARTILAGE

By

Alek Erickson

A DISSERTATION

Presented to the faculty of
the University Nebraska Graduate College
in Partial Fulfillment of the Requirements
for the Degree of Doctor of Philosophy

Genetics, Cell Biology, and Anatomy
Graduate Program

Under the Supervision of Professor Andrew Dudley

University Nebraska Medical Center
Omaha, Nebraska

February 2017

Supervisory Committee:

Hamid Band, Ph.D.
Angela Pannier, Ph.D.
Andrew Dudley, Ph.D.
Karen Gould, Ph.D.
John G Sharp, Ph.D.

ACKNOWLEDGEMENTS

Andrew Dudley, I am so grateful for your mentorship. My development as a scientist I owe to you. When we first met, my mind was an amorphous blob of curiosity, lacking direction. You built my scientific communication skills from the ground up, demonstrated the beauty of experimental design, showed me the power of attention to detail in every part of science, and taught me how to focus on the important questions. At the same time, you gave me freedom and independence to obsess. I will never forget your strange robotic intensity, endless patience, constant encouragement, and your uncanny ability to explain with excellent reasoning every decision you have ever made. Thank you so much.

Thank you to all members of my committee: Drs. Hamid Band, Karen Gould, Angie Pannier, and Graham Sharp. Our meetings were my first awakening to the scientific world outside the bubble of Andy's lab. You pushed me to be clear, knowledgeable, and concise enough to effectively communicate. Your expertise, the ideas you contributed, and your constructive criticism, have all been so important for progressing the project. In particular I want to thank Dr. Pannier, who through extensive (and fun!) collaborations, I began viewing as a second (more organized) mentor.

All the people working in Andy's lab were crucial to my experience at UNMC. Krishna Sarma, you were the perfect partner with to share everything we went through in graduate school. Our friendship brought extremely rare levels of mutual understanding. Thanks for the arguments (scientific, philosophical, metaphysical, moral, petty, drunk, or otherwise). I could probably write an entire dissertation of Krishna-centric acknowledgements. Sarah Romereim, I still remember your unique brand of goofy and serious. Thank you for showing me the ropes during my first couple years. You taught me invaluable techniques and skills in the lab as well as helped me develop writing skills, and you laid the foundations for the project through developing the live imaging

experimental setup and initial validation of the alginate system. Nicholas Conoan, thank you for grounding me. Thank you for helping me practice presentations, and for your fountain of good questions. You gathered countless electron microscopy images for the project. Jamming out to your Rhapsody account every day at lab and watching you play chess over lunchtimes—both major highlights.

I want to especially thank the brilliant collaborators from the College of Engineering at UNL: the inimitable Donghee Lee, who devised the cell compression device and was essential for the development of mechanical testing and adhesion assays; Taylor Laughlin, who worked closely with me to characterize the alginate culture system; and Sophie Walsh, my twin who will be continuing the alginate project. Each one of you has been a gift.

Thank you to so many friends in my academic communities like department of Genetics, Cell Biology, and Anatomy, in the Regenerative Medicine program, and all those people I see every day on the sixth floor. I am sorry I cannot list all the names of those whom I have spent such valuable time with. Additionally, I give huge thanks to friends within Omaha music, art, and game communities. You know who you are, even though many of you will never read this.

Finally, I think of my family. Lars, Lisa, Hootie, Helen, and Emma are an amazing support network. Each one of you is a bastion of creativity, passion, and intellect, and without you none of this would be possible.

ABSTRACT

Functional architectures of complex adaptive systems emerge by dynamic control over properties of individual components. During skeletal development, growth plate cartilage matches bone geometries to body plan requisites by spatiotemporally regulating chondrocyte actions. Bone growth potential is managed by the proximodistal patterning of chondrocyte populations into differentiation zones, while growth vectors are specified by the unique columnar arrangement of clonal groups. Chondrocyte organization at both tissue and cell levels is influenced by a cartilage-wide communication network that relies on zone-specific release and interpretation of paracrine signals. Despite genetic characterization of signaling interactions necessary for cartilage maturation, the regulatory mechanisms that couple positional information with polarized chondrocyte activities to coordinate skeletal morphogenesis remain poorly understood. Building on previous kinematic descriptions of column formation, the work contained in this dissertation suggests cytoskeletal regulation mediates crosstalk between long-range signaling and local cell behavior. Rearranging daughter chondrocytes specifically recruit actomyosin contractility to cortical surfaces, indicating a primary role for the actin cytoskeleton as the engine powering column formation kinetics. Disrupted chondrocyte contractility patterns are observed after genetic perturbation of planar cell polarity signaling, and after inhibiting integrin extracellular matrix binding, implicating actomyosin as a sensor able to integrate global with local signaling cues. To gain greater analytical control towards dissecting the mechanochemical patterning systems underlying cartilage architecture, an alginate hydrogel-based model of growth plate was developed. Daughter chondrocytes encapsulated in alginate beads deposit extracellular matrix in anisotropic and hierarchical configurations that resemble myosin localization in vivo, hinting cytoskeletal forces may sculpt the solid-state environment. Single-cell transcriptomic analysis of chondrocytes stimulated with recombinant ligands

demonstrates the functionality of the IHH/PTHrP circuit in alginate beads, and points towards a novel role for PTHrP signaling gradients in transcriptional regulation of cytoskeletal and ECM proteins. Basal bead cultures tend towards resting/proliferative phenotypes driven by endogenous PTHrP expression, but activating IHH signaling induces position-dependent gene expression, consistent with a model of zone formation where concentration gradients generate spatial cues. Together, the work suggests that in addition to regulating chondrocyte differentiation, the tissue-wide signaling network in cartilage can influence cell-matrix interactions that may be important for cell behavior, and presents a novel culture model that can be used for future studies investigating how chondrocytes discern positional information to shape the growing tissue.

TABLE OF CONTENTS

CHAPTER 1: CURRENT ISSUES IN GROWTH PLATE CARTILAGE MORPHOGENESIS

CHAPTER 2: CYTOSKELETAL DYNAMICS UNDERLIE GROWTH PLATE CARTILAGE MORPHOGENESIS

CHAPTER 3: A TUNABLE, THREE-DIMENSIONAL IN VITRO CULTURE MODEL OF GROWTH PLATE CARTILAGE USING ALGINATE HYDROGEL SCAFFOLDS

CHAPTER 4: TRANSCRIPTOMICS ANALYSIS OF THE IHH/PHTRP SIGNALING LOOP IN ALGINATE CULTURE

CHAPTER 5: FUTURE DIRECTIONS AND CONCLUDING COMMENTS

LIST OF FIGURES

LIST OF TABLES

LIST OF ABBREVIATIONS

2D	Two-dimensional
3D	Three-dimensional
AER	Apical ectodermal ridge
AFM	Atomic force microscopy
ANOVA	Analysis of variance
AP	Anterior-posterior
APEX	Ascorbate peroxidase
APS	Ammonium persulfate
APTES	3-aminopropyltrimethoxysilane
ARP	Actin-related protein
BAPN	Beta-aminoproprionitrile
BCR	Blastocoel roof
BMP	Bone morphogenetic protein
BRDU	Bromo deoxyuridine
CaCl2	Calcium chloride
CamkII	Calcium/Calmodulin-Dependent Kinase 2
cAMP	Cyclic adenosine monophosphate
CCA	Cell-cell association
CDH	Cadherin
cDNA	Complementary deoxyribonucleic acid
CMA	Cell-matrix association
COL	Collagen
CSPG	Chondroitin sulfate proteoglycans
DAH	Differential adhesion hypothesis
DAPI	4',6-diamino-2-phenylindole, dihidrochloride
DCDMS	Dichlorodimethylsilane
ddPCR	Digital droplet polymerase chain reaction
diH2O	Deionized water
DITH	Differential interfacial tension hypothesis
DKO	Double knockout
DMEM	Dulbecco's Modified Eagle's Medium
DNA	Deoxyribonucleic acid
DV	Dorsal-ventral
E	Embryonic day
E	Young's Modulus
ECM	Extracellular matrix
EDC	1-ethyl-3-(3-dimethylaminopropyl)carbodiimide hydrochloride
EDTA	Ethylenediaminetetraacetic acid disodium salt dihydrate
eGFP	Enhanced green fluorescent protein
EGTA	Ethylene glycol tetraacetic acid
FACS	Fluorescence activated cell sorting
FBS	Fetal bovine serum
FDR	False Discovery Rate
FE	Finite element analysis
FGF	Fibroblast growth factor
FISH	Fluorescent in situ hybridization
FN	Fibronectin
Ft	Trigger force
G	Shear modulus

GDC-0449	Vismodegib
GFP	Green fluorescent protein
GPI	Glycosylphosphatidylinositol
GTPase	Guanosine triphosphatase
HIP-1	Hypoxia inducible protein 1
HISS	Heat inactivated sheep serum
HSPG	Heparan sulfate proteoglycan
HYAL	Hyaluronidase
IFT	Intraflagellar transport
IHH	Indian hedgehog
IPA	Integrative Pathway Analysis
ITG	Integrin
ITM	Interterritorial matrix
JNK	Jun-kinase
M	Mitosis
MDG	Muscular dysgenesis
MMP	Matrix metalloproteinases
mRNA	Messenger ribonucleic acid
MSCs	Mesenchymal stem cells
Myo2b	Myosin 2B
MyoD	Myoblast determination protein 1
N	Newton
NCAM	Neural Cell Adhesion Molecule
NCBI	National center for biotechnology information
NGS	Next Generation RNA Sequencing
OMIM	Online Mendelian inheritance in man
PAAM	Polyacrylamide gel
PBS	Phosphate buffered saline
PCA	Principal component analysis
PCM	Pericellular matrix
PCP	Planar cell polarity
PD	Proximal-distal
PES	Polyether sulfone membrane
PKA	Protein Kinase A
PLL	Poly-L-Lysine
PMA	Purmorphamine
pMLC	Phosphorylated myosin light chain
PSS	Presphenoidal synchondrosis
PTH	Parathyroid hormone
PTHrP	Parathyroid hormone-related protein
QPS	Glutamine, penicillin, streptomycin
qRT-PCR	Quantitative real time polymerase chain reaction
RA	Retinoic acid
Rb	Retinoblastoma
RCS	Rat chondrosarcoma
RGD	Arginylglycylaspartic acid (Arg-Gly-Asp)
RGE	Arginylglycylglutamic acid (Arg-Gly-Glu)
RNA	Ribonucleic acid
ROCK	Rho-associated protein kinase
RPM	Revolutions per minute
RQ	Reaction quotient (normalized gene expression)

SEM	Standard error of the mean
SEM	Scanning electron microscopy
SHFM	Split hand/foot malformation
SHH	Sonic hedgehog
SpD	Splotch Delayed
ssRNAseq	Single Cell RNA Sequencing
Sulfo-NHS	N-hydroxy-sulfosuccinimide
t-SNE	T-distributed stochastic neighbor embedding
T4	Thyroxine
TBST	Tris-buffered saline with triton-X100
TEM	Transmission electron microscopy
TEMED	Tetramethylethylenediamine
TGFβ	Transforming growth factor beta
TIFF	Tagged image file format
TM	Territorial matrix
UMF	Uncertainty magnification factor
VEGF	Vascular endothelial growth factor
VWC	Von willebrand factor type C domain
WASP	Wiscott aldrich syndrome protein
WAVE	WASP family verprolin homologous protein
WNT5a	Wingless/int-5a
ZPA	Zone of polarizing activity
α-cat	Alpha-catenin
β-cat	Beta-catenin
e	Strain
n	Poisson's ratio

CHAPTER 1: CURRENT ISSUES IN GROWTH PLATE CARTILAGE MORPHOGENESIS

AN INTRODUCTION TO SKELETAL BIOLOGY

The musculoskeletal system is the organ system that provides the form and structural integrity of our bodies, while also enabling us to move, bend, stretch, and execute complicated motor processes such as locomotion. In this system, the placement, connectivity, shape and size of the bones, cartilage, muscles, ligaments and tendons are crucial for their function. These features are irrevocably tied to tissue growth properties, which are partially determined during development, but dynamically change throughout one's lifespan. Diseases affecting growth (chondrodysplasias) can arise from diverse genetic, environmental, or trauma-related sources and have extremely serious consequences for affected individuals. With the hope of understanding and developing therapeutics to treat chondrodysplasias, there has been an immense corpus of basic research attempting to disentangle the complex mechanisms that regulate growth behavior. The linear elongation of the long bones in the developing limb has been a principal model for biologists to understand the formation of the musculoskeletal architecture. In this chapter, we will outline some of the major principles that govern limb morphogenesis. In particular, we discuss the interlocking roles of morphogen signaling gradients with mechanical forces as cues to induce and maintain cellular and tissue polarity, and explore the interdependencies among cells and tissues, across time and space, in tissue patterning, architecture, and growth.

Basics of vertebrate bone formation:

During an individual's growth, hundreds of developing bones undergo unique paths of precise patterning, shaping and scaling (Alberch 1979). Some flat bones, mostly in the skull, undergo intramembranous ossification, where mesenchymal stem cells differentiate into osteoblasts and directly deposit bone matrix without a cartilaginous

intermediate (Hojo 2016). However, the long, short, and irregular bones that make up the endochondral skeleton are formed by the regulated maturation of a collagenous growth plate cartilage template (Kronenberg 2003). In this process of endochondral ossification, mesenchymal stem cells differentiate into cartilage, which grows the skeletal element outward from each epiphysis before forming a primary ossification center at the diaphysis, where the growth plate template is invaded by blood vessels, osteoblasts, and osteoclasts that transform the area into the mineralized bone matrix. At the same time, a thin layer of cells that surrounds cartilage (perichondrium) undergoes periosteal ossification to give rise to the bone collar. The remaining growth plate continues to expand for as long as the individual grows, eventually developing secondary ossification centers that separate the existing growth plate from the nascent articular cartilage lining each joint surface. In humans, the secondary ossification center finally overtakes the entire growth plate region, halting growth and completing the mature bone anatomy.

Evolution towards the vertebrate skeleton:

The aforementioned processes are one route towards achieving a mineralized skeleton. One of life's major innovations, skeletons brought about a breathtaking diversity of body types, each containing bones of all shapes and sizes ranging from the thin shell of an ant to the massive skull of blue whales. This ancient strategy can be classified into two groups, endoskeleton and exoskeleton (Hirasawa 2015). Because phylogenetic continuities are traditionally inferred through fossil remains, definitions of each skeletal system were historically founded on presumed evolutionary lineage. One assumption was that skeletons of similar morphologies share cell origins, modes of histogenesis, genetic regulatory mechanisms, or position on the body. This belief has been challenged by recent comparative studies decoupling those parameters across phyla to reveal a very complicated picture of skeletal evolution (Hirasawa 2015, Brunet 2016).

Exoskeletons are usually defined by an enameloid/dentine coating on the exterior of the body, where endoskeletons are thought to have a deep position within the body, and feature a cartilage intermediate. However, body position is not a reliable criteria: fingernails and turtle carapaces are considered “exposed endoskeleton”, jaws and clavicle are considered “sunken exoskeleton” based on their contrary positioning, and some bones are actually fusions containing elements of both systems (Hirasawa 2013). Similarly, distinguishing these systems by the presence of a cartilage template runs into a number of counterexamples. Even cell lineage may also be more plastic than previously thought during evolution of “homologous” bones, based on studies of skull development in closely related phyla (Gross 2008). The presence of at least 18 analogous types of exoskeletons that independently evolved shows even chemical composition fails to define this term. (Roer 2015) Although terminology used for comparative skeletal anatomy mirrors the arbitrary, the complexity, and the historicity inseparable from all evolving systems, it is a humorous consequence of the symbiosis among skeletal biology and evolutionary theory (Alberch 1979).

However, it is possible to construct a timeline leading to the modern long bones of man. The story begins in the Metazoan, where multicellular organisms began experimenting with cell-cell junctions and extracellular matrices containing collagen and sulfated mucopolysaccharides, leading to the emergence of various chondroid connective tissues including hyaline cartilage (Cole 2004). Henceforth, cartilage was either conserved across distant clades of Bilateria, or independently evolved into the exact same tissue many times, based on detailed comparative assessments of tissue and cell histology, composition of the extracellular matrix, and genetic regulation (Tarazona 2016). By being relatively stiffer than most tissues, cartilage was able maintain various novel body structures. In some of these primordial endoskeletons, cartilage was calcified but did not ossify until the appearance of the jawless fish

Osteostracans 510 million years ago. Even then, these fish merely formed intramembranous bone on the surface of the cartilage (perichondrial ossification). Finally the bony fishes Osteichtyes in the late Silurian (419 million years ago) discovered true endochondral ossification, forming bone through the entire cartilage tissue as well as on its surface (Hirasawa 2015). Shortly afterwards, a group of creatures migrated onto land and, through a modification of the Hox gene code of spatial patterning, established a fin-to-limb transition that marked the beginning of tetrapods containing appendages that are deeply homologous to our own (Leite Castro 2016).

Diseases affecting skeletal growth – is regeneration a viable treatment option?

During these millennia of evolution, vertebrates gained the ability to precisely define bone geometries to match unique body plan requirements. Despite the natural variability of bone sizes across species, the mechanisms underlying endochondral bone shaping are remarkably conserved. Directional growth of bones occurs through strict orchestration of maturation, architecture, and remodeling of growth plate cartilage by an intricate regulatory system that is not yet fully elucidated. Tragically, the groundwork for our understanding has been built through careful analysis of conditions that adversely impact growth plate cartilage development to cause serious growth defects.

Over four hundred heritable bone growth disorders fall under the umbrella classification of osteochondrodysplasias, which collectively affect nearly 0.025 percent of all newborns (Geister 2015). Since the skeleton maintains the basic structure for every other organ, bone malformations can devastate an individual's life in diverse ways (Spranger 2012). Some common skeletal dysplasias, such as asymmetric limb length, make walking painful and difficult, and can often be spurred by a local traumatic injury to the growth plate during childhood. Some disorders progressively worsen, such as the

rare metaphyseal chondrodysplasias where excessive cartilage deposits at each epiphysis calcify to produce clubbed hands and feet. More serious conditions like disproportionate short stature (achondroplasia) can result in hypotonia, spinal cord compression, chronic ear infections, and obesity. Dysplasias that also affect the craniofacial skeleton in addition to long bones, such as Rhizomelic chondrodysplasia punctata, are associated with respiratory problems, cataracts, severe intellectual disability, and a significantly shortened lifespan. Even victims of chondrodysplasias that survive into adulthood are almost guaranteed to suffer from osteoarthritis. In general, diseases that disrupt skeletal formation have far-reaching secondary consequences that exacerbate their emotional, social and economic burden.

Because dysplasias are often characterized by morphological abnormalities in the growth plate, decades of intense research focused on understanding cartilage growth regulation, with the hope of preventing or correcting skeletal defects. Fueled by advances in genetics and molecular biology, thousands of dysplasia-associated alleles were identified, providing early clues as to which structural and signaling factors are necessary to promote healthy cartilage growth (Chen 2016). Genetic studies in vertebrate model systems came to describe some of the major hormonal interactions that impact cartilage maturation (Zelzer 2003, Hojo 2016, Kronenberg 2003). Nevertheless, our knowledge of the regulatory mechanisms that malfunction to drive skeletal disease is still insufficient to produce targeted clinical options in most cases. Efforts to stimulate growth using hormone or gene-based treatments are usually nullified by patient-specific genetic blockades. When bone length correction is absolutely necessary, manual techniques are used that rely on principles of distraction osteogenesis developed by Ilizarov in the 1950's (Spiegelberg 2010). Ilizarov therapy, which is the gold standard for bone lengthening, is an extremely painful and intensive surgical procedure that involves repeated fracturing of a single bone over several

months to a year. Thus, given limited alternatives, palliative care is the current norm for patients with chondrodysplasias.

Partially because of the prevalence and lack of therapeutic options for skeletal diseases such as osteoarthritis and chondrodysplasias, one long-standing dream of medicine has been the successful replacement or regeneration of injured or diseased cells, tissues, or entire organs by transplanting artificial tissue constructs grown *in vitro* to patients in need. The desire for regenerative therapeutics propelled advances in tissue engineering (the use of combined cells, scaffolds, and biologically active molecules for the sake of designing functional tissue systems), which since the early 1990's has blossomed into a mature field of research. Using this now-classic approach, clinics have had success with tissue replacement strategies targeting simple body parts like skin, arteries, bladder, and even entire trachea. Yet, rational design of tissues with controllable growth properties such as the growth plate remains unrealized, despite the early selection of cartilage as a promising candidate by many tissue engineers viewing it as a simple substance containing only one cell type (chondrocytes) with the sole function of extracellular matrix secretion. Since then, many of the early assumptions have since been discarded, and there has been some acceptance of the need to faithfully recapitulate the native molecular, cellular, and tissue-wide organization of cartilage so crucial for its mechanical integrity and growth. However, to succeed in recreating cartilage architecture, it is crucial to understand the underlying mechanisms. The next sections arrange a timeline of significant developmental processes, and review the current approaches being taken to model them by tissue engineers and cartilage biologists.

Cellular sequence of events during skeletal development:

The entire limb structure arises from the lateral plate mesoderm in three steps: a limb bud outgrowth stage, a cell fate specification stage (chondrogenesis), and endochondral ossification (Romereim 2011, Kronenberg 2003, Zeller 2009, Tickle 2015). The limb bud is composed of a thin layer of surface epithelium called the apical ectodermal ridge (AER), which covers a mesenchymal tissue core (Tickle 2015). Signaling between these tissues establishes a three-dimensional system of positional information that organizes growth along the anterior-posterior (AP), dorsal-ventral (DV), and proximal-distal (PD) axes (Figure 1.1a, the specific genetic interactions shown in this figure will be discussed shortly).

In mouse, limb bud outgrowth begins at the cervical-thoracic and lumbosacral boundaries at embryonic day 9 with thickened regions in the flank mesoderm called mesenchymal condensations. In these structures, increased cell-cell adhesion separates the limb bud from the adjacent mesoderm, and cell cycle activation drives isometric growth (Hamburger and Hamilton 1951, Romereim 2011, Tickle 2015). However, distal tissue soon expands along the AP axis and thins along the DV axis to produce a paddle-like shape (Figure 1.1b). During this stage, limb bud outgrowth is founded in regulation of cell shape, cell migration, and oriented cell division by signaling centers that produce ligands important for growth and patterning (Gros 2010). As mesenchymal cells at the tissue edges migrate towards the distal AER, vectors of tissue deformation and direction of cell movement correspond to orientation of the cell body, and angle of the mitotic spindles (Gros 2010). Meanwhile, mesenchymal cells from the lateral plate mesoderm collectively move towards the distal-posterior mesenchyme called the zone of polarizing activity ZPA (Tickle 1975, Romereim 2011, Tickle 2013). As a result, the directional bias of growth is initially distal but becomes posterior.

Throughout these growth phases, anisotropic tissue elongation is uniform at different points along the PD axis and can still occur independently of cell proliferation (Morishita 2015). Thus, the induction of polarized cell behavior produces directional growth in the limb bud. As the limb bud continues to elongate along the PD axis, cell fate specification begins via the progressive formation of mesenchymal condensations that specify position of the future bone. This is a highly ordered temporal sequence where the most proximal elements begin the differentiation process first, followed by more distal elements. For each limb, the proximal stylopod contains a single long bone (femur), followed by the zeugopod, which contains two bones (tibia/fibula), and the distal autopod contains many skeletal elements (ankle/toes). For each element, portions of the limb mesenchyme differentiate into the early cartilage anlagen (eventually giving rise to each bone). To form the anlagen, a correct number of chondrocyte progenitors, and increased levels of cell-cell adhesion between these progenitors are required to distinguish the presumptive cartilage from a surrounding sheath of perichondrial cells, which will eventually give rise to the bone collar (Widelitz 1993). Simultaneously, the cells that will occupy the joint spaces are specified (Mak 2006). At this point, the shape of each cartilage anlagen already resembles the geometry of the final bone (Figure 1.1c), indicating that important shaping events occur prior to cartilage formation.

Figure 1.1: Developmental origins of growth plate cartilage

A) Morphology of the early limb bud is depicted. The 3D coordinate space defining positional information is superimposed on the bud. (Pr-proximal, Di-distal, Do-Dorsal, Ve-ventral, An-anterior, Po-posterior). B) During limb bud outgrowth, mesenchymal tissue elongates along the PD axis. Signaling gradients of WNTS, FGFs and RA emanating from the apical ectodermal ridge (AER) control growth and patterning along the PD axis. Sonic Hedgehog (SHH) protein from the distal ZPA and the transcription factor Gli3 underlie growth and patterning along the AP axis. C) Digit specification in the distal mesenchyme of the limb bud. A gradient of SHH signaling that depends on time, concentration, distance from SHH source, and cell-matrix interactions, interacts with the limb bud environment to specify position of the future cartilage anlagen. D) Embryonic day 11.5. Cartilage anlage of the presumptive metacarpal resides among the chemical milieu of the distal mesenchyme. Even this early in development, the cartilage is geometrically elongated. E) Embryonic day 12.5. Wnt5a signals specify a region (colored green) of chondrocytes that become polarized in the plane perpendicular to the PD axis, via asymmetric localization of Vangl2. IHH expression is detected in the center of the cartilage element, but markers of hypertrophic (very large cells expressing ColX) and resting zones (PTHrP) are absent. F) Embryonic day 13.5. Markers of tissue-wide polarity are observed after localized cell differentiation occurs. PTHrP expression is observed near the articular surfaces, large hypertrophic cells are observed in the center of the cartilage, flanked by IHH-expressing cells. Some polarized chondrocytes reside between domains of PTHrP and IHH-expressing cells. G) Embryonic day 14.5. Eventually, columns of proliferative zone chondrocytes are observed. WNT5a expression moves to the perichondrium, where it may form a secondary gradient in cartilage. Zonal arrangement of cartilage is observed henceforth until growth plate closure, when the element stops elongating in postnatal skeletal development.

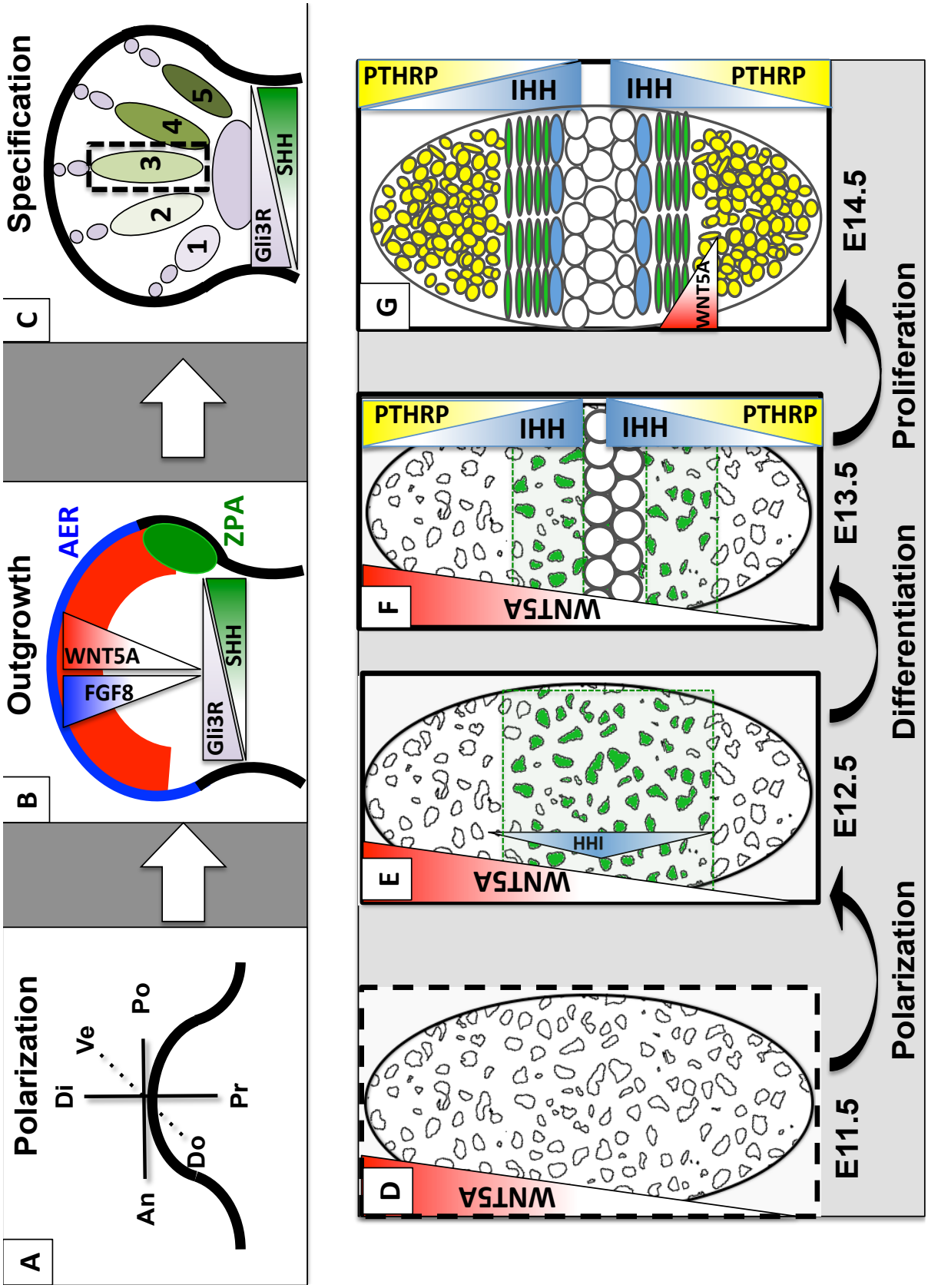
A
Polarization
Di
Ve
Po
An
Do
Pr
B
Outgrowth
AER
ZPA
WNT5A
FGF8
Gli3R
SHH
C
Specification
1
2
3
4
5
Gli3R
SHH
D
WNT5A
E11.5
E
WNT5A
HHI
E12.5
F
WNT5A
PTHRP
IHH
IHH
PTHRP
E13.5
G
WNT5A
PTHRP
IHH
IHH
PTHRP
E14.5
Polarization
Differentiation
Proliferation

The final stage of limb development, called endochondral ossification, begins as newly differentiated chondrocytes secrete a cartilage matrix and initiate a maturation process that forms the growth plate cartilage. During endochondral ossification, this cartilage serves as a master regulator of bone formation and growth through spatiotemporal regulation of chondrocyte differentiation, proliferation, and morphogenetic behavior. Each growth plate displays tissue-wide polarity, in that it is partitioned along the proximal-distal axis into morphologically distinct zones that control growth in unique ways (Figure 1.2b). At the epiphyseal surface, rounded and slowly dividing resting zone chondrocytes serve as a reservoir of progenitor cells. The number of these cells determines the total growth potential, because the maintenance of the adjacent maturation phases relies on recruiting cells from this resting zone (Abad 2002).

Next, quiescent resting zone chondrocytes mature by entering into a transit-amplifying phase called the proliferative zone. These cells rapidly activate the cell cycle and obtain several important morphogenetic characteristics based on oriented cell behavior. Namely, proliferative chondrocytes adopt a discoid shape that polarizes the cell body in the plane perpendicular to the proximal-distal axis (Dodds 1930). During this stage, many other hallmarks of cell polarity become visible, such as lateral secretion of matrix vesicles and planar alignment of the primary cilium (de Andrea 2010, Romereim 2014b). Most importantly, oriented cell movements in this zone establish the vectors underlying bone elongation. Each cell division displaces daughter chondrocytes laterally, and polarized 90-degree rearrangement of daughter cells produce cell columns that lengthen along the proximal-distal axis (Figure 1.2c). By this iterative process, isogenic groups of proliferative chondrocytes form clonal columns that resemble stacks of coins (Romereim 2014). The length of proliferative zone columns establishes the primary growth vector, and maximizes potential tissue elongation along the proximal-distal axis while minimizing oppositional thickening (Li 2009).

Finally, the columnar cells undergo a process of pre-hypertrophy and then hypertrophy, where cells directly drive tissue expansion by volumetric expansion of each cell, and increased extracellular matrix deposition. Hypertrophic chondrocyte enlargement has a linear relationship to longitudinal growth, and occurs in three distinct cell growth stages that underlie differences in skeletal proportions among bones (Cooper 2013). After hypertrophy, terminally differentiated chondrocytes undergo apoptosis (although some portion of these cells has been proposed to transdifferentiate into osteoblasts, see Yang 2014), while the remaining cartilage matrix is remodeled into bone (Tsang 2015). Thus, by controlling the rate of maturation across resting, proliferative, and hypertrophic zones, the growth plate cartilage determines the final shape and size of each skeletal element.

During skeletal development two separate tissue systems, the limb bud and growth plate cartilage, exhibit tissue-wide polarity in the form of discrete ordered regions of cell differentiation and behavior along the PD axis. In fact, proximal-distal polarity is quite apparent during skeletal development no matter which grain of analysis is taken. At the organ-scale, we can see the proximal-distally determined patterning of the entire limb bud, the beautiful elongated geometry of entire bones, and the symmetry of tissues (bone, capped by cartilage growth plates) along the proximal-distal axis (Figure 1.2a). At the tissue level, each piece of cartilage is segmented into maturation zones that reflect a PD-oriented pattern of cell differentiation (Figure 1.2b). This polarity is mirrored at the cell level, with PD-oriented columnar cytoarchitecture and cell shape in the proliferative zone of growing cartilage (Figure 1.2c), and PD-oriented cell migration and division in the growing limb bud.

Figure 1.2: Multi-scale organization of growth plate cartilage.

A) Morphology of an E14.5 developing mouse hind limb skeleton stained using Alcian Blue /Alizarin Red to visualize cartilage and bone, respectively. The body axes are shown in the top right. From left to right, notice the characteristic patterning of bones (many little bones in the autopod, two long bones in the stylopod, one large bone in the zeugopod). Notice the elongation of the femur along the proximal-distal axis. Each bone is symmetrical, with a growth plate capping each end. At this length scale, the skeletal system mechanically interacts with many tissues including muscle and ligaments that contribute to skeletal development. B) Schematic representation of the growth plate cartilage of the distal femur boxed in (A). Growth plate cartilage contains a high degree of organization in the form of maturation zones. Near the joint, resting zone (RZ) chondrocytes secrete PTHrP to maintain a pool of less differentiated cells. Near the bone center, IHH-secreting cells signal to promote the hypertrophic differentiation program, characterized by cell swelling and increased matrix deposition. Between these zones, the column-forming proliferative zone cells mature and proliferate at rates controlled by the reciprocal interactions of PTHrP and IHH. At this length scale, properties of the cartilage matrix and bulk tissue dynamics caused by growth affect cartilage development. C) Schematic of the cellular events underlying chondrocyte column formation in the cartilage proliferative zone boxed in (B). Proliferative chondrocytes orient the mitotic spindle such that daughter cells are side-by-side. An adhesion surface connects the two daughter cells following cytokinesis. The daughter cell adhesion interface rotates to drive column formation. Finally, chondrocytes secrete new ECM to separate. At this length scale, molecular forces between cells and their mechanical environment drive interface remodeling and cell organization.

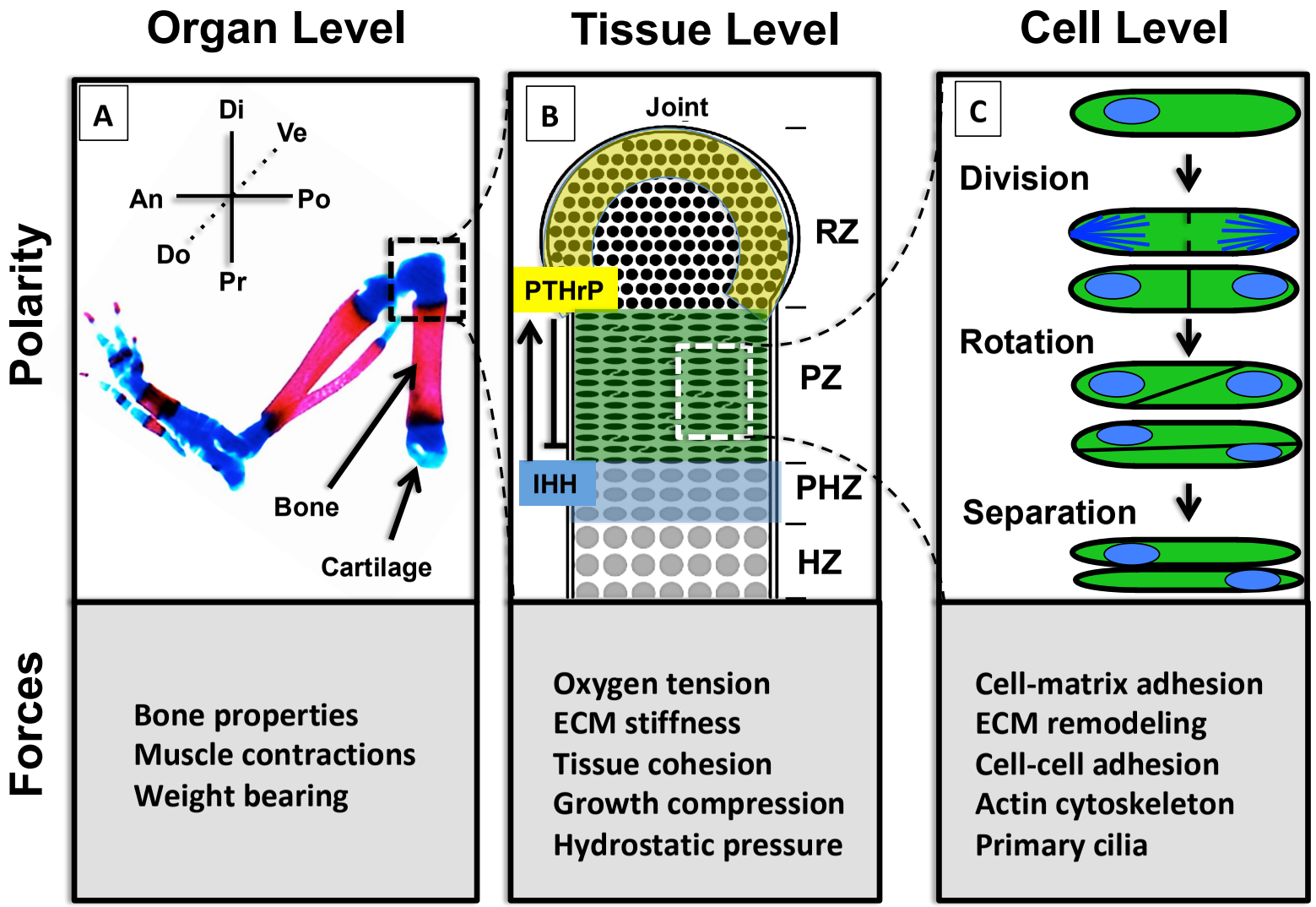
Organ Level
Tissue Level
Cell Level
Polarity
Forces
A
Di
Ve
An
Po
Do
Pr
Bone
Cartilage
B
Joint
RZ
PTHrP
PZ
IHH
PHZ
HZ
C
Division
Rotation
Separation
Bone properties
Muscle contractions
Weight bearing
Oxygen tension
ECM stiffness
Tissue cohesion
Growth compression
Hydrostatic pressure
Cell-matrix adhesion
ECM remodeling
Cell-cell adhesion
Actin cytoskeleton
Primary cilia

Strategies for modeling cartilage development in culture

The integration of shaping mechanisms across length and time scales during limb cartilage development is under the control of both gene regulatory networks as well as mechanics of the physical environment (outlined in Figure 1.2). These complexities have hindered the production of accurate and useful *in vitro* representations of growth plate cartilage that could facilitate cell-based therapies for chondrodysplasias. However, biologists and engineers have made progress towards control over the functional properties of cartilage constructs by the development of various *in vitro* cartilage culture models. While most of these studies focused on articular chondrocytes, some of the approaches have been applied towards reproducing the growth plate structure, with varying rates of success.

Cartilage regeneration has been a subject of primary concern for decades. Being the structural support of the body, all cartilage types are at high risk for injuries. Damage to the permanent cartilages of load-bearing joints can cause osteoarthritis, and injuries of the growth plate lead to ectopic bone formation that usually halt growth and tend to recur after surgical removal. Because cartilaginous tissues are populated only by chondrocytes and develop mostly in the absence of vasculature or innervation, they are limited in their capacity for spontaneous repair following damage (Vinatier 2016). The clinical strategies employed to reconstruct injured skeletal tissues vary widely and depend on the anatomic context, and have primarily focused on joint cartilages that are most commonly affected by osteoarthritis such as the knees and hips. Generally, classical techniques such as cartilage autografts, autologous chondrocyte implantation (ACI), and microfracturing bone to stimulate repair by the underlying marrow have been used to fill osteochondral defects with cartilage, although these methods usually present practical difficulties that impair the healing process such as improper integration with

host tissues, insufficient mechanical properties to carry out normal load-bearing function, and in some cases of head-and-neck cartilage repair, inappropriate activation of immune responses (Liu 2017). A deeper underlying problem is that historically, reconstruction attempts have not successfully recapitulated the fine tissue architecture so important for cartilage function and mechanical integrity. Many tissue-engineering groups are now motivated to achieve this goal (Kock 2012).

One apparent theme in cartilage engineering research has been that chondrocytes are responsive to culture parameters such as dimensionality, scale, nutrient availability, mechanical properties of the environment, and various physical, chemical, and biological stimulations. This could be taken to mean that relevant phenomena may be modeled in culture if optimal conditions are attained. However, a wide range of tested conditions eventually lead to either dedifferentiation into fibrocartilage characterized by increases in Collagen I production, which results in mechanically inferior constructs, or spontaneous hypertrophy leading to terminal differentiation and a loss of proliferative potential (Kock 2012). Thus, many of the early studies developing chondrocyte culture models were plagued by loss of the chondrocyte phenotype (Benya 1978). This was most poignantly illustrated in attempts to culture chondrocytes in monolayer (Schabel 2002); neither stimulation with growth factors, nor coating the substrate with cartilage-specific matrix molecules (Brodkin 2004) is sufficient to truly regain a chondrocyte identity in two-dimensional culture (Pei 2012). Environment dimensionality is then a principal concern for maintaining chondrocytes in culture.

Three-dimensional culture models can improve chondrogenic differentiation, usually determined by chondrocyte markers such as rounded morphology, expression of the transcription factor Sox9, and production of a proteoglycan- and Collagen 2-rich ECM. There are two basic types of commonly used 3D chondrocyte culture systems: scaffold-free cultures, and the implementation of scaffolds to simulate the cartilage environment.

Scaffold-free techniques include bioprinting, the creation of cell sheets or aggregates, and particularly pellet cultures, which have been used to show a curious potential for *in vitro* cartilage self-organization.

For many pellet cultures, spontaneous hypertrophy actually still occurs after one week without additional supplementation by growth factors (Kameda 2000). This response may be triggered because pellet cultures do not facilitate biomolecule diffusion, and can result in nutrient deprivation over time depending on their size. One consequence of this is an overall lack of investigator control with respect to the spatiotemporal delivery of signaling factors to chondrocytes in micromass. Additionally, the extensive cell-cell contacts characteristic of micromass culture is not a feature of the mature, ECM-dense growth plate (although it could be argued to mimic early chondrogenic condensations). Despite this, a few studies have claimed that pellet cultures treated with the correct cocktail of growth factors could support growth plate-like morphogenesis. In one notable example, addition of serum to 28-day pellet cultures led to the generation of cell columns resembling those found in the proliferative zone (Ballock 1994). In this study, it was deduced that of the known molecules contained in serum, thyroxine alone was sufficient to recapitulate this phenotype. Later, similar chondrocyte pellet cultures transformed and treated with components of the planar cell polarity-signaling pathway were claimed to generate columnar cell morphology compared to normal control pellet cultures (Randall 2012). Unfortunately, these preliminary studies were not pursued further, and in both cases, there is very little information about whether these columns were derived from clonal cell groups, or otherwise formed by known biological processes. Furthermore, the presence of maturation zones in these constructs was not shown. Thus, pellet cultures occupy an important and controversial space in studies of growth plate cartilage tissue engineering.

Three-dimensional scaffolds offer more precise control over the chondrocyte's signaling environment, and can help retain the chondrocyte phenotype. These include scaffolds that are modeled after one or more components of the cartilage matrix itself, as well as those that use naturally occurring or synthetic polymers foreign to cartilage. For example, studies have utilized various forms of decellularized cartilage or mesenchymal matrix, which seems to support cartilage formation well. Additionally, isolated components such as collagen, laminin, fibrin, and fibronectin scaffolds have been used to provide a protein substrate in 3D that mimics the protein-rich cartilage ECM. Proteoglycan and other glycosaminoglycan scaffolds have been explored that use pericellular matrix molecules such as hyaluronic acid and chondroitin sulfate to which chondrocytes closely associate in vivo. More generic polysaccharide-based scaffolds are also common such as chitosan, agarose and alginate. Finally, synthetic polymers such as polyethylene glycol (PEG), polylactic acid (PLA), and poly(lactic-co-glycolic) acid (PLGA) have been employed (Dhandayuthapani 2011).

Polymeric scaffolds can be presented to cells as hydrogels, which from a practical viewpoint allows precise control of cell culture parameters such as oxygenation, nutrient diffusion, mechanical attributes (Dhandayuthapani 2011). Furthermore, hydrogels usually have high biocompatibility and low toxicity, making them suitable for many types of *in vitro* modeling applications. Hydrogel culture has been utilized to generate some of the most compelling evidence of growth plate reconstruction. One notable result arose from co-culturing chondrocytes and osteoblasts in a hydrogel construct made of alginate, conjugated to RGD peptides to stimulate cell adhesion (Alsberg 2002). When this construct was injected into mice, histological analysis after 7 months revealed tissue that grossly resembled growth plate structure complete with columns and zones, while untransplanted constructs did not. Agarose hydrogels have also been used in attempts to recreate the spatially separated maturation zones of

cartilage by exploiting their diffusion properties to present gradients of chondrogenic signaling factors to encapsulated chondrocytes (Schmitt 2012). Although cells at the periphery expressed markers of hypertrophy, such spatial variation can be found to be byproducts of long-term, high-density culture (Park 2007). Further, no information about the sequential cartilage maturation was presented in this study.

Detailed, comprehensive characterizations of how different scaffolds compare in terms of promoting chondrocyte proliferation, differentiation, and cartilage formation are not available, and technical details for any given method are by no means completely standardized across this field. Ultimately, no single scaffold has been demonstrated to recapitulate all major features of growth plate biology, such as the spatially organized zonal maturation along with clonal column formation of chondrocytes. Indeed, many studies of cartilage formation in culture do not even make attempts to assess these parameters. Furthermore, while there are many studies that deliver signaling factors and other forms of directed stimulation to chondrocytes in culture, there is little to argue for or against whether these conditions resemble the highly coordinated suite of signaling cues presented to chondrocytes by the *in vivo* signaling environment of the growth plate. Thus, of the many candidate scaffolds, there is no real “golden standard” to compare a given type of chondrocyte culture to, other than cartilage itself. Ultimately, although the versatility of hydrogel and other tissue engineering systems opens virtually unlimited design options, our ability to make rational design choices based on a mechanistic understanding of cartilage development remains a critical bottleneck. Knowing how individual signaling cues affect chondrocyte behavior, or which genes are required for different aspects of cartilage formation, will not be enough; it is also imperative to discover how genetic and physical factors form an integrated regulatory system that functions across multiple length and time scales to generate shape and form. The following sections will draw from classic work, recent progress, and overlooked

experimental and theoretical studies to begin to address how genetic and mechanical factors could serve as positional cues during skeletogenesis.

GENETIC REGULATION OF CARTILAGE ARCHITECTURE

Signaling interactions that coordinate limb bud positional information:

The events of limb bud patterning and outgrowth that initiate morphogenesis of the limb skeleton are believed to depend on several molecular gradients derived from the overlying ectoderm via a three-dimensional system of positional information for interpretation by the limb bud mesenchyme cells (Figure 1.1a). Once the signaling environment created by the limb bud organizers have established the primary axes, limb bud continues to develop autonomously (Stephens 1993). Proximodistal outgrowth begins when Hox genes signal transcription of FGF and WNTs in the mesenchyme to establish the apical ectodermal ridge (AER), a strip of ectoderm along the limb bud tip, which primarily functions through producing an FGF signaling gradient (Lewandowski 2000, reviewed by Bokel 2013). In the forelimbs, FGF signaling is antagonized by retinoic acid (RA) produced by the proximal mesenchyme but degraded by distal mesenchyme, creating opposing morphogen gradients (Nishimoto 2015, Mercader 2000). One result of this is a distally biased gradient of motility, where cells closest to the AER move with greater velocity (Gros 2010, Wyngaarden 2010). The AER also maintains the zone of polarizing activity (ZPA), which is located on the posterior region of the ectoderm and controls anterior-posterior polarity by secreting SHH (Mao 2009, Zhang 2009, Tickle 2013). In turn, ZPA-derived SHH signaling maintains FGF4 expression in the AER (Laufer 1994, Niswander 1994). Further, both the AER and ZPA maintenance requires induction of dorsal-ventral polarity by ventrally secreted BMP and dorsally secreted Wnt7a from the ectoderm (Ahn 2001, Pizette 2001). Thus, positional

information here relies on abundant molecular feedback and disruption of cell polarity along a single axis can have serious consequences for cell polarity signaling in other directions (Figure 1.1b). As a result of the highly ordered signaling environment, different cell domains within the limb bud displays cell polarity manifested by unique regimes of oriented cell shape, cell division and migration (Gros 2010, Wyngaarden 2010). While FGF signaling from the AER promotes scalar properties of growth such as the speed of migration, the orientation of cell behavior along the PD axis seems to depend largely on the actions of Wnt5a signals that originate from the distal mesenchyme and ventral ectoderm and are maintained by reciprocal interactions between the AER and ZPA (Gros 2010, Kawakami 1999, Barrow 2003). Thus, to understand the mechanisms generating anisotropy in the developing skeleton, we will begin by learning to what extent Wnt5a serves as an instructive cue for cells in the limb bud.

Wnt5a signaling controls proximal-distal polarity to regulate limb bud growth:

Wnt (Wingless-related integration site) molecules are a highly conserved family of nearly twenty secreted protein ligands that activate discrete signaling pathways that can be categorized into both canonical (beta-catenin dependent) and noncanonical (beta-catenin independent) pathways (Geetha-Loganathan 2008). Historically, canonical Wnt ligands were discovered for their role in carcinogenesis and formation of the body axes in the early drosophila embryo (Nusse 1992, Nusse 2005). Some noncanonical Wnt ligands can activate calcium signaling, but the noncanonical Wnt/JNK/Planar Cell Polarity (PCP) signaling is a primary pathway that gives rise to cellular and tissue polarity in many developmental contexts, including skeletogenesis (reviewed in Vladar 2009). Planar polarity refers to the coordination of cell behavior along any single plane. The central components of the planar cell polarity pathway are the cell-surface proteins

Frizzled (Fzd), Van-Gogh-like (Vangl, Stbm), and Celsr1 (Flamingo) that signal downstream to the cytoplasmic proteins Disheveled (Dvl), Prickle (Pk), and Diego (Dgo). It is thought that these proteins work in coordination with components of the Wnt signaling pathway to directionally drive cell proliferation, migration, and other polarized cell behaviors during limb bud and growth plate development to promote skeletal elongation. Early studies established Wnt5a signaling in the developing limb as a regulator of cell cycle. $Wnt5a^{-/-}$ limb mesenchyme shows reduced proliferation by BRDU label and subsequently, reduced tissue growth (Yamaguchi 1999). However, quantitative deformation mapping suggest that spatial heterogeneity in cell cycle cannot explain anisotropic mesenchymal tissue deformation in the limb (Morishita 2015). In addition to regulating scalar growth via cell cycle, Wnt5a through PCP signaling was shown to also promote oriented cell behaviors to regulate cell organization during limb bud outgrowth (Gros 2010, Wyngaarden 2010).

Formation of the AER from the ventral/distal ectoderm is a crucial step in limb bud development, and relies in part on convergence-extension movements to form a stratified cytoarchitecture that displays both apicobasal and planar polarity. Wnt5a signaling is probably involved in the establishment of AER organization, since the Dlx5/6 DKO model of split hand/foot malformation (SHFM) characterized by cell shape and polarity defects reduce Wnt5a expression and can be rescued by exogenous Wnt5a treatment (Conte 2016). In this study, inhibiting the JNK pathway led to loss of AER marker RhoU expression, which could not be rescued by FGF8 treatment. Thus, defects in AER-stratification dependent limb bud growth could be reflected in $Wnt5a^{-/-}$ mice, suggesting that tissue-scale polarity has roots in the cell-level polarity of tissue-organizer regions.

In addition to regulating epithelial stratification of the AER, Wnt5a seems to affect cell polarity in the underlying limb bud mesenchyme. Time-lapse video microscopy

combined with lineage tracing has also shown that mesenchymal cells are polarized and organized by position within the tissue and that local growth vectors are aligned with flattened cell bodies, mitotic spindle orientation, and cell migration (Gros 2010). In Wnt5a$^{-/-}$ embryos, elongated cell shape was lost, cell divisions in the dorsal and ventral domains were disorganized, and cell movements were randomized. These phenotypes were copied by inhibiting the JNK pathway.

Wnt5a is also recognized as a regulator of cell polarity in the perichondrial cells which can affect cell fate specification (Kuss 2014). Wnt5a$^{-/-}$ cartilage lacks a perichondrium (personal observation). In mice with Synpolydactyly (spdh mice), Wnt5a expression is reduced, and orientation and polarity of perichondrial cells is lost. The consequences of lost polarity here is the transformation of some long bones into cuboidal bones.

How could a secreted ligand such as Wnt5a act to produce such oriented cell behavior? In vitro experiments indicate that Wnt5a through JNK/PCP may act as a chemoattractant to confer cell polarity upon mesenchymal cells and promote oriented cell behaviors (Wyngaarden 2010). Together, WNT5a and FGF8 signaling integrate cell motility with cell polarity to define the mesenchymal cell migration trajectories that characterize limb bud outgrowth.

Do morphogen gradients control skeletal patterning in the limb bud?

Patterning of future bones in the limb bud depends on the actions of many locally secreted signaling molecules, but the mechanisms that translate these signals in the dynamic tissue environment into discrete cartilage elements is still unclear. This is important because at a glance, the known topology of the signaling environment does not precisely predict the numbers, positions, and geometries of the various bones of the

limb skeleton. To explain these phenomena, biologists have grappled with the concept of morphogen gradients as positional cues. Alan Turing introduced the concept of "morphogen" almost a century ago in a seminal theoretical study describing how reaction kinetics of a diffusible molecule could generate patterning in a field of cells (Turing 1952). Since this work, developmental biologists have almost unilaterally adopted the paradigm of "positional information based on a morphogen gradient" as a major mechanism in morphogenesis, and much of the theory behind this concept has been experimentally verified to play important roles during development (Sheth 2012, Hiscock 2015). While the role of gradients in proximal-distal patterning in the limb bud has been hotly debated for decades, there is some consensus that anterior-posterior patterning gives rise to digit cartilage from the distal mesenchyme according to a SHH signaling gradient.

Proximal-distal patterning:

There have been several competing models proposed throughout the last century to explain how the limb reproducibly arranges the zeugopod, stylopod, and autopod pattern across the proximal-distal axis, and many of them use a proximal flank-derived RA gradient that opposes a distal AER-derived FGF8 gradient to specify differentiation within different segments of the skeleton. It was originally proposed that progressive specification of cell fates in a "progress zone" subadjacent the AER started as proximal, and became increasingly distal throughout development (Summerbell 1973). Later, a pre-pattern model was conceptualized in which cell fates were determined from a very early stage, potentially by reading relative RA/FGF concentrations (Chiang 2001, Dudley 2002). Recent data suggests that specification of the limb field is initiated by RA/FGF antagonism, which could account for the most proximal limb segment, but that distal mesenchyme do not require RA signaling for patterning, and that FGF signals

permissively regulate patterning by simply promoting growth (Cunningham 2013, Saiz-Lopez 2015). Rather, patterning of the zeugopod and autopod may rely on an intrinsic clock to coordinate differences in cell cycle, expression of Hoxa11/Hoxd11 and Hoxa13/Hoxd13 genes, and cell adhesion properties to specify proximal-distal values (Saiz-Lopez 2015). This may play a role in determining differences in size among bones along the proximal distal axis, as it was proposed that mesenchymal cells that give rise to the more proximal stylopod bones, having proliferated fewer times prior to differentiation, contain greater proliferative potential and thus grow to much greater sizes compared to autopod bones, explaining the fact that most mesenchymal condensations initially form to similar sizes irrespective of proximal-distal value (Tabin 2007). Thus, the importance of signaling gradients for proximal-distal patterning is still unclear.

Anterior-posterior patterning:

SHH, locally secreted from the tiny posterior-distal ZPA domain, controls the anterior-posterior polarity of the limb mesenchyme during outgrowth and digit specification (Figure 1.1c). Localized expression of SHH can be clearly viewed at the mRNA level by in situ hybridization (Marigo 1996) and immunohistochemistry (Gritli-Linde 2001). Also, several downstream molecular, cellular, and morphological readouts clearly exist to produce a graded outcome. Downstream transcriptional targets of SHH signaling, Ptc1 and Gli1, are expressed in a gradient emanating from the ZPA (Drossopoulu 2000, Tickle 2013). Furthermore, PKA-mediated Gli3 post-translational processing interacts with SHH in the limb bud to control digit patterning (Marigo 1996). Graded SHH signaling has been shown to translate to a gradient of the Gli3 activator/Gli3 repressor ratio to relieve posterior cells from Gli3 transcriptional repression of SHH targets (Litingtung 2002, te Welscher 2002, Wang 2007). Experiments using SHH-expressing cell grafts and SHH-soaked beads have demonstrated that this anterior-posterior gradient is

dependent on SHH dose, and duration of cells to SHH exposure, and distance from the SHH source (reviewed in Tickle 2013). Cells in the ZPA also contain an intrinsic cell cycle clock that regulates SHH expression, suggesting both SHH-expressing and interpreting cells sense time (Chinnaiya 2013). This means that during digit patterning, SHH does not act in a simple concentration gradient, but rather, time, distance, and slope of the concentration gradient all cooperate to produce a signaling activity gradient that varies across time and space to determine digit number. As a result of the gradient of SHH signaling along the AP axis, quantitative maps of tissue deformation anisotropy have shown that the regions of greatest tissue deformation correspond exactly with regions of greatest SHH signaling, and that SHH-dependent growth rate also emanates from the ZPA in a gradient (Morishita 2015).

The SHH signaling gradient is just one of the many examples of clearly graded distributions of signaling molecules in space that result in generating a gradient of cellular signaling response that can differentiate between multiple thresholds to produce tissue patterning. What determines these thresholds is beginning to be understood, but more research is needed to uncover the exact mechanisms used by cells in the limb bud to interpret the SHH gradient. Further, we need to know how SHH signaling, in conjunction with other positional cues, is used by dynamically moving mesenchymal cells in the growing limb bud to make cell fate decisions.

Chondrogenesis:

Once growth and patterning of the limb bud have defined the position of future bones in the limb skeleton, each specified domain of mesenchyme undergoes a compaction process where cells become highly cohesive to demarcate the shape of new cartilage elements by a mechanism that resembles cell sorting (Widelitz 1993, Oberlander 1994, Barna 2007). Cells within the forming cartilage begin to express Sox9, which is the

master transcription factor underlying chondrogenic differentiation (reviewed in Hojo 2016). Sox9 expression promotes rapid deposition of Collagen II and Aggrecan, the primary constituents of the early cartilage ECM, and induces the rounded cell shape characteristic of early chondrocytes (Barna 2007, reviewed in Kozhemyakina 2015). At this point, cartilage has formed, but does not show any large-scale organization, other than the fact that the entire cartilage anlagen somewhat resembles the gross geometry of the future bone (Figure 1.1d). Further, cells within the new cartilage anlagen do not exhibit specific polarity along any of the axes defined in the limb bud. However, to achieve the polarized growth so crucial for bone elongation, primordial chondrocytes must give rise to the growth plate, cartilage, the highly ordered array of cells that displays both tissue- and cell- scale organization along the proximal-distal axis (Figure 1.1g). Establishing tissue polarity means that distinct zones of maturation including resting, proliferative, prehypertrophic, and hypertrophic zones must be aligned along the PD axis of the future bone. At the cell level, proliferative zone chondrocytes must form the idiosyncratic columnar structures that restrict future hypertrophy-driven growth along the PD axis to specifically promote tissue elongation. Knowing this, one current challenge is to identify the cell source as well as identify the specific polarizing cue driving zone and column formation.

Tissue autonomous mechanisms may underlie growth plate cartilage polarity:

One strategy to identify a polarizing cue for cartilage is to identify the location of endogenous factors that modulate polarity in the growth plate. There are several lines of evidence pointing to the existence of tissue-wide cues intrinsic to the growth plate that support the high degree of cell and tissue organization required for bone elongation. It was discovered that zonal and columnar architecture of growth plate cartilage does not

depend on its positioning relative to bone (Abad 1999). In this study, inversion of growth plates in a mouse model induced repolarization of surrounding bone tissue while maintaining cartilage structure, suggesting that cartilage spatial polarity is intrinsic, and further, that it regulates polarity of the underlying bone. It was later demonstrated that resting zone chondrocytes are capable of regenerating all other zones after resection of proliferative and hypertrophic zones of the developing distal ulnar growth plate, and that transplant of resting zone cartilage next to the proliferative zone is sufficient to induce orthogonally directed columns, suggesting that resting zone cells produce a signal that directs cartilage polarity. More recently, time-lapse confocal microscopy has revealed polarized cell behavior in growth plate cartilage explants cultured in minimal media (Romereim 2014). This study demonstrated that cultured cartilage explants could add new cells to preexisting columns and even establish *de novo* cell polarity in the absence of external tissues. The above information suggests that the resting zone of cartilage produces some factor that can regulate cell polarity, but the identity of this factor is unknown.

Cartilage-wide signaling - Role of PTHrP – IHH loop in growth plate organization:

If column formation in the postnatal growth plate depends on the spatial orientation of cartilage zones, one strong candidate in the search for tissue-intrinsic cues can be found in the reciprocal interactions of Parathyroid hormone-related protein (PTHrP) and Indian hedgehog (IHH). The PTHrP/IHH signaling axis has long been known for its importance for tissue architecture during growth plate maturation. PTHrP is expressed and secreted from sub-articular resting chondrocytes, while IHH is secreted specifically from pre-hypertrophic chondrocytes and both expression domains are observed prior to the formation of columns (Figure 1.1g and 1.2b) (Chen 2006, Vortkamp 1996, Gao 2009,

Provot 2007, Yang 2003). It is thought that the two ligands form complementary signaling gradients along the PD axis to control the rate of cell proliferation and differentiation in the cartilage proliferative zone (Samsa 2016, Kronenberg 2003). Manipulation of PTHrP or IHH signaling has profound ramifications for growth plate organization at the level of column formation and zonal architecture. Complicated genetic experiments have revealed that both IHH and PTHrP control the rate of chondrocyte proliferation and hypertrophy via mechanisms both independent of, and dependent on, the activities of each other. IHH promotes proliferation of early proliferating chondrocytes (Kobayashi 2002, Kobayashi 2005), and hypertrophy of maturing proliferative zone chondrocytes independently from PTHrP (Mak 2008), and is thought to be the principal activator of PTHrP expression in resting zone cells (Kronenberg 2006). Conversely, PTHrP inhibits hypertrophic differentiation independently from IHH (Chung 1998, Mau 2007), while also repressing IHH expression and activity (Mau 2007, Karp 2000, Lanske 1996). Impaired IHH signaling in vivo or cartilage explants results in loss of PTHrP expression, resulting in premature hypertrophy and loss of proliferative zone columns (St Jacque 1999, Gao 2009, Kobayashi 2002, Minina 2001). Similarly, mouse models of altered PTHrP signaling exhibit severely disorganized growth plates and defects in hypertrophy (Miao 2008, Lanske 1999, Weir 1996). What drives IHH expression in naive chondrocyte condensations is unclear; however, IHH precedes PTHrP and hypertrophic markers during growth plate morphogenesis; thus, IHH likely induces PTHrP in some cells while inducing hypertrophy in other cells, originating tissue-wide growth plate organization (Figure 1.1e-f).

Do gradients of IHH/PTHrP signaling in the growth plate affect cell organization?

The existence of long-range paracrine signaling pathways that have such importance for limb bud and growth plate development and function suggests intuitively that signaling gradients control bone growth. The observations of localized gene expression of crucial ligands (PTHrP, IHH, Wnt5a, FGF8 etc.), coupled with localized expression of paired receptors (PPR, PTC1, FGFR) have been interpreted as evidence for a gradient of signaling activity. This sort of conclusion is sometimes prematurely made, as studies detecting graded ligand-receptor interactions at the protein level in cartilage are scarce. For example, IHH is a crucial signaling ligand in cartilage known to have dose-dependent effects on cell biology *in vitro*, and its paralog SHH has been proven to cause a gradient of Gli3 processing during limb bud development. Comparing overexpression models with classic allelic series also shows genetic dose of IHH is positively correlated with growth plate length, proliferative zone column length, and PTHrP expression (Kobayashi 2005). However, although PTHrP expression is presumed to occur in response to an IHH signaling gradient in periarticular chondrocytes, a gradient of IHH protein in cartilage has not been definitively shown to extend to periarticular cells (Ma 2011, Minina 2001, Koziel 2004). This maybe caused by poor limits of detection of cartilage immunostaining, or to the existence of a secondary signaling interaction that bridges the prehypertrophic and resting zones. Second, phenomena that are known to be dose-dependent in two-dimensional culture models *in vitro,* such as IHH-dependent phosphorylation of Smo (Li 2016, reviewed in Chen 2013) have not been demonstrated to exhibit a gradient in cartilage. This is important because a gradient of IHH ligand demonstrated at the protein level does not account for the morphogen-sequestering activities of the extracellular matrix (i.e. local heterogeneity in ECM composition can repress signaling activity even in regions of high morphogen concentration, reviewed in

Yan 2009). The effect of the extracellular environment on diffusion of secreted ligands is a poorly understood topic, but a linear, one-to-one relationship between mRNA expression of any given ligand, and downstream signaling should not be assumed (Hynes 2009). Particularly, the effects of extensive growth on the interpretation of all gradients in the proximal-distal axis should be under question, given the large distances involved in continued allometric growth during puberty, relative to the presumed concentration gradients. Essentially, this means directly detecting the cell interpretation of a signal is the only way to show true signaling gradients, since upstream or downstream measures are subject to overwhelming spatiotemporal complexity.

Furthermore, in situ hybridization studies describing the expression domains of genes targeted by signaling regulation, particularly markers of growth plate maturation (PTHrP, FGFR3, BAPX, PTC1, IHH, COLX) show clearly defined boundaries that resemble discrete differentiation switches, or at least punctuated equilibria (Ahrens 2009, Romereim 2014). This suggests that ligand-receptor signaling in the growth plate depends on at least one threshold to determine morphogen presence/absence (thus specifying range), but does not necessarily imply multiple thresholds within signaling range. This primary (on/off) IHH threshold can be modulated by extracellular matrix composition as well as point mutations in IHH that affect its binding to HIP-1, but the function, let alone existence, of secondary or tertiary thresholds of IHH signaling activity in cartilage has not been explored (Gao 2009, Cortes 2009, Koziel 2004). However, it has been shown that repressive interactions between multiple morphogens can generate sharp, stepwise and on-off boundaries of gene expression from simple diffusion gradients in the nervous system development (Ashe 2006), and thus further research may identify new repressive signaling mechanisms that control cartilage zone boundary formation.

Even if the presumed IHH signaling gradient does exist in the growth plate, how does it affect the mechanism by which the IHH/PTHrP loop build cartilage architecture? Excellent work by Vortkamp's group demonstrate that the importance of IHH for growth plate development is contingent on the presence of Gli3, a transcription factor that can regulate gene expression depending on post-translational cleavage from an activator to repressor form (Koziel 2005). Double mutants of IHH/Gli3 rescue the column formation phenotype seen in single IHH mutants; thus, IHH seems to function mainly in the repression of Gli3 activity. Furthermore, PTHrP signaling via PKA/cAMP promotes Gli3 processing to repress transcription of IHH target genes, possibly including PTHrP itself (Mau 2007). This suggests that IHH does not act as a polarity cue for chondrocytes, despite a possible spatial IHH signaling gradient lengthwise along the growth plate.

If not IHH, would PTHrP signals be acting in a gradient? Theoretically, PTHrP could action independently to regulate column formation as long as transcriptional repression by Gli3 is lifted, which is consistent with an organizer-like role for resting zone cells during establishment of cartilage polarity. Interestingly, it was also discovered that overexpressing SHH (presumably activating expression of PTHrP) under a Col2a1 promoter causes orthogonally directed columns, possibly caused by the failure of chondrocyte rotation, or alternatively a total repolarization of the tissue (Tavella 2004). Similar defects were caused by PTHrP overexpression in chick (Li and Dudley, unpublished data), suggesting the importance of chondrocyte interpretation of PTHrP ligands for properly oriented column formation. Additionally, recent live imaging experiments demonstrated that proliferative zone chondrocytes within growth plate cartilage explants treated overnight with an excess dose of PTHrP fail to rearrange into columns, suggesting that PTHrP could directly impact the signaling network that controls column formation. However, whether or not a PTHrP gradient is required for column formation is still under debate, since constitutive activation of PTH1R in cartilage partially

rescues the growth and polarity defects seen in PTHrP null mice, which strongly suggests that uniform levels of cAMP/PKA signaling within cartilage are sufficient to support zone and column formation. However, intersections between the PTHrP/IHH circuit and several pathways critical for chondrocyte differentiation (FGFs, BMPs, WNT, to name a few) are still being discovered. Because the level of crosstalk in the entire signaling network that controls column formation is still unclear, excluding cooperative, multidimensional, or alternative gradients would be hasty.

Wnt5a signaling gradients may provide a cue to establish chondrocyte polarity:

Endochondral skeleton formation and bone elongation is controlled by a complex signaling network, yet many genetic models that block cartilage growth or modulate differentiation leave the mechanisms that determine proximodistal axial polarity intact (for example, some chondrocyte-specific disruptions of FGF signaling have minimal effect on column formation while still producing growth abnormalities by affecting proliferation and hypertrophy, Jacob 2006, reviewed in Lui 2014). In stark contrast, the genes that mediate non-canonical Wnt signaling and planar cell polarity signaling seem to be required for growth plate tissue and cell polarity. Human chondrodysplasias that disrupt cell polarity in cartilage have been linked to Ror2/Vangl2 (Geister 2015, Zelzer 2003, Wang 2011). Null mutations in Wnt5a, Ror2, Vangl2, and Prickle in mouse all result in failure to establish columnar chondrocyte arrangement (Schwabe 2004, Gao 2011, Liu 2014, Yang 2003). In chick, mosaic overexpression of dominant-negative or wild type Wnt5a, Fzd7, Vangl2 result in cell-autonomous disruption of cell polarity and cell shape, demonstrating a clear relationship between cartilage column formation and noncanonical Wnt signaling (Li 2009). Allelic series by Yang's group and others demonstrated genetic interactions between the Wnt5a, Ror2 and Vangl2 proteins in

mouse (Wang 2001, Gao 2011). In this study it was shown that Wnt5a protein is capable of binding Ror2 and Vangl2 receptors in mammalian cells to induce the formation of Ror2/Vangl2 protein complex, promoting dose-dependent phosphorylation of Vangl2 (Gao 2011, Yang et al 2017). Specifically, Vangl2 contains two clusters of serine/threonine phosphorylation sites on its N-terminus, some of which exist in a state of basal phosphorylation. Increased interaction with Wnt5a/Ror2 can phosphorylate the remaining residues, and bring Vangl2 to a fully activated state to promote its polarized localization on the cell membrane. Wnt5a/Ror signaling can also phosphorylate and activate Dvl. In fact, binding Ror receptors seems to account for a significant portion of Wnt5a's function, demonstrated by the exacerbated Ror2 $^{-/-}$ skeletal phenotype by concomitant Ror1 deletion (Ho 2012).

A standard readout for cell polarity is the presence of molecular or morphological asymmetries in any given cell. In early cartilage, Vangl2 was observed to localize in a planar-polarized manner along the proximodistal axis (Gao 2011). This is the earliest known sign of cell polarity in chondrocytes. Vangl2 asymmetric localization begins at 12.5 in the metacarpals (prior to column formation for this growth plate), depends on its phosphorylation downstream of Wnt5a/Ror2, and is influenced by the presence of Pk1 (Figure 1.1e). Other PCP effectors Pk1 and Dvl have been reported to localize specifically to the chondrocyte lateral edge at E14.5 in mouse (Kuss 2014). Although a comprehensive analysis of PCP protein localization across growth plates and along developmental stages has not been reported, the data agrees with several developmental contexts (drosophila, c. elegans) in which distinct membrane domains enriched for different PCP proteins confer polarity information to each cell (Vladar 2009, Rozco 2015, Axelrod 2011). Such specialized domains are maintained by positive feedback among pairs of transmembrane PCP molecules (i.e. Ror2/Vangl2) as well as stabilizing intercellular interactions, counterbalanced by lateral inhibition of separate

PCP modules (i.e. mutual inhibition of Vangl2/Pk1 within a cell). In the majority of these systems, a Wnt signaling gradient provides the first symmetry-breaking cue (Yang 2015). In E12.5 mouse embryos, Wnt5a is expressed in a graded manner along the distal mesenchyme of the limb bud while IHH/PTHrP/COLX expression remains barely detectable in this presumptive growth plate until E13.5 (Figure 1.1f). Thus it was proposed that a Wnt signaling gradient might be transduced into planar cell polarity by promoting asymmetric membrane domains during the initial stages of cartilage differentiation (Gao 2011).

Is there a continuous requirement for Wnt signaling in chondrocyte polarity?

One question critical to growth plate development *in vivo* and *in vitro* is whether the mechanisms that initially establish chondrocyte polarity are continuously responsible for providing positional cues for the duration of cartilage elongation. Later stages in development show the Wnt5a expression domain moves to the perichondrium surrounding the proliferative and prehypertrophic zones of each growth plate (Yang 2003, Hartmann 2000), raising the question of whether Wnt5a functions continuously to maintain preexisting planar cell polarity, or acts transiently to initiate a self-maintaining polarity signaling cascade in chondrocytes (Figure 1.1g). Polarized cell rearrangements underlying column formation were observed in tissue explants of cranial base growth plate cartilage lacking a perichondrium, suggesting that cell polarity can be maintained in the absence of Wnt5a signals (Romereim 2014). It was shown that SOXC genes are required for WNT5A expression, however deletion of SOXC in limb bud (Prx-Cre) but not chondrocytes (Col2a1-Cre) produced defects resembling the Wnt5a homozygous null phenotype, leaving open the possibility that WNT5A expression in the early limb bud, but not perichondrial cells, supports its primary function (Kato 2015). WNT5a deletion in perichondrial cells would be a crucial experiment to demonstrate the continued

requirement for PCP in growth plate cartilage polarity. Alternatively, inducible Col2-cre mediated deletion of Wnt5a receptors such as Ror2/Vangl2 at later time points after growth plate formation would be a fair test of this hypothesis. One study has claimed that chondrocyte column formation could be induced in vitro by addition of Wnt5a and transfection of PCP receptors, suggesting the Wnt5a pathway maintains polarity in mature chondrocytes (Randall 2012). However, the analysis used in this study does not distinguish isogenic groups (a putative characteristic of chondrocyte column formation) and cannot account for the possibility of physical cell deformation in their cell pellet culture caused by increased cell proliferation rather than acquisition of planar cell polarity via graded actions of WNT5a on the pellet. Finally, asymmetric localization of PCP effector genes was not presented in the study, leaving open the possibility that activating WNT5a encourages crosstalk with alternative cell polarity signaling modules.

What is the proper interpretation of skeletal defects in Wnt5a mutants?

There is an important distinction to be made between failed column formation phenotypes; between not differentiating to the proliferative zone (developmental delay), hypertrophying before proliferation would result in columns (developmental acceleration), and differentiating correctly to a proliferative zone that is still unable to form columns (cell polarity defect). However, the phenotype caused by disrupting PCP signaling appears to have equal importance for the limb bud development and cartilage differentiation as for chondrocyte polarity, raising the caveat that polarity defects in Wnt5a and associated receptor genes may be simply caused by abnormalities in cartilage maturation. For example, deficiencies in Wnt5a signaling lead to defects in the cell cycle, resulting in reduced cell number (Yang 2003, Yamaguchi 1999). This can be illustrated by significantly reduced phalanx size in embryos expressing dominant-

negative Ror2 (Witte 2010). Importantly, hypocellularity has been demonstrated to interfere with mesenchymal condensation, a critical step in cartilage formation (Hall 2000, Wolpert 1979). In fact, almost all of the germline and limb-bud-deleted PCP mutant mice fail to express early markers of chondrogenesis such as SOX9 at the appropriate developmental stages (Yang 2003, Yang 2013, Schwabe 2004, Gao 2011). Further, the distal phalanges are entirely missing in Wnt5a $^{-/-}$ and Ror2/Vangl2 $^{-/-}$ embryos, suggesting a delay in the development of the distal skeleton (Yamaguchi 1999, Gao 2011). Point mutations in gene Pk1, which is reported to affect growth plate organization, also causes growth and differentiation defects in the limb bud as early as E11.5 (prior to cartilage formation in the metacarpals, but after cartilage formation in the proximal limb), concomitant with greatly reduced expression of Wnt5a and Vangl2 (Yang 2013). Thus, mutations affecting Wnt5a signaling could produce crippling defects in skeletal morphogenesis even before chondrocytes would be competent to interpret Wnt5a signals.

Developmental aberration by disrupting Wnt5a signaling could also occur after cartilage formation but long before chondrocytes form columns, as both Wnt5a $^{-/-}$ and Ror2$^{-/-}$ mutations abrogated IHH expression in cartilage (Yang 2003, Schwabe 2004). Even if the cartilage maturation prompted by IHH was simply delayed in these experiments, the observed reduction in proliferation in Wnt5a$^{-/-}$ cartilage could delay chondrocyte exodus from the PTHrP signaling domain, resulting in a very large resting zone. This caveat applies to the studies that suggested a continuous requirement for noncanonical Wnt signaling in chicken growth plate polarity (Li 2009). Alternatively, Wnt5a signaling could affect column formation independently of cell polarity through suppression of canonical Wnt/beta-catenin signaling. Disruption of canonical Wnt signaling has been reported to be sufficient to disorganize the growth plate (Yuasa 2009). Wnt5a, in a context-dependent manner, either stabilizes or increases turnover of

beta-catenin (Mikels 2006). While loss of beta-catenin does not render chondrocytes unable to form columns (they are shorter, Ahrens 2011), it is possible to that deregulation of canonical Wnt signaling may phenocopy a polarity defect. Studies from chick, however, dispute this hypothesis, as overexpressing canonical Wnt inhibitors seems to have no effect on chondrocyte column formation (Li 2009). A comprehensive analysis of column formation across growth plates and developmental stages in planar cell polarity mutant mice is needed. Until then, the question of whether mature growth plates rely on Wnt5a signaling to form columns, at least in mouse, is still unclear.

MECHANICAL REGULATION OF CARTILAGE ARCHITECTURE

Diverse signaling mechanisms such as receptor-ligand binding and mechanotransduction have been shown to contribute to cartilage maturation by acting at multiple length scales, from the level of single molecules and cells to the level of bulk tissue-tissue interactions. Recently, the relative contributions of various signaling modalities across length scales and their mutual interactions are coming into focus. Particularly, the information presented here will highlight the many different types of force generating mechanisms. Later we discuss their cross-scale and intermolecular feedback, and the complex routes by which they are managed by the cell-signaling environment to generate tissue architecture.

Polarity and mechanics: common threads along skeletal development:

At each length scale, different mechanical forces from the external environment influence polarized growth and cell behavior for the proper development of every part of the musculoskeletal system. Muscle contractions, compression, torsion, and stretch are examples of organ-level forces that signal through large-scale architectural changes to

influence the long-term development of cartilage and bone (Figure 1.2a). At the tissue level, variation in the composition and remodeling of the extracellular matrix (ECM) and forces caused by bulk cellular dynamics creates a complex mechanical environment that is characterized by extensive reciprocal interaction between ECM structure and cell organization (Figure 1.2b). These interactions are founded in mechanical forces produced at the cell level, including mechanotransduction via cell-ECM adhesion, cell-cell adhesion, and cytoskeletal dynamics (Figure 1.2c). Together, cell-level forces orchestrate polarized cell behavior such as oriented cell division, cell migration, cell shape changes, and the creation of a structured ECM. Thus, the signaling mechanisms that govern cell- and tissue- scale polarity cooperate with cell and tissue mechanics to generate the polarized growth of each mature bone in the limb skeleton. In this section, the force-producing modules that are thought to play important roles in forming the logic of cartilage organization and growth will be introduced. Discussion will focus on the role of mechanotransduction from the interactions between individual cells to the contributions of tissue-wide and tissue-extrinsic forces during the formation of growth plate cartilage architecture.

Cell level forces: integrins, cadherins, cytoskeleton, and cilia

Most cells use cell-surface receptors called integrins to transfer mechanical stimuli to and from the external environment. Chondrocytes express several integrin receptor subtypes (β1, β3, β5, α1, α2, α5, αV, α6, α10) that form heterodimers to bind the various collagen, fibronectin, laminin and minor proteins of the cartilage ECM. The cell-matrix interactions mediated by β1 integrin complexes are incredibly important for cartilage growth, because mutations in ITGβ1 and integrin-linked kinase (ILK) both result in chondrodysplasia (Aszodi 2003, Bengtsson 2004, Grashof 2003, Kyostila 2013,

Enomoto-Iwamoto 1997). Of the alpha subunits only ITGα10$^{-/-}$ can, to a certain extent, reproduce the phenotype of ITGβ1$^{-/-}$ cartilage indicating that chondrocytes are particularly reliant on adhesion to collagen. In these mutant conditions, several disturbances are noted within cartilage. First, loss of integrin function completely abolished cell polarity and the ability for chondrocytes to form columns. Second, the mutations disrupted the actin cytoskeleton, resulting in punctate organization of the cortex compared to the even distribution of the actin network in wild-type controls. Third, integrin deficient chondrocytes showed G2/M defects due to failed cytokinesis. In many cell types, cytokinesis depends on adhesive forces as well as contractile forces of the cleavage furrow, suggesting that to produce stereotypical cartilage tissue architecture, chondrocytes rely on forces produced cooperatively among the actin cytoskeleton, the integrin adhesion complexes, and the cartilage ECM.

Recently, a novel time-lapse imaging assay of live murine growth plate cartilage explants has provided fundamental insight into the cellular processes underlying cartilage architecture and growth by demonstrating a requirement for cell-cell adhesion (Romereim 2014). Live imaging revealed that the chondrocyte division plane is always arranged perpendicular to the long axis of the mother cell body, so that daughter cells sit laterally adjacent. This is in accordance with Hertwig's rule, that division plane assumes the minimum possible distance across daughter cells. Following cell division, instead of immediately separating, daughter chondrocytes form a tight association rich in putative cell-cell adhesion complex proteins such as cadherins and beta-catenin. The daughter cell adhesion interface then rotates 90 degrees in the span of 4-5 hours until it is perpendicular with the primary growth axis, thereby stacking the chondrocytes into a column. By contrast, cells in the resting zone and chondrocytes in culture are capable of forming adhesion surfaces following cell division, but are not observed to rotate. This corroborates previous work in chicken showing that chondrocyte columns are clonal, and

that the initial division plane is randomly oriented in the resting zone but non-randomly oriented in the proliferative zone (Li 2009). Further, correct rotation in resting-proliferative transitioning cells occurred independent of cell shape (Romereim 2014). Importantly in this study, disruption of intercellular adhesion by inhibiting cadherin-cadherin binding halts rotation of the daughter cell interface, demonstrating that chondrocyte rearrangement depends on cell-cell in addition to cell-matrix adhesive interactions.

The above findings provide a theoretical framework to dissect the local mechanisms promoting tissue architecture, leading to the following question: how does a pair of daughter chondrocytes coordinate adhesion dynamics on two distinct cell surfaces to achieve collective movement? One classic explanation is called “differential adhesion” and has roots in the self-organizing properties of surfactants (Manning 2010). Soap bubbles that are in contact with each other minimize free energy by maximizing the surface area of their shared interface (Besson 2007). According to the “differential adhesion” hypothesis, the adhesive forces are balanced between cell-cell and cell-ECM surfaces under static conditions, but increases in adhesive force favor expansion of the stronger interface, resulting in rearrangement (McMillen 2015). Since the amount of cadherin-cadherin *trans* dimerization determines the adhesive forces connecting two cells, regulation of cadherin enrichment at the daughter cell interface could cause breakage of existing integrin-matrix bonds to result in interface expansion, leaving the daughter cells in a lower energy state post-rotation (Chen 2005, Zhang 2009).

The above model does not account for the actions of alternative force-generating mechanisms available to the chondrocyte, such as the actin, microtubule, or intermediate filament networks. In fact, modern perspectives derived from “differential adhesion” now recognize the cooperative nature of adhesive and cytoskeletal forces. Cell-patterning phenomena that were originally thought to derive from differences in

cadherin adhesion were later demonstrated to be potentiated by surface tension produced by actomyosin, such as self-sorting in cell aggregates from different germ layers (Lecuit 2015). In cartilage, electron micrographs of the adhesion surface in rotating daughter cells show formation of nanoscale protrusions at the interface periphery that resemble lamellopodia (Romereim 2014b). Further, actin organization is altered in B1 integrin mutant chondrocytes (Aszodi 2003). Actin networks are capable of self-regulating the connectivity, elasticity, flow, and turnover of individual components to control cell movements and shape change, and are extremely sensitive to upstream signaling cues (Banerjee 2017). Thus, despite experimental challenges caused by the coupling of cytokinesis with cell rotation, cytoskeletal forces could be an important part of the column formation mechanism by generating protrusive and/or tensile forces on the cadherin- and integrin- adhesion surfaces.

In the growth plate, the primary cilium has received attention as a way chondrocytes transduce various mechanical and chemical cues from the extracellular environment (Serra 2008). The primary cilium is a non-motile, microtubule-based organelle on the surface of most cells including chondrocytes and mesenchymal cells of the limb bud mesenchyme (Satir 2010). Intraflagellar transport (IFT) proteins bring hundreds of proteins to the primary cilia including acetylated tubulin, which is used as a cilia marker (Yuan 2016). Originally hypothesized to be vestigial, and to sense the centriole, it is now known that this structure is mainly used as a cellular sensory mechanism (Satir 2010). While enriched with cellular receptors to transduce chemical cues, the primary cilium can sense physical cues by bending in response to mechanical stimulation such as fluid flow, shear stress, and hydrostatic pressure, which leads to activation of intracellular signaling and transcriptional responses (Yuan 2016). Mutations in IFT genes can result in the loss of cilia formation, causing skeletal disorders known as ciliopathies. Many of these disorders have ramifications for the limb bud, often affect

chondrocyte differentiation in the growth plate and are associated with altered HH and WNT signaling, resulting in cartilage mechanical instability (Ross 2005). Specifically, the chondrocyte response to externally applied tensile strain depends on activation of IHH signaling and downstream ECM metabolism that depends on the presence of the primary cilia (Shao 2012). Polydactyly is a common consequence of abnormal primary cilium, consistent with defects in digit patterning during limb bud growth (Haycraft 2006). Primary cilium seems able to regulate the actin cytoskeleton as well as microtubule network, as primary cilium assembly affected the amount and organization of stress fibers produced by chondrocytes in culture and in vivo, leading to changes in cell shape and cortical tension (McGlashan 2007, Rais 2015). Some groups have used the primary cilium to assess chondrocyte polarity, because proliferative zone chondrocytes have the shortest cilia and orient them parallel to the longitudinal axis of the growing bone, and conditions that alter cell polarity result in random orientation of primary cilium. Accordingly, primary cilia have been proposed by some to play a role in cartilage polarity (de Andrea 2010). However, inspection of cartilage histology in *Col2a1cre-IFT80*$^{f/f}$, *Tg737*^{orpk}, and *Col2a1cre-KIF3A*$^{f/f}$ mutants, shows little effect on column formation at birth, despite the total loss of primary cilia (Mcglashan 2007, Song 2007, Koyama 2007, Haycraft 2006). Interestingly, in the absence of primary cilia, the postnatal growth plate cartilage becomes gradually more disorganized over time (Song 2007). Whether this is due to the compromised mechanosensory mechanisms in proliferative chondrocytes, or a loss of PTHrP/IHH regulation remains unknown. Thus, while signaling by the primary cilia is probably not related to the network that establishes chondrocyte polarity, it is possible that cilia-mediated signaling contributes to maintenance of chondrocyte polarity.

Transduction of cell-extrinsic and tissue-wide forces: roles of extracellular matrix:

Cartilage is composed of distinct populations of chondrocytes that are spatially segregated into zones based on their differentiation state. Each zone of chondrocytes produces a unique extracellular matrix with distinct morphology and mechanical properties. One reasonable hypothesis is that ECM with locally variant composition could produce bifurcations in cell mechanics at the level of membrane domains (cell polarization), cell population domains (tissue polarization), or both. That is to say, structural anisotropies within cartilage could act as global or local cues to promote cell polarity and tissue growth.

Zone-specific variation in mechanical stiffness and compressive force has been demonstrated in the developing cartilage. Computational modeling results suggest that chondrocytes near the reserve/proliferative zone border are subjected to combinations of high compressive hydrostatic stresses that vary as a function of position within the tissue (Gao 2016). Finite element analysis showed that compressive force is conducive to endochondral ossification, in contrast to tensile force, which promotes fibrocartilage formation. In general, many labs have found the resting zone to be stiffer than the proliferating and hypertrophic zones by bulk mechanical testing (reviewed in Villemure, 2009). Others completed an analysis of rabbit and porcine growth plates that revealed a steady increase of ECM stiffness as a function of position throughout cartilage maturation (Radakrishnan, 2004). Porcine growth plate stiffness also increases until 4 weeks of age (Wosu 2010). Extracellular matrix stiffness was also shown by atomic force microscopy to increase with cartilage maturation in mouse embryos (Prein 2016). Zone-specific differences in ECM stiffness are likely to result from dynamic regulation of ECM deposition and remodeling, illustrated by the marked increase of pericellular/territorial ECM, interterritorial ECM, and fibrillar collagen mass per cell in

lower hypertrophic versus upper proliferative zone cartilage (Noonan 1998). Thus, either increased or decreased matrix stiffness and mechanical compression are associated with the transition from non-column-forming resting zone cells to column-forming proliferative zone chondrocytes.

Anisotropic mechanical properties of the cartilage matrix have also been demonstrated in the proliferative zone. Orientation of collagen fibrils is biased towards the mediolateral axis in the pericellular matrix surrounding every cell, while collagen residing in the interterritorial matrix surrounding each column/chondron is polarized along the proximodistal axis during early and postnatal cartilage development (Godwin 2016, Prein 2016). Furthermore, the interterritorial matrix is shown to be much stiffer than pericellular matrix in proliferative zone chondrocytes (Prein 2016). Thus, an asymmetric mechanical environment exists around each column of chondrocytes that could potentially differentially resist movement, resulting in consistency in the direction of daughter cell rotation. In 1974, Gould proposed a simple explanation for cylindrical shape of growth cartilage in chick based on differential matrix deposition leading to differential compression along the proximodistal axis. Ten years later, it was demonstrated that certain compositions of collagen/fibronectin ECM could drive translocation of cells or even polystyrene-latex beads from regions of low fibronectin concentration to regions of high fibronectin concentration by a process that did not depend on diffusion, convection, or electrostatic distribution effects, providing proof of concept that anisotropies in the cartilage matrix could promote column formation (Newman 1985, Loganathan 2016).

Genetic studies have clearly demonstrated the importance of the extracellular matrix for cartilage organization, chondrocyte polarity, and formation of cell columns in the proliferative zone. Integrin-mediated cell-matrix interactions are thought to participate in mechanotransduction between chondrocytes and the ECM that depend not only on

the presence of matrix components, but also on the organization in which secreted molecules form the supramolecular ECM network. Genetic disruption of almost any component of the cartilage extracellular matrix results in tissue architecture defects. So far, the list of matrix genes necessary for column formation includes Col2a1, Col9, Col11, Aggrecan, Glypican 4, Hyaluronic acid, Fibrillin 1, Matrilin (Blumbach 2008, Dreier 2008, Gustafsson 2000, Matsumoto 2009, Jeong 2014, Rogers 2007, Li 2001). Collagen II is specifically well studied, as a number of point mutations have been generated that each affect cartilage growth in various ways (Arita 2002, Hering 2014, Ritvaniemi 1995, Korkko 1993, Maddox 1997). Interestingly, processing of pro-collagen into helical fibrils seems to have an effect on column formation, as pro-collagen surrounds every resting chondrocyte but demarcates chondrons in the proliferative zone, and mutations that disrupt pro-collagen organization also disrupt column formation (Patra 2014). Chondrocytes seem to require cell-collagen binding interactions, because alpha 10 beta 1 integrin heterodimers recognize and bind collagen II (Reviewed in Plow 2000). Further, many of the aforementioned ECM genes affect the fibril formation and network organization of Collagen II, particularly Col9, Col11, Fibrillin, and Matrilin (Brachvogel 2012, Budde 2005, Posey 2008, Gustafsson 2000, Huang 1999). These studies show Collagen 9 is actually required for the maintenance of the structure of Collagen 2 fibrils, so it seems that collagen structure feeds back to cell structure and shape (potentially due to the relationship between molecular structure and stiffness), even if ECM structure is a downstream consequence of cell organization. Accordingly, $Col2a1^{-/-}$ chondrocytes have been reported to exhibit normal cell polarity and shape very early in cartilage development, but fail to maintain proper tissue architecture (Raducanu 2009). Thus, feedback between chondrocyte polarity and cartilage biomechanics is likely to play a role during tissue growth.

Why is the cartilage ECM so important for column formation and growth? One simple answer is that ECM is a crucial component of chondrocyte biology, influencing a wide range of cellular processes including cell differentiation, proliferation, and survival. Many of these processes are integrin-dependent and can affect tissue architecture, which adds complexity to the question of the ECM's role in cartilage growth. For example, mechanotransduction from the ECM could affect the PTHrP cartilage signaling domain, as PTHrP gene expression is stretch-sensitive (Chen 2005, Torday 2002), and B1-integrin dependent cell-ECM interactions are required for normal levels of cell proliferation (Aszodi 2003).

In addition to signaling to cells through integrin and other adhesion receptors, the ECM can also regulate cartilage growth and tissue architecture through adhesion-independent mechanisms. Matrix constituents regulate the biochemical landscape at the level of morphogen availability to shape signaling gradients in cartilage. For example, the matrix protein Fibrillin binds and sequesters TGFB to control its diffusion (Reviewed in Hynes 2009). Defects in bone growth arise from altered TGFB signaling in Marfan's syndrome, which is caused by loss-of-function mutations in Fibrillin (Judge 2005). Moreover, the major collagen in cartilage, collagen II, controls the diffusion of secreted BMP2 and TFGB1 in early cartilage via its ligand-binding VWC domain (Zhu 1999). This interaction is developmentally regulated, as mature chondrocytes splice collagen II pre-transcripts to omit the VWC domain (Hynes 2009). This ligand-sequestering domain can release growth factors upon interactions with matrix metalloproteinases (MMPs), making TGB1 and BMP2 immediately available to chondrocytes. Competitive ligand binding is a feature of many cartilage ECM components such as Laminin, which also contains EGF domains that can activate signaling upon degradation (Swindle 2006, Prieto 1992). In addition to a role in ligand sequestration, many ECM components such as heparin sulfate and chondroitin sulfate are used as cofactors to activate receptor signaling

(Hynes 2009). For example, zebrafish mutants of chondroitin sulfate proteoglycan-synthesizing enzymes accelerate chondrocyte differentiation via FGF, BMP and IHH pathways (Eames 2011). Thus, the ECM can concentrate or limit growth factors to particular sides of the cell to maintain polarity by controlling spatial availability of signaling factors, which contributes to the establishment of morphogen gradients, and thus could guide cell polarity in both chemical and mechanical fashion.

One example from the limb bud mesenchyme illustrates how cell-matrix interactions can be used to alter the signaling environment. Using specialized cellular filopodia-like projections called cytonemes, cells exchange signaling proteins and transmit mechanical tension across cells at the tissue level (Kornberg 2014). Cytonemes stretch several cell diameters to provide SHH and WNT signals from the cytoplasm to responding cells, thus regulating the availability of morphogens in the growing limb bud mesenchyme (Sanders 2013). The outgrowth of cytonemes through the collagen matrix is dependent on the actin cytoskeleton and has shown to require planar cell polarity signaling in Drosophila (Huang 2016). Cytoneme-mediated signaling requires integrin adhesion and heparin sulfate proteoglycans (Huang 2016). Therefore, by influencing the outgrowth and signal transduction of cytoneme projections in the early limb bud, the ECM potentially shapes the SHH and WNT signaling gradients to control cell fate determination and growth (Stanganello 2014, Umulis 2013, Hadjivasiliou 2016).

Tissue-extrinsic forces: muscle and gravity, in and after the womb

We have outlined basic mechanical modules at the cell and tissue level that can affect cartilage growth. However, cartilage is an open system, subject to a wide range of external mechanical stimuli during embryonic and postnatal development. In particular the extent to which musculature-derived stresses are important for bone growth and

structural properties has been controversial. It is known that developing bones are subject to increasing stress caused by muscular forces. However, the claim that muscle-derived force transmission influences the cell polarity and organization of chondrocytes in the growth plate lacks a definitive body of evidence.

First, the effects of weight bearing on bone growth seem to be minimal. Spaceflight does not reduce growth in growing rat bones (Spengler 1983). Alternative methods of gravitational unloading versus single (1N) and double gravitational loading (2N) have no effect on rat hind limb length, although unloading is associated with decreased total bone mass, reduced bone mineral density, external bend of the shaft and rotation of the distal tibia (Van der Meulen 1995, Ohira 2006). Even artificial systems to deliver large, non-physiological compressive forces to the limb have very subtle effects on growth, but are commonly cited to describe the importance of external mechanotransduction on bone length (Kozhemyakina 2015). Dynamic axial loading was shown to suppress growth proportional to load, yet this suppression recovered after 1 week except at highest loads (17N) (Ohashi 2002, Duke 1999). Centrifugation of rats (2N to 4N) was reported to inhibit bone growth, yet this study did not report control for potential endocrine responses and trauma-induced behavioral effects such as reduced feeding compared to non-centrifuged rats (Vico 1999). Therefore, the fact that cartilage responds to large compressive forces may not be relevant to normal bone growth aside from disease models.

Furthermore, the data surrounding the role of muscle-derived forces in bone length has remained ambiguous for decades. Neuromuscular blocking reagents in chick show growth defects that appear to affect geometric scaling on the organ scale rather than cell polarity or tissue architecture, although differences in bone collar formation were observed (Hall 1990, Nowlan 2008, reviewed in Shea 2015). These studies revealed that IHH and ColX expression patterns were altered compared to untreated

control, reflecting a developmental delay rather than a tissue polarity defect. Further, the effects of these agents on overall chondrocyte proliferation, total extracellular matrix production, or their effects in organotypic bone culture were never assessed. Species-specific peculiarities are also possible, as much of the information surrounding the effects of neuromuscular disruption on bone growth in mammalian systems suggests the view that cartilage growth is somewhat mechanically autonomous. Human patients with immobilizing neuromuscular defects develop characteristic growth plate patterning and ultimately produce skeletons of normal proportions and size. Application of oligohydramnios to rat fetus produces no significant reductions in final bone length (Palacios 1992). In MDG null mice lacking muscle contractions, abnormal joint cavitation was observed, and periosteal bone formation (circumferential growth) was reduced due to effects on osteoblast number, but long bone length remained unaffected (Sharir 2011). This suggests that muscle-derived mechanical forces may influence the shape of the cortical bone after cartilage growth has occurred to influence cross-sectional bone geometry to optimize the skeletal element for load bearing, but does not explain column formation or allometric cartilage growth. In fact, muscle-less MyoD and SpD mutant mice, femur and tibia were shortened by 10% of the total length compared to controls, and long bones of the forelimb were not significantly shortened (Shwartz 2011, Shwartz 2013). The mutant mice formed morphologically normal columns in the growth plate cartilage, even if column size is somewhat altered. However, absence of musculature did not affect cell organization in the mandibular cartilage of zebrafish (Schwartz 2012). Therefore, while cartilage elongation may still require tissue-wide compressive or tensile stress, mechanical stimuli derived from the musculature probably has a minor impact on the processes that originally generate growth vectors.

However, tissue-extrinsic forces still play an important role in skeletal development and patterning. Perichondrium stripping induces cartilage overgrowth, and

thus it has been argued to inhibit cartilage growth via compression (although a caveat to this observation would be the effects of perichondrium removal on paracrine signaling) (Warell 1979, Lynch 1987). Joint cell progenitor fate for specification of joint formation and cavitation was found to rely on tissue-extrinsic mechanical loading, and it was proposed that beta-catenin acted as a molecular sensor to transduce muscle-derived forces (Kahn 2009). Bone formation correlates with muscular contractions as determined by FE analysis (Roddy 2011). During fracture regeneration, bone realigns by forming an ectopic, bidirectional growth plate that can fuse bone fragments via endochondral ossification (Rot 2014). This mode of regeneration requires muscular mechanotransduction, but the mechanisms of regulatory muscle-bone crosstalk in this situation remain unclear. Thus, muscle contractions do appear to be crucial for a suite of morphogenetic processes during skeletal development and can even influence endochondral ossification during healing, but subtle growth defects indicates that presence of the musculature plays a minor role in bone elongation, and cannot be viewed as a polarizing cue for cartilage tissue architecture.

Tissue-extrinsic forces also appear to play important roles before cartilage forms, during growth of the limb bud. The AER is an epithelial layer, which stratifies based on cell intercalation. Recently, it was proposed that dorsal-ventral anisotropic tissue tension caused by growth of the mesoderm orients remodeling of the limb bud ectoderm by driving cell intercalation processes to result in the formation of the AER (Lau 2015). Much like the growing cartilage, cell division in the AER progenitors precipitates neighbor exchange in the remodeling ectoderm in a process that uses actin and beta-catenin mediated cell-cell adhesion (Conte 2016). In this example, the physical outcomes of mesenchyme growth further participate in shaping the cell organization of the growing tissue. This can also be seen during chondrogenic specification in the limb bud, where increased cell adhesion via cadherins and NCAM molecules are thought to

cause the presumptive cartilage to separate from the surrounding mesenchyme and form a coherent oval-shaped condensation. Bulk mechanical stretching can disrupt that process, which can inhibit cartilage differentiation through an integrin-dependent mechanosensory process that increases formation of actin stress fibers (Onodera 2005).

Mechanotransduction at the chondrocyte level, as well as extrinsic forces acting on cartilage, have distinct influences on chondrocyte behavior and cartilage growth. Ultimately, both mechanical stimuli and biochemical signaling factors are probably integrated in the overall regulatory mechanisms that govern chondrocyte behavior. Investigating the regulation of gene products that are known to produce force, such as the mechanochemical motor proteins of the cytoskeleton, may help peel back the initial layers of complexity at the intersection of these signaling modalities. In the next chapter, the potential role of chondrocyte cytoskeletal dynamics during column formation is investigated. Actomyosin is identified as a candidate molecular tool that could link daughter cell behaviors with reception of signaling cues from the external environment.

CHAPTER 2: CYTOSKELETAL DYNAMICS UNDERLIE GROWTH PLATE CARTILAGE MORPHOGENESIS

INTRODUCTION

During skeletal development, the long bones of the vertebrate limb achieve optimal structure by maximizing elongation while restraining oppositional thickening (Hamburger & Hamilton 1951, Kaufman 1992, Summerbell 1981). Bone morphogenesis is driven primarily by the growth plate cartilage, in which chondrocytes produce a three-dimensional environment that determines cell signaling, cell shape, rates of cell proliferation, and extracellular matrix (ECM) deposition to control the progressive maturation and lengthening of cartilage tissue until it is replaced by bone (Kronenberg 2003, Kozhemyakina 2015, van der Eerden 2003). During endochondral ossification, growth plate chondrocytes become organized into zones of differentiation that each function uniquely to control growth (Dodds 1930). The least mature resting zone near the articular surface serves as a reservoir of progenitor cells dispersed in a collagen II matrix (Abad 2002). Long-range paracrine signaling across zones drives proximal resting zone cells to be recruited into a transient proliferative phase marked by discoid cell shape, upregulation of cell cycle, and columnar arrangement of cells (Kronenberg 2003). Further differentiation of columnar proliferative zone chondrocytes causes hypertrophy, where cell enlargement and increased matrix deposition effectively elongates the tissue before ossification.

The extent of longitudinal hypertrophic growth in cartilage is the major determinant of bone length, and is potentiated by the extent of columnar cell organization, which specifies the primary growth vector (Breur 1991, Cooper 2013, Romereim 2011). Column formation in the proliferative zone is crucial for skeletal morphogenesis, and this has been demonstrated in several vertebrates including man (Geister and Camper 2015). Genetic studies have identified key regulators of cartilage tissue architecture, such as planar cell polarity (PCP) signaling via Wnt5a and Ror2 (Li

2009, Gao 2011, Liu 2014, Wang 2011, Schwabe 2004), a PTHrP-IHH signaling feedback loop (Vortkamp 1996, Weir 1996, Kronenberg 1997, Miao 2008), cell adhesion via B1 integrin (Aszodi 2003, Kyöstilä 2013, Terpstra 2003, Bengtsson 2005), and various constituents of the cartilage ECM (Fernandes 2007, Ritvaniemi 1995, Jeong 2014, Li 2001, Thur 2001, Rodgers 2007, Wiweger 2011). However, while the regulation of bone growth by such signaling networks has been well studied, the physical and molecular mechanisms that govern the organization of chondrocytes into columns remain unclear.

Our recent work using time-lapse imaging of live growth plate cartilage explants demonstrated that column-forming daughter cells become laterally displaced by mitosis, and intercalate by using a dynamically spreading cell-cell adhesion surface that rotates 90 degrees, leaving daughter cells stacked in the direction of the growth axis (Romereim 2014). Importantly, cadherin function is required for cell rearrangement, supporting a model in which relative strengths of adhesion, or surface tension, between the daughter cell interface and cell-matrix associations drive rotation and thus promote column formation. One prediction of this model is that the surface with greater tension will be enriched for some force-generating mechanism during cell intercalation. Although tools needed to carry out in vivo mechanical testing of intracellular forces have not been optimized for a living growth plate, it is possible using microscopy-based techniques to track the cytoskeletal dynamics that are the primary means of managing cellular forces.

To investigate the role of cytoskeletal dynamics during rotation, we determined the spatiotemporal relationships among the actomyosin contractile apparatus and cell adhesion surfaces. We report myosin activity is excluded from the daughter cell interface during column formation, instead accumulating at cell-matrix associations near the daughter cell junction. Furthermore, myosin-ECM domains are associated with rearrangement, as non-column forming cells in the resting zone, as well as in column-

deficient mutant mice, show reduced myosin localization at chondrocyte-matrix associations. Finally, we demonstrate a regulatory link between planar cell polarity and myosin localization in vivo. Our data suggests that signaling networks mediate differences between cell-cell and cell-matrix interactions by regulating the position of cellular actomyosin contractility to promote chondrocyte column formation and skeletal morphogenesis.

RESULTS

Nanoscale protrusions observed in rearranging chondrocytes:

Previous work using time-lapse imaging of live cartilage explants led to the model that following chondrocyte division, daughter cells form a cadherin-based adhesion surface that dynamically spread to drive proliferative zone column formation. In this model, differences in adhesion force or surface tension between the cadherin and integrin surfaces would be sufficient to drive cell rotation. This model seemed attractive compared to an active migration model, since by submicron resolution of confocal fluorescence microscopy the daughter cell interface appeared to be a smooth, straight line that lacked a leading edge (Romereim 2014). However, analysis of cranial base growth plate cartilage using improved electron microscopy techniques revealed that in fact rotating chondrocytes display nanoscale protrusions that resemble actin-based lamellopodia at the leading edge of migrating cells (Appendix 2.1). ARP2/3 is widely recognized to promote branching actin polymerization at lamellopodia. Analysis of the protrusions after disruption of ARP2/3 complex function by a small-molecule inhibitor suggests they could be related to the actin cytoskeleton, since electron micrographs of the treated cranial bases revealed protrusions were blunted or collapsed upon inhibition

of actin branching, concomitant with loss of cadherin adhesion at the interface periphery. Further, there was a dose-dependent inhibition of chondrocyte rearrangement with cells displaying substantially delayed and slightly disoriented rotation at a lower dose of the inhibitor and almost complete inhibition of cell rearrangement at a higher dose (Appendix 2.2). These results support the notion that branched polymerization of the actin network could drive chondrocyte rearrangement in concert with cell adhesion at the daughter cell interface, but whether other types of actin dynamics such as contractility were involved was unclear.

A screen of myosin protein localization in growth plate cartilage:

To address this question, we sought to identify several reliable markers of daughter cell adhesion and cellular contractility in growth plate cartilage. We performed immunofluorescence assay on histological sections using antibodies recognizing components of the cadherin adhesion complex as well as several myosins. Cadherins, beta-catenin, p120 catenin, myosin 2b, myosin 2c, and phosphorylated myosin 2 light chain (pMLCII) all showed specific membrane localization in nearly all chondrocytes, respectively (Figure 2.1). Myosin 2a showed specific localization to the Golgi, consistent with previous reports, and thus was not selected for further analysis (Petrosyan 2012). For all other epitopes, equivalent immunolocalization was observed among adhesion molecules, as well as among myosins, in all columnar chondrocytes analyzed.

Previous live-imaging analysis of column formation determined three major steps to column formation. 1) Cell division and formation of cadherin interface between daughter cells, 2) Rotation of the adhesion surface resulting in stacked daughter cells, and 3) Separation of daughter cells caused by *de novo* matrix secretion. Because remodeling of cell-cell junctions is often associated with regulation of actomyosin, we hypothesized that during column formation, a non-random relationship

Figure 2.1: Surveying cadherin adhesion complex proteins and myosin isoforms in growth plate cartilage. Immunolocalization of cadherins using a pan-cadherin antibody (A), beta-catenin (B), p120-catenin (C), phosphorylated myosin light chain S19 (D), myosin 2c (E), myosin 2b (F), and myosin 2a (G) in daughter cell pairs in the proliferative zone that already completed rotation. Nuclear staining by DAPI is shown in blue. Scale bar = 5 um. Each localization pattern was observed in nearly all daughter cell pairs examined (over 100 proliferative zone chondrocyte pairs from at least 2 biological replicates).

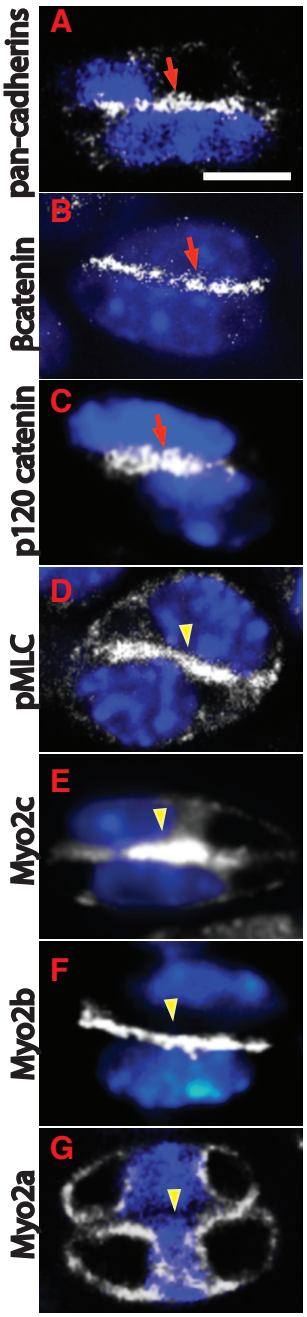
A
pan-cadherins
B
βcatenin
C
p120 catenin
D
pMLC
E
Myo2c
F
Myo2b
G
Myo2a

existed between cell adhesion and myosin activation. To test this hypothesis in vivo, we exploited the fact that a single tissue section of embryonic cartilage contains on average 200 daughter cell pairs exhibiting all three stages of column formation. We noted that throughout all stages of column formation, immunofluorescence probing for beta catenin and plasma membrane-targeted GFP equivalently labels interstitial surfaces between daughter cells (Appendix, 2.3). From this information, we were able to infer that a gap in the center of the beta-catenin interface constitutes dividing cells, and shortening of the beta-catenin interface is evidence of true cell separation. Therefore, using beta catenin as a marker for cadherin cell-cell adhesion, and Myo2b/pMLC2 as markers for potential generation of tension by the actomyosin contractile apparatus, we analyzed Z-stacked, tiled images of double-labeled cartilage to test the relationship between cadherin adhesion and myosin localization throughout the dynamic process of column formation.

Analysis of cytokinesis-associated adhesion dynamics:

Dividing cells were first identified by the appearance of a myosin-enriched cleavage furrow (Figure 2.2, arrowheads). In these cells, size of the contractile ring indicated progression through cytokinesis. Close inspection of dividing cells along the z-plane revealed that an enrichment of beta-catenin was always observed between the ingressing cleavage furrow and the periphery of the surface connecting the dividing daughter chondrocytes. Furthermore, nearly all cells with a discontinuous adhesion interface show myosin specifically localized to the gap between cell-cell adhesion domains, regardless of the zone or myosin isoform analyzed. This indicates that the cadherin adhesion interface forms progressively throughout cytokinesis from the outside inwards towards the midbody (Figure 2.2 arrows).

Figure 2.2: Daughter cell adhesion interface forms during cleavage furrow ingression. Schematic of daughter cells undergoing cytokinesis is shown in (A). Green dotted lines represent optical sections captured in the z-plane. Representative images of dividing cells stained for phosphorylated myosin light chain (pMLC, yellow arrowheads) and Myosin 2B (Myo2b, yellow arrowheads) in (B) and (C), respectively. Selected planes (1-3um spacing) from z-stack images are shown to illustrate the structure of the cleavage furrow (shown in a schematic in A) marked by Myosin 2b (D, yellow arrowheads) and phosphorylated myosin light chain (E, yellow arrowheads). Note that beta-catenin-enriched adhesion domains adjacent to the cleavage furrow at the cell periphery (B'-D', red arrows). Nuclear staining by DAPI is shown in blue. Scale bar = 5 um. N.S = distribution of localization patterns between zones and between epitopes not significantly different by chi-squared test (cells pooled from 5 biological replicates, for pMLC comparison n > 75 cells from each zone, for Myo2b comparison n > 25 cells from each zone)

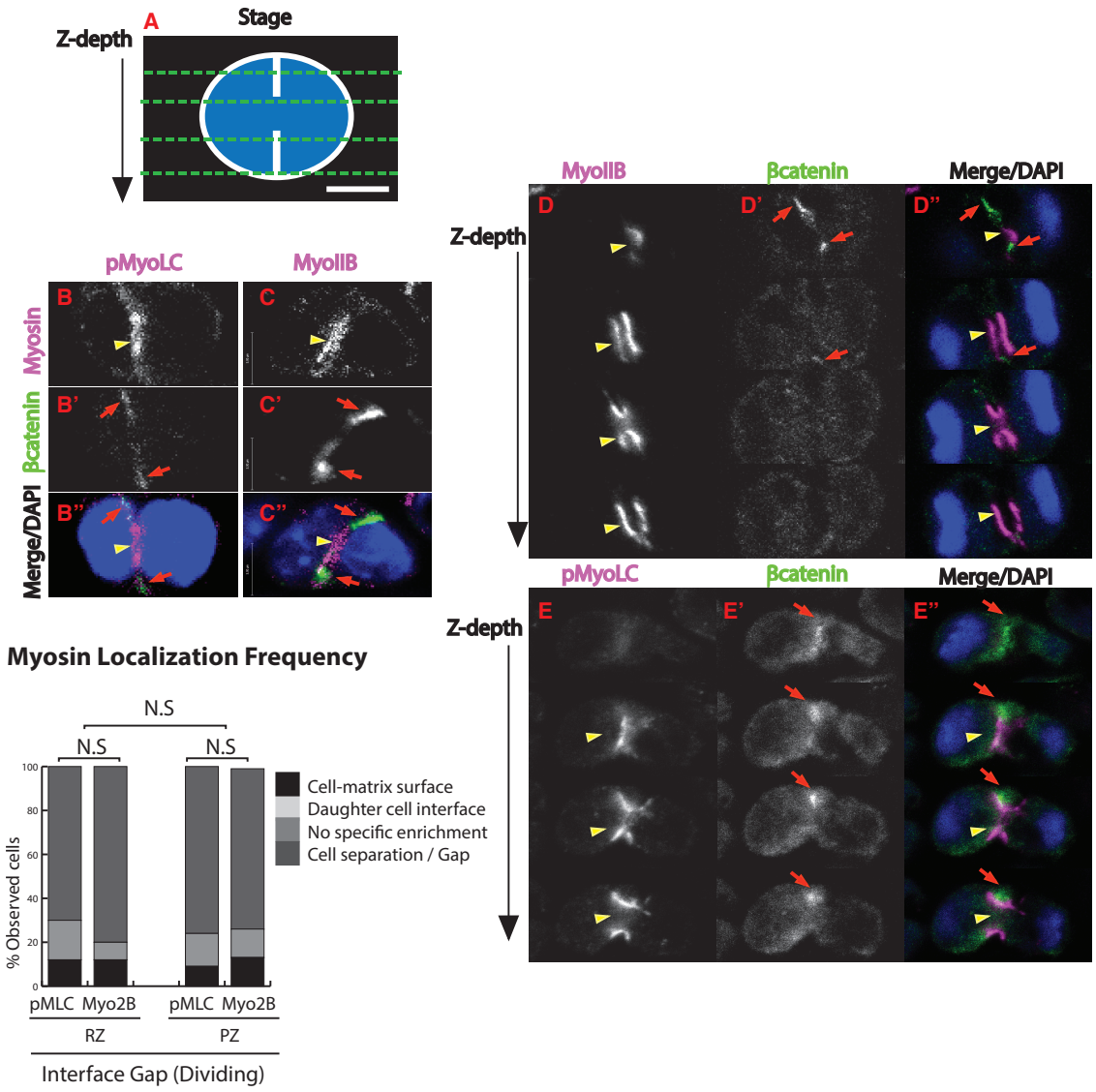
A
Stage
Z-depth
pMyoLC
MyoIIB
Myosin
βcatenin
Merge/DAPI
B
B'
B''
C
C'
C''
MyoIIB
βcatenin
Merge/DAPI
Z-depth
D
D'
D''
pMyoLC
βcatenin
Merge/DAPI
Z-depth
E
E'
E''
Myosin Localization Frequency
N.S
N.S
N.S
% Observed cells
100
80
60
40
20
0
Cell-matrix surface
Daughter cell interface
No specific enrichment
Cell separation / Gap
pMLC
Myo2B
pMLC
Myo2B
RZ
PZ
Interface Gap (Dividing)

Determining myosin localization patterns associated with rotating chondrocytes:

We next identified chondrocytes that appeared to be actively forming columns by rotation. To do this, we segregated daughter cells in the proliferative zone that were fully connected by beta-catenin surfaces into separate classes based on the angle of the interface relative to the primary growth vector (vertical, rotating, horizontal), and recorded the predominant localization of myosin in each daughter cell pair. A large majority of observed rotating cells exhibited myosin enriched solely at regions of cell-matrix associations (75%, Figure 2.3), often concentrated around the edges of the beta-catenin interface. The remaining minority of daughter cell pairs showed myosin localization either at the cell-cell surface, ubiquitous membrane localization of myosin, or very weak staining. This was true for both Myo2B and pMLC, indicating that total myosin, as well as myosin activity, are both excluded from sites of cadherin adhesion during column formation. Compared to actively rotating cells, there was significantly reduced mutual exclusion between myosin activity and cadherin adhesion in cells with interfaces parallel to the growth axis (vertical interfaces found prior to rotation, Figure 2.3), and cells with interfaces perpendicular to the growth axis (horizontal interfaces after having completed rotation, Figure 2.3), although these groups also predominantly excluded myosin from the beta-catenin surface. Because the resting zone of growth plate cartilage does not form columns, we reasoned that if actomyosin contractility functioned to promote column formation, there would exist an observable difference in either the localization or phosphorylation of myosin when comparing total populations of resting and proliferative zone chondrocytes (Figure 2.3). We analyzed the myosin activity patterns of resting zone daughter cell pairs that expressed complete cadherin adhesion surfaces and compared that data against the total proliferative zone dataset. We found that the majority of resting cells evenly distribute myosin around all cell surfaces including the beta-catenin interface. The portion of cells showing myosin

activity at cell matrix borders was lower than in the proliferative zone (Fig 5M), indicating that actomyosin contractility at the cell-matrix border is reduced in resting zone daughter cells compared to column-forming cells. Importantly, both myosin 2b and pMLC staining patterns were different across zones indicating a general shift in myosin localization rather than specific differences in myosin phosphorylation among daughter cells (Fig 2.3 E and I versus G and K). Together, this data suggests that myosin activity at the cell-matrix border could be part of the mechanism that enables cells to rotate into columns.

Myosin supplants the separating cadherin interface:

After rotation, separation of the daughter cell membranes is accompanied by disengagement of the cadherin adhesion surface and therefore loss of the beta-catenin label. We analyzed daughter cells with partial beta-catenin labels (<75% of the interface) and/or obvious disruptions in the cell-cell interface to determine predominant myosin patterns. Nearly every separating cell pair was observed to have strong enrichment of Myo2b and pMLC at nascent separations caused by regional losses of daughter cell adhesion (Figure 2.4 a, d, j, Appendix 2.4). In 20% of cells, enrichment at separations was accompanied by additional myosin signal at alternate sites along the cell membrane (Figure 2.4, Appendix 2.4). Interestingly, a large portion of cells were observed that maintained a myosin-enriched surface facing the most recent sister cell, even after the cell-cell adhesion surface had completely disengaged (Figure 2.4 e, k). Chondrocytes without an obvious most recent sister cell were almost always observed to distribute myosin in “arcs” along the lateral edges of the cell where membrane curvature is greatest (Figure 2.4 f, l).

Figure 2.3. Myosin activity localizes to cell-matrix borders during daughter chondrocyte rotation. Localization is shown for phospho-myosin light chain S19 (pMLC, yellow arrowheads, E-H) and Myosin 2B (Myo2B, yellow arrowheads, I-L) in resting zone (E, I) and proliferative zone daughter cell pairs prior to (F, J), during (G, K) and following (H, L) rearrangement. Percentage of cells observed expressing myosin activity at cell-matrix associations versus cell-cell associations, for each zone (M) and each given position of the cadherin cell-cell adhesion interface during rotation (N) marked by beta-catenin (red arrowheads). Nuclear staining by DAPI is shown in blue. Scale bar = 5 um. Statistical significance determined by chi-squared test (n = 228 resting zone cell pairs, 64 “beginning rotation”, 203 “actively rotating”, and 150 “completed rotation” proliferative zone cell pairs).

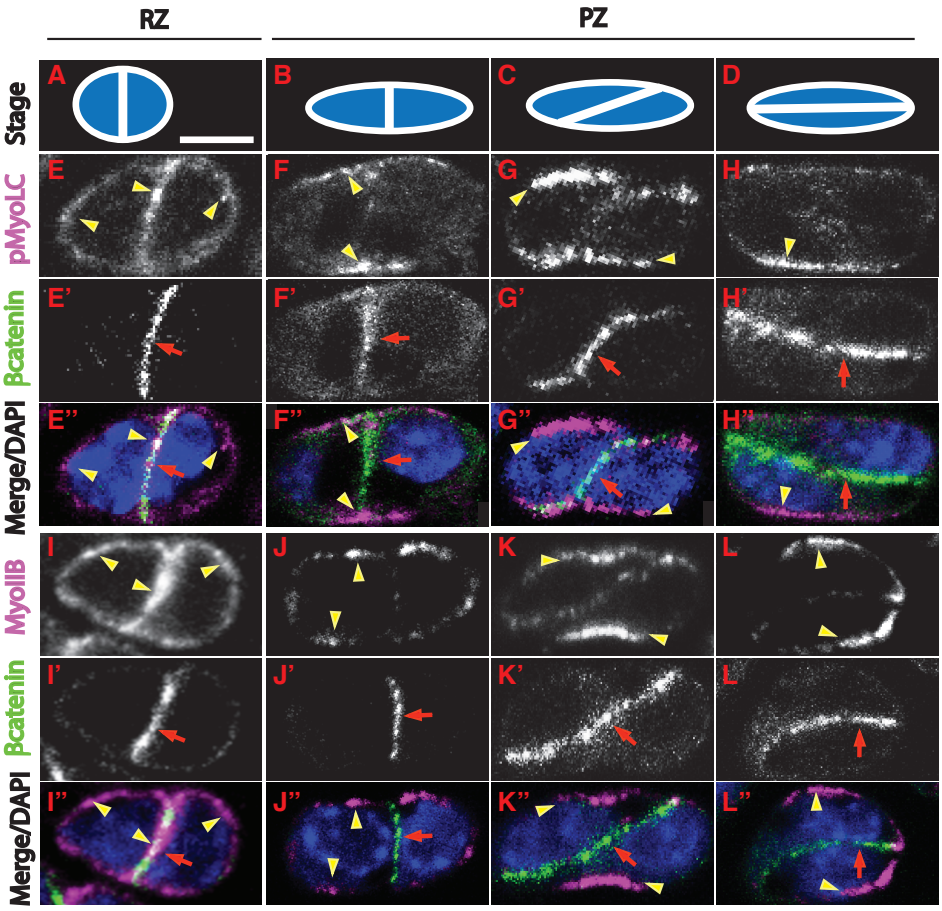

pMLC Localization Frequency

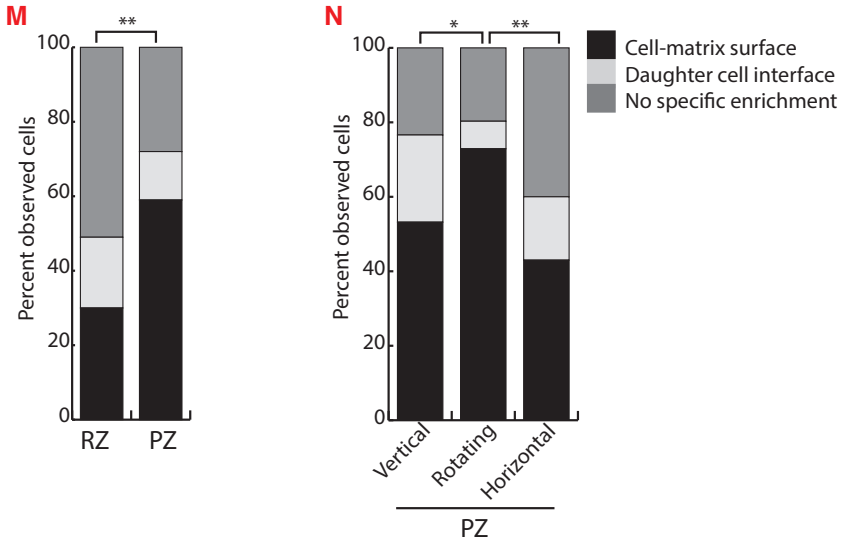

Figure 2.4: Myosin is activated at nascent cell separations.

Immunolocalization of phosphorylated myosin light chain (pMLC, yellow arrowheads) in proliferative zone (D-F) and resting zone (J-L) daughter cells that are disengaging, detected by apparent shortening (A, G) and eventual loss (E, H) of the beta-catenin-rich adhesion interface (red arrows). Myosin localization for actively separating cell pairs is summed over the entire population and represented as a stacked bar chart. As chondrocytes become more distant from sister cells, myosin activity becomes redistributed away from the prior cadherin interface (F, L). Nuclear staining by DAPI is shown in blue. Scale bar = 5 um. N.S = not statistically significant by chi-squared tests (for pMLC, n= 342 proliferative zone cell pairs, 252 resting zone cell pairs; for Myo2b, n= 118 proliferative zone cell pairs, 64 resting zone cell pairs, pooled from 5 biological replicates). Images of completely separated cells are representative of the two major observed patterns that account for nearly all single cells observed from 5 biological replicates.

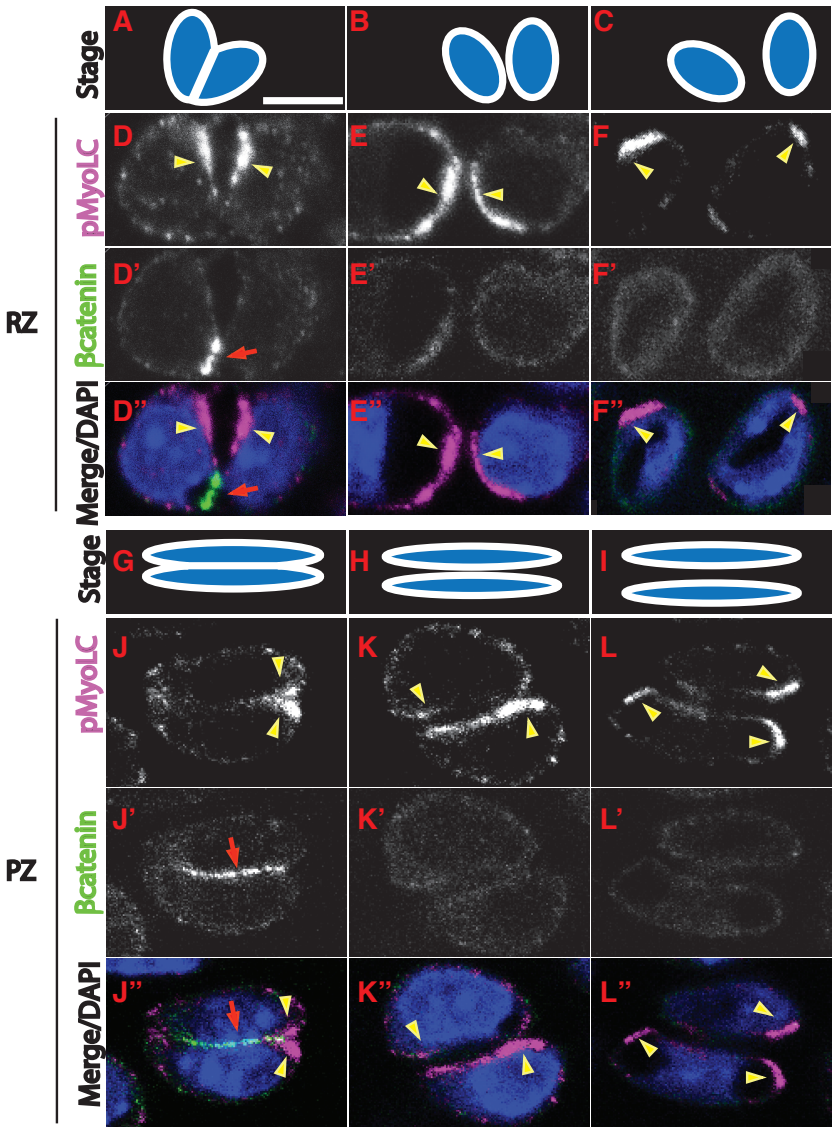
Stage
A
B
C
RZ
pMyoLC
D
E
F
βcatenin
D'
E'
F'
Merge/DAPI
D''
E''
F''
Stage
G
H
I
PZ
pMyoLC
J
K
L
βcatenin
J'
K'
L'
Merge/DAPI
J''
K''
L''

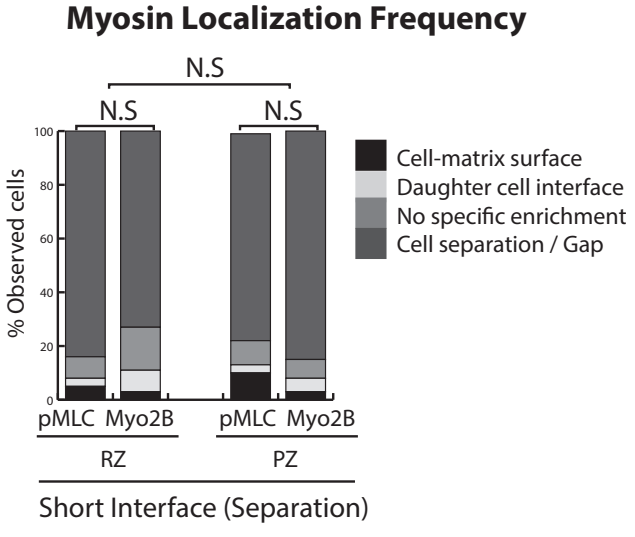
Myosin Localization Frequency
N.S
N.S
N.S
% Observed cells
100
80
60
40
20
0
Cell-matrix surface
Daughter cell interface
No specific enrichment
Cell separation / Gap
pMLC
Myo2B
pMLC
Myo2B
RZ
PZ
Short Interface (Separation)

Separating cell pairs showed the same myosin localization distribution regardless of the myosin (pMLC or 2B) or zone being analyzed (Appendix, 2.3). Thus, myosin localization at the cell-extracellular matrix interface is highly correlated with separating, and rotating, cells. Strong cortical localization of activated myosin at the cell-matrix surface suggested a connection between cell contractility and integrin activity. We explored the possibility that myosin was being recruited to regions of integrin adhesion by treating cartilage explants in culture with soluble arginine-glycine-aspartate (RGD) peptide to broadly inhibit cell-matrix binding, using RGE peptides as an inactive control treatment. In these cartilage cultures, the number of daughter cell pairs was reduced. However, in some RGD-treated daughter cells, myosin 2b localization completely redistributed to the cell-cell interface (Figure 2.5a), which was not observed in RGE-treated cultures (Figure 2.5B). This observation is consistent with a functional connection between integrin-matrix binding and myosin localization.

The previous experiments indicated that the signaling networks that control column formation might regulate cytoskeletal organization. The planar cell polarity (PCP) signaling network is a major regulator of growth plate cartilage architecture (Li 2009). Mice lacking either the ligand Wnt5a, or co-receptor Ror2 develop extreme skeletal defects, lack proliferative zone columns, and show disrupted cell polarity and shape (Gao 2011). We hypothesized myosin activity in growth plate chondrocytes is influenced by PCP signaling *in vivo*. To test the hypothesis, we generated Wnt5a and Ror2 null mice and analyzed the patterns of myosin localization in mutant embryonic cartilage. Strikingly, the majority of PCP-signaling deficient daughter cell pairs displayed extensive co-localization between the beta-catenin, and pMLC/Myo2b at the cell-cell adhesion surface (Figure 2.6 E-L and Appendix 2.5). PCP-deficient mutant cartilage exhibited a significantly different myosin localization profiles as compared to the matrix-restricted myosin within wild-type proliferative zone cells and randomly distributed myosin within

resting zone cells (Figure 2.6, Appendix 2.5). A subset of myosin protein appeared to be affected as many cells still expressed limited CMA-domains in addition to the predominating CCA-domains. Notably, some myosin/beta-catenin co-localization was also observed in dividing and separating cells, although there did not appear to be a defect in the contractile ring, or in the accumulation of active myosin at the prior interface during cell separation. Together, this data suggests that polarity signaling influences myosin localization in daughter chondrocytes during column formation.

DISCUSSION

Cytoskeletal dynamics are associated with column formation.

Vertebrate limb growth and morphogenesis result from the actions of a complex tissue-wide signaling network on chondrocyte cytoarchitecture. Earlier studies elucidated many of the genes and long-range signaling interactions that were required for column formation, but the local processes driving cell organization are unclear. In particular, the role of cytoskeletal dynamics, which is crucial for other directed cell behaviors such as cell migration, cell sorting, and convergent extension of epithelial tissue (reviewed in Lecuit 2011, Parsons 2010), is unknown within the context of growing cartilage. In this study, electron microscopy demonstrated the existence of nanoscale, branched actin polymerization-dependent protrusions at the periphery of the cell-cell interface during column formation.

Figure 2.5. Myosin localization is disrupted by inhibition of integrin binding. Immunolocalization of myosin 2B (Myo2B, yellow arrowheads) in daughter cell pairs after the cell-cell adhesion interface has matured in embryonic growth plate cartilage treated in culture with RGD peptide (X) or RGE inactive control (). Cadherin adhesions are labeled using antibody specific to beta catenin (red arrows). Nuclear staining by DAPI is shown in blue. Scale bar = 5 um. Images representative of 28 cells for each condition pooled from 2 biological replicates.

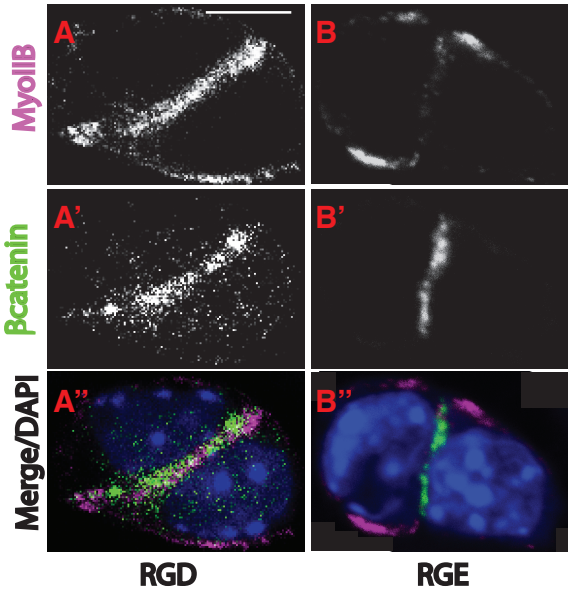
A
B
MyoIIB
A'
B'
Bcatenin
A''
B''
Merge/DAPI
RGD
RGE

Figure 2.6. Myosin activity is mislocalized in planar cell polarity signaling deficient cartilage. Immunolocalization of phosphorylated myosin light chain S19 (pMLC, yellow arrowheads) in daughter cell pairs during cytokinesis (E, I) after the cell-cell adhesion interface has matured (F, J), during separation (G, K) and after complete separation (H, L) in embryonic growth plate cartilage from Wnt5a (E-H) and Ror2 (I-L) mutant mice. Cadherin adhesions are labeled using antibody specific to beta catenin (red arrows). Percentage of cells observed expressing myosin activity at cell-matrix associations versus cell-cell associations is tabulated in the stacked bar chart below. Nuclear staining by DAPI is shown in blue. Scale bar = 5 um. Statistical significance compared to wild-type datasets from Figure 2.3 determined by chi-squared test (n = 70 Ror2 mutant daughter cell pairs, 62 Wnt5a mutant daughter cell pairs, each pooled from 3 mutants).

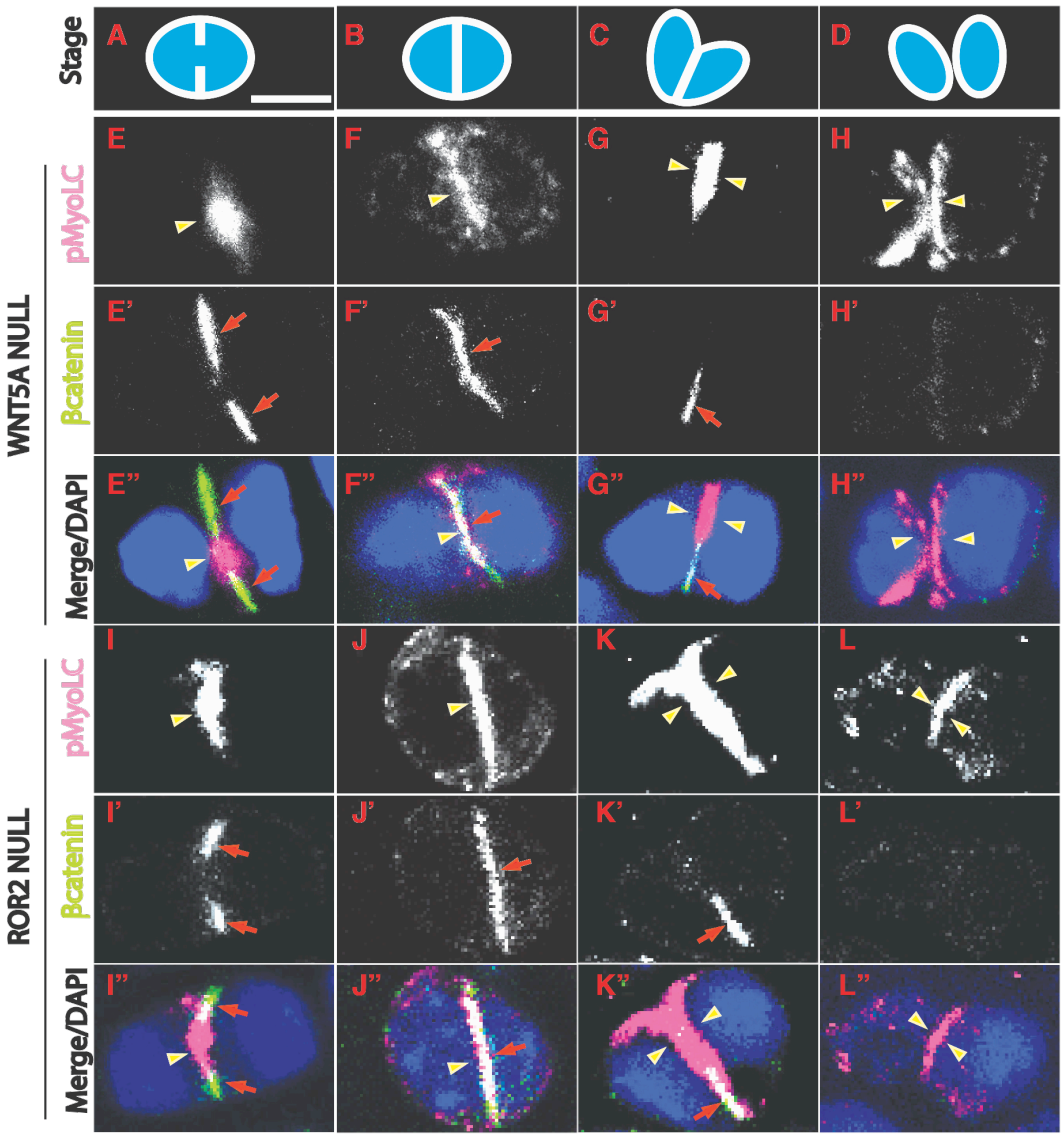
Stage
A
B
C
D
WNT5A NULL
pMyoLC
βcatenin
Merge/DAPI
E
F
G
H
E'
F'
G'
H'
E''
F''
G''
H''
ROR2 NULL
pMyoLC
βcatenin
Merge/DAPI
I
J
K
L
I'
J'
K'
L'
I''
J''
K''
L''

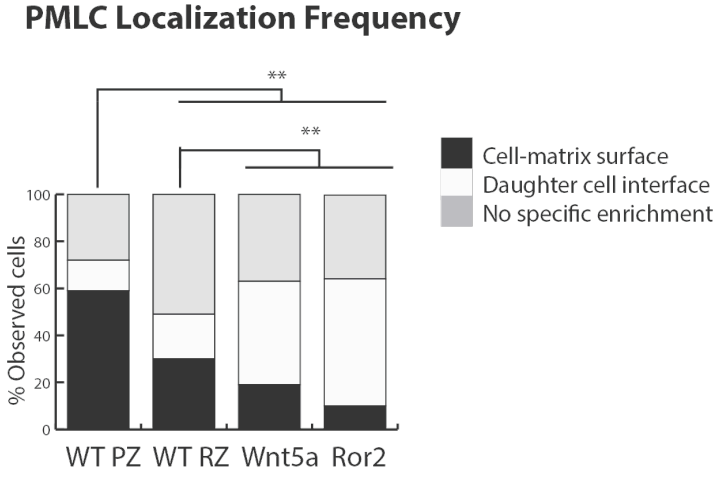
PMLC Localization Frequency
**
**
Cell-matrix surface
Daughter cell interface
No specific enrichment
% Observed cells
100
80
60
40
20
0
WT PZ
WT RZ
Wnt5a
Ror2

Time-lapse imaging assay of column formation in growth plate cartilage explants, which previously demonstrated daughter chondrocytes use a dynamic cadherin-dependent adhesion surface to rotate into columns, were here used to demonstrate a requirement for ARP2/3 complex function during column formation. Electron microscopy of ARP2/3 inhibited explants suggested nanoscale protrusions as well as peripheral cell adhesion were disrupted, implying a possible relationship between ARP2/3-mediated actin dynamics and cadherin adhesion during movement of the cell-cell interface, as in many other tissues (Romereim 2014, Verma 2004).

Previous studies also introduced an important marker of column formation, beta-catenin (Romereim 2014). This marker enabled the current study to investigate the role of actomyosin in cell rotation by inferring the dynamic progression of column formation using detailed analysis of histological sections, which was previously impossible. To accomplish this, we tracked the localization of total and phosphorylated non-muscle myosin 2 during the stages of division, rotation, and separation. Using this approach we present data that suggests preferential recruitment of myosin to cell-matrix surfaces and/or exclusion from the cadherin junction during and after cell rotation. Conversely, conditions that prohibit column formation, such as the resting zone of the growth plate cartilage, and mutant cartilage defective in planar cell polarity signaling, fail to exclude myosin from the cadherin interface in daughter cell pairs, highlighting a potentially important role for regulation of myosin localization during chondrocyte rearrangement. One limitation of the study is that because these experiments are mostly correlative, the observed myosin localization patterns may be a downstream effect, rather than a causal factor, in the mechanism that produces cell rearrangement. To demonstrate a requirement for myosin function during rearrangement will be challenging, but may be possible by performing live cell imaging after precisely-timed blebbistatin treatments in cell-cycle synchronized cartilage explants.

How could myosin function to promote column formation?

Non-muscle myosin 2 typically functions in a complex with actin, and is not yet recognized to exhibit actin-independent functions. A role for myosin in column formation would require actin binding, which was not specifically measured but is likely for three reasons. First, we visualized specific staining of Myo2b and pMLC at the contractile ring in dividing cells, a structure that is known to require actin in all mammalian cells. Second, the use of actin-binding labels such as phalloidin in growth plate cartilage reveals ubiquitous expression of actin at the cell membrane in all chondrocytes (Li 2011, Aszodi 2003), so co-localization between these proteins is inevitable. Third, phosphorylation of myosin promotes the formation of actomyosin complexes via actin binding.

Based on its known activities, functional actomyosin could influence cytoskeletal architecture by either crosslinking actin filaments to generate tension, or by using motor function to generate cytoskeletal flow (Laevsky 2003, Levayer 2013, Ma 2012, Martin 2009, Murrell 2015). Which of these functions, if any, are utilized during column formation remains an open question. Since cadherin adhesion and B1 integrin protein are both required for cell rearrangement (Aszodi 2003, Romereim 2014), the finding that myosin activity localizes to the cell-matrix adhesion surface during rearrangement is consistent with a model in which actomyosin dynamics at cell-matrix adhesions promotes column formation. Although truly distinguishing between myosin localized to integrin surfaces versus the protrusions found at the periphery of the cell-cell interface is difficult at the resolution of confocal microscopy, disrupted integrin-matrix coupling led to an apparent defect in myosin localization. This finding favors the idea that actomyosin could interact with integrin adhesion complexes during rotation. Thus, one prediction is that ILK and ITGB1 mutant cartilage should similarly fail to recruit myosin to cell-matrix

adhesions (Aszodi 2003, Terpstra 2003), which may be partially responsible for the chondrodysplasia-like phenotypes in these animals.

How does the daughter cell interface function to promote rotation?

Although cadherin function is required for cell rotation, our data does not support the idea that cell-cell junctions produce cytoskeletal tension during this process. Rather, the proposed model by Aszodi et al from 2003 is probably correct to assume a primary role for integrin adhesion surfaces as a driver of cell rotation. However, in their model, integrins were proposed to hold the daughter cells together by binding a thin layer of interstitial extracellular matrix. By contrast, our data indicates that only after cell rotation does the daughter chondrocyte cadherin adhesion interface separate and thus becomes replaced by a *de novo* myosin-enriched cell-matrix interface. One simplistic explanation is that the cell-cell junction holds cells together to coordinate rates of movement, as occurs during collective migration of cell ensembles (Haeger 2015). Alternatively, because inhibiting branched actin polymerization led to disrupted cell adhesion at the interface periphery, cadherins may cooperate with ARP2/3 and/or WAVE complexes during rotation (Verma 2004). However, it is still an open question whether entire cells or only the cell-cell junctions physically move during rotation, which will be a key piece of information in determining the role of cadherins.

Planar cell polarity signaling regulates actomyosin patterns during column formation.

Wnt signaling, through both beta-catenin dependent and beta-catenin independent networks, plays a pivotal role in the growth and morphogenesis of various tissues including growth plate cartilage (Mak 2006, Yang 2003, Tamamura 2005, Olivia 2003). While the canonical Wnt/beta-catenin pathway mainly regulates chondrocyte differentiation, studies in chick and mouse models have demonstrated that noncanonical

ligand Wnt5a and associated receptors (Ror2, Vangl2, Fzd7) mediate planar cell polarity in chondrocytes, which is crucial for column formation (Li and Dudley 2009, Gao 2011). Although much is known about PCP signaling in simple model systems such as fly, the mechanism downstream of Wnt5a that promotes polarized cellular rearrangements in vertebrate cartilage remains to be elucidated (Goehring and Grill 2013, Yang and Mlodzik 2015). Our discovery that total and phosphorylated myosin localize to the daughter chondrocyte interface in PCP-deficient cartilage suggests a model in which noncanonical Wnt5a signaling through Ror2 influence myosin localization in daughter chondrocytes to promote cell rearrangement. Such a model is in agreement with studies of melanoma cell migration, in which Wnt5a stimulates polarized recruitment of actin and myosin II to the cell periphery in a process requiring Rab4-mediated endosomal trafficking (Witze 2008). However, the large fraction of Wnt5a mutant cells lacking any pMLC staining suggests Wnt5a could also promote myosin activation. One possible intermediate of PCP-induced myosin activation would be the Rho family of GTPases. RhoA and associated kinase ROCK are commonly found to be downstream mediators of noncanonical Wnt/PCP signaling, and are putative regulators of myosin contractility (Winter 2011). Alternatively, the similarities in myosin patterns among PCP-deficient mutant cartilage and RGD-treated cartilage offer the possibility that Wnt5a signaling may influence myosin indirectly by regulating the amount or activity of adhesion receptors such as integrins, at the chondrocyte cell surface. Indeed, Wnt-PCP stimulates collagen-dependent focal adhesion dynamics in migrating cells (Matsumoto 2010), and is required for cell adhesion to fibronectin during zebrafish gastrulation (Dohn 2013). Overall, the complex feedback among chondrocyte adhesion surfaces and cytoskeletal organization will require rigorous genetic and real-time testing to determine the direct effects of Wnt5a signal transduction during column formation.

CONCLUSION

The current study utilized histological analysis of an in vivo mouse model to investigate the relationship between cadherin cell adhesion and force generation via the actomyosin contractile apparatus. We found that myosin is more likely to be interacting with extracellular matrix adhesion molecules during cell rotation, and that control of the cellular contractile machinery via the planar cell polarity signaling network seems to be an important part of the mechanism for chondrocyte column formation. We propose a model in which signaling networks cooperatively guide the localization and activity of cytoskeletal and adhesion proteins that drive chondrocyte rotation and promote the cartilage elongation so crucial for vertebrate skeletal morphogenesis.

MATERIALS AND METHODS

Mice

Mice harboring either the tdTomato reporter allele [Gt(ROSA)26Sortm4(ACTB-tdTomato,-EGFP)Luo/J; Jackson Laboratories] (Muzumdar ., 2007) or col2a1::creERT [FVB-Tg(Col2a1-cre/ERT)KA3Smac/J; Jackson] (Feil ., 1997; Nakamura ., 2006) were maintained on a Swiss Webster background (Jackson). For clonal analysis, female mice homozygous for the Td reporter allele were mated with homozygous col2a1::creERT males. Wnt5a$^{+/-}$ mutant mice (Jackson) were incrossed to produce homozygous mutants for analysis. To derive Ror$^{-/-}$;Td;Cre mice, Ror2$^{fl/-}$ mice were generated by germ line recombination of Ror2$^{fl/fl}$ conditional mutant mice (B6;129S4-Ror2$^{tm1.1Meg/J}$, Jackson) with Prm-Cre [129S/SV-Tg(Prm-cre)58Og/J, Jackson] and subsequent outcrossing to Td;col2a1::creERT mice. For all matings, noon on the day of the postcoital plug was

designated as embryonic day (E) 0.5. Pregnant females were injected intraperitoneally with one 2 mg dose of tamoxifen (20 mg/ml in 90% corn oil, 10% ethanol) on E12 to generate a pulse of cre activity in a mosaic pattern to switch reporter allele expression from tdTomato to myristoylated eGFP. All procedures performed on animals were consistent with regulatory agency policies and were approved by the Institutional Care and Use Committee at University of Nebraska Medical Center.

Histology and Immunofluorescence

On embryonic day E17, long bones were harvested, fixed in 4% paraformaldehyde in PBS overnight at 4°C, and embedded for cryosectioning or paraffin sectioning as previously described (Ahrens and Dudley, 2011). Immunofluorescence was performed as described (Ahrens and Dudley, 2011), with the following pretreatments: autofluorescence quenching in 0.25% ammonia/70% ethanol for one hour; 2 mg/ml hyaluronidase in 100 mM NaCl, 10 mM sodium acetate, pH 5.6, 0.1% Triton X-100 at 37°C for 30 min; antigen retrieval in boiling 10 mM sodium citrate; and permeabilization in 0.5% Triton X-100/PBS for 20 min. Primary antibodies were diluted in 2% HISS in TBST at the following ratios: Myosin 2a (1:500, Cell Signaling), Myosin 2b (1:500, Cell Signaling), Myosin 2c (1:500, Cell Signaling), phosphorylated myosin 2 light chain (1:50, Cell Signaling), alpha-catenin (1:100), beta-catenin (1:250, BD), p120 catenin (1:100), pan-cadherins (1:500, Sigma). After secondary antibody incubation, slides were mounted in ProLong Gold plus DAPI, and imaged the next day.

Confocal Microscopy

Imaging of slides was performed using a Zeiss 710 laser scanning confocal microscope with an oil-immersion 63X objective. 3-6 optical sections (line averaging of 8, scan speed

of 8, and typical resolution of 1024×1024) were collected at 1.5-μm intervals. To capture entire tissue sections, multi-channel z-stacks were tiled with 10% overlap and stitched into single TIFF files. Images were then exported from ZEN 2010 acquisition software and imported into Volocity 3D (Perkin Elmer) for analysis.

Image analysis, cell classification.

Resting and proliferative zones of growth plate cartilage were distinguished for individual analysis by the stereotypical arrangement of proliferative zone cells into columns. Each zone was screened for daughter cells that expressed an adhesion interface (strong enrichment of beta-catenin between cells). Daughter cell pairs with fully convex geometry and BCAT interfaces that spanned 90-100% of the shared outline were classified as having a “full interface”. Proliferative zone daughter cells with full interfaces were further subdivided into classes “0-9 degrees”, “10-79 degrees”, or “80-90 degrees”, by calculating the relative angle of the interface with the long axis of shared daughter cell outline. Significant gaps in the interface (greater than 20% of the beta-catenin signal missing between daughter cells), or regions of concavity in the shared outline caused by incomplete cell-cell association, signified the class “cell separation”. Daughter cell pairs with separations occurring exclusively in the middle of the interface were given a unique class “separation in middle”. After categorizing each daughter cell pair based on the adhesion surface morphology, myosin localization relative to the interface and cell bodies was described (for example, “associated with the matrix near the edges of the interface”, “a single dot in the middle of the interface”, “arcs concentrated around the lateral edges of the cell body”, “mostly cytoplasmic”, “no bias along the plasma membrane”). Cells with the same description were tallied, and relative preeminence of myosin patterns among any given adhesion class was calculated by dividing each count

by total number of cells in that class. Statistically significant differences in pattern abundance among experimental groups of a given class were determined using a Pearson's Chi-squared test (* $p < 0.01$, ** $p < 0.001$).

Explant Cultures

Neonatal mice at postnatal day (P) 1-4 (with P0 being the day of birth) were euthanized and cranial bases including a small amount of attached bone were rapidly harvested into PBS then transferred into cartilage culture media: MEM alpha medium without Phenol Red (Invitrogen, 41061-029) supplemented with 50 µg/ml penicillinstreptomycin-glutamine (Invitrogen, 10378-016), 10 mM β-glycerophosphate, 50 µg/ml ascorbic acid and 10 nM β-mercaptoethanol. All cartilage explants were maintained briefly in a passively humidified incubator at 37°C and 8% CO2, then explants were embedded in 1% agarose in a LabTek 35 mm glass-bottom culture dish and an 18•18 mm glass coverslip was gently placed on top. After gelation, 5 ml of medium was added to the dish and the culture was equilibrated to the microscope environmental chamber. For the ARP2/3 inhibitor-treated cranial bases, the media added to the culture dish contained either 1.5µM or 2µM ARP2/3 inhibitor (EMD Millipore, 89135-652). For RGD and RGE peptide treated cultures (Sigma-Aldrich, 99896-85-2), peptides were solubilized in PBS, and diluted into media at a concentration of 1mM. Explants were treated overnight.

Confocal Imaging Setup and Image Acquisition

Ex vivo imaging was performed using a Zeiss 710 laser scanning confocal microscope equipped with a 37°C heated chamber and a stage-mounted Pecon environmental control system (passive humidity, 37°C, 8% CO2). Optical sections (line averaging of 2, scan speed of 4 or 5, and typical resolution of 1024•1024) were collected at 1.8 µm

intervals for between 15 and 25 sections (total depth of 30-40 μm) every30 min forupto24 h with manual focus adjustments and occasional increases in z-stack size to compensate for thermal fluctuations and tissue growth. For some experiments, image tiling with 10% overlap and subsequent stitching of adjacent images was performed to visualize a greater area of the explant.

Live Image Processing, Quantification and Biostatistics

Volocity by Perkin Elmer was used to remove noise and assemble z-stacks into movies of 3D reconstructions. Cell shape/size measurements were performed with manual assignment of points in Volocity for distance and angle measurement. The division angle was defined with respect to a horizontal 0° defined to be perpendicular to the long axis of surrounding columns. The final orientation angle was measured with respect to that same 0° horizontal, with clockwise movement decreasing the angle and counterclockwise movement increasing the angle. The raw angle data was plotted as circular histograms using Oriana version 4 software (Kovach Computing Services).

Transmission Electron Microscopy Analysis

Cranial base cartilage was harvested from neonatal mice at P3. The tissue was fixed in a modified Karnovsky's fixative containing 2.5% glutaraldehyde, 2% paraformaldehyde, 0.1 M sodium cacodylate and 0.7% (w/v) safranin O (R. Wilson ., 2010). The addition of Safranin O served to preserve the proteoglycan network of the pericellular matrix, which proved to be crucial in maintaining proper cell morphology. Samples were then post-fixed with 1% osmium tetroxide for 1 h, dehydrated, and embedded in Araldite resin (Electron Microscopy Sciences). Thick sections (1 μm) were taken in order to identify regions of interest within the tissue. Once identified, thin sections (100 nm) were

collected on tri-slotted, carbon-coated Formvar grids (Ted Pella) and incubated at 65°C overnight to promote section adherence. Thin sections were contrast stained with 2% uranyl acetate and Reynold's lead citrate. Imaging was performed on a FEITecnai G2 Spirit transmission electron microscope equipped with a LAB6 crystal operating at an accelerating voltage of 80 kV.

CHAPTER 3: A TUNABLE, THREE-DIMENSIONAL *IN VITRO* CULTURE MODEL OF GROWTH PLATE CARTILAGE USING ALGINATE HYDROGEL SCAFFOLDS

Published in Tissue Engineering Part A. January 2018, 24(1-2): 94-105.

INTRODUCTION

During embryonic and postnatal skeletal development, the shape and length of bones is determined by the activities of the growth plate cartilage. Growth plate cartilage promotes elongation of long bones via regulation of chondrocyte maturation that is reflected in morphologically and functionally unique cellular domains (van der Eerden 2003). Toward the distal (epiphyseal) end resides the resting (or reserve) zone composed of the least mature chondrocytes (Kozhemyakina 2015). These resting zone chondrocytes are progressively recruited into the proliferative zone, where cell cycle activation and changes in cell morphology and cell organization result in expansion of isogenic columns of chondrocytes along the axis of growth (Romereim 2014). As columns lengthen, chondrocytes at the proximal (metaphyseal) end of the column withdraw from the cell cycle and increase in volume (hypertrophy) in two steps that are characteristic of the prehypertrophic and the hypertrophic chondrocytes (Tsang 2015, Kronenberg 2003). Growth is generated from chondrocyte hypertrophy through increased cell mass and deposition of specialized matrix (Pacifici 1990). Hypertrophic chondrocytes are subsequently replaced by bone through the process of endochondral ossification (Mackie 2011). Thus, continuous growth over the two-decade span of human development requires tight coordination between cell production in the resting and proliferative zones, and cartilage loss in the hypertrophic zone.

Chondrocyte maturation in growth plate cartilage is coordinated by a complex paracrine signaling network that is rooted in reciprocal interactions between two major signal transduction pathways that include the secreted ligands Parathyroid-related protein (PTHrP, encoded by *Pthlh*), produced by periarticular resting chondrocytes, and Indian hedgehog (IHH), produced by prehypertrophic chondrocytes (Karp 2000, Kronenberg 2006, St-Jacques 1999). In this context, PTHrP acts to maintain resting

chondrocytes, and stimulates formation of proliferative chondrocytes (Ogawa 2002, Minina 2001). In addition, PTHrP signaling represses hypertrophy in part through inhibition of IHH signal transduction (Harrington 2010, Zhang 2009, Koziel 2005, Mau 2007, Guo 2002). Conversely, IHH induces hypertrophic differentiation in a PTHrP-independent manner while promoting PTHrP expression in periarticular resting chondrocytes (Tavella 2004, Oji 2007). Therefore, crosstalk between PTHrP and IHH paracrine signaling forms the core of a feedback circuit that maintains long-term growth by balancing chondrocyte production with chondrocyte loss through endochondral ossification.

Despite a deep understanding of the regulatory pathways that regulate growth, few options exist for clinical intervention in growth disorders (Lin 2006, Ballock 2003, Geister 2015). In vitro models of growth plate cartilage that reveal the network structure of regulatory interactions would advance both drug discovery efforts and tissue engineering solutions for growth disorders. One challenge is that chondrocytes readily form cartilage in vitro, but do not spontaneously assemble into functional growth plates (Gosset 2008, Bashey 1991, Guo 1989, Paige 1996). Results using pellet cultures generated from postnatal growth plate chondrocytes suggest that growth plate-like structure can be induced by the addition of exogenous factors. For example, pellet cultures treated with the hormone thyroxine or the signaling molecule Wnt5a form rudimentary chondrocyte columns and regionally display morphological evidence of chondrocyte hypertrophy (Ballock 1994, Randall 2012). While these observations suggest that chondrocytes respond appropriately to growth factor stimulation in vitro and that isolated chondrocytes are competent to organize into columns, these studies did not confirm formation of definitive growth plate structure through gene expression or demonstrate that columns formed via known cell biological mechanisms. Therefore, it remains to be determined whether a limited repertoire of signaling molecules is sufficient

to establish growth plate structure in vitro. Furthermore, pellet cultures significantly limit mechanistic studies by affording minimal control over the spatial distribution of growth factors and matrix structure. A culture system that allows precise spatial and/or temporal manipulation of the cellular microenvironment is needed to finely dissect the molecular mechanisms that regulate vertebrate growth.

To establish an in vitro model of growth plate cartilage, we encapsulated primary growth plate chondrocytes in beads composed of alginate hydrogel. Alginate is a linear polysaccharide that forms hydrogels when crosslinked in the presence of divalent cations (Loty 1998). It is widely used in tissue engineering applications because of its inherent non-fouling nature and ease of functionalization of the alginate molecule, and because the pore size of alginate hydrogels allows for the diffusion of waste out and nutrients and growth factors into the tissue engineered construct (Sargus-Patino 2014). Growth plate chondrocytes that have been encapsulated in “semi-solid” alginate beads maintain a rounded morphology (Rowley 1999, Lee 2012). More recently, groups have utilized alginate to inject growth plate chondrocytes into mice for long-term culture, and have even observed zonal arrangement and column formation (Alsberg 2001, Alsberg 2002). However, due to the complex nature of the in vivo culture environment, the crucial factors for growth plate development were not elucidated.

In the current study, we describe a novel three-dimensional *in vitro* culture model where chondrocytes encapsulated within alginate hydrogel scaffolds display zonal arrangement of gene expression domains consistent with growth plate cartilage architecture. In our culture system, chondrocytes display cell cycle properties and generate extracellular matrix consistent with growth plate chondrocytes. Moreover, we show that chondrocyte hypertrophy can be regulated by exogenous manipulation of PTHrP and IHH signaling. Importantly, treatment of alginate bead cultures with soluble IHH protein or thyroxine induces formation of spatially distinct gene expression patterns

consistent with a hypertrophic zone. Our results indicate that we have developed a viable model for studies of the genetic regulatory network that maintains the growth plate cartilage and thereby promotes bone growth.

RESULTS

Alginate culture maintains the growth plate cartilage phenotype

The objective of this study was to investigate the use of alginate hydrogels as three-dimensional scaffolds for development of an in vitro growth plate model. As a starting point, we analyzed the short-term cellular response of mouse chondrocytes to encapsulation within 1.5 % alginate hydrogels for up to seven days. The culture conditions used resulted in cell viability greater than 90% on days 0, 1, 4, and 7 (Figure 3.1A, Appendix Table 3.1). Individual chondrocytes progressively elaborated a pericellular matrix, as evidenced by extracellular domains of collagen IV and collagen VI, during the 7-day culture period (Figure 3.1 B). Since spontaneous dedifferentiation and hypertrophy are common problems in chondrocyte cultures, we next assessed chondrocyte differentiation via quantitative digital droplet PCR (ddPCR) analysis of gene expression. Chondrocytes in our alginate bead cultures express high levels of *collagen2a1* (Col2, Figure 3.2A), low levels of the fibroblast marker *collagen1a1* (Col1, Figure 3.2B), and maintain a stable ratio of Col2:Col1 gene expression (Figure 3.2C), a measure commonly used to assess chondrocyte dedifferentiation. Although the Col2:Col1 ratio did not significantly change over time, ColX expression, a marker of chondrocyte hypertrophy, decreased rapidly and significantly (Figure 3.2D).

Figure 3.1. Culture in alginate hydrogel promotes chondrocyte growth. (A) Invitrogen Live/Dead assay to determine chondrocyte viability for at least a week of alginate culture. Notice evident cell proliferation over time, but low amounts of dead cells in all time points (n=3). (B) Immunofluorescence assay demonstrating the formation of pericellular matrix in alginate culture using antibodies against Collagen 4 (left) and Collagen 6 (right). Freshly isolated chondrocytes lack ECM staining, but produce *de novo* ECM after 1 day in alginate culture. On day 4 (right), a secondary ECM structure is observed resembling territorial matrices (n=4).

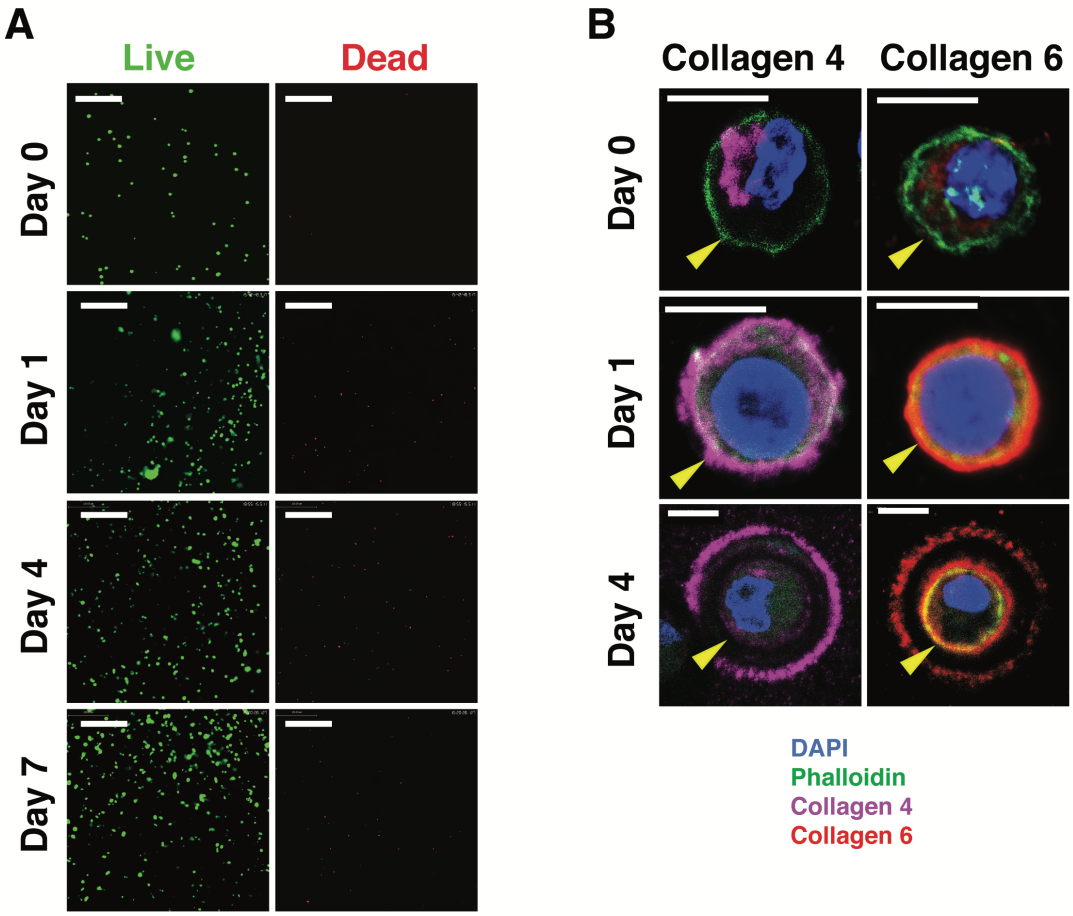
A
Live
Dead
Day 0
Day 1
Day 4
Day 7
B
Collagen 4
Collagen 6
Day 0
Day 1
Day 4
DAPI
Phalloidin
Collagen 4
Collagen 6

We also noted that cell density within the beads increased over time (Figure 3.1A) and many of the initial single cells become doublets in our cultures (data not shown); two observations that are consistent with cell proliferation. Therefore, we performed cell cycle analysis of our cultures using flow cytometry (FACS). FACS analysis revealed two populations of chondrocytes in our cultures that were distinguished by both forward and side scatter measures of cell size, and thus will be referred to as “larger” and “smaller” chondrocyte populations (Appendix 3.1). Smaller chondrocytes constituted less than 10% of the chondrocytes recovered from the beads and were associated with the only observable instances of sub-G1 peaks. In related experiments, we have observed that these small cells remain in the G1 phase of the cell cycle regardless of condition or treatment (data not shown), whereas larger cells are growth factor responsive (see below). Thus, only the larger, growth factor-responsive, cells were included in the reported cell cycle analysis. In this population of larger chondrocytes, FACS analysis revealed that only 5-7% of chondrocytes were in S-phase at the initiation of alginate culture (Figure 3.2E), whereas 15-20% of cells are in S-phase in embryonic growth plate cartilage (Yang 2003). However, during seven days of culture within the alginate hydrogel beads, we observed a statistically significant increase in the percentage of cells in S-phase that approached the level reported in vivo (Figure 3.2E). Since PTHrP has been shown to both inhibit hypertrophy and promote cell proliferation in cartilage, we next asked whether PTHrP was expressed by chondrocytes in our alginate culture. ddPCR analysis confirmed a significant upregulation of PTHrP expression over seven days of culture (Figure 3.2F).Taken together, these data suggest that our minimal culture conditions are sufficient to maintain the growth plate chondrocyte phenotype in vitro.

Figure 3.2. Culture in alginate hydrogel restrains cartilage differentiation. Gene expression analysis of alginate cultures using ddPCR (n=4) to count mRNA transcripts of Collagen 2 (A), Collagen 1 (B), Collagen X (D), and PTHrP (F). Values are reported as fold change in gene expression relative to day 1. (C) Ratio of mRNA transcript counts of Collagen 2 and Collagen 1. (E) Propidium Iodide cell cycle analysis by FACS to quantify percentage of cells in S-phase (DNA synthesis for cell proliferation/growth). Alginate cultures tend to increase the number of proliferating cells over time, compared to D0 and D1 (n=3).

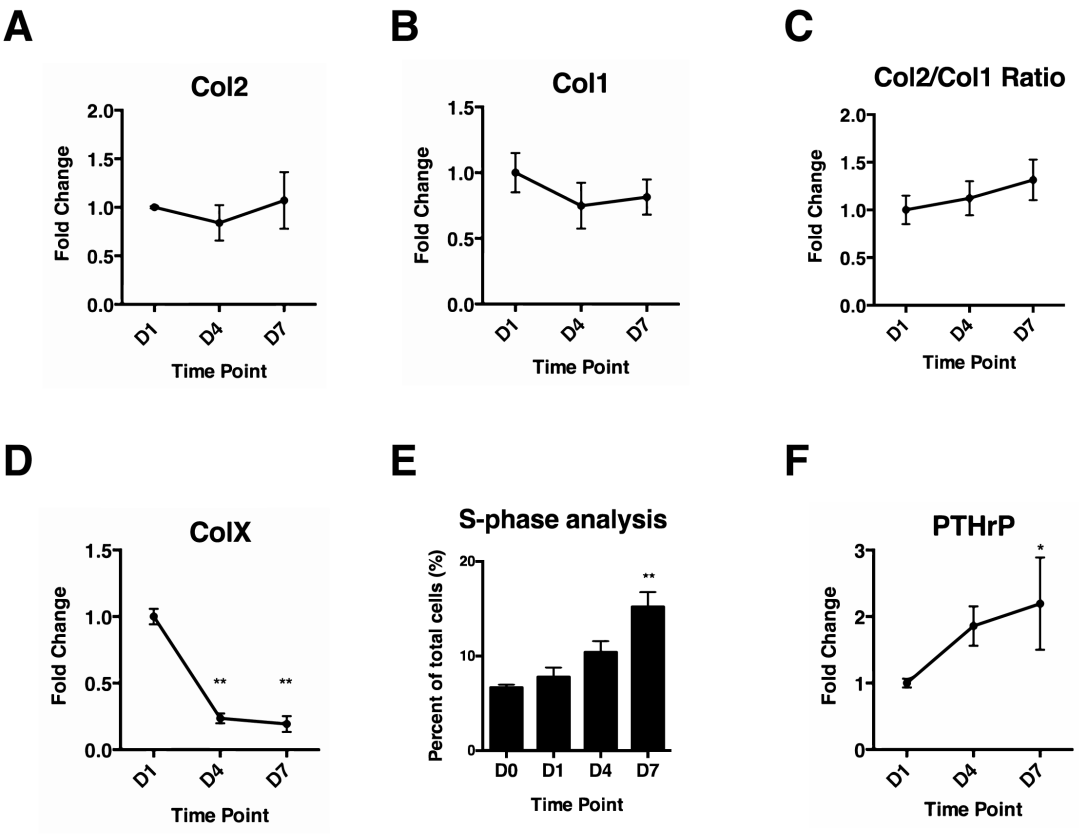
A
Col2
Fold Change
2.0
1.5
1.0
0.5
0.0
D1
D4
D7
Time Point
B
Col1
Fold Change
1.5
1.0
0.5
0.0
D1
D4
D7
Time Point
C
Col2/Col1 Ratio
Fold Change
2.0
1.5
1.0
0.5
0.0
D1
D4
D7
Time Point
D
ColX
Fold Change
1.5
1.0
0.5
0.0
**
**
D1
D4
D7
Time Point
E
S-phase analysis
Percent of total cells (%)
20
10
0
**
D0
D1
D4
D7
Time Point
F
PTHrP
Fold Change
3
2
1
0
*
D1
D4
D7
Time Point

PTH (1-34) treatment promotes cell proliferation in alginate bead culture

Given the correlations between PTHrP expression, cell proliferation, and chondrocyte differentiation, we next asked if stimulating PTHrP signaling could further enhance cell proliferation and chondrogenesis. We cultured chondrocytes in the presence of recombinant human PTH1-34, a 34-amino acid peptide derived from the N-terminus of parathyroid hormone that has been shown to activate the same receptor and downstream signal transduction pathways as the natural ligand PTHrP in chondrocytes (Kronenberg 2006). FACS analysis showed that one day treatment with PTH1-34 increased the fraction of cells in S-phase as compared to untreated controls, whereas no significant difference was observed after four days of treatment even when culture medium and factors were replaced every day (Figure 3.3A). It should be noted that the fraction of S-phase cells in PTH1-34 stimulated cultures was identical after one- and four-days of treatment (compare 100 nM PTH on day 1 and day 4). Therefore, the apparent desensitization to PTH1-34 treatment results from the increase in cell cycle activation over time in untreated cultures (compare 0 nM PTH on day 1 and day 4). Thus, exogenous stimulation of PTHrP signaling enhances chondrocyte cell proliferation in the short-term, but does not appear to have long-term benefits.

In addition to stimulating cell cycle progression, PTH1-34 also significantly reduced expression of ColX (hypertrophic chondroctyes, Figure 3.3B) and IHH (prehypertrophic chondrocytes, Figure 3.3C), as well as endogenous expression of PTHrP after one day of treatment as compared to control cultures (Figure 3E). One interesting observation was that PTH1-34 treatment continued to repress COLX expression after four days, whereas expression of other genes (i.e. IHH and PTHrP) had already returned to the level of untreated cultures. Therefore, we decided to validate the ddPCR results by analyzing gene expression at single cell resolution using fluorescent *in*

Figure 3.3: Treatment with PTH(1-34) accelerates the chondrocyte response to alginate bead culture. (A) Propidium Iodide cell cycle analysis by FACS to quantify percentage of cells in S-phase (DNA synthesis for cell proliferation/growth). PTH treatment on day 1 stimulates proliferation similar to levels typically seen in day 4 cultures. However, 4 days of PTH treatment has little effect (n=4). (B-E) Gene expression analysis was performed on PTH-treated alginate cultures with ddPCR to count mRNA transcripts. On day 1 (left), PTHrP inhibits expression of Collagen X (B), IHH (C), and PTHrP (E), but not collagen 2 (D). After 4 days of culture (right), the effects of PTHrP on gene expression are greatly attenuated (n=3).

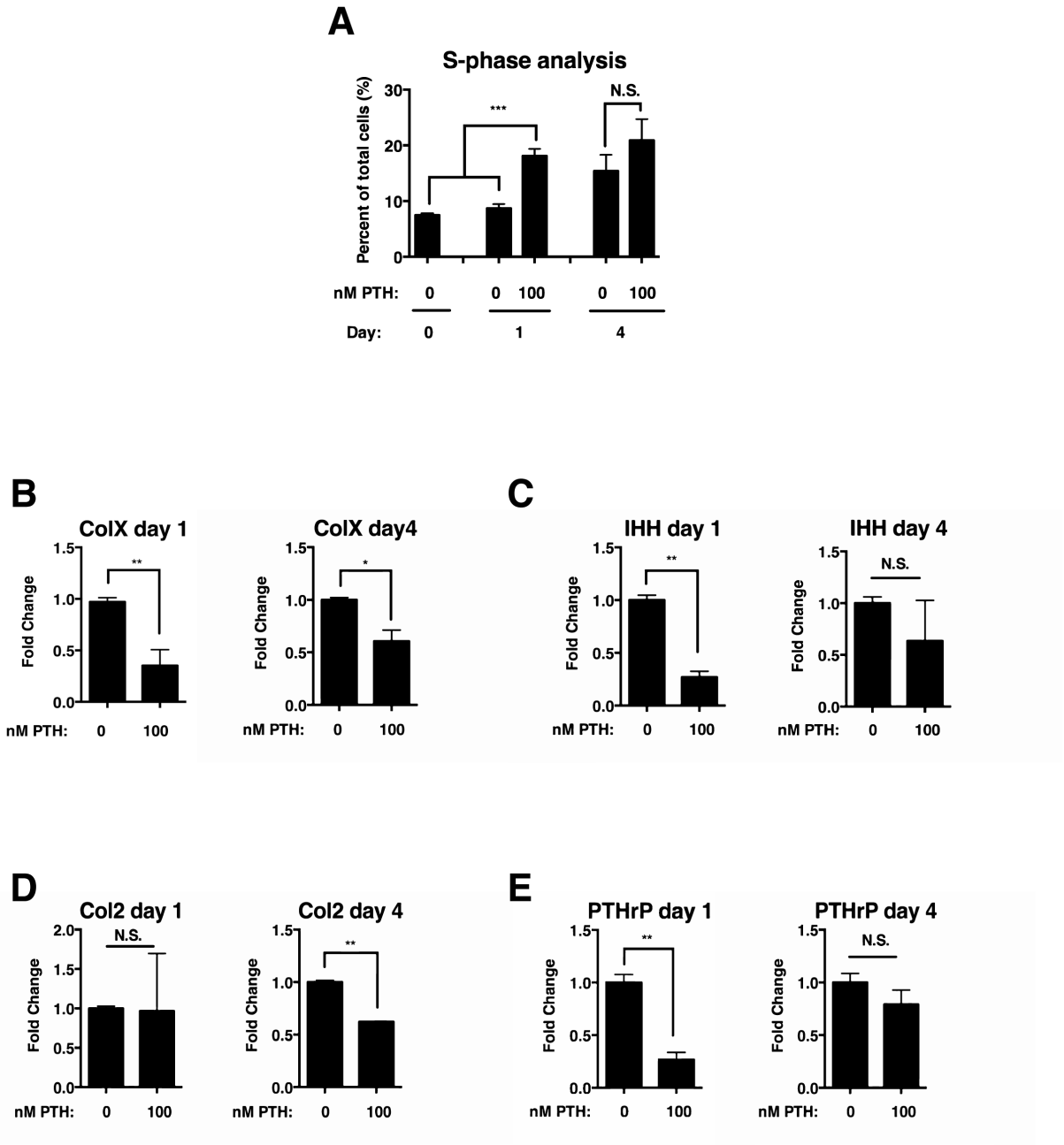
A
S-phase analysis
Percent of total cells (%)
30
20
10
0
***
N.S.
nM PTH: 0 0 100 0 100
Day: 0 1 4
B
ColX day 1
ColX day4
Fold Change
1.5
1.0
0.5
0.0
**
*
nM PTH: 0 100
C
IHH day 1
IHH day 4
N.S.
D
Col2 day 1
Col2 day 4
2.0
E
PTHrP day 1
PTHrP day 4

situ hybridization (FISH). *In situ* hybridization in alginate beads is difficult because the elevated hybridization temperatures, denaturing conditions, and metal ion chelation of hybridization buffers promote depolymerization of the alginate scaffold. To address this issue, we devised a novel tissue processing protocol in which alginate beads are stabilized prior to cryo-embedding by infiltration with acrylamide and induction of polymerization with ammonium persulfate. Using this method, we were able to carry out FISH on slides without disrupting the integrity of bead architecture, which allowed the spatial relationships between cells in our culture to be accurately determined. We visualized gene expression in each cell with fluorescence microscopy (Figure 3.4A, left), and quantified the total cell number (DAPI), as well as the number of hypertrophic chondrocytes (COLX) and immature chondrocytes (COLII) using an object-counting macro in ImageJ (see Supplemental Material). These values were used to calculate the hypertrophic index (ratio of COLX positive cells:COLII positive cells) that describes the state of chondrocyte maturation in regions of the alginate beads. Using this approach, we found that PTH1-34 treatment reduced the hypertrophic index following both 1-day and 4-day treatments (Figure 3.4B). Although the downward trend on each day was not statistically significant, the overall effect of PTH1-34 treatment across days was a significant reduction in hypertrophic index. Thus, together, in situ hybridization image analysis and ddPCR transcript quantification demonstrate long-term repression of COLX expression by continuous PTH1-34 treatment.

Activation of IHH signaling induces chondrocyte hypertrophy in alginate bead culture

In vivo, IHH signaling both promotes chondrocyte hypertrophy and activates PTHrP gene expression, which antagonizes chondrocyte maturation, including hypertrophy. Therefore, we next asked which effect would dominate following exogenous activation of

IHH signaling in alginate culture. To answer this question, we used three known activators of IHH signaling: purmorphamine, a commonly-used agonist of Smoothened, the signaling component of the hedgehog receptor complex (Sinha 2006); thyroxine, a hormone that activates IHH expression in chondrocytes (Williams 2013, Robson 2000); and bone morphogenetic protein 4 (BMP4), which is known to upregulate IHH expression (Grimsrud 2000). At all time points analyzed, IHH-activating agents increased the hypertrophic index as determined by FISH analysis (Figure 3.5A-B). After pooling data from different time points, it was determined that overall, 1 and 5 ng/mL BMP4, 0.5 μg/mL purmorphamine, and 500 ng/mL thyroxine each significantly increased hypertrophic index of bead cultures. In addition, both purmorphamine and thyroxine maintain the proportion of large (growth factor responsive) cells in alginate culture (Figure 3.5C-D). Given that direct activation of IHH signaling by the Smoothened agonist purmorphamine increased the hypertrophic index to a greater extent than the indirect activators thyroxine and BMP4, we next asked if recombinant IHH protein could similarly induce chondrocyte hypertrophy. As expected, hypertrophy was induced by IHH as determined by the ColX:ColII ratio (Figure 3.5A-B). However, induction of hypertrophy (COLX positive cells) was observed exclusively in cells near the bead surface, appearing as a ring illuminating the bead edges when analyzed by epifluorescence microscopy (Figure 3.6A). Conversely, COLII positive cells were enriched within core of the bead (Figure 3.6A, quantification in Figure 3.6B-C). Interestingly, treatment with thyroxine, but not purmorphamine, also induced formation of a peripheral ColX expression domain (Figure 3.6D). These data demonstrate regionalization of chondrocytes within alginate bead cultures into a layer of hypertrophic-zone-like cells on the bead periphery that surrounds a core of less mature chondrocytes. To our knowledge this is the first example of an inducible zonal chondrocyte organization in a tissue engineered cartilage construct using alginate hydrogel scaffolds.

Figure 3.4: Visualizing chondrocyte gene expression in alginate bead culture. (A) Fluorescent images generated using our improved protocol exploiting acrylamide embedding of fixed beads in conjunction with fluorescent *in situ* hybridization (FISH) to visualize cells that highly express Collagen 2 (left) and Collagen X (right) as a cell-by-cell measure of hypertrophic differentiation. Images are analyzed via a fully automated macro in ImageJ to quantify percentage of cells expressing each gene relative to a nuclear DAPI stain. Ratio of these percentages was calculated (ColX/Col2) to yield a hypertrophic index (refer to methods for more details). (B) Quantification of hypertrophic index in PTH1-34 treated and untreated cultures (n=3).

A

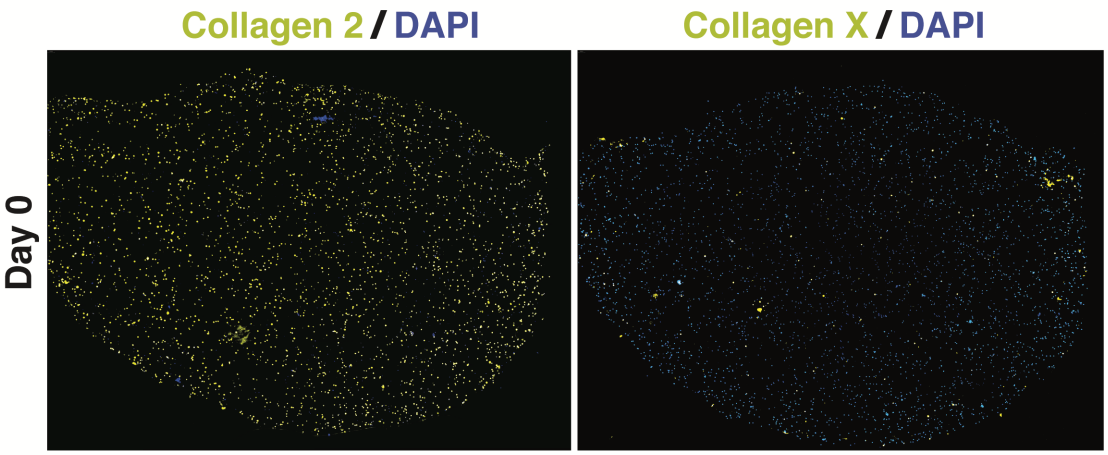
Collagen 2 / DAPI
Collagen X / DAPI
Day 0

B

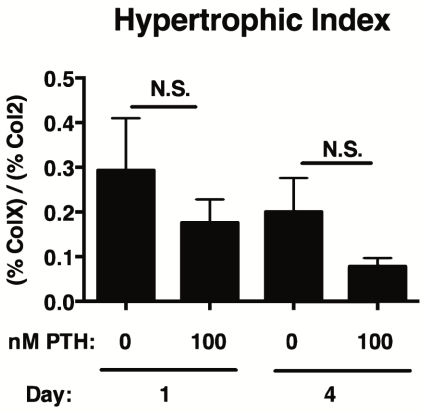
Hypertrophic Index
(% ColX) / (% Col2)
0.5
0.4
0.3
0.2
0.1
0.0
N.S.
N.S.
nM PTH: 0 100 0 100
Day: 1 4

Figure 3.5: Increased levels of hypertrophic gene expression following exogenous activation of IHH signaling. (A-B) Analysis of FISH-derived images to calculate the extent of hypertrophy in alginate cultures treated with Thyroxine (10, 500 ng/mL), BMP4 (1, 5 ng/mL), Purmorphamine (0.5, 5 μg/mL), and IHH (100 ng/mL) for a single day (A) and for 4 days in culture (B) (n=3)**.** On panel A, purmorphamine 20 day 4, the error bar is much larger than the rest of the data points and therefore is clipped by the axis. (C-D) Propidium Iodide analysis of stimulated bead cultures was performed to quantify percentage of cells in S-phase (n=3) on days 1 (C) and 4 (D).

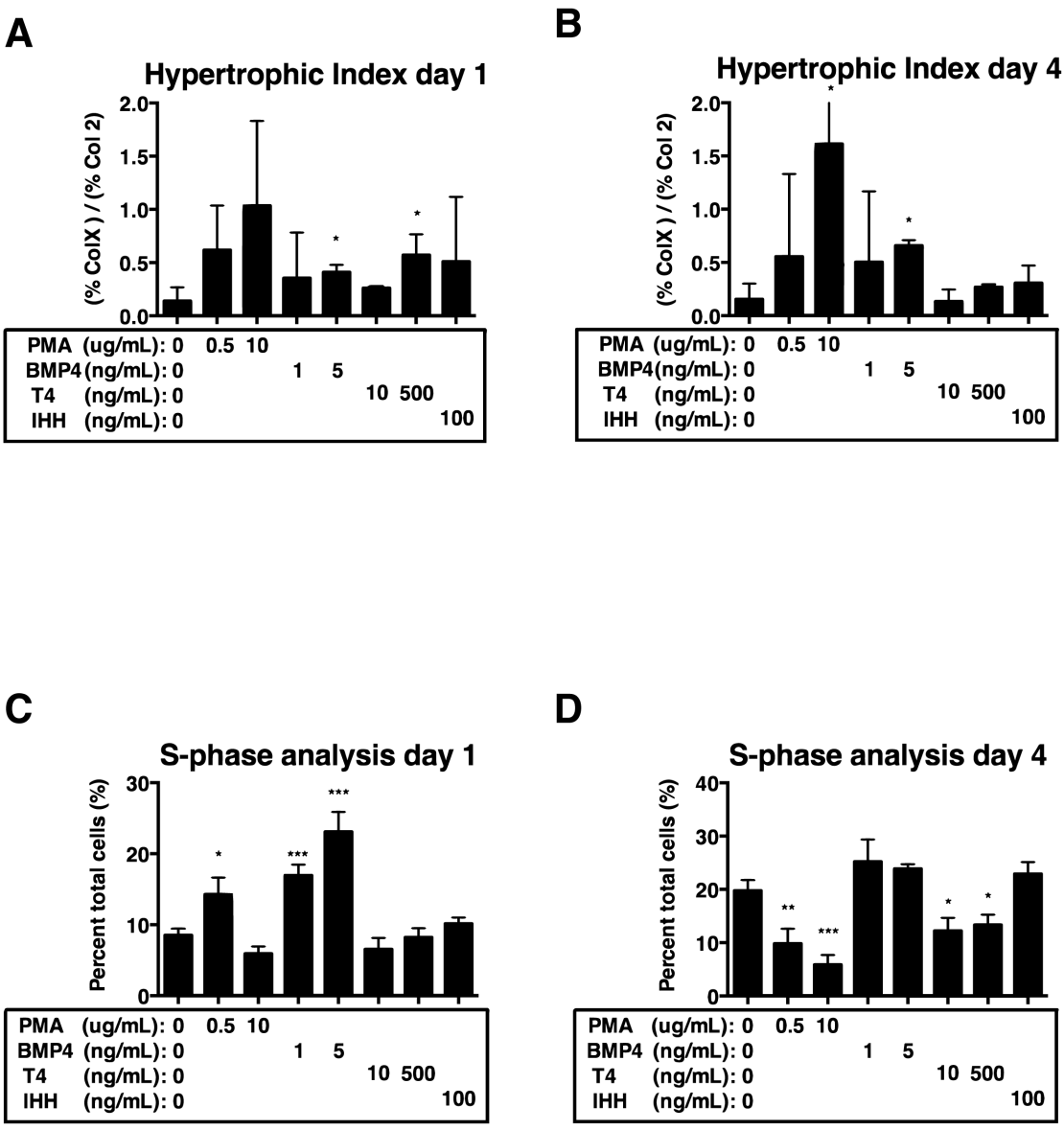
A
Hypertrophic Index day 1
(% ColX) / (% Col 2)
2.0
1.5
1.0
0.5
0.0
*
*
PMA (ug/mL): 0 0.5 10
BMP4 (ng/mL): 0 1 5
T4 (ng/mL): 0 10 500
IHH (ng/mL): 0 100
B
Hypertrophic Index day 4
(% ColX) / (% Col 2)
2.0
1.5
1.0
0.5
0.0
*
*
PMA (ug/mL): 0 0.5 10
BMP4 (ng/mL): 0 1 5
T4 (ng/mL): 0 10 500
IHH (ng/mL): 0 100
C
S-phase analysis day 1
Percent total cells (%)
30
20
10
0
*
***
***
PMA (ug/mL): 0 0.5 10
BMP4 (ng/mL): 0 1 5
T4 (ng/mL): 0 10 500
IHH (ng/mL): 0 100
D
S-phase analysis day 4
Percent total cells (%)
40
30
20
10
0
**
***
*
*
PMA (ug/mL): 0 0.5 10
BMP4 (ng/mL): 0 1 5
T4 (ng/mL): 0 10 500
IHH (ng/mL): 0 100

DISCUSSION

A novel culture system for studies of growth plate formation:

In children, growth plate cartilage is crucial to skeletal morphogenesis. Defects in growth plate function due to genetics (incidence of chondrodysplasia - 1 in 5000 births), metabolic disease, radiation and chemotherapy, and high-impact fractures affect skeletal growth, which can lead to deformities, growth arrest, or structural instability of developing long bones (Krakow 2010). However, an incomplete understanding of the molecular and cellular processes that produce growth has resulted in few clinical options to treat growth defects and has severely limited advances in tissue engineering and regenerative strategies to replace damaged or diseased tissue. While genetic models have identified many important molecules that regulate cartilage morphogenesis, deeper mechanistic understanding of growth regulation in vertebrates has been confounded by the lack of tools for precise and combinatorial genetic manipulation that is needed to determine mechanism. In vitro models offer the potential to simultaneously regulate multiple secreted, matrix, and mechanical factors in space and time (Langer 1993, Antoni 2015, Rowley 2002, Inoue 2014). Here we describe development of a 3D chondrocyte culture system using mouse neonatal growth plate chondrocytes encapsulated in an alginate hydrogel to investigate the mechanisms underlying growth plate formation, regulation, and growth disorders.

Three-dimensional alginate culture maintains immature chondrocytes.

For many tissues, two-dimensional cultures are sufficient to preserve cell phenotypes and cell-specific responses to growth factor signaling. However, in the case of growth plate cartilage, monolayer cultures promote dedifferentiation of chondrocytes, abnormal gene expression profiles, and inappropriate responses to signaling factors (Grant 1985,

Figure 3.6: IHH treatment in alginate bead culture is sufficient to establish spatiotemporal patterns of gene expression resembling chondrocyte zonal arrangement. (A) FISH (top) was used to visualize ColX-expressing (left) and Col2 expressing (right) cells in 100 ng/mL IHH-treated cultures. White dotted lines delineate the observed zones of predominant expression. Red dotted lines delineate outer boundary of the bead. Beads form a ColX-enriched ring (outer portion) surrounding a Col2-enriched core (inner portion). DAPI (middle) is shown on right to demonstrate cells are still evenly dispersed in hydrogel culture after 4 days, aside from isogenic groups, (n=3). (B) Counts of Col2-expressing and ColX-expressing cells (divided by the count of DAPI-positive nuclei in each FISH image), stacked in a bar graph to illustrate the relative predominance of hypertrophic versus non-hypertrophic chondrocytes in different domains of the IHH-treated alginate beads. (C) Hypertrophic indexes of different domains of the IHH-treated alginate beads. (D) FISH was used to visualize ColX-expressing (left) and total (right) chondrocytes in alginate cultures treated with 10 ng/mL thyroxine.

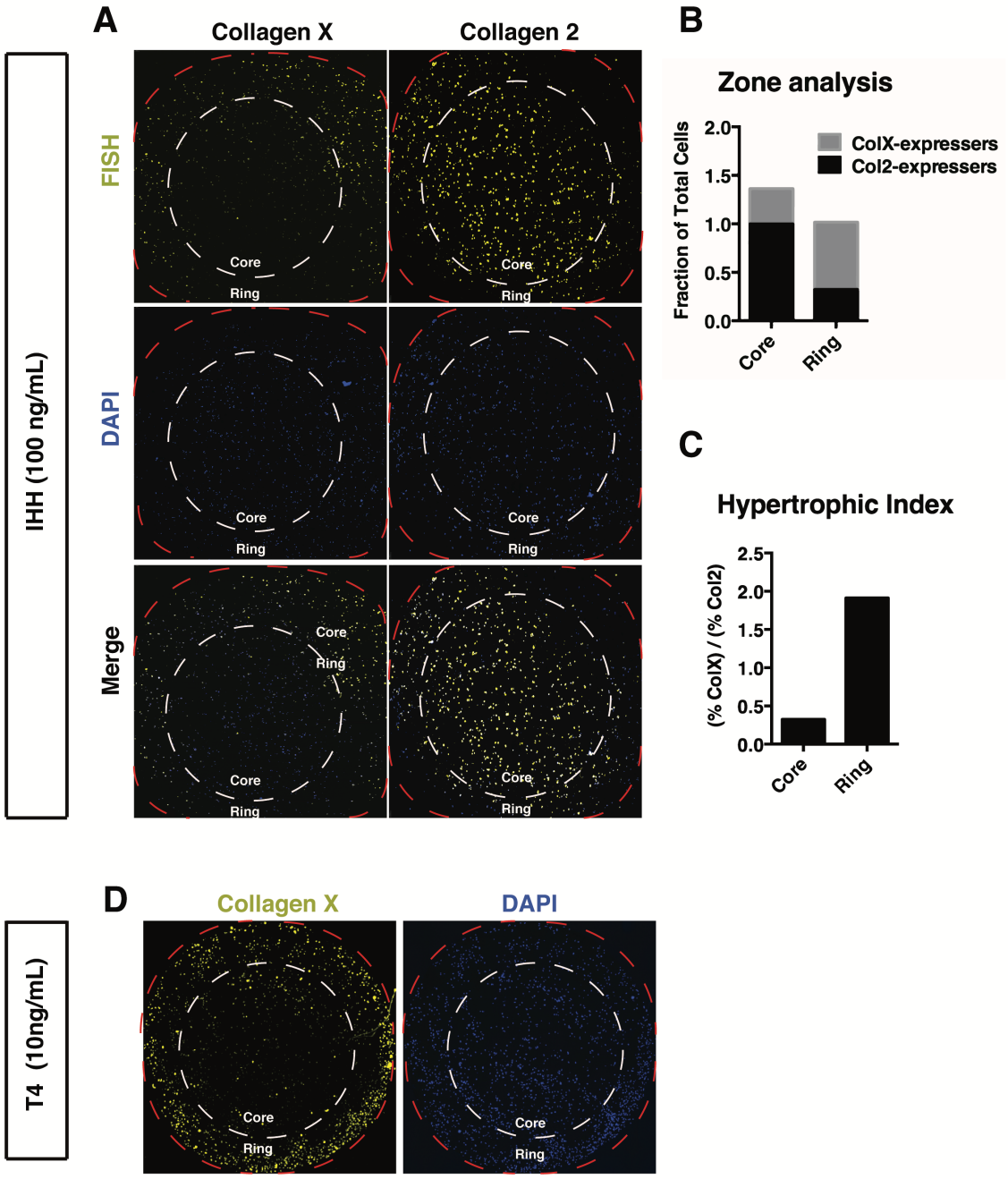
A
Collagen X
Collagen 2
IHH (100 ng/mL)
FISH
DAPI
Merge
Core
Ring
B
Zone analysis
Fraction of Total Cells
ColX-expressers
Col2-expressers
2.0
1.5
1.0
0.5
0.0
Core
Ring
C
Hypertrophic Index
(% ColX) / (% Col2)
2.5
2.0
1.5
1.0
0.5
0.0
Core
Ring
D
Collagen X
DAPI
T4 (10ng/mL)
Core
Ring

Shin 2016). Three-dimensional culture of chondrocytes in pellets, micromass, or artificial scaffolds has been shown to maintain the chondrogenic phenotype (Caron 2012, Liu 1998). Although pellet cultures have been induced to generate growth plate-like architecture, the difficulty of manipulating these cultures to generate regional differences in signaling factor concentrations or matrix composition inspired us to explore culture models in which chondrocytes are encapsulated in hydrogel scaffolds that have defined composition. The choice of scaffold is potentially important, since physical interaction of scaffold materials with cells and growth factors might significantly alter outcomes of these models. Therefore, we chose alginate as a scaffold material because low cell adhesion, limited protein binding, and minimal cell toxicity of this material renders alginate a “blank slate” for the introduction of defined signaling and matrix factors. The many advantages of alginate also include mild gelation conditions, fluid diffusion of nutrients and wastes into and out of the construct, and accessible functional groups for modifications. For these reasons, many cell types, including articular chondrocytes (Paige 1996), have been successfully cultured in alginate gels.

Our basal culture conditions display high viability and extracellular matrix deposition that are consistent with previous reports (Guo 1989), which suggests that the basal culture conditions are permissive for chondrogenesis. However, unlike previously described growth plate cartilage cultures, we observed rapid and significant decrease in chondrocyte hypertrophy and a concomitant increase in cell proliferation during seven days in culture. These findings are important because induction of hypertrophy and cell cycle exit are common observations in monolayer and micromass culture of chondrocytes (Gosset 2008, Bashey 1991). In these contexts, hypertrophy is often accompanied by expression of IHH and BMPs, and thus it has been assumed that isolated growth plate chondrocytes are unable to maintain expression of factors that are required to repress chondrocyte maturation (Grimsrud 2000). By contrast, our results

demonstrate that these alginate culture conditions promote maintenance of proliferating and growth factor-responsive chondrocytes that exhibit minimal hypertrophy. Although the mechanism remains to be defined, endogenous production of PTHrP might underlie preservation of the chondrocyte phenotype in alginate since PTHrP expression continued to increase during the 7 day culture period and the addition of exogenous PTH1-34 inhibited expression of both COLX and IHH, transcriptional markers of chondrocyte hypertrophy. These data strongly suggest that resting/proliferative chondrocytes, not hypertrophic chondrocytes, are the default maturation state in our alginate cultures.

PTHrP signaling drives cell proliferation in alginate culture

Although endogenous PTHrP production likely plays an important role in maintenance of chondrogenesis, PTHrP expression in our culture system increases at a rate that is probably suboptimal for chondrocyte cultures. For example, during 7 days in basal medium, our cultures display increased cell cycle entry from approximately 5% of cells in S phase at day 0 to approximately 15% by day 7. In contrast, approximately 20% of resting and proliferative chondrocytes are in S phase in embryonic growth plate cartilage (Yang 2003). However, after only 1 day of treatment with PTH1-34, cell proliferation within our cultures was restored to in vivo levels in our cultures. PTH1-34 stimulation of cell proliferation occurs concomitant with loss of IHH expression, suggesting that PTHrP signaling alone is the primary driver of cell proliferation in these cultures. The apparent primacy of PTHrP signaling is surprising given the genetic evidence for roles of IHH, Wnt5a and Wnt5b in cell cycle control (Yang 2003, Minina 2001). This paradox could be explained if these growth factors regulate PTHrP expression or if PTH1-34 induces expression of additional endogenous growth factors.

The *in vivo* observation of 20% S phase cells likely represents a limit to the rate of proliferation in heterogeneous chondrocyte populations, since this rate was not exceeded using lower or higher concentrations of PTHrP (data not shown). Together, our data suggest that establishment of PTHrP signaling is a crucial step to restore normal cell proliferation levels in growth plate chondrocyte cultures. However, one potential challenge to using PTH1-34 in long-term cultures is the potential for desensitization of the PTHrP signaling pathway (Figure 3.3), which could alter the cell proliferation rate and possibly lead to induction of cell hypertrophy. Results presented here suggest that chronic treatment is not detrimental to cultures since continuous stimulation with PTH1-34 maintained maximum levels of cell proliferation and minimum levels of *ColX* and *Ihh* expression for at least 7 days in our cultures. Given these results, we suggest that PTHrP signaling plays a crucial, yet underappreciated role, in maintaining cultures of growth plate chondrocytes.

IHH signaling induces hypertrophic zone-like gene expression patterns in alginate:

PTH1-34 stimulation of the cell cycle and repression of hypertrophy (Figure 3.3A-B) demonstrate that PTHrP pathway functions are maintained in chondrocytes within our alginate cultures. Likewise, our data show that functions of the IHH signaling pathway are also preserved in these cultures. Specifically, activation of IHH signaling either directly (IHH or purmorphamine) or indirectly via BMP signaling (thyroxine or BMP4) increased the proportion of COLX-expressing chondrocytes in bead cultures (Figure 3.5A-B). Induction of chondrocyte hypertrophy is an important PTHrP-independent function of IHH in vivo (Karp 2000). Thus, in combination with the data from PTH1-34 treatments, our results demonstrate preservation in alginate culture of the crucial functions that comprise the PTHrP-IHH signaling feedback loop, a key node in the regulatory network of growth plate cartilage.

Although treatment with IHH, purmorphamine, or thyroxine resulted in similar effects on chondrocyte hypertrophy, we observed one crucial difference – IHH and thryoxine treatments both produced regional differences in chondrocyte hypertrophy in alginate beads. Specifically, treatment with IHH or thyroxine was sufficient to stratify alginate bead cultures into an inner core consisting of non-hypertrophic (resting/proliferative) chondrocytes and an outer ring of *ColX*-expressing hypertrophic chondrocytes, which mimics the layered organization of growth plate cartilage *in vivo*. Regional differences were unexpected from treatment with a single factor, but could occur if diffusion of the hypertrophy inducing factors into the bead was rate limiting. Restricted diffusion of IHH might be expected since the pore size in 1.5% alginate gels restricts diffusion of molecules in the 10-70 kD range to varying degrees (Tanaka 1984) and mature IHH protein has a molecular mass of 20 kD. However, IHH is sufficiently small that it could be expected to equilibrate in concentration throughout the bead during four days in culture and therefore distinction between the core and periphery should lessen over time. An additional argument against a requirement for sustained exogenous concentration gradients is the observation that the small molecule thyroxine also induced a hypertrophic domain. Thyroxine has a negative charge that should limit interaction with the alginate scaffold and a low molecular weight (0.78 kD) that should allow unimpeded diffusion in alginate gels (Williams 2013). Therefore, the current data do not support a model in which sustained concentration gradients of signaling molecules are required to establish zonal differences in growth plate chondrocytes. If not by sustained concentration gradients of exogenous signaling molecules, what mechanism might account for regionalization of chondrocytes in alginate beads? An alternative model is that a concentration gradient is only transiently required to initiate

Figure 3.7: Hypothetical model exploring potential mechanisms of IHH-driven zonal demarcation. Possibilities include an outside-in IHH-diffusion gradient (Left) where cells exposed to high levels of IHH are induced to hypertrophy, but at the center of the bead, cells are seeing less IHH and maintain static differentiation state. Alternatively, IHH diffuses into the bead rapidly, creating a uniform IHH concentration in media (Right). Under this model, IHH induction of hypertrophy is balanced by endogenous PTHrP expression (differentiation block). Since PTHrP rapidly diffuses out of alginate but is constantly produced, this forms a radial gradient of PTHrP from the inside out where cells on the outer ring are exposed to a higher IHH/PTHrP ratio causing induction of hypertrophy.

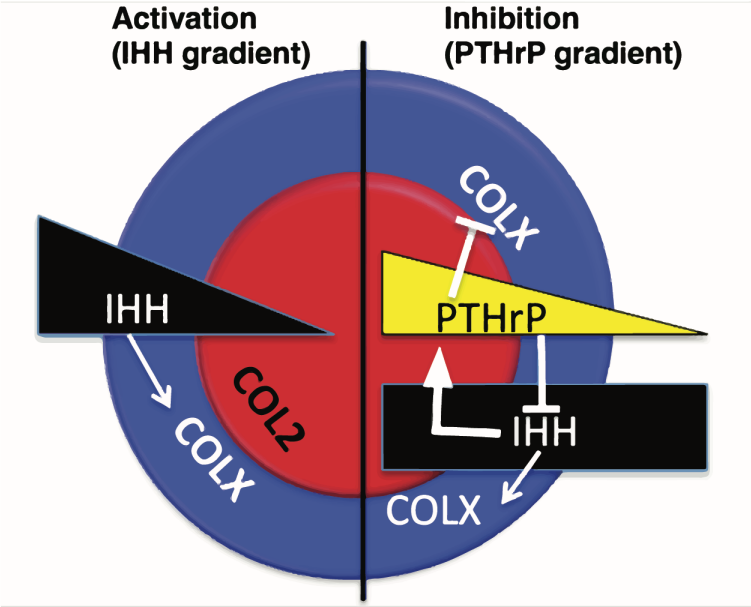
Activation
(IHH gradient)
Inhibition
(PTHrP gradient)
COLX
IHH
PTHrP
COL2
COLX
IHH
COLX

formation of distinct maturation domains. In this context, the current results most likely indicate induction of PTHrP expression in the non-hypertrophic core chondrocytes in response to IHH produced by the peripheral hypertrophic chondrocytes (Figure 3.7). In turn, endogenously produced PTHrP from the core chondrocytes might diffuse toward the periphery inhibiting IHH-dependent hypertrophy. Consequently, an initial anisotropic growth factor stimulus can activate the endogenous IHH-PTHrP signaling feedback interaction that generates distinct zones of chondrocyte maturation as observed in vivo.

CONCLUSION

Our results are the first demonstration of a tunable, three-dimensional culture model of growth plate cartilage. This culture system will be an important tool for elucidating the mechanisms underlying chondrocyte differentiation, cartilage architecture. In addition, our *in vitro* model could be used to advance drug discovery by facilitating high-throughput screening for molecules that regulate cartilage growth. Finally, our results encourage future studies that aim to use alginate hydrogel scaffolds to engineer cartilage constructs of defined proportions in vitro.

MATERIALS AND METHODS

Materials

Unless otherwise indicated, chemicals and reagents were obtained from Sigma Aldrich (St. Louis, MO), EMD (Darmstadt, Germany) or Thermo Fisher Scientific (Waltham, MA); cell culture media from Gibco/Life Technologies (Grand Island, NY); oligonucleotides from IDT (Coralville, IA); and consumables from Thermo Fisher Scientific or VWR (Radnor, PA). Growth factors were obtained from Sigma-Aldrich, EMD

Calbiochem (San Diego, CA), Tocris (Ellisville, MO) or R&D Systems, Inc. (Minneapolis, Minnesota).

Chondrocyte Isolation

Neonatal Swiss Webster mice (Jackson Laboratories, Bar Harbor, ME) at postnatal day 4 (P4, with P0 being the day of birth) were euthanized, and the growth plate cartilage from both hind limbs was harvested into Hank's Balanced Salt Solution (HBSS). Cartilage was transferred into Complete Medium composed of Dulbecco's Modified Eagle Medium (DMEM) containing 10% fetal bovine serum (FBS; Atlanta Biologicals, Flowery Branch, GA), 1% glutamine-penicillin-streptomycin. Collagenase was added to 0.25% (w/v) and the cartilage was digested for 4 hours in a passively humidified incubator at 37°C and 8% CO_2 and pipetted several times to break up remaining tissue. Chondrocytes were pelleted by centrifugation at 125 x g for 5 minutes using a Sorvall Legend RT centrifuge (Kendro Laboratories, Newtown CT) and resuspended in Complete Medium. Cell density was quantified using a haemocytometer. Chondrocytes were maintained in the incubator until time for alginate encapsulation. All procedures performed on animals were consistent with regulatory agency policies and were approved by the Institutional Care and Use Committee at University of Nebraska Medical Center.

Chondrocyte Encapsulation in Alginate

Sodium alginate powder (Pronova UP MVG, >60% guluronic acid, 200,000 – 300,000 g/mol; NovaMatrix, Sandvika, Norway) was dissolved in sterile phosphate buffered saline (PBS) to a concentration of 1.5% (w/v) and the solution was filtered sterilized using 0.20 μm Rapid-Flow PES filters. Growth plate chondrocytes were

pelleted by centrifugation at 125 x g for 5 minutes and resuspended in an appropriate volume of alginate solution (to $8x10^6$ cells/ml) by gentle pipetting and vortexing. Homogenous alginate beads were formed using the basic "drop" method previously described previously (Sargus-Patino 2014). Briefly, 10 µL of alginate-cell solution was drawn into a pipette tip and the tip was wiped with a Kimwipe® to ensure the alginate could drop freely from the tip. The plunger was rapidly depressed to release a drop of the cell suspension into 2 mL of crosslinking solution (50 mM $CaCl_2$/140 mM NaCl at 37^{o}C) contained in a 24-well tissue culture dish from a height of 2-3 inches. Only one bead was prepared in an individual well. After 2 minutes of crosslinking, beads were transferred to a well containing 2-mL of Complete Medium for up to 10 minutes and then washed in MEM-alpha medium without Phenol Red (α-MEM) for up to 10 minutes. After both washes, the bead was placed into cartilage culture media (described below).

Culture Conditions

Cartilage culture media was prepared using previously described methods (Romereim 2014): α-MEM supplemented with 50 µL/mL QPS, β-glycerophosphate (10 mM), and L(+) ascorbic acid (50 µg/ml). In addition, dexamethasone (1 nM), proline (1 mg/mL), 1% antioxidant (Sigma Aldrich), sodium pyruvate (1 mM), 1% nonessential amino acids (Gibco), and 1% Insulin-Transferrin-Selenium+3 media supplement (ITS +3; Sigma Aldrich). In some cultures, parathyroid hormone 1-34 (PTH1-34), Indian hedgehog (IHH), Purmorphamine (PMA), bone morphogenetic protein-4 (BMP4), or Thyroxine (T4) was added to the media at the concentrations indicated in the text. Beads were cultured in a 48-well plate in a humidified incubator at 37°C and 8% CO2 for up to 7 days with medium changes every day.

Evaluation of Viability

Viability of encapsulated chondrocytes was determined using a Live/Dead Cell Viability kit (Invitrogen). Briefly, after culture, beads were incubated in PBS containing 2 μM Calcein AM/4 μM ethidium homodimer-1 for 30 minutes in the dark, washed in several changes of PBS and fluorescence signal of live (green) and dead (red) cells was imaged using a Leica DMI6000B inverted microscope. Live and dead cell counts were quantified from the resulting images using a basic ImageJ macro (Supplemental File 1) to calculate percent viability.

Immunofluorescence Imaging

For immunofluorescence (IF) analysis, all reagent and wash solutions contained 2mM $CaCl_2$ to maintain crosslinking of alginate. Beads were fixed with 4% paraformaldehyde (PFA) for 20 minutes, permeabilized with TBST (0.1% Triton X-100/15-mM Tris-HCl/136-mM NaCl, pH 7.6) , and then blocked for 2 hours with 10% heat-inactivated sheep serum (HISS, Sigma Aldrich) in TBST. Subsequently, beads were incubated with gentle rocking at 4º C in either rabbit-anti-Collagen VI (1:500; Abcam, Cambridge, UK) or rabbit-anti-Collagen IV (1:500; Abcam) primary antibody in 2% HISS/TBST overnight. The beads were then incubated in a secondary anti-mouse AlexaFluor 647 antibody (1:1000; Jackson Laboratories) and phalloidin-labeled AlexaFluor 488 (1:100; Invitrogen) for 2 hours in 2% HISS/TBST. After washing 3 x 5 minutes in TBST, the beads were mounted with Prolong Gold antifade reagent with DAPI (Invitrogen) on a glass microscope slide with a coverslip. Images were obtained on a Leica DMI6000B inverted microscope or a Zeiss 710 laser scanning confocal microscope. For confocal microscopy, optical sections were collected at 1.8-μm intervals

for between 15 and 25 sections (total depth of 30-40-μm) with line averaging = 2, scan speed = 4 or 5, and resolution = 1024×1024).

Transcript Expression Analysis

For each experimental condition, four beads were depolymerized in 50 μL of 50 mM ethylenediaminetetraacetic acid disodium salt dihydrate (EDTA) and chondrocytes were recovered by centrifugation. RNA was isolated from cells using the NucleoSpin® RNA Plus kit (Thermo Fisher) according to the manufacturer's instructions and quantified using a Thermo Fisher Scientific NanoDropOne spectrophotometer. cDNA was synthesized using Superscript IV (Thermo Fisher) according to the manufacturer's instructions and analyzed by ddPCR (Bio-Rad Laboratories, Inc., Pleasanton CA). Thermal cycling conditions were 95°C for 5 min, 40 amplification cycles (95°C for 30 seconds and 60°C for 30 seconds), and a final signal stabilization step (4°C for 5 minutes, 90°C for 5 minutes). The transcript count of each gene of interest was normalized with a geometric average of transcript counts of three normalization control transcripts: actin, RPL13a, and HPRT. Data from this analysis are reported as fold change in the geometric mean ± SEM over the transcript count of the non-treated control and significance was calculated using two-way ANOVA analysis using Prism software (GraphPad Software, Inc, La Jolla, CA). A full list of primer sequences and gene accession numbers used to generate primers is included in Supplemental Table 2 (Peng 2012, Zhai 2013,Everaert 2011, Bougault 2008, Hiramatsu 2011, Sahar 2005, Kruger 2010).

Flow Cytometry

Fluorescence-activated cell sorting (FACS) was used to analyze cell cycle progression in cultured chondrocytes. Alginate beads were dissociated in 200 µL of 50 mM EDTA for 5 minutes. Cells were washed by with PBS and centrifuged at 125 x g for 5 minutes. The cell pellet was resuspended in 200-µL of PBS and fixed by adding 2.8 mL of ice-cold 90% ethanol dropwise while vortexing. Fixed cells were stored at -20°C for up to 7 days. For cell cycle analysis, DNA in fixed cells was stained with 0.05 mg/mL propidium iodide in Telford's reagent (33.62 µg/mL EDTA, 26.8 µg/mL RNAse A at 93 U/mg, and 0.1% Triton X-100) for 1 hour at 4°C in the dark. Labeled suspensions of cells were filtered through 5-mL filter-cap polypropylene Falcon tubes (Corning Labs, Tamaulipas, Mexico) and were then immediately analyzed on a BD FACSCaliber 2 flow cytometer (BD, Franklin Lakes, NJ). The resulting cell cycle data was represented as stacked bar graphs of the geometric mean ± SEM of percentage of cells in each phase of the cell cycle and significance was calculated using a two-way ANOVA using GraphPad Prism software.

In Situ Hybridization

For fluorescence in situ hybridization (FISH) analysis of gene expression in cell cultures, whole alginate beads containing chondrocytes were fixed in 4% paraformaldehyde in TBS containing 5mM $CaCl_2$ overnight at 4°C. To maintain structural integrity of the sample, beads were infiltrated with in 37.5:1 40% acrylamide (JT Baker, Center Valley, PA) overnight at 4ºC and the acrylamide was polymerized using 10% ammonium persulfate (10 µL/mL acrylamide) and TEMED (1 µL/mL acrylamide). Polymerized samples were subsequently incubated in 30% sucrose overnight at 4^{o}C before embedding in Tissue-Tek Optimum Cutting Temperature embedding medium

(OCT) and freezing on dry ice. Sections (60 μm) were collected on glass microscope slides and FISH was performed using fluorescein labeled RNA probes for *collagen2a1* (ColII) and *collagen 10a1* (ColX) as previously described (Ahrens 2009). Slides were mounted using Prolong Gold antifade reagent with DAPI (Life Technologies) and images were obtained on a Leica DMI6000B inverted microscope. The images presented in this paper are montages that were assembled by tiling and stitching images from several optical planes as a z-stack (10-μm width between individual slices in the z-stack, 3 total slices per z-stack, total width of the z-stack equaling 20 μm) to visualize the entire section of the bead for downstream quantification. To quantify cell counts we used a batch processing analysis in Image J using a macro programmed in-house using FIJI software (http://fiji.sc/) to quantify the number of cells expressing the respective gene (for macro, see Supplemental Information). Typically, each image yielded cell counts of approximately 1000 and the data for each experimental condition derived from approximately 10,000 cell counts. The fraction of cells expressing a given gene was determined by dividing the number of cells expressing the gene by the number of DAPI positive nuclei observed in the section. The ColX:ColII ratio was calculated as the geometric mean of the ColX:DAPI ratio for each replicate divided by the geometric mean of the Col2:DAPI ratio for each replicate (n=3 or 4 sections for each replicate). The ratio is reported as the geometric mean of the ColX/Col2 ratio for each replicate ± SEM. To determine statistical significance, a Student's t-test was used. To determine whether a given treatment had significant overall effects on hypertrophy, datasets from different time points were pooled into treated or untreated groups and compared using a paired Wilcox signed-rank test.

CHAPTER 4: TRANSCRIPTOMICS ANALYSIS OF THE IHH/PHTRP SIGNALING LOOP IN ALGINATE CULTURE

INTRODUCTION

Endochondral bone elongation rates are determined by the sequential passage of chondrocytes in the epiphyseal growth plate cartilage across a maturation trajectory spanning at least four recognized subtypes. A tissue-wide regulatory network that relies on zone-specific release and interpretation of paracrine signals regulates the zonal arrangement of these chondrocyte subpopulations along the proximodistal axis. At the heart of this control system, the well-studied PTHrP/IHH negative feedback circuit masterminds rates of cell proliferation and differentiation, and holds the key to organizing the complex signaling environment found in cartilage throughout its development. Thus, a thorough understanding of IHH/PTHrP signaling behavior as a function of both chondrocyte positioning in space, as well as specific chondrocyte subtype, is a crucial criterion for studies attempting to recreate zonal growth plate architecture in culture.

The previous chapter discusses the development of a hydrogel-based *in vitro* model of growth plate cartilage by describing how chondrocytes encapsulated in alginate respond to exogenous stimulation with growth factors. Basal bead cultures exhibit a predominately PTHrP-driven baseline phenotype that progressively favors cell cycling, while repressing transcription of hypertrophic marker Col10a1. Conversely, activation of IHH signaling triggers gene expression patterns consistent with hypertrophy in a chondrocyte population located close to the bead periphery. This results in transcriptionally distinct and spatially segregated chondrocyte subdomains reminiscent of early cartilage patterning. The results emphasize the potential power of alginate culture to dissect developmental interactions that organize the growth plate, and lead to a hypothesis that activating the IHH/PTHrP signaling feedback loop is sufficient to establish zonal architecture *in vitro*. However, limitations of the study left several key assumptions of the model untested. Recombinant PTHrP affected gene expression and

cell cycle of bead cultures, but whether treatment invoked the transcriptional regulatory mechanisms native to cartilage is not clear based on the limited number of markers used. Further, *In situ* hybridization experiments did not utilize probes to specifically identify resting, proliferative, prehypertrophic, or IHH-responsive chondrocytes, instead only measuring hypertrophy using Col10a1, and non-hypertrophic chondrocytes via Col2a1. Thus, although two distinct cell domains were observed, IHH-treated beads were not definitively proven to contain spatially ordered arrangement of all four subtypes, and the specific identity of target populations directly mediating IHH signals in alginate remain mysterious. Without additional molecular markers to confirm cell identity, the possibility that Col10a1-expressing cells were transcriptionally distinct from bona fide hypertrophic cells also could not be excluded. Thus, the predicted negative feedback loop of transcriptional regulation by IHH-mediated induction of PTHrP has not yet been verified in alginate culture. To validate our *in vitro* model, we characterized the chondrocyte signaling response to PTHrP by transcriptomic analysis using next-generation RNA sequencing (NGS), and determine how IHH treatment affects identity and signaling profile of individual chondrocytes and subpopulations by applying single cell RNA sequencing (scRNAseq). The results demonstrate, in proof of concept, a powerful tool towards dissecting specific actions of individual growth factors across heterogeneous cartilage culture.

RESULTS/DISCUSSION

Transcriptomic analysis of PTH-treated bead cultures:

To identify transcriptional targets of the PTHrP signaling pathway, we chose optimal conditions based on parameter sweeps described in Chapter 3. Our preliminary dose-response assessments of PTH (1-34) treatment on primary chondrocyte gene

expression in alginate showed that a 100nM dose caused similar transcriptional changes compared with a 1uM treatment, but was more potent than 10nM treatment (data not shown). In the same experiments, a 24-hour treatment produced much greater effects compared to a 4-day treatment duration, which was attributed to the increases in endogenous PTHrP expression seen in longer-term alginate culture (Figure 3.2). For these reasons, a 1-day culture period and a 100nM dose of PTH (1-34) were selected to characterize the genome-wide transcriptional response to activation of PTHrP signaling. We performed RNA sequencing analysis on PTH-treated and untreated beads (n=3 of each condition). Analyzing the principal components of these six samples shows overall gene expression differences between the two experimental conditions mostly exceeded the heterogeneity of replicates (Figure 4.1a). We saw a total of 393 genes were significantly differentially expressed in chondrocytes cultured in alginate ($p < 0.05$ after Benjamini-Hochberg FDR correction) compared to the non-treated controls (Figure 4.1b). The average fold change across all detected genes was 1.045. The magnitude of change in all genes, calculated by the absolute value of $\log_2$-fold change in chondrocytes, was 0.46 (38% change in expression, 1.38). The magnitude of change in the significantly differentially expressed genes was 0.715 (64% change in expression, 1.64). The results indicate that PTH treatment caused a shift in the chondrocyte transcriptional profile without affecting overall levels of transcription. We compared the data with results of real-time quantitative PCR experiments shown in the previous chapter that initially defined the chondrocyte response to PTHrP in the alginate context. After PTHrP treatment, Col10a1 and PTHLH were significantly reduced (fold change 0.39, corrected p-value < 0.05), IHH was significantly reduced before BH-FDR p-value correction (fold change 0.40), and Col2a1 is not significantly altered. The agreement among the ddPCR and RNAseq data suggests the culture environment provided by alginate bead encapsulation is likely suitable for accurate studies of gene expression.

Figure 4.1: Summary of NGS analysis following PTH treatment of chondrocytes.

A) Multidimensional scaling plots illustrating the transcriptional relationship between PTH-treated and untreated samples. Each axis is based on the dimensionality reduction of transcriptomic datasets by identifying groups of principal component genes that vary across samples. Although PTH and untreated cells both vary along the Y-axis, they are segregated by a group of genes that constitute the entire X-axis. B) Volcano plot illustrating the direction, magnitude, and significance of differential expression for every measured gene following PTHrP treatment. Black dots are not considered significant differences after p-value correction. Red dots fall above the significance threshold of $p < 0.05$ after correction.

A

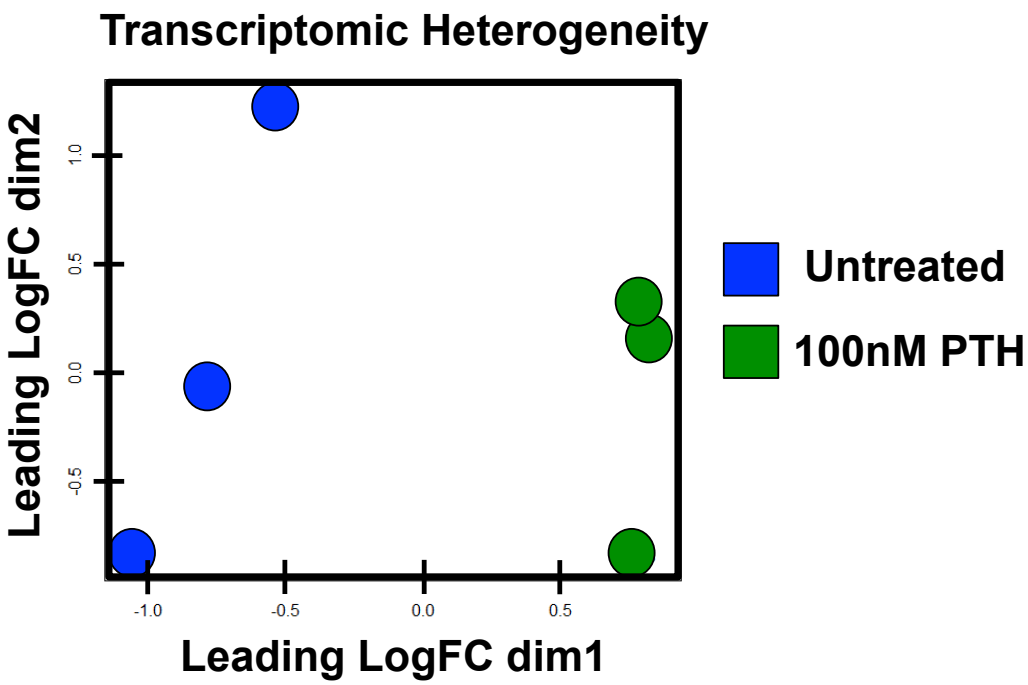
Transcriptomic Heterogeneity
Leading LogFC dim2
1.0
0.5
0.0
-0.5
-1.0
-0.5
0.0
0.5
Leading LogFC dim1
Untreated
100nM PTH

B

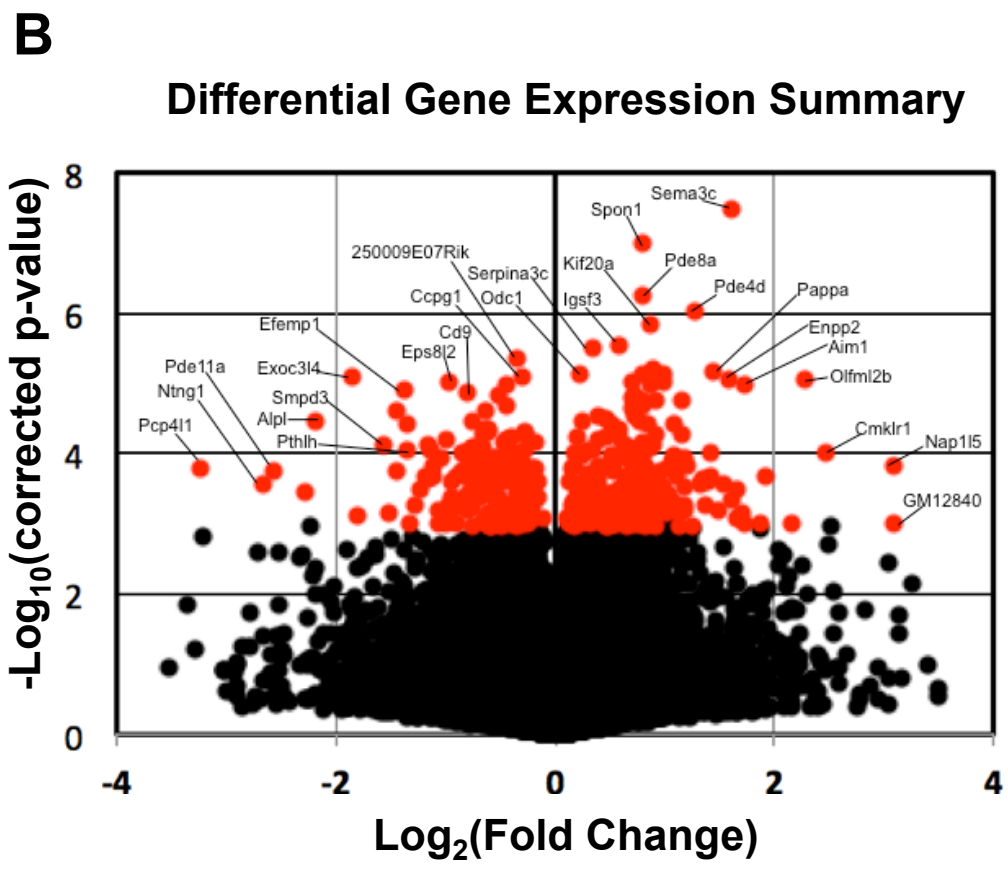
Differential Gene Expression Summary
-Log10(corrected p-value)
8
6
4
2
0
-4
-2
0
2
4
Log2(Fold Change)
Sema3c
Spon1
250009E07Rik
Serpina3c
Kif20a
Pde8a
Ccpg1
Odc1
Igsf3
Pde4d
Pappa
Efemp1
Cd9
Eps8l2
Enpp2
Aim1
Pde11a
Exoc3l4
Olfml2b
Ntng1
Smpd3
Alpl
Cmklr1
Pcp4l1
Pthlh
Nap1l5
GM12840

Pathway analysis reveals conserved and novel targets of PTHrP signaling:

Expression data from differentially regulated genes (corrected $p < 0.05$) identified from treated alginate cultures were further characterized using the Ingenuity Pathway Analysis (IPA) tool to identify cellular and molecular functions associated with exposure to PTH (Figure 4.2). Based on the directionality of gene expression changes, IPA calculates z-scores that predict activation/inhibition status of these particular pathways as well as probable upstream regulatory networks that could hint at a mechanism for PTH-mediated gene expression differences. In parallel, enrichment analysis with the online tool Enrichr was used to mine three independent databases (Reactome, WikiPathways, and Panther) to test whether multiple software packages interpret the gene set similarly (Table 4.1). IPA software found over 40 genes participating in pathways that affect cell cycle, including Polo-like kinase role in mitosis, chromosomal replication, G2/M DNA damage checkpoint, and p53 signaling to be the most significantly affected by the treatment. Enrichr also consistently identified cell cycle processes, such as DNA strand elongation, M-phase, and Mitotic Prometaphase, and sister chromatid resolution as the most enriched pathways in the gene set. The results show that genes associated with the activation of Polo-like Kinase, which is required for progression through several cell-cycle checkpoints, are significantly upregulated by PTH treatment. These genes include AURKA, AURKB, PLK1, PLK2, CCNF, CDCA3, CDCA2, and CDK1 (Appendix table 4.1 lists the entire suite of differentially regulated genes). Similarly, genes participating in cycling inhibition at the G2/M checkpoint such as the p53 and CDKN1A pathways are downregulated. Although qPCR will be needed to validate these gene expression changes, this data suggests that PTH-signaling mediated induction of Polo-kinase-dependent cell cycle progression, and p53 checkpoint relief, could explain our finding that PTH treatment leads to increased chondrocyte proliferation in alginate culture.

Figure 4.2: Ingenuity Pathway Core Analysis Summary of molecular networks and cell processes affected by PTH treatment. Signaling effects of PTH treatment are summarized in a bar graph listing pathways IPA predicts to be most significantly altered in treated samples versus control. The vertical orange line is a threshold value for determining significance ($p<0.01$), which all reported pathways exceed. The color of each bar determines its predicted activation or inhibition status. Deeper colors indicate a greater directional change in activity. Orange signifies activation, whereas blue signifies the pathway is inhibited by PTH treatment.

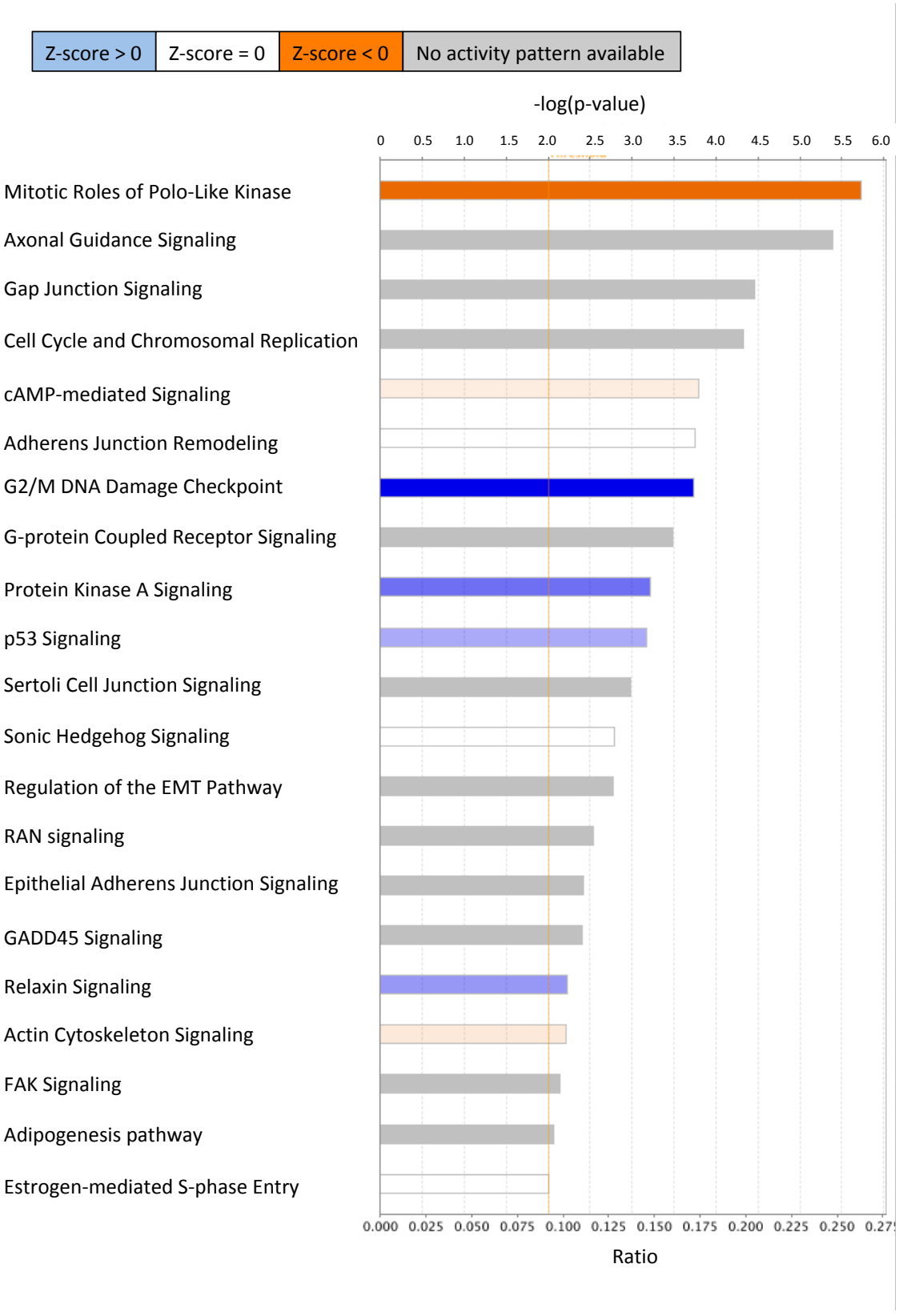
Z-score > 0
Z-score = 0
Z-score < 0
No activity pattern available
-log(p-value)
0
0.5
1.0
1.5
2.0
2.5
3.0
3.5
4.0
4.5
5.0
5.5
6.0
Mitotic Roles of Polo-Like Kinase
Axonal Guidance Signaling
Gap Junction Signaling
Cell Cycle and Chromosomal Replication
cAMP-mediated Signaling
Adherens Junction Remodeling
G2/M DNA Damage Checkpoint
G-protein Coupled Receptor Signaling
Protein Kinase A Signaling
p53 Signaling
Sertoli Cell Junction Signaling
Sonic Hedgehog Signaling
Regulation of the EMT Pathway
RAN signaling
Epithelial Adherens Junction Signaling
GADD45 Signaling
Relaxin Signaling
Actin Cytoskeleton Signaling
FAK Signaling
Adipogenesis pathway
Estrogen-mediated S-phase Entry
0.000
0.025
0.050
0.075
0.100
0.125
0.150
0.175
0.200
0.225
0.250
Ratio

IPA result also indicated differential regulation of many known mediators of PTHrP signaling including genes related to cAMP-mediated signaling, G-protein coupled receptor signaling, Protein Kinase A (PKA) signaling, and Hedgehog signaling, which again were listed among the top hits of the Enrichr screen. The specific affected genes that IPA categorized into these groups showed a complex pattern of up- and downregulation by PTH treatment. As expected, Hedgehog-associated genes such as PTCH1 and GLI1 were both downregulated, although GAS1 and interestingly DHH, a member of the Hedgehog family expressed mainly in the germline, increased in expression. Many differentially expressed genes were categorized commonly into the HH, PKA, and cAMP-associated groups, and of these genes, several were upregulated (DUSP1, CAMK4, AGTR2, STAT3, PDE8A, PDE7B, PDE3A) as well as down (CTNNB1, PRKAR2B, ADCY2, GNAS, GPER1, PDE11A, AND PTH1R). Together, these data suggest that stimulation of the cAMP/PKA-signaling axis by PTH treatment led to inhibition of the HH pathway as expected from *in vivo* studies. If this were true, chondrocytes in alginate should be capable of mimicking at least some of the PTHrP-responsive signaling behaviors seen in cartilage. Also noteworthy is the downregulation of the PTH receptor, PTH1r in response to its ligand, as well as downregulation of the PTHLH gene itself, a result we previously found via ddPCR. These data could reflect the existence of a negative feedback and/or compensatory mechanism used by the chondrocytes to prevent saturation of the signaling environment (Barolo 2002), or the natural consequences of repressing IHH signaling by PTHrP treatment (Karp 2000).

Unexpectedly, genes that regulate local interactions between cells and their surrounding environment made up a large fraction of the gene classes found by Enrichr and IPA to be influenced by PTH treatment (Figure 4.2 and Table 4.1). Specifically, these groups included genes that participate during cell-cell interactions (gap-junction signaling, adherens junctions), cell-matrix interactions (axonal guidance, integrin and

focal adhesion signaling, collagen formation, chondroitin sulfate synthesis, ECM organization), and regulation of the cytoskeleton (Actin cytoskeleton signaling, Rho-GTPase regulation of cytoskeleton, Rho-GTPase activation of formin). Differential expression of G-protein and Rho/Rac GTPase signaling effectors (H2AFZ, PLK1, KIF14, IQGAP2, RANGAP1, IQGAP3, NDC80, ACTG1, TIAM2, KIF18A, RACGAP1, INCENP, PRC1, DLC1, NUF2, CTNNB1, CENPN, PAK3, ECT2, MAD2L1, PRKAR2B, PDE4D, GNAS, ARHGEF1, ADCY2, PDE7B, PDE8A, TUBB6, TUBB4B) was detected. One or more of these targets may affect Rho/Rac-mediated control of chondrocyte cytoskeletal organization (Rac promoting actin polymerization, Rho promoting actomyosin contractility). Altered Rho/Rac activity and subsequent disruption in actin architecture would be expected to affect adhesion dynamics at the cell surface (Katsumi 2002, Ren 2000). Similarly, a large number of differential expression of genes related to cartilage ECM organization and cell-ECM adhesion (IBSP, PDGFD, COL5A2, ERBB2, ITGA5, PAK3, THBS2, ACTG1, ADAMTS3, LOX, CTSL, COL25A1, COL12A1, COL8A2, LOXL4, COL10A1, GDF5, DCN, COMP, VCAN, EFEMP1, CAPN6, SDC1, ARF1, RND2) were detected. The sheer number of ECM and cell-ECM adhesion proteins that are differentially expressed after PTH treatment, suggests that PTHrP signaling could influence cell-matrix engagement by modulating composition of the cartilage ECM, the chondrocyte's repertoire of available adhesion proteins, or both. Taken together, the RNA sequencing data agrees with our previous work and many of the expectations from the literature, but also revealed new possible target nodes downstream of PTHrP. These targets should be confirmed by alternate methods, and future studies should investigate whether they are involved in linking the diffusible ligand-receptor interactions with local cell processes such as daughter cell rearrangements during proliferative zone column formation.

Table 4.1 – Enrichr analysis of PTHrP-affected genes

Function (Reactome 2016)	**P-value**	**Adjusted p-value**	**Z-score**	**Combined**
Cell Cycle	7.01E-15	2.82E-12	-2.45	79.92
Mitotic Prometaphase	2.81E-09	7.52E-07	-2.03	40.02
M Phase	8.66E-08	0.00001738	-2.42	39.4
Chondroitin sulfate biosynthesis	0.000001701	0.0002277	-2.28	30.23
Resolution of Sister Chromatid	5.56E-07	0.00008932	-2.06	29.61
DNA strand elongation	0.000002362	0.000271	-2.1	27.16
S Phase	0.000006168	0.002433	-2.14	25.65
Rho GTPase Activate Formins	0.00008482	0.00073	-1.8	16.91
Extracellular Matrix Organization	0.00001371	0.00073	-2	22.42
Collagen Formation	0.00004397	0.00161	-1.84	18.41
Function (WikiPathways 2016)	**P-value**	**Adjusted p-value**	**Z-score**	**Combined**
Retinoblastoma in Cancer	2.31E-10	6.08E-08	-1.95	43.33
Cell Cycle	8.57E-07	0.0001127	-1.87	26.09
Endochondral Ossification	0.00001912	0.001257	-1.86	20.16
Adipogenesis	0.0000457	0.001668	-1.74	17.35
DNA Replication	0.0001209	0.003179	-1.72	15.51
Hedgehog Signaling Pathway	0.00005708	0.001668	-1.54	15.04
G Protein Signaling Pathways	0.002693	0.04165	-1.52	9.01
Extracellular vesicle mediated signaling	0.00269	0.04165	-1.07	6.36
Osteoblast Signaling	0.00233	0.0409	-0.27	1.64
Focal Adhesion	0.00463	0.0554	-1.62	8.71
Function (Panther 2016)	**P-value**	**Adjusted p-value**	**Z-score**	**Combined**
DNA replication	0.0004504	0.02522	-1.36	10.47
Angiogenesis	0.007095	0.09933	-1.37	6.8
Integrin signaling pathway	0.01213	0.1012	-1.4	6.17
Hedgehog signaling pathway	0.004934	0.0921	-0.85	4.49
Cytoskeletal regulation by Rho GTPase	0.01218	0.1012	-0.93	4.11
CCKR signaling map ST	0.04481	0.2509	-0.94	2.93
Endothelin signaling pathway	0.06019	0.3064	-0.74	2.08
Cadherin signaling pathway	0.07598	0.3546	-0.59	1.51
Huntington disease	0.09788	0.364	-0.4	0.93
Formyltetrahydroformate biosynthesis	0.003703	0.0921	-0.15	0.87

Single-cell sequencing reveals chondrocyte subpopulations targeted by IHH signaling:

The transcriptional profiles of PTH-responding chondrocytes in alginate determined by RNA sequencing provides a benchmark by which to test the activation of PTHrP signaling among alginate-cultured chondrocyte subpopulations in other experimental settings. To test our hypothesis that IHH treatment stimulates the IHH/PTHrP negative feedback loop in alginate culture, we performed a pilot experiment (n=1 treated and untreated sample) where we replicated the culture and IHH stimulation conditions from the previous chapter. Primary chondrocytes were given 4 days in alginate culture, in the presence or absence of 100-ng/mL dose of IHH recombinant protein. We analyzed the transcriptional profile of individual cells by single-cell RNA sequencing. This analysis pipeline, developed by 10X Genomics, inputs the raw sequencing reads for each cell, and generates a dimensionally reduced scatter plot using the principal components (PC) of gene expression across all cells. The visualization method, called t-SNE, applies a nonlinear, probabilistic algorithm that projects high-dimensional datasets into 2D for visualization (Maaten 2008). This algorithm recursively transforms the relative point arrangements based on local and global considerations until equilibrium is reached, so distances along x- and y- axes have no direct interpretation. Additionally, data points that appear highly similar in high-dimensional space may scatter due to the 2D projection. However, the resulting graph allows a general view of sample heterogeneity, where the distance between two points represents their overall differences in gene expression.

Using an unbiased, graph-based method of clustering the t-SNE space results in the detection of 7 subpopulations from a total population of 2368 untreated control chondrocytes (Figure 4.2a, left), and 8 subpopulations of from a total population of 2566 IHH-treated chondrocytes (Figure 4.2a, right). Clusters are color coded by the number of cells residing in that cluster, summarized below (Figure 4.2b). As with individual cells, t-

SNE distance between clusters represents transcriptional similarities. Results from this initial cluster analysis suggest that IHH treatment led to the formation of at least one transcriptionally distinct subpopulation of chondrocytes.

Genes that were used to generate the clustering results, and their expression levels in each cluster relative to all other cells in the dataset were analyzed for both treated and control samples (Supplemental Table 2). A visual representation of relative expression levels of all PC genes for each cluster relative to the total sample population is shown via heat maps (Figure 4.2b), as well as the number of cells residing in that population. Both cluster plot and heat map enable a rough assessment of the transcriptional distances among chondrocyte subpopulations, within each sample. Because the IHH-treated and control samples were analyzed independently by the 10X Genomics pipeline, PC genes were not strictly held constant by the software. In all, 149 genes were used as PC's for the IHH-treated sample, and 137 PC genes were used for the control. Of these genes, 84 PC genes were shared across samples, meaning that although PC gene definitions were not exactly identical in similar groups across samples, the majority of the PC genes necessary for distinguishing subpopulations in both IHH and untreated samples were the same. Among these PC genes we observed many familiar cartilage zone markers and genes that are well established to exhibit specific expression domains in the growth plate. Expression of most canonical zone marker genes were segregated into respective clusters, suggesting that growth plate chondrocyte subtypes retained transcriptional identity in alginate culture, or differentiated into other known subtypes during culture.

Figure 4.3: Single-cell RNA sequencing workflow schematic. Top left: Primary chondrocytes were harvested from the growth plate cartilage. Colored labels reflect the spatial organization of transcriptionally similar chondrocyte subtypes in the cartilage. Top right: chondrocytes become encapsulated in alginate hydrogel. Colored dots show how chondrocyte maturation status becomes decoupled from their relative positions. During this stage, cells were cultured in the presence or absence of IHH. Bottom right: cells were removed from alginate gel and prepared for single-cell capture and barcoding. RNA was isolated from single cells and the resulting libraries were sequenced using Illumina NextSeq 550. Bottom left: transcriptional heterogeneity among single cells is visualized using a t-SNE plot, where each cell is sorted into clusters according to their transcriptional output, based on their cell identity. This plot does not in any way explicitly represent the spatial positioning of each cell, but may reflect cell organization in cases where spatial and transcriptional heterogeneity are closely correlated.

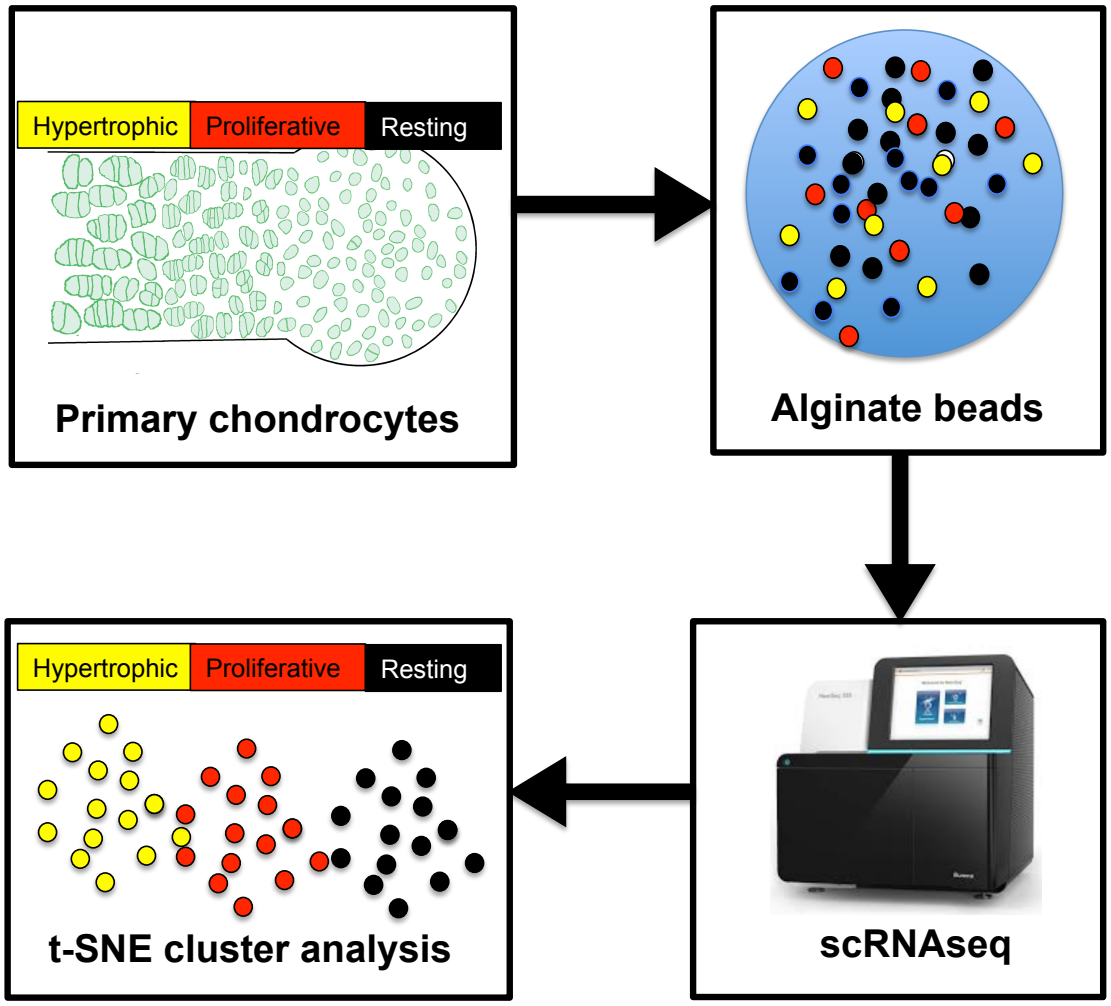
Hypertrophic
Proliferative
Resting
Primary chondrocytes
Alginate beads
scRNAseq
Hypertrophic
Proliferative
Resting
t-SNE cluster analysis

By matching the PC genes of each cluster to known zonal markers, cell populations could be reasonably identified in terms of chondrocyte maturation. For the sake of discussion, cell populations that show expression levels of any given marker that exceeds that of all other populations will be said to have “high” expression of that marker. These primary markers include PTHrP (resting zone marker), BMP3 (previously shown to be expressed specifically in resting zone cells, see Nilsson 2007), IHH (prehypertrophic zone marker), Col10a1 (hypertrophic zone marker), and extreme upregulation of cell cycle genes such as Ccna2, Pbk, Top2a, and Mki67 (proliferative zone chondrocytes), and are only part of the larger suite of cartilage zone-specific PC genes that characterize these subpopulations (for examples, see Romereim 2014, Ahrens 2009). By using these marker genes to identify clusters, subpopulations representing each of the four stereotypical growth plate cartilage zones segregate into clusters in both the treated and untreated conditions.

Cells with high expression of the marker genes were for the most part confined to unique single clusters in the non-treated chondrocytes; a high PTHrP-expressing cluster contained 474 cells, the highly proliferative cluster contained 130 cells, high IHH-expressing cluster contained 303 cells, and the high Col10a1 cluster contained 410 cells. However, gene expression indicative of hypertrophy was heightened in cells receiving IHH treatment, resulting in two distinct Col10a1-rich clusters (365 cells expressing 6.4-fold more Col10a1 than the total population and 278 cells expressing 1.86-fold more Col10a1 than the total population). Enrichr analysis of the top 40 locally distinguishing PC genes in t-SNE space shows enrichment for lipid and carbon metabolic processes in the medium-high Col10a1-expresssing group, and some zone markers (IHH, MMP13, and WNT4) enriched in the highest Col10a1-expressing group.

Figure 4.4: Single-cell transcriptomics of alginate cultures could uncover the subpopulation-specific signaling actions of IHH. A) Multidimensional scaling plots showing the transcriptional heterogeneity of single chondrocytes cultured in alginate beads in the presence (right) or absence (left) of IHH. Each point represents a single cell within t-SNE (transcriptional) space at positions determined by overall expression of principal component genes. Some cell groups are distant from the total population; this distance signifies a highly transcriptionally distinct subpopulation. Group shapes do not have direct interpretation, as t-SNE tends to expand dense regions. Scatterplots are color-coded to show cell clusters that were determined by the graph-based cluster analysis to transcriptionally segregate into unique subpopulations. Clusters are ranked by number of cells residing within the cluster to generate the color scheme. B) Mapping of each observed cluster to specific chondrocyte identities. Heat maps show the relative expression of PC genes by clusters compared to total dataset. Briefly, leftmost regions display expression of resting zone markers, middle-right regions show prehypertrophic and hypertrophic markers, and rightmost regions mark cell proliferation genes. Green arrows match each cluster in untreated sample to corresponding clusters in IHH-treated sample to compare cell counts. C) PC genes of each cluster (and overall population) were compared to PTH-responsive genes reported by NGS. The numbers of principal component genes displaying expression values within a cluster (relative to total dataset) matching direction of differential expression induced by PTH are shown in the bar graph. Blue bars = untreated clusters, red bars = IHH-treated clusters. N=1 untreated and 1 treated sample submitted for analysis.

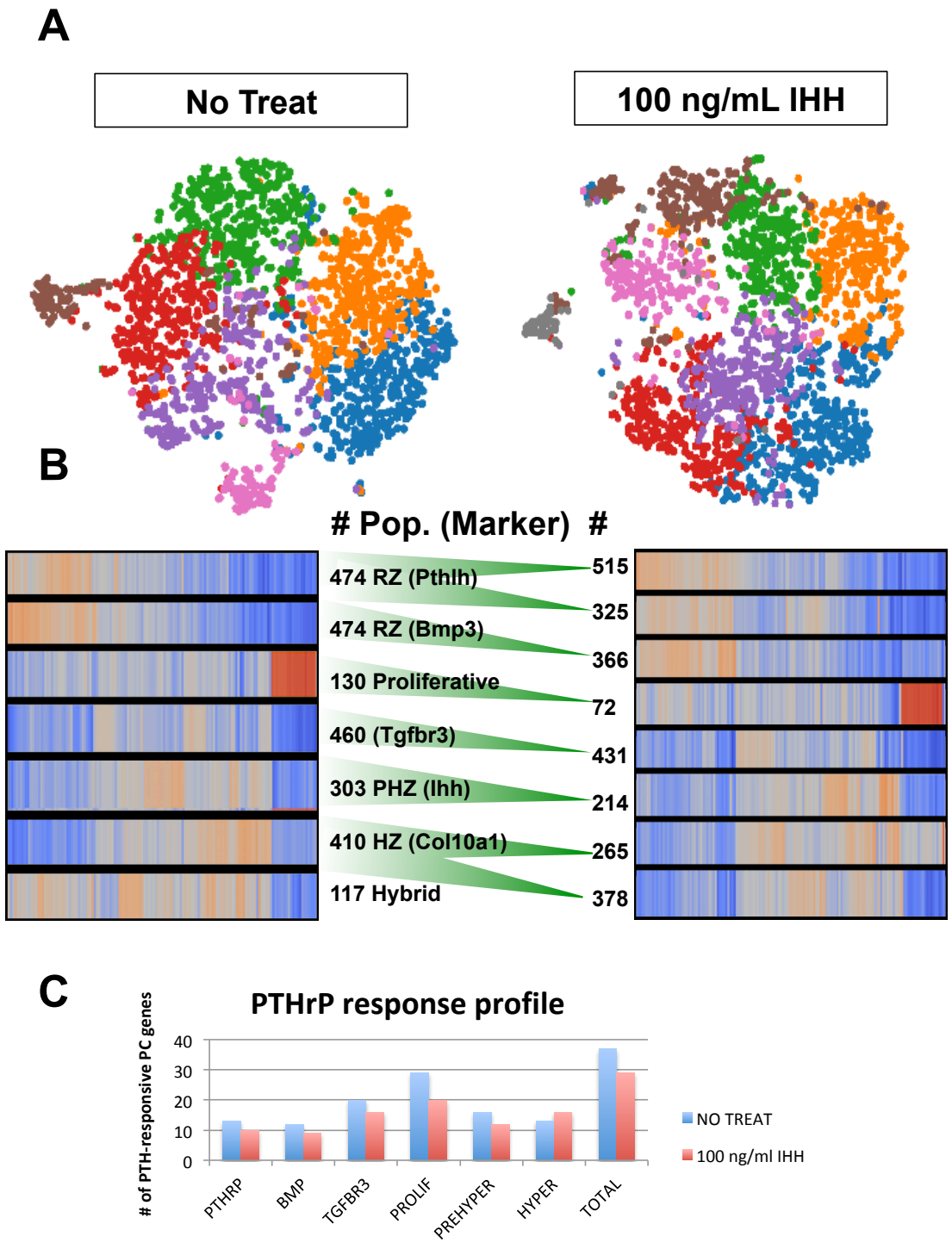
A
No Treat
100 ng/mL IHH
B
Pop. (Marker)
474 RZ (Pthlh)
515
474 RZ (Bmp3)
325
130 Proliferative
366
460 (Tgfbr3)
72
303 PHZ (Ihh)
431
410 HZ (Col10a1)
214
117 Hybrid
265
378
C
PTHrP response profile
# of PTH-responsive PC genes
40
30
20
10
0
PTHRP
BMP
TGFBR3
PROLIF
PREHYPER
HYPER
TOTAL
NO TREAT
100 ng/ml IHH

In addition, PTHrP expression was increased in the IHH treated group, resulting in two distinct PTHrP-expressing clusters (515 cells producing 8.28-fold more PTHrP than total population, 325 cells expressing 1.46-fold more PTHrP than total population) Enrichr analysis of 40 PC genes that locally distinguish these resting populations in t-SNE space shows medium-level PTH expressing population enriched for mitochondrial function, as well as transcription, translation and protein folding machinery whereas the highest-level PTHrP expressing cells are characterized by genes regulating ECM production (UCMA, LUM, MFAP2, PRELP) and cell adhesion (SNAI1, TNS1, NDRG1, ILSR). Notably, both the highest PTHrP- and Col10a1-expressing groups are characterized by a similar pattern of gene expression relative to their neighbors in t-SNE space: 2-fold increases in the expression of cartilage matrix protein PRELP, cell migration factor NREP, and secreted protein FAM180A, and 2-fold decreases expression in the ER-stress-related gene ERO1L, and three calcium-binding proteins (PLA2G2A, TPD52, and ESPN). These genes may represent a transcriptional signature that occurs in response to IHH. All other clusters in the IHH-treated sample had decreased cell counts compared to untreated (for example only 214 prehypertrophic and only 72 proliferative zone), despite the overall larger total cell population.

Figure 4.5: Schematic illustrating chondrocyte subtype distribution as determined by analysis of scRNAseq results. t-SNE scatterplots superimposed with manually drawn maps of individual clusters to show their shape and position. Each cluster is labeled with a group identity based on PC gene definitions, and a percentage value describing each subtype's representation among the total population of chondrocytes. More replicates, and parameter sweeps using the Cell Ranger software will be necessary to understand whether cluster shape or position is biologically meaningful. Top: untreated chondrocyte cultures. Bottom: IHH-treated chondrocyte cultures.

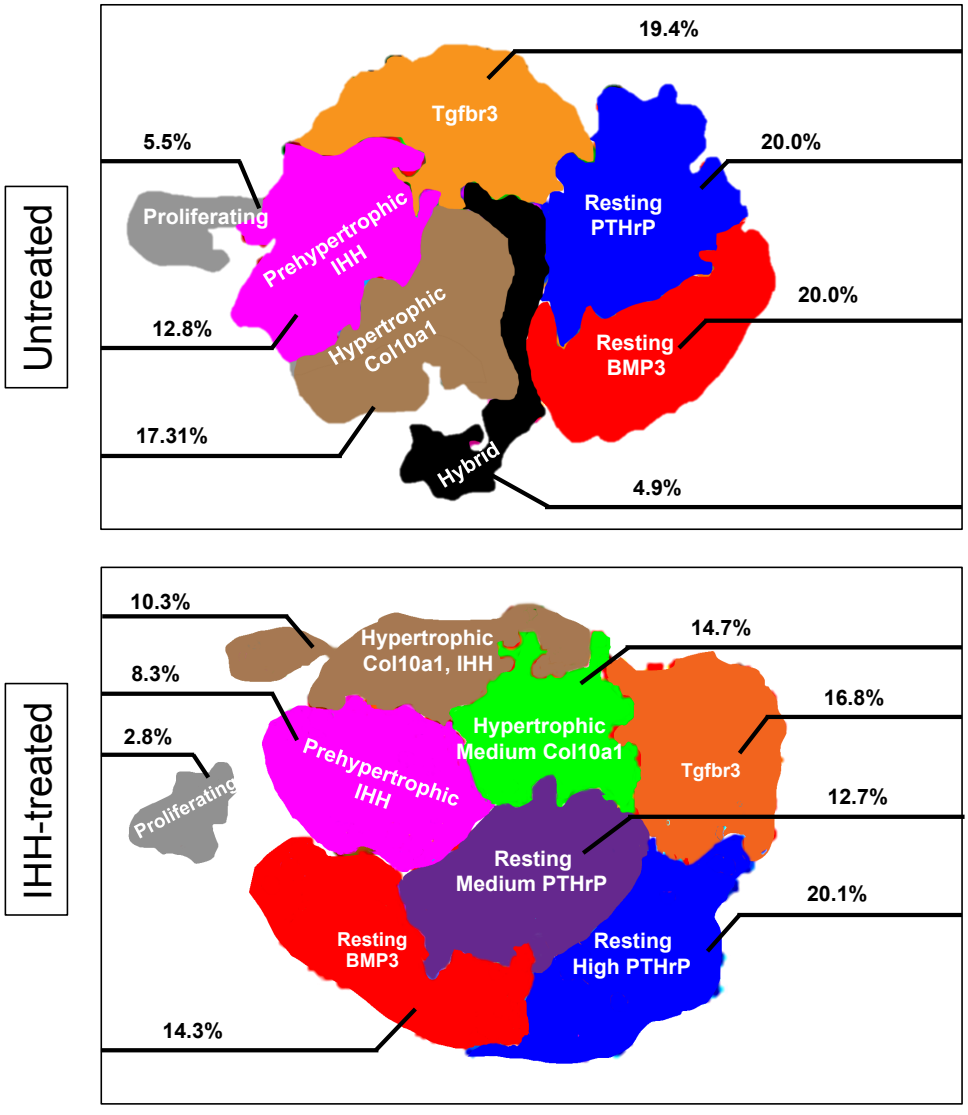
Untreated
19.4%
Tgfbr3
5.5%
20.0%
Proliferating
Prehypertrophic IHH
Resting PTHrP
20.0%
12.8%
Hypertrophic Col10a1
Resting BMP3
17.31%
Hybrid
4.9%
IHH-treated
10.3%
Hypertrophic Col10a1, IHH
14.7%
8.3%
16.8%
Hypertrophic Medium Col10a1
2.8%
Prehypertrophic IHH
Tgfbr3
Proliferating
12.7%
Resting Medium PTHrP
20.1%
Resting BMP3
Resting High PTHrP
14.3%

Novel chondrocyte subtypes identified by scRNAseq:

In addition to categorizing much of the heterogeneous population into known chondrocyte subtypes, the pipeline identified unique subpopulations of chondrocytes that have not previously been appreciated as transcriptionally distinct. High BMP3-expressing resting chondrocytes segregated into a unique cluster in both IHH-treated (366 cells) and untreated (474 cells) samples. This population lies proximal to the high-PTHrP expressing resting cells both in vivo, as well as in t-SNE space (Nilsson 2007, Garrison 2017). In addition to differential regulation of PTHrP and BMP3, analysis of the PC genes that separate these two clusters from one another (Supplemental table 3) by Enrichr analysis shows enrichment of pathways such as Integrin signaling (SPP1, F13A1, TGM2), Extracellular matrix organization (TIMP1, TIMP4, EFEMP1), transcription factors (BHLHE41, KLF2, KLF3, MEF2C, CRIP1, CRIP2), cytoskeletal regulation (TMSB4X, TNNI2, MAP2, MARCKS, S100A6, CALM3), and genes involved in the trafficking or transport of calcium ions. It is possible that these transcriptionally distinct BMP3-high resting chondrocytes represent a previously underappreciated zone in the growth plate. A second novel cluster was identified in both IHH-treated (431 cells) and control (460 cells) preparations that was defined primarily by moderately high expression of SERPINA3N, C4B, TSPAN7, SL6A6, SMOC1, TGFBR3, MLLT4 AND SH2B2. This population is labeled TGFBR3. None of the molecules that define this novel cluster have been localized to a particular zone in cartilage. Many of the markers of this novel cluster are not well studied, particularly with respect to cartilage, and thus little is known about the interactions between them. Nonetheless, analysis of general cartilage marker genes (COL2A1, SOX9) confirm that these clusters express nearly equal amounts compared with resting and proliferative zone clusters (Appendix), indicating that all identified clusters are in fact chondrocytes, and not artifacts due to cellular contamination, warranting further investigation as to whether this phenotype is unique to

alginate culture, or represents a novel population in the growth plate. It remains possible that correcting for cell cycle differences may lead to overlap between this TGFBR3 and proliferating populations. The final novel cluster determined in this experiment was a population of 117 cells in the untreated sample that expressed markers of almost all PC genes ranging from the resting zone to the hypertrophic zone, except that of rapid cell proliferation. This chondrocyte population, which has been labeled hybrid cells, probably arises in response to the unique conditions alginate culture, since in situ hybridization clearly demonstrates spatial segregation of these genes in cartilage. Hybrid cells were not observed in the IHH-treated sample, suggesting that IHH could be overriding a level of stochasticity that chondrocytes experience in cultures where specific signaling cues are absent.

We suspected gene expression changes could result from secondary effects from IHH-induced PTHrP production. Whether a negative feedback loop was active may be manifested in subpopulation-specific transcriptional profiles. PC genes from each group were compared to the gene expression signature of PTH-treated beads (Figure 2c). Proliferating chondrocytes from basal culture exhibited 29 PC genes matching the relative transcriptional levels seen in PTH-treated beads (Supplemental table X), more so than any other cluster. This is expected since PTHrP drives cell proliferation in alginate culture. The number of PTHrP-responsive PC genes fell after IHH treatment almost uniformly across all clusters, as did the number of proliferative cells, suggesting that instead of forming a new PTHrP-responsive subpopulation, IHH primarily acts on PTHrP-responsive cells to stimulate either the hypertrophic program, or PTHrP expression. Analysis of gene expression of ligand and receptor genes for the PTHrP/IHH pathways across all clusters provides proof-of-concept that these pathways are mutually capable of responding to one another, possibly by long-range signaling in the bead (Appendix 4.1).

Figure 4.6: T4-mediated Col10a1 expression patterns may require Smo signaling. Positions of hypertrophic cells are shown as a function of distance from bead center normalized to bead radius. Images from N=2 independent beads per condition were used for image analysis. Left, untreated chondrocytes. Middle, thyroxine treated. Right, thyroxine and GDC-0449 treated. Box plots are superimposed on the raw data such that horizontal line marks median value of dataset, and upper and lower edges of boxes represent 75% and 25% values of dataset, respectively.

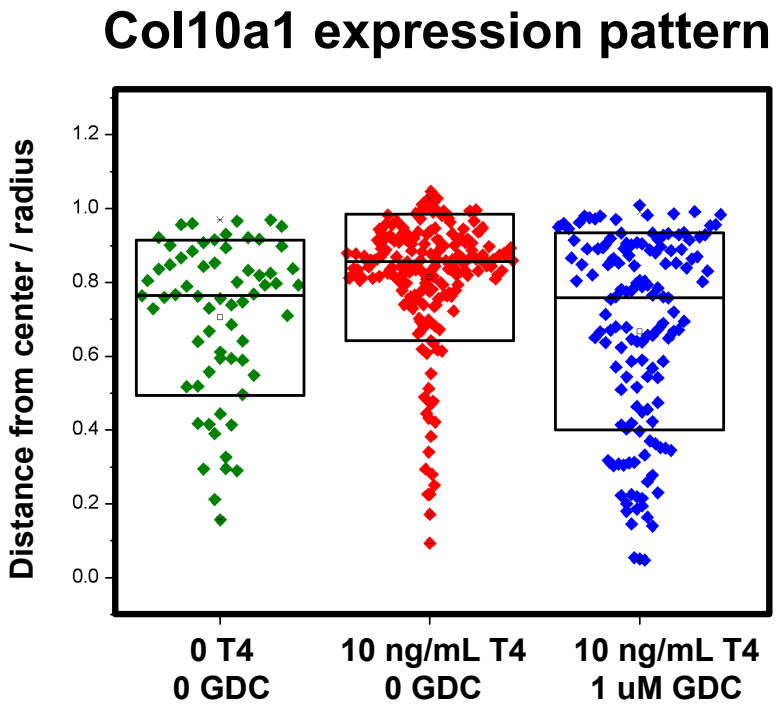
Col10a1 expression pattern
Distance from center / radius
1.2
1.0
0.8
0.6
0.4
0.2
0.0
0 T4
0 GDC
10 ng/mL T4
0 GDC
10 ng/mL T4
1 uM GDC

Similarly to direct stimulation of IHH signaling pathway by exogenous treatment with the ligand, exposure to the hormone thyroxine induced gene expression patterns consistent with hypertrophy localized to the periphery of alginate bead cultures. Thyroxine is thought to drive expression of IHH but has also been reported to actuate BMP signaling in growth plate chondrocytes. Although treatment with BMPs did not lead to similar ring patterns in cultures we analyzed (data not shown), it was unclear whether zonal formation in thyroxine treated beads occurs by BMP-related mechanisms, or via indirect activation of the IHH/PTHrP loop. To test whether IHH signaling mediates patterning actions of thyroxine in alginate, we wrote a custom MATLAB script to quantitatively measure hypertrophic zone formation (Appendix). The script records the position of chondrocytes labeled with DAPI or FISH probes targeting COL10A1, calculates the distance of each cell from the center of the bead, and outputs a distribution that describes the regions of alginate culture where hypertrophic cells are most prominent. Because surface area increases proportional to the square of the distance from the center of a circular cross-section, a slightly top-heavy distribution is expected to occur in conditions where hypertrophic cells are randomly scattered, such as in untreated chondrocytes (Figure 4.5). However using this approach, hypertrophic zone formation is still apparent after thyroxine treatment compared to untreated beads. Beads treated with the small molecule Smoothened inhibitor GDC-0449 exhibited a random spatial distribution of hypertrophic cells resembling untreated beads, suggesting that inhibition of IHH signaling can rescue the thyroxine-mediated effects on hypertrophic gene expression patterns (Figure 4.5). However, whether BMP signaling is involved in the thyroxine response will require further testing, possibly by co-treatment with Noggin.

The results of this study, taken together with the previous chapter, suggest that activation of IHH signaling is sufficient to induce spatial patterns of gene expression that resembles a hypertrophic zone. ISH results showed that after four days of IHH or

thyroxine treatment, Col10a1-expressing cells are restricted to the periphery, while Col2a1-expressing cells remain in the bead core. At this time point, this ring pattern is not observed in the untreated cultures. However, spontaneous peripheral Col10a1 expression is observed in some 2-3 week bead cultures, which matches the tendency for high-density pellet cultures to exhibit edge hypertrophy over long culture periods. Since the mechanism underlying hypertrophy in alginate beads is unknown, determining whether IHH treatment accelerates a preexisting differentiation program, or directly induces hypertrophy, remains a challenge. For example, exposure to normal oxygen tension in culture remains basically a constant factor at the bead periphery, while during culture the bead core may experience varying degrees of hypoxia, which has been shown to inhibit hypertrophy (Leijten 2012), influence early chondrogenesis (Provot 2007), elicit a hedgehog signaling response (Bijlsma 2009), and induce PTHrP expression (Pelosi 2013). Since the growth plate and chondrogenic condensations are typically hypoxic, it will be worthwhile to ask to what degree oxygen tension contributes to the observed gene expression patterns. One way to accomplish this would be to replicate the ISH studies under variable oxygen concentrations, as well as measure patterns of HIF1-alpha expression. Ultimately, chondrocyte signaling behaviors are expected to adapt to the physical conditions of culture, but to what extent this would override explicit signaling cues is uncertain.

Our scRNAseq data suggests that IHH treatment increases the number of PTHrP and Col10a1- expressing chondrocyte subpopulations. Alternative methods will need to be employed to unequivocally confirm their identity by mapping activity of hypertrophic functions such as volumetric swelling, alkaline phosphatase, and metalloproteinases. However, the dataset defines these clusters by multiple known marker genes, as well as a downregulation of cell-cycling genes, suggesting that Col10- and PTHrP- expressing clusters are likely to be similar to, if not bona-fide hypertrophic and resting chondrocytes,

respectively. In normal cartilage development, IHH signaling can directly stimulate hypertrophy, but is also necessary for formation of a stable PTHrP expression domain, which then feeds back to spatially restrict hypertrophic differentiation. If the chondrocyte response to IHH in the context of alginate in any way mimics native chondrocytes, induction of PTHrP-expressing chondrocytes could be a key event.

However, our results suggest that even in untreated cultures, endogenous PTHrP expression significantly increases over time, and that chondrocytes in basal alginate culture behave in a manner consistent with a PTHrP response (activation of cell cycle genes, upregulation of S-phase, repression of hypertrophy-associated and prehypertrophy-associated genes). Further studies may clarify when this trend of spontaneous PTHrP expression plateaus, since the available data only addresses the first week in culture. The factors causing this expression are still unknown; if beads cultures naturally become hypoxic within a few days, PTHrP expression may be expected to gradually increase. However, the encapsulation protocol does include prehypertrophic cells from the growth plate that may continue to secrete IHH during culture.

It is important to understand whether the PTHrP/IHH interactions are fully intact in alginate. Careful mapping of spatiotemporal dynamics by 3D reconstructions of daily FISH applied to untreated cultures may reveal small domains of PTHrP and IHH-expressing cells that grow and collapse according to the local signaling. The use of Smoothened null cells, or treatment with GDC-0449 in alginate beads are both ways to test whether chondrocytes unable to respond to either endogenous or treatment-induced production of IHH ligands maintain stable PTHrP domains. If PTHrP is not lost in such conditions, this experiment may reveal alternative mechanisms by which chondrocytes regulate differentiation rates. One possible pathway could occur via through BMPs, treatment of which led to significant increases in bead-wide proliferation rates that

matched PTHrP responses. NGS analysis of PTHrP treatment revealed differential expression of multiple BMP inhibitors CRIM1 and GREM1. Testing transcriptional responses to BMP activation will be crucial to identify if additional feedback exists among these signaling pathways.

The context of alginate bead culture combined with the use of omics technologies to investigate the bulk and single-cell transcriptional effects of signaling factors, as well as FISH-based assays to quantify spatiotemporal patterns of gene expression, is proving to be a powerful system in which to dissect the mechanisms that regulate chondrocyte differentiation. Future work replicating the scRNAseq results will be necessary to understand specifically how consistent chondrocyte responses are at the single cell and subpopulation levels. For example, although the analyzed bead cultures roughly match the expected distributions of chondrocyte subtypes based on in situ hybridization of native cartilage (Romereim 2014b, Ahrens 2009), standard error values based on multiple replicates will be crucial to fully trust the percentages each subpopulation occupies, and test how much variance to expect before drawing conclusions about differences in cell count. Still, it will be exciting to proceed by applying such a fine-grained approach towards cultures treated with other signaling factors such as thyroxine, BMP proteins, and Wnt5a to discover novel subpopulation-specific transcriptional crosstalk that defines the regulatory zone-patterning network responsible for constructing a growing cartilage tissue.

MATERIALS AND METHODS

Next generation RNA sequencing workflow:

RNA from four beads was pooled to generate the RNA samples for NGS. 100nM PTH-treated and untreated 1-day bead cultures were placed in PBS containing 50mM EDTA

and 0.01% BSA to dissolve alginate for 5 minutes at 37C before pelleting by centrifugation at 125xg for 5 minutes. Cell pellets were lysed with chilled TRIZOL and RNA was immediately isolated according to manufacturers protocol. RNA was tested on the Bioanalyzer for RNA quality and all samples displayed RIN values greater than 9.0. A minimum of 1 ng RNA for each sample was submitted to the Genomic Sequencing Core Facility at the University of Nebraska Medical Center. cDNA libraries were created using Illumina TruSeq RNA library prep kit prior to sequencing on the Illumina NextSeq550 at a depth of ~20 million paired-end reads (150 base). Six total cell samples were sequenced using RNA-seq method (3 samples were from the control group, 3 samples from PTH-treated group. Read quality was assessed using FASTQC (version 0.11.5). Reads were mapped to the mouse genome “mouse_GRCm38”. RNA-seq data were quantified and normalized in TPM values, and available for 50600 genes. To normalize for sequencing depth and gene length we calculated TPM values by dividing the read counts by the length of each gene in kb to generate reads per kilobase (RPK), dividing total RPK values in each sample by 1,000,000 to calculate a scaling factor, and dividing RPK values of each gene by the scaling factor. 17791 genes having nonzero TPM values for at least one of the two groups were kept and each expression value is log2 transformed for later analysis. Differential expression analysis between two groups was conducted using the limma package in R (R Development Core Team 2004, Richie 2015). Multidimensional scaling plot of distances between gene expressions profiles were used to examine the relationship of samples (Smyth 2004). The Bejamini-Hochberg method was used to control the false discovery rate (FDR) to be no more than 0.05 (Benjamini and Hochberg, 1995). Differentially expressed genes (corrected $p < 0.05$) were entered into Enrichr, an online tool that utilizes Fisher’s exact test to identify biological functions and pathways that are enriched in a list of genes. TPM values were submitted to ingenuity pathway analysis (IPA), software that uses individual known

relationships from the literature to construct causal networks underlying differential gene expression between control and PTH-treated chondrocytes, and the core analysis capability of IPA was utilized to generate the list of predicted upregulated and downregulated pathways.

Single cell RNA sequencing workflow:

Chondrocytes from four beads from each condition were pooled to generate the cell samples used for scRNAseq. 100ng/mL IHH-treated and untreated 4-day bead cultures were placed in PBS containing 50mM EDTA and 0.01% BSA to dissolve alginate for 5 minutes at 37C before pelleting by centrifugation at 125xg for 5 minutes. The cell pellet resuspended with cartilage culture media and passed through 5-mL filter-cap polypropylene Falcon tube to remove debris and cell aggregates. Cells were counted by haemocytometer to achieve concentrations of 1000 cells/uL. Trypan blue was used to ensure viability of all captured cells. Cells were placed onto a 10X Genomics chip for single-cell capture and barcoding. cDNA libraries were quantified for using qPCR to dilute to 1pmol for sequencing on the Illumina NextSeq 550. To generate fastQ files from raw sequencing data of single chondrocyte libraries, we used the software called Cell Ranger v 2.0.0, freely available from 10x Genomics website (https://www.10xgenomics.com/solutions/single-cell/). This pipeline uses the command “cellranger mkfastq” for demultiplexing, and a command “cellranger count” for alignment, filtering, and UMI counting. This pipeline outputs cluster plots that are visualized in the software Loupe Cell Browser, also available from 10x Genomics. The algorithm for clustering performs a modified principal components analysis that identifies genes that are coordinately expressed in subpopulations relative to the rest of the dataset to iteratively reduce matrix dimensionality. The program outputs a t-SNE scatterplot that can be divided into clusters. Options are given for k-means or graph-based method for

biased or unbiased clustering. Unbiased graph-based method was chosen for analysis, although selecting k values equal to the cluster numbers generated by graph-based method outputs nearly identical principal component genes. Individual gene expression visualization and principal component heat maps of clusters were also performed in Loupe.

Post-clustering analysis of scRNAseq data:

For both IHH- and untreated samples, tables of PC genes, their relative expression for each cluster compared to the rest of dataset, and p-values were analyzed in Excel to identify unique versus shared PC genes across total datasets, to locate individual clusters that share identity (common PC genes in clusters across IHH- and untreated samples) and to match clusters with known cartilage zones based on PC genes. Once identification of clusters was accomplished, number of cells residing in each cluster could be found from Loupe Cell browser to compare differences between IHH-treated versus untreated samples.

CHAPTER 5: FUTURE DIRECTIONS AND CONCLUDING COMMENTS

FEEDBACK AMONG FORCES, TOWARDS POLARITY

Every step of cartilage formation, including the elaboration of proliferative zone columns, occurs within the context of the cartilage extracellular matrix (ECM). In cartilage, ECM constitutes the entire external environment of chondrocytes for most of their lifetime (with the exception of the direct cell-cell adhesive contacts that follow cell divisions). As such, nearly every signaling factor relevant to chondrocyte behavior is potentiated by the physical, chemical, and topological properties of the ECM. In fact, genetic evidence suggests both molecular composition and organization of the ECM are crucial for the creation of fine cartilage architecture. However, at this time it is difficult to decouple novel regulatory functions of ECM network from the previously identified permissive roles in the general maintenance of chondrocyte homeostasis.

Work from this dissertation sheds a new light on the involvement of chondrocyte-environment interactions in the production of growth vectors. Detailed tracing of the actomyosin machinery suggests that cytoskeletal dynamics at the cell-ECM boundary plays an important role during chondrocyte rotation, and suggests that positioning of myosin motor protein is responsive to Wnt5a/Ror2 signaling and integrin adhesion. One implication is that positioning and assembly of the proper ECM molecules is needed to properly engage the cytoskeleton via integrins, but many questions stand in the way of testing this directly. Primarily, how chondrocytes differentially interact with the cartilage ECM components, and the extent to which these specific interactions affect cytoskeletal organization, cell mechanical properties, cell adhesion strength, and resulting cell body movement, are still poorly elucidated.

In order to dissect the signaling interplay between growth factor signaling and cell-ECM interactions that were hypothesized to drive cartilage architecture formation, we

developed an in vitro model of growth plate cartilage using alginate hydrogel bead culture and show that chondrocytes in alginate can interact with components of the IHH/PTHrP signaling loop and are capable of generating a pericellular matrix *de novo*. This discussion outlines how our novel culture system is being used to develop an array of tools that can begin to probe the interactions between growth factor signaling and chondrocyte mechanobiology during critical processes such has the formation of zones and columns in the growth plate cartilage, and how the new information could be incorporated into the existing knowledge.

In Chapter 1, knowledge in the literature about the contributions made by forces at levels ranging from the molecular to the organismic was reviewed. From this, it seems that disrupting mechanics at different length scales have unique ramifications for cartilage architecture and growth, but that cartilage-extrinsic mechanics are secondary to cartilage-intrinsic mechanics. Tissue-level forces within the extracellular matrix, and the cell-level actions of integrins, cadherins, and the actin cytoskeleton could be basic units in a simplistic physical model for the rearrangement mechanism underlying cartilage morphogenesis. Do these molecules cooperate with signaling and the mechanical environment to give rise to tissue structure?

Do cell-cell junctions mechanically integrate neighboring cells to drive patterning?

Much of the knowledge about the relationship between cellular mechanics and morphogenesis are found in the literature surrounding elongation and invagination of epithelial tissue. Epithelial cells attach to a basement membrane by integrin adhesions and acquire apical-basal polarity via that association (Scarpa 2016). On the apical surface, cell-cell attachments are made via E-cadherin-based adherens junctions that transduce cytoskeletal-derived forces between cells (Lecuit 2015). Cadherin complexes

experience constitutive endogenous tension via association with actomyosin, but this tension spikes in response to external mechanical stimuli, driving cadherin clustering at cell junctions (Borghi 2012). Ultimately, maturation and remodeling of the adherens junction relies on positive feedback between cortical tension-dependent cadherin clustering and cadherin-dependent myosin recruitment to junctions (Yang 2015, Delanoe-Ayari 2004, Levayer 2013). Distinct modes of tissue morphogenesis are achieved by regulating the size and geometry of cadherin-mediated adherens junctions that connect epithelial cells (Lecuit 2015). The two major modes driving epithelium shape changes are tissue elongation, which is founded in cell intercalation (neighbor exchange), and tissue invagination, which is driven by apical constriction. In both situations, spatiotemporal control over actomyosin tension drives a pulsatile ratchet-like mechanism that gradually remodels adherens junctions to implement cell- and tissue-wide shape changes (Bertet 2004, Rauzi 2010, Munjal 2015, Collinet 2015). Tissue extension utilizes a self-organized biomechanical network to drive cell shape changes (Munjal 2015). In this system, two different pools of myosin (medial and junctional) flow back and forth across different cell surfaces in a feedback loop that potentiates the activities of upstream cytoskeletal regulators Rho1 and Rok (Drosophila analogs to mammalian RhoA and ROCK. Engagement of actomyosin promotes tension and Rho/ROCK, but high levels of myosin concentration negatively feeds back to reduce further tension (Munjal 2015, Ponik 2013). Such pulsatile behavior is governed by myosin phosphorylation dynamics downstream of Rho, as well as advection due to myosin-induced contraction of F-actin. In other words, Rho/Rock signaling is regulated by the physical outcomes of actomyosin (force and contraction). Together, these mechanical behaviors of the cytoskeleton regulate epithelial morphogenesis in a wide range of developmental contexts.

Figure 5.1: Schematic model of cytoskeletal dynamics hypothesized to drive column formation. A) Two actin-based force-generating mechanisms are shown. Left, actions of ARP2/3 complex-mediated actin branching that drives protrusions shown below (B, left cell). The protrusion forces are directed towards the growing actin branches. Right, actomyosin contractility drives production of cellular tension. Pulling forces may effectively originate from points where actin filaments are connected to the cell surface. Green background and arrows illustrate direction of cortical flows. B) Three-way fork between rotating daughter cells and ECM. Actin polymerization protrudes to define the direction of rotation (left cell) while integrin-anchored myosin provides force to pull the cadherin interface periphery rightward. As cadherin interface expands, integrin adhesions are broken, and myosin is briefly sent to the junction before recycling back to the cortical surface. Later, new integrin adhesion sites may form. C) Three-way fork between separating chondrocytes and newly secreted ECM. Myosin-rich integrin surfaces overtake the shortening cadherin junction. Similar dynamics may be involved involving cortical, junctional, and medial pools that flow as tension is produced.

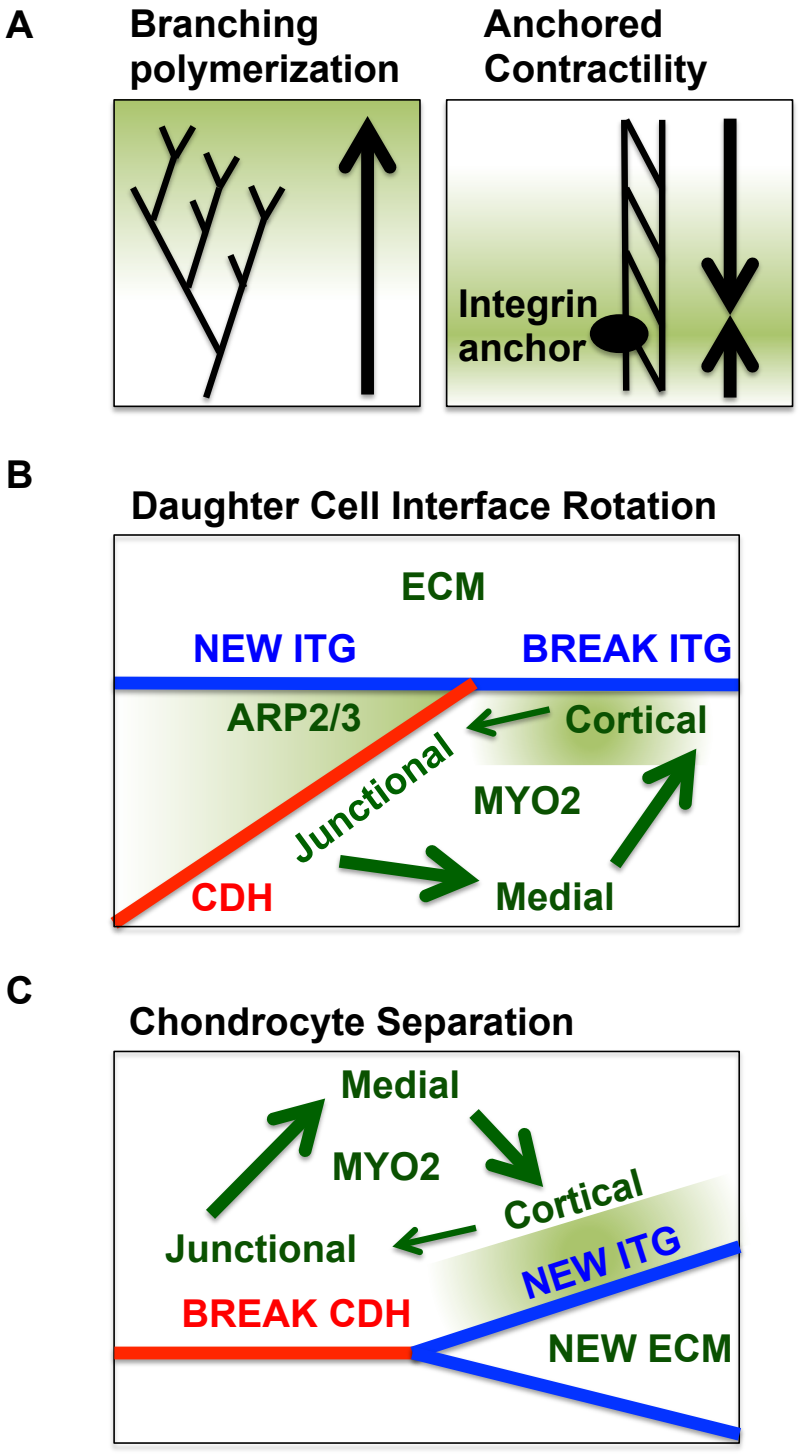
A
Branching polymerization
Anchored Contractility
Integrin anchor
B
Daughter Cell Interface Rotation
ECM
NEW ITG
BREAK ITG
ARP2/3
Cortical
Junctional
MYO2
CDH
Medial
C
Chondrocyte Separation
Medial
MYO2
Cortical
Junctional
NEW ITG
BREAK CDH
NEW ECM

Hypothetical model of cytoskeletal dynamics during chondrocyte column formation

If the cytoskeleton plays an important role in chondrocyte column formation, it probably does not exactly mirror the epithelial situation. However, it is a useful starting paradigm that can be applied to cartilage to envision possible traits of the mechanisms underlying cell behaviors. For example, In addition to medial and junctional pools, our studies of actomyosin localization and activity suggest an alternative active pool in chondrocytes: the cortex where actin physically associates with the integrin adhesome to connect cells to the ECM. Loss of junctional myosin, and high levels of cortical myosin were highly correlated with cell rearrangement. Non-column forming cells such as integrin-inhibited and Wnt5a/Ror2 mutant cartilage displayed a preference for junctional myosin. However, minority populations were observed in all conditions that defied this pattern (e.g. small number of proliferative chondrocytes mid-rotation with adherens-junctional myosin). One interpretation of this result invokes epithelial morphogenesis by envisioning cytoskeletal flows downstream of myosin activity and/or actin polymerization, resulting in highly dynamic movement of network components throughout the cell cycle. In this hypothetical model, the initial state of the contractile apparatus is junctional, as cytokinesis-associated tension concurs with cadherin zippering. Afterwards, advection due to motor activity exchanges actomyosin across multiple pools, where differential affinity for each cell surface determines relative workload at the cortical (versus junctional/medial) pool to control the rate of cell rearrangement. Live cell imaging of growth plate explants labeled with LifeAct probes and/or fluorescently tagged myosin could be one way to begin to visualize the predicted cytoskeletal dynamics. One expectation is that in the resting zone, concurrent expression of junctional, cortical, and medial pools would create a force balance that does not favor movement. The use of molecular tension sensors during the live imaging experiments would be an important experiment to confirm this

prediction (Wang 2011c). Conversely, each pair of rearranging daughter cells in the proliferative zone would be biased towards cortical myosin to a level that matches the observed population levels that were measured by immunofluorescence (70%, which in this model would correspond to 3.5 out of 5 total hours). This metric, taken across a field of chondrocytes, could finely map cytoskeletal workload as a function of position in the cartilage. Such a map could be used to locate inflection points for calculating the slope of graded intermediates. Using this method to study cytoskeletal management profiles at the single-cell level could then identify a specific population between the resting and proliferative zones that is transitioning towards a column-forming phenotype.

Single-cell sequencing identifies candidate transition zone:

Within the zonal array of the growth plate, a predicted “transition zone” might display some characteristics of resting cells, but activate cytoskeletal regulatory mechanisms that resemble column-forming chondrocytes. The early live imaging studies that characterized chondrocyte rotation did in fact report a population of chondrocytes in between resting and proliferative chondrocytes that would begin to rotate, but halt early in the process before completely rearranging into columns (Romereim 2014b). Additionally, these experiments demonstrated that some late resting chondrocytes were capable of complete, oriented cell rotation independent of prior cell geometry, but that mother cell shape was maintained by daughter cell cortex throughout the entire rearrangement process. From this, it was concluded that an ECM remodeling phase would be necessary to achieve the flattened and elongated cell form observed in the proliferative zone. Transcriptional profiling of chondrocyte subpopulations in alginate revealed two clusters that largely match a resting zone identity, but are defined by alternative genes that may act as paracrine signaling outputs, PTHrP versus BMP3. PTHrP-expressing chondrocytes reside near the epiphyses in the most distal

compartment of the resting zone (Ahrens 2009), whereas BMP3 expression has been observed by *in situ* hybridization in resting cells proximal to the proliferative zone columns (Nilsson 2007). Comparing gene expression signatures across these clusters, if they end up being comparable to the in vivo context, reveal major differences in ECM metabolism and adhesion. Decreased TIMP1 and TIMP4 expression indicates that BMP3-expressing chondrocytes lift inhibition of matrix metalloproteinases, while beginning to secrete new ECM molecules such as Osteopontin, the calcium-binding EFEMP1, and the fibronectin-fibrin cross-linker F13a1. Single-cell RNAseq needs to be repeated using native growth plate cartilage tissue in future studies, because these processes could account for the matrix-remodeling process predicted to be a crucial step towards column formation. Secondly, increased expression of many calcium-sensitive actin regulators in the BMP3-high cluster versus the PTHrP cluster is consistent with a model where position-dependent cytoskeletal reorganization gradually prepares chondrocytes to form columns. Together, these results suggest BMP3 could be a marker of the predicted “transition” zone.

Could there be a novel role for calcium signaling?

Our alginate culture system was analyzed by transcriptomics methods to investigate the actions of the IHH/PTHrP signaling loop. Both bulk- and single-cell RNA sequencing datasets hint that it may be fruitful to revisit the role of calcium signaling in the growth plate as a possible driver of actin dynamics. Calcium/Calmodulin-dependent kinases (CAMK), which are predominant effectors of calcium signaling, have been studied in the growth plate (Li 2011). These proteins contain numerous phosphorylation sites that promote self-assembly into multimeric holoenzyme structures with diverse kinase activities. In cartilage, CAMKII is primarily phosphorylated in the prehypertrophic zone

and regulates chondrocyte proliferative potential by promoting hypertrophic differentiation, and both PTHrP and WNT5a negatively regulate activity of CAMKII. However, CAMKII phosphorylation can be visualized in some resting and proliferative chondrocytes using high-sensitivity methods, and *in situ* hybridization studies of cartilage maturation in the presence of CAMKII inhibitor KN93 shows disruption of PRELP and COL9A1 expression in the resting/proliferative regions of cultured metatarsals. Further, CAMKII overexpression in chick growth plate results in loss of cortical actin in proliferative chondrocytes, which can be countered by treatment with PTHrP. It is worth investigating whether junctional/cortical myosin residencies depend on sensitivity to calcium signaling. This connection would provide an alternative interpretation of the live imaging studies that initially established the importance of the daughter cell cadherin junction (Romereim 2014). These experiments involved manipulation of free calcium and cadmium concentrations, which could directly disrupt actomyosin dynamics independently of cadherin function.

Does feedback among integrin and cadherin cell surfaces control cell organization?

If cadherins are a necessary part of the mechanism that drives column formation, but do not directly drive chondrocyte rearrangement, there may be important feedback between cell surfaces. Generally, biological systems that contain multiple adhesion surfaces usually feature crosstalk among them, and particularly cell-cell junctions have several ways of regulating cell-ECM interactions. During Xenopus and zebrafish convergence extension, cadherin-mediated actomyosin tension activates fibronectin-bound integrins (Dohn 2013, Dzamba 2009), inducing a conformational change in fibronectin to expose cryptic residues that promote fibril assembly and alter cell-ECM adhesion dynamics. In these systems, cell cohesion-driven matrix organization is

needed to power the cell intercalation underlying tissue extension. Cadherins can also stabilize integrin-integrin homodimers that sequester integrins in an inactive conformation, restricting fibronectin assembly to cell surfaces depleted of cadherins (Julich 2015). These examples are mostly taken from systems where the functioning forces are cumulatively derived from many adherens junctions across a field of cells, whereas chondrocytes are limited to pairs. Because myosin is not enriched at the cell-cell interface during rotation, it is unlikely that tension produced via cadherin adhesion could drive cell movement. However, the observation that daughter cell interface length significantly increases throughout rotation intuitively suggests that this process involves locally remodeling the cell-ECM boundary at three-way forks where peripheral junction of both daughters meets the pericellular matrix (one possible configuration is shown in Figure 5.1). Within this nanoscale domain, each cell on either side of the junction could, in theory, cooperate to produce directional movement using distinct physical mechanisms: the protruding forces of ARP2/3-mediated branched actin polymerization on one daughter, and actomyosin contractility on the other daughter, pulling the interface in the same direction. While polymerization is inherently polarized towards barbed end of actin filament, contractility need not be unless an anchor is present (Huber 2011). Either way, this coordination would break integrin-ECM bonds and lengthen the cadherin junction; as a consequence, cortical actomyosin would be redistributed to junctional or medial pools. Because these chondrocyte protrusions are only visible at the ultrastructural level, live imaging and standard immunofluorescence both are not sufficient to examine this specific relationship. Advanced electron microscopy methods utilizing ascorbate peroxidase (APEX) to detect protein localization with nanometer resolution will be very beneficial to understand the cytoskeletal and adhesion dynamics occurring at the extreme junction periphery (Martell 2012). For example, it is difficult to predict whether the protruding daughter would form new integrin adhesion sites in the

same position immediately after procession, and if so, whether replacement cell-matrix associations are identical or distinct from their precursor. Using EM-resolution microscopy, tags of specific integrin binding interactions, combined with selective binding inhibition may be able to resolve whether rearrangement endows cell surfaces with access to novel microenvironmental cues, and may provide a clue towards characterizing the specific functions of ECM domains that surround daughter chondrocytes. Similarly, whether cadherin concentration at the membrane is diluted, or held constant during lengthening is unknown but the latter would imply an active trafficking or recruitment mechanism that would be manifested by homodimer-resolution microscopy. In the above scenario, cadherins and integrins are either directly competing for access to the actin filaments, or passively antagonistic, both passengers in a mechanism driven by cytoskeletal interplay.

Do chondrocytes embed anisotropic signals in the cartilage matrix?

Following chondrocyte rearrangement, daughter cells begin to detach from one another and secrete interstitial pericellular matrix. At this moment, the point between the shortening cadherin junction and the newly assembled ECM becomes yet another three-way fork that illustrates cadherin/integrin feedback on the cell surface (Figure 5.1c). Cortical myosin is highly activated at the site of disengagement. It is unclear whether force is required to pull apart the cadherin surface, which would suggest that myosin may be directly involved in cell separation, or if ECM secretion sufficiently signals towards cadherin internalization for dismantling the junction. One interpretation is that the shortening cadherin junction is being replaced with sites of active integrin adhesion marked by cortical actomyosin. If myosin simply marks integrin adhesion sites, the observation that myosin lingers interstitially after total separation before relocating to

lateral arcs would indicate that chondrocytes execute a specific order of ECM composition that depends on the final position of the cell-cell junction following rotation. Aside from the previously discussed and numerous examples of anisotropic ECM patterning in cartilage in vivo, analysis of ECM development in alginate beads demonstrates that chondrocytes are capable of building specialized and specifically localized ECM structures *tabula rasa*: single chondrocytes cultured in alginate build concentric rings of collagen 6 that would at first suggest a radially symmetrical matrix, but after cell divisions new collagen 6 is secreted in a way that strikingly resembles the myosin distribution at separating chondrocytes in vivo (Figure 5.2). Further, while collagen 6 patterning is symmetrical across the daughter cell interface, the fibronectin matrix develops anisotropically, nearly always being secreted by a single daughter cell into an arc-like structure that points away from the paired daughter (Figure 5.2, e-g). These observations, in connection with what we are learning from live imaging studies and the myosin staining experiments, suggest that cell division is tightly linked with chondrocyte polarity, possibly bestowing asymmetry to each pair of daughter cells, and this asymmetry inherent to chondrocytes eventually manifest through ECM production. Testing how the interstitial compartment forms might first depend on whether disrupting cadherin adhesion would restore complete radial isotropy. Alternatively, the final position of mitotic spindle could be the information used to assign unique network construction to medial versus lateral cell surfaces. However, an additional symmetry-breaking mechanism is needed to account for differential fibronectin deposition between daughter cells. A parsimonious hypothesis is that daughter cells become stochastically

Figure 5.2: Anisotropic ECM patterning in alginate bead culture. Images shown are representative of hundreds of cells observed across 3 independent experiments. Although quantitative statistics are unavailable because the complexity of matrix deposition and formation of cell clusters are not amenable to standard image analysis programs, these are major and noteworthy patterns among the total ECM-depositing behaviors of alginate-encapsulated chondrocytes. A-D) Immunofluorescence showing Collagen 6 deposition (red) in daughter cells appears reminiscent of myosin localization patterns. Nuclei are shown in blue and actin is shown in green. A) Multinucleated chondrocyte preparing to divide. Collagen 6 has been deposited in a radially symmetric ring around the cell body as previously shown. Scale bar = 3 um. B-C) Daughter chondrocytes in the process of cell separation. Collagen 6 is deposited strictly at the new separations. D) Completely separated daughter cells share a Collagen 6 – rich interface, breaking radial symmetry. Scale bar = 5 um. E-G) Immunofluorescence staining showing fibronectin (yellow) deposition builds up in a single direction over time. E) Day 1 beads show little to no fibronectin deposition. Scale bar = 8 um. F) Day 4 beads exhibit daughter cell pairs where one cell has built a fibronectin matrix laterally (arrowheads). G) This accumulation of fibronectin continues to increase for many days in culture. Here, the fibronectin matrix at day 14 is shown.

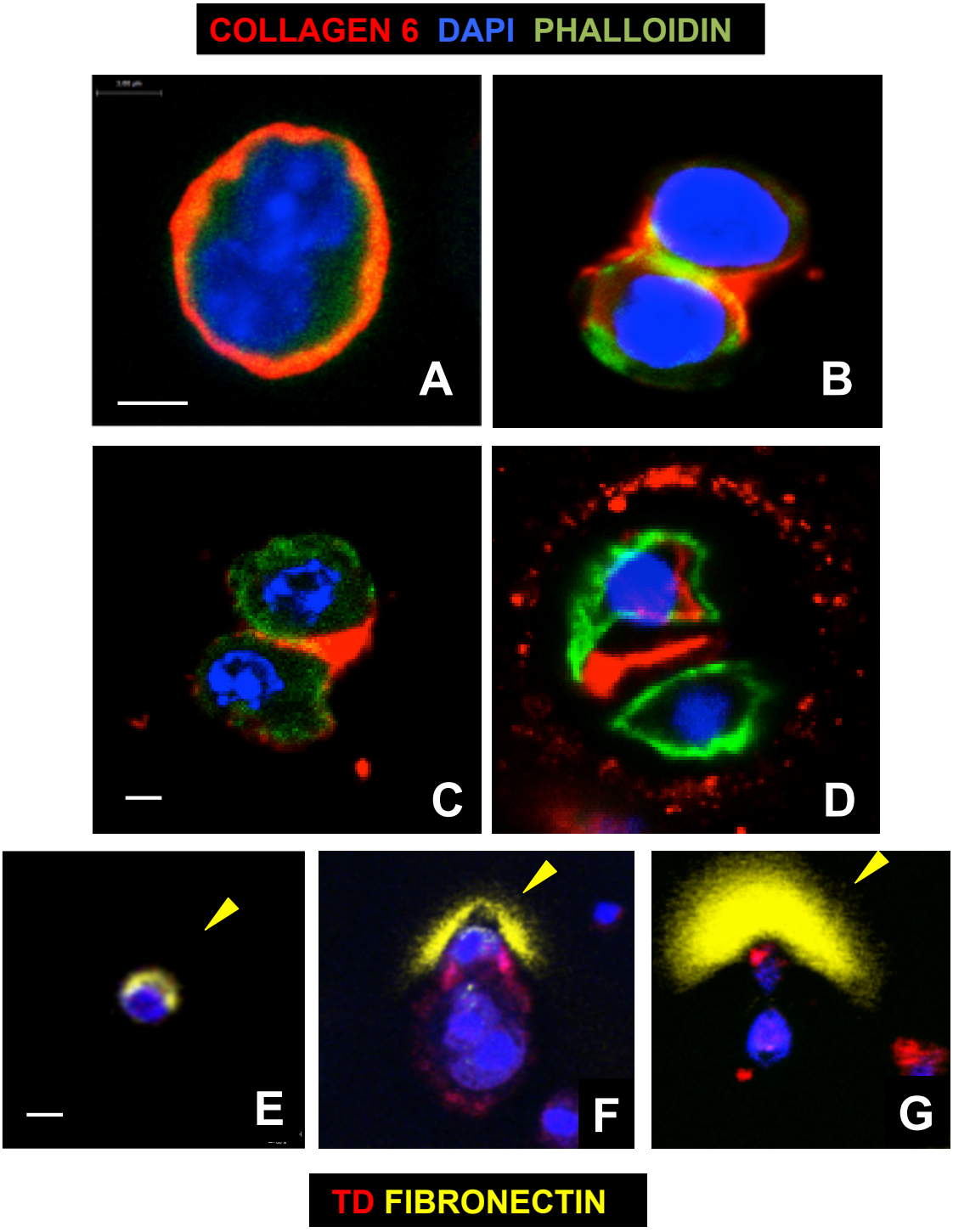
COLLAGEN 6 DAPI PHALLOIDIN
A
B
C
D
E
F
G
TD FIBRONECTIN

distinguished by inheritance of the midbody, which is the densely compacted tubule-based organelle representing the vestiges of the contractile ring after cytokinesis. Possession versus absence of the midbody could generate “leader” and “follower” cells whose relative position would determine the clockwise or counterclockwise direction of rotation, which seems to occur stochastically (Romereim 2014b). Crosstalk between the midbody remnant and cortical myosin flows has been documented to participate in dorsal-ventral axis formation in early *C. elegans* embryos (Singh 2014) and adherens junction formation in the Drosophila dorsal thorax pupal epithelium (Herszterg 2013). Interestingly, daughter cells in monolayer chondrocyte cultures have been observed to produce starkly asymmetric levels of myosin activity (Appendix 5.1). Because fibronectin among other ECM proteins requires mechanical stimulation by the cytoskeleton for proper construction of the supramolecular network, cortical myosin activity might well be a critical step in assembling daughter-cell specific structures in the cartilage matrix. Cell cycle synchronization of alginate-cultured chondrocytes, in conjunction with cytoskeletal inhibitors such as blebbistatin, could be used to ask whether cell contractility affects ECM production routines in newly divided daughter cells.

What could be the role of such ECM patterning? Why would chondrocytes spend the effort to create an anisotropic matrix? The answer may lie in understanding the roles of each ECM component within the context of the overall biomechanical landscape of a chondrocyte, and their ability to support short-range mechanical signaling. One major thrust to identify the importance of outside-in mechanotransduction for tissue organization has utilized the basal surface of epithelial sheets as a model system. Studies of epithelial cell pairs showed that cell-ECM traction force controls the orientation of the division plane to specify the position of daughter cell interface (Thery 2005), and can modulate endogenous tension at cell–cell contacts to promote cell shape changes (Maruthamuthu 2011, Ng 2014). Other studies show that integrin-dependent

adhesion to fibronectin or collagen can negatively or positively impact cadherin cell adhesion depending on the context (Robinson 2002, Robinson 2004, Al-Kilani 2010). Recently, it was shown that populations of collectively migrating epithelial cells could be induced into various “tissue-scale” organizational regimes in vitro by varying substrate stiffness (Ng 2012, Ravasio 2015). In these studies, tuning cell shape change and lamellopodia-driven motility at the edges of colonies caused by cell-ECM mechanotransduction produced a direct effect on emergent morphogenetic cell behavior. Interestingly, softer substrates induced higher-scale actin organization in the form of multicellular cables, while stiffer substrates actually allowed propagation of polarity by a front-back Myosin II gradient dependent on intercellular force transmission. This suggests that the mechanical environment integrates with cell contractility and cell-cell adhesion in a feedback loop, producing a “tug of war” between cell-cell and cell-ECM tensile forces to regulate collective migration, and causing qualitative differences in the pattern-forming properties among these cells. In essence, the ECM patterning of chondrocytes, based on precise positioning of adhesion strengths and differential engagement with cytoskeletal components like myosin and ARP2/3, could influence where the division plane begins, whether and how fast it rotates, and where the rotation will cease.

How do growth plate chondrocytes respond to physical cues?

One implication of the above information is that rearranging chondrocytes may have multiple sensory mechanisms to read positional cues. In addition to sensing concentration gradients of diffusible ligands, haptic perception of the solid-state environment could result in local mechanical responses, which may be modulated by extrinsic and globally acting cartilage-intrinsic forces. Mediators of this system may

directly observe mechanical properties of the environment, or require membrane deformation to become active. To investigate whether growth plate chondrocytes are capable of responding to compressive stimuli, the alginate culture system was used as a basis for engineering a microfluidics-based pneumatic cell compression device (manuscript in preparation). This device functions by encapsulating chondrocytes in cylindrical pillars of alginate attached between parallel glass plates. Compressive force is delivered by controlling airflow through five parallel channels to inflate PDMS balloons that compress each pillar according to balloon height. Confocal microscopy-based visualization of compressed chondrocytes confirmed balloon height-dependent cell deformation ranging from 7% to 19% strain. Single-cell mechanical profiling of chondrocytes using atomic force microscopy (AFM) was employed to ask about the relationships between environment, mechanical stimuli, and cell stiffness (for detailed methods, see Lee 2017). In these experiment, Poly-L-Lysine was used as a default substrate for AFM testing, and was compared to other ECM coatings to detect substrate-dependent effects on cell mechanical properties. The role of compression was tested by culturing chondrocytes in alginate with or without dynamic compression (1 hour, 1 Hz, 19% strain) before seeding onto Poly-L-Lysine for AFM measurements. Chondrocytes simply cultured on standard poly-L-Lysine coated plates exhibit Young's Modulus (*E*) distribution peaking around 0.3 kPa (n=70 cells, Figure 5.3a). The adhesive environment was tested using chondrocytes cultured on gelatin, Collagen 2, and Fibronectin-coated surface. Gelatin and Fibronectin cultured cells display a slightly different mechanical profile with smaller range, increased average, and only single peaks centered at 0.5 kPa, while Collagen 2 seems to lead to cell stiffening, although this may be due to the additional hour of culture time prior to AFM testing in this sample. Effect of culture dimensionality was controlled using cells cultured in alginate compression device (without compression) prior to AFM testing. These cultures display

an increase in overall cell stiffness (mean of 0.78 +/- 0.5 kPa, range from 0.1-2 kPa, peaks centered at 0.3 and 1.3 kPa, n=76 cells), opening up the possibility that the alginate environment mechanically stimulate chondrocyte subpopulations. However, cells that are compressed to 19% strain in the chip are much softer than uncompressed controls (average E = 0.56 +/- 0.33 kPa, distribution ranging from 0.1-1.6 kPa with only a single peak at 0.3 kPa, n=65 cells). Interestingly, repeated AFM indentation generates local mechanical response in single cells, causing them to stiffen further with each measurement. This observation has been noted before in chondrocytes but not other cell types (personal communication, Donghee Lee). One way to interpret this seemingly paradoxical data is the possibility of dual mechanosensory systems that allow chondrocytes to differentiate between local versus globally applied forces. How could such contradictory responses beget from nearly similar induced strain rates? One explanation takes into account the high osmotic pressure of cartilage due to the water-absorbing actions of the proteoglycan matrix. If cartilage ECM constantly pressures chondrocytes by physical control of cell shape, the default cytoskeletal stiffness in vivo would be expected to remain low. In this case, such a mechanism may sensitize chondrocytes to mechanical stimuli that locally exceeds baseline compression levels, allowing appropriate activation of local cytoskeletal stiffness responses against a deactivated background. For instance, strain caused by ARP2/3 mediated protrusions (causing a local indentation) may contribute to the mobilization of actomyosin on the opposing daughter cell (stiffening response) during column formation. The complexity of these responses, given heterogeneity of different zones, also highlights the need to assess individual responses of subpopulations at the single cell level, possibly by FACS prescreening on zonal markers, or comparing stiffness profiles to cell sizes and geometries.

Figure 5.3: AFM testing reveals subtle mechanical response of chondrocytes to adhesive substrate. Chondrocytes were seeded on Poly-L-Lysine (A), Gelatin (B), Fibronectin (C), and Collagen 2 (D) coated culture dishes for one hour to adhere before AFM testing was commenced (Collagen 2 cells were seeded two hours, being tested after Gelatin in a single AFM run). Poly-L-lysine and Fibronectin were both tested on independent days. The histograms depict the distribution of cell stiffness upon sampling the chondrocyte population by AFM indentation.

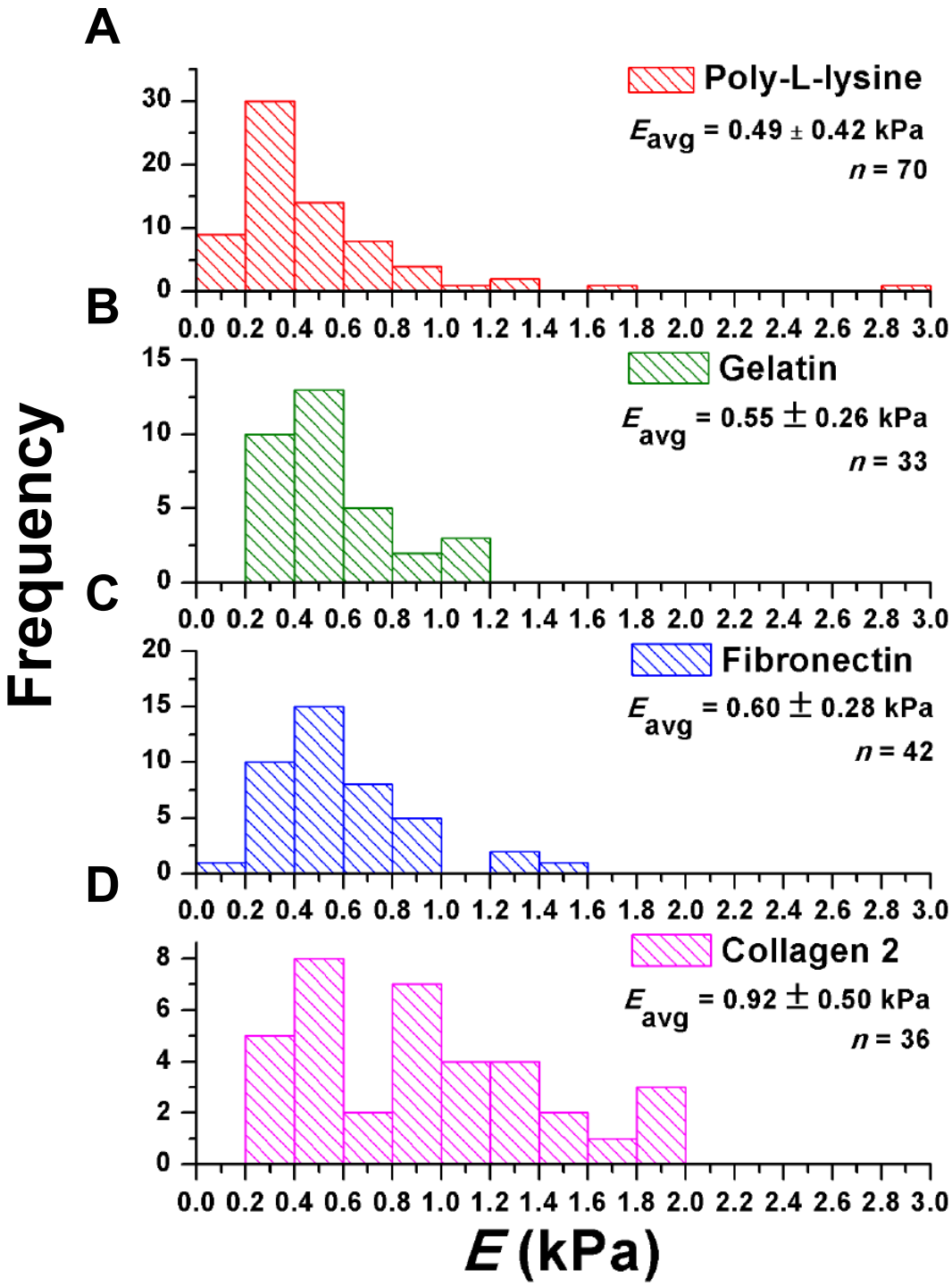
A
Poly-L-lysine
E_{avg} = 0.49 ± 0.42 kPa
n = 70
B
Gelatin
E_{avg} = 0.55 ± 0.26 kPa
n = 33
C
Fibronectin
E_{avg} = 0.60 ± 0.28 kPa
n = 42
D
Collagen 2
E_{avg} = 0.92 ± 0.50 kPa
n = 36
Frequency
E (kPa)

Figure 5.4: AFM testing suggests differential chondrocyte response to global versus local mechanical stimulation. Chondrocytes cultured in alginate for 1 hour without compression (A) or with dynamic compression (B, 19% strain, 1Hz) and then seeded onto poly-L-lysine for one hour prior to AFM testing. The histograms depict the distribution of cell stiffness upon sampling the chondrocyte population by AFM indentation. Data is pooled from n=2 devices per condition. C) Cells were seeded onto Poly-L-lysine for 1 hour prior to AFM indentation measurements. The plot shows stiffness of a single chondrocyte after repeated indentation at a single position by AFM. Similar strain and frequency was generated by the AFM pulsing regime compared to the dynamic compression device. This plot is representative of experiments done on n=5 cells.

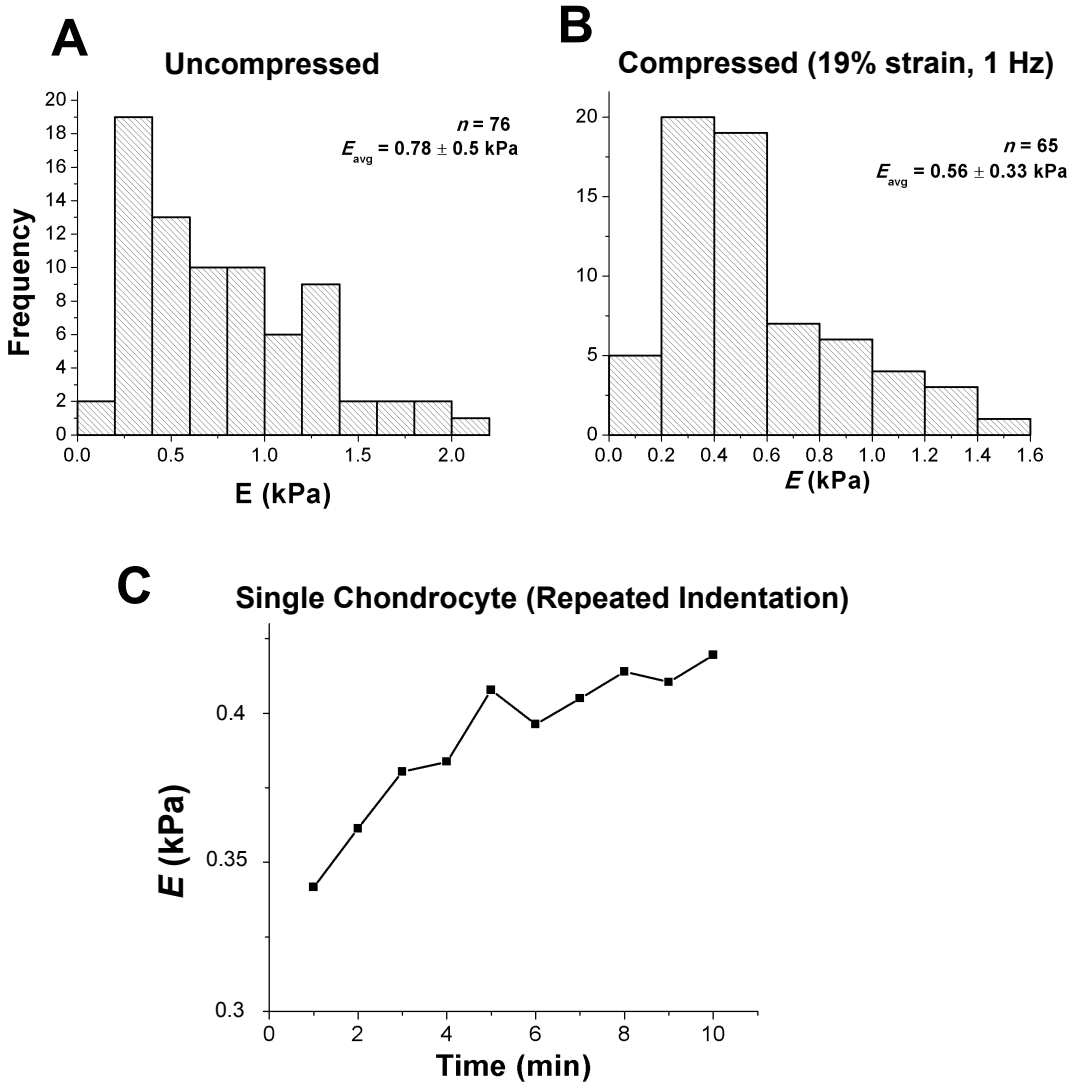
A
Uncompressed
n = 76
E_avg = 0.78 ± 0.5 kPa
Frequency
E (kPa)
B
Compressed (19% strain, 1 Hz)
n = 65
E_avg = 0.56 ± 0.33 kPa
E (kPa)
C
Single Chondrocyte (Repeated Indentation)
E (kPa)
Time (min)

Cell migration: complex interplay between ECM, adhesion, and cytoskeleton.

The observed responses to force probably depend on a suite of mechanosensitive proteins, and it is a crucial task to identify them. How do these results fit into the context what is known about coupling among various cell mechanical modules during individual or collective cell migration? Classically, migrating cells use integrin adhesion to gain traction against a substrate (Haeger 2015, Collins 2015). Integrin activation occurs through a conformational change mediated by binding of B-tails with intracellular cytoskeletal proteins (Liu 2000, Calderwood 2004). Therefore, the cytoskeleton, along with scaffolding and signaling molecules can be linked to the extracellular matrix through the activated integrins to convey mechanical signals in and out of the cell via actomyosin-generated force (Clark 2014). The known major molecular connections occur through talin, filamin, actinin, tensin, vinculin, paxillin, FAK and Src family kinases (Lee 2007, Sawada 2006, Liu 2000, Mitra 2006, Zaidel-Bar 2007, Garvalov 2003, Goksoy 2008, Demali 2002). The activation of focal adhesions and integrin clustering functions by a LALI mechanism whereby positive feedback promotes the clustering of integrins nearest the growing adhesion (local activation) to cause oppressive membrane tension that inhibits the formation of focal adhesions at distal sites in the cell, for example the rear (lateral inhibition, Goehring 2012). As a result during migration, integrin adhesions form at the leading edge allowing traction forces to mediate motility, while adhesions at the rear break (Scarpa 2016). This dynamic adhesion cycle directly activates Rho-GTPases that promote force-generating activities such as actin polymerization and actomyosin contractility (Ren 2000, Parsons 2010, Provenzano 2011, Alfandari 2010). Downstream of Rho, myosin II promotes adhesion stability and maturity through activation of cryptic integrin sites by mechanisms that include actin

bundling and generation of tension, often sending mechanical signals to the leading edge from contractility produced in the rear (Parsons 2010). Thus, in both migratory and intercalating cells, cytoskeletal tension applied to an integrin or cadherin adhesion surface stimulates Rho-GTPases to perpetuate polarized adhesion dynamics.

Different types of adhesions (eg. focal adhesion complexes, fibrillar adhesion) are associated with distinct strength of adhesive forces. Furthermore, the length and duration of adhesions depend critically on the stiffness, dimensionality, organization, and composition of the extracellular matrix. Even simple mechanical deformability of the matrix can control adhesion, migration and differentiation of various cell types (Pelham 1997, Kim 2013, Sun 2016). Differences in the stiffness of substrate determine the amount of actomyosin-dependent force cells produce on that substrate, and the size of focal adhesions present (Ng 2012, Murrell 2015, Friedland 2009, Von Wichert 2003). ECM stiffness is interpreted by integrins, because inducing integrin clustering can mimic the effects of stiffness, and RGD-driven integrin activation promotes focal adhesion growth regardless of substrate stiffness (Taubenberger 2007, Paszek 2009, Yang 2015). This applies to both integrin and cadherin adhesions, since cadherins and cytoskeletal organization respond to differential stiffness of cadherin-coated substrates, producing more traction force on stiffer cadherin substrates in a myosin II and cadherin dependent manner (Ladoux 2010). Interestingly, substrate rigidity, porosity, and crosslinking also determines lifetime of actin filaments, and can synergistically signal to cells to affect migratory and morphogenetic cell behavior (Hu 2007, Lo 2000, Gupta 2015, DeMali 2014). Migrating cells first sense the substrate composition before sensing substrate stiffness by adapting their rheology, adhesive surfaces, and actin organization (Murrell, 2015, Gupta 2015). Thus, a plausible mechanism that could underlie the chondrocyte force and substrate response could have roots in the ECM-integrin-actin signaling axis.

RELATIONSHIPS BETWEEN GLOBAL SIGNALING AND MECHANICAL EFFECTORS OF CELL ORGANIZATION

Dynamic daughter cell rearrangements promote column formation and allometric tissue elongation in the proliferative zone of growing cartilage. In the previous discussion, it is hypothesized that with the proper symmetry-breaking mechanism, interactions among adhesion, cytoskeletal, and ECM proteins could potentially assemble into self-regulating mechanical loops. However, the specific signaling mechanisms upstream of these short-range behaviors are still unknown. Next we will discuss a scenario in which a global signaling network, in this case the planar cell polarity (PCP) pathway, can sculpt the cell- and tissue- scale biomechanical environment in various ways to effect morphological change. Here we ask: Wnt5a signaling gradients might be present during the initials stages of chondrogenesis, but how would chondrocytes remain polarized throughout an individual's lifespan? Perhaps by examining some putative signaling targets of this pathway, we may get a better understanding of the mechanisms that translate these global signaling cues into cartilage architecture. We propose that one possible role of Wnt/PCP signaling is rallying the cellular biomechanical effectors such as adhesion, matrix, and cytoskeletal proteins into determined positions, and in parallel, modifying the signaling environment that produces zonal architecture.

Planar cell polarity often utilizes cell adhesion:

PCP was first discovered by examining Drosophila mutants with altered polarity of hair and cilia-bearing cells on the epithelium of the wing (Axelrod 2001, Strutt 2001, Winter 2001). In these initial experiments a number of genes were identified to be crucial for proper polarization along the plane of the epithelium (not apical-basal polarity) in hair cells of the wing, bristles, and ommatidia of the drosophila eye. Several of these genes

were observed to localize to cell junctions to establish polarized domains at the cell surface, and these molecules became known as the “core” PCP proteins (Vangl, Prickle, Frizzled, Dishevelled, Ror2, and Celsr) (Peng 2012). However, a mechanism for translating asymmetrical cell localization into cell polarity began to manifest when it was found that atypical cadherins Fat and Ds cooperate with core PCP effectors to polarize hair cells in the wing (Peng 2012), and that DE- and DN- cadherins cooperate with Frizzled to regulate ommatidia morphogenesis in the eye (Mirkovic 2006). In both of these systems, polarized domains utilized not only cell-autonomous feedback mechanisms to stabilize membrane occupancy, but also cooperated with cell-cell adhesion pathways to strengthen the polarity of neighboring cells (Axelrod 2011). The theme of “intracellular inhibition, intercellular adhesion” has been repeatedly shown in studies of planar polarity including the drosophila SOP cell, vertebrate hair follicles, multi-ciliated epithelium, and the inner ear of mammals (Simons 2008, Vladar 2009, Yang 2015).

Even in polarized systems in which lateral stabilization – local destabilization has not yet been definitively proven, there are abundant examples of PCP components interacting with cell adhesion molecules to control tissue morphogenesis. Cadherins seem to be a particularly conserved target of PCP intermediaries, but regulatory mechanisms are context dependent. For example, in the developing chick limb mesenchyme, Fzd7 controls N-cadherin expression specifically at the initial precartilage condensations to regulate the initiation of chondrogenesis (Tufan 2002), whereas during synapse development, Vangl2 and Prickle compete with beta-catenin to bind and regulate the cell surface expression of N-cadherin (Nagaoka 2014). Similar Vangl2-dependent mechanisms promote E-cadherin endocytosis in the developing kidney (Nagaoka 2013) and inhibit VE-cadherin-based adherens junctions to enable

rearrangement of endothelial cells during intraluminal valve formation in lymphatic vessels (Tatin 2013).

Applied to the problem of cartilage column formation, these data would seem to suggest polarity signaling could influence the daughter cell adhesion surface, despite a few constraints that ought to be placed on this model. First, the observation of similar cadherin-rich daughter cell adhesion surfaces in all resting zone, proliferative zone, polarity-deficient, and cultured chondrocytes, leads to the requirement that small quantitative differences in cadherin levels would need to be sufficient to promote or inhibit rotation. Second, that the daughter cell interface is transient requires signaling to cadherins to reactivate after each cell division to elongate the column. This point is particularly important because in cartilage, the effects of deregulated Wnt/PCP signaling are cell-autonomous, in sharp contrast to most PCP-dependent systems that exhibit domineering non-autonomous effects of mutant cells on neighboring wild-type cells in a mosaic mutant (Li 2009, Axelrod 2011). This divergence is somewhat expected because cell-cell adhesion is only present between isogenic daughter chondrocytes for a short duration relative to the 24-hour doubling time. Furthermore, cell frequency and morphology of the daughter cell cadherin adhesion interface is not obviously disrupted in Wnt5a or Ror2 mutants. Thus, the “intracellular inhibition, intercellular stabilization” paradigm cannot exclusively utilize daughter cell interaction to stabilize the location of transmembrane polarity protein complexes, but could conceivably rely on additional factors such as cell-matrix adhesion, ECM remodeling, and/or cell tension.

Figure 5.5: Mechanochemical feedback could underlie tissue architecture

Simplified schematic illustrating a model that polarity signaling and mechanotransduction contains a high degree of feedback. Different types of positional cues can result in the formation of new positional cues. Many of the molecular outputs of polarity signaling are mechanically active. Force-generation in cells often results in complex interplay among different parts of each cell, among cells, and throughout the extracellular environment. Mechanical behavior of cells can result in new types of cellular and molecular organization. A) Typical scenario of epithelial PCP maintained by cell junctions. B) Two daughter cells embedded in a complex extracellular matrix environment (black). Cells are connected to the matrix by integrin adhesions (blue), and connected to each other by a cadherin-based adhesion surface (red). On the top cell, yellow and grey boxes indicate membrane domains where planar cell polarity proteins are enriched. On the middle, active mechanical components of the cell including the actin cortex, integrins, and cadherins, are labeled in two daughter chondrocytes. As the chondrocytes rotate, PCP proteins may be interacting with adhesion or cytoskeletal proteins to regain their former position after cell separation. C) The arrows indicate regulatory relationships between different molecules that are known to occur in other systems to promote polarized tissue growth. Thus, complex, context-dependent interactions between cell polarity and forces could produce adaptive systems-level behavior in chondrocytes.

A. Stereotypical polarized epithelium

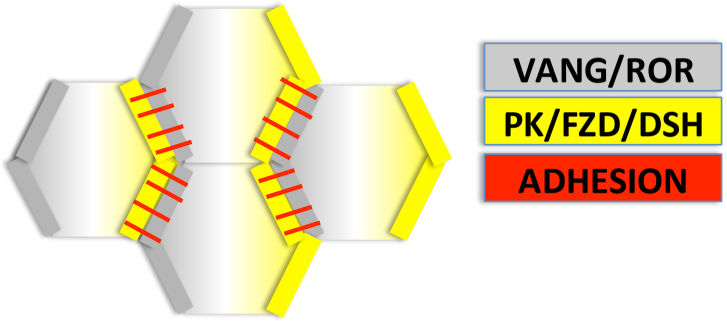

B. Chondrocyte rotation

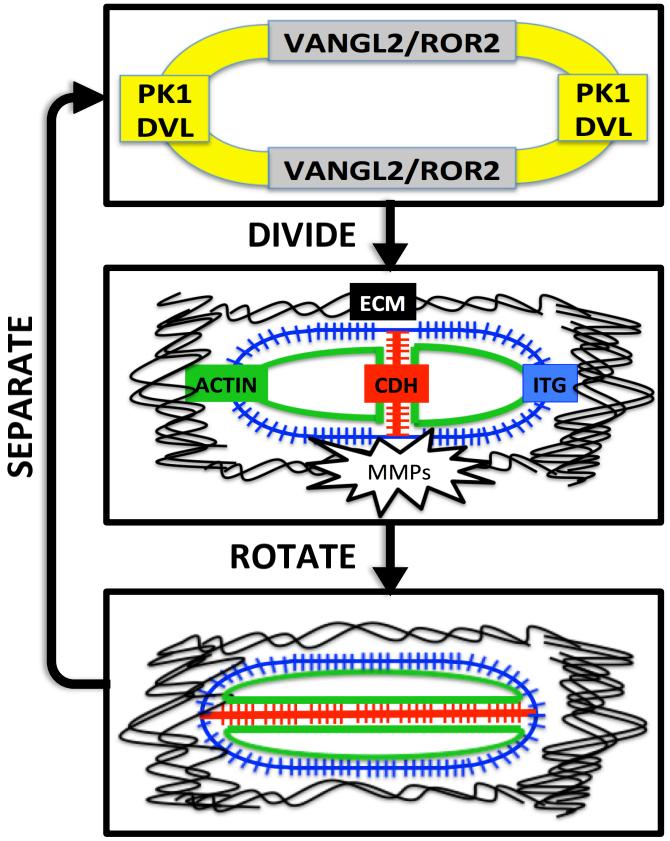

C. Regulatory network

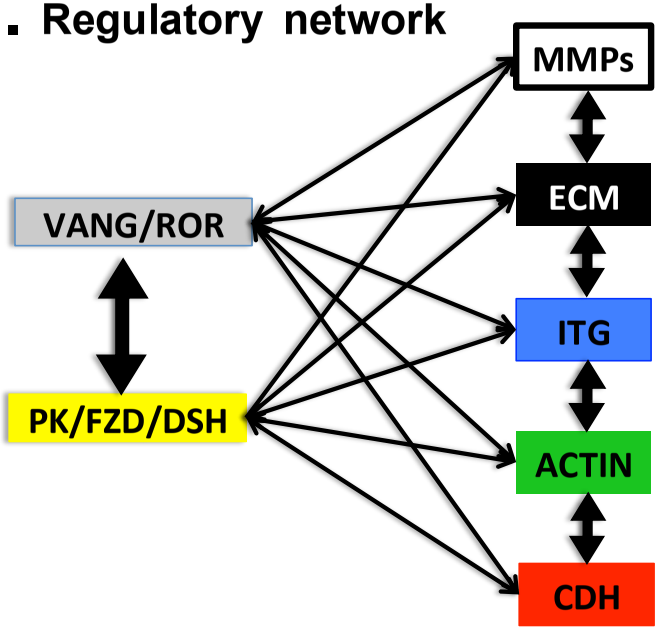

Does Wnt / PCP regulate adhesive interactions to promote ECM organization?

Planar cell polarity signaling protein modules are capable of coordinately regulating several cellular processes that become mechanically coupled during development. In the case of zebrafish gastrulation, convergence-extension cell movements are achieved by both noncanonical Wnt11 signaling, cadherin adhesion, integrin adhesion to the fibronectin matrix, and planar cell polarity. In this system, the cell-surface proteoglycan Gpc4 (also known as *Knypek*) and Fzd7 cooperate to regulate E-cadherin-based intercellular adhesion and tissue-wide tension propagated by the actomyosin cytoskeleton (Dohn 2013, Puech 2005). The tension produced at these cadherin interactions instigates cell-matrix mechanotransduction at integrin-fibronectin binding sites, which promote ECM fibril assembly (Dohn 2013). The actions of Fzd7/Gpc4 on ECM formation are counterbalanced by a dynamic intracellular distribution of Vangl2, which regulates retrograde trafficking of MMP14 to control its cell-surface expression, leading to ECM catabolism and polarized disassembly of integrin-ECM contacts (Roszko 2015, Williams 2012, Page-McCaw 2007). Together, these studies showed that Vangl2/Prickle and Glypican/Frizzled signaling exert mutually antagonistic influences on cell adhesion and ECM organization to effect mediolateral cell alignment and tissue elongation. A similar mechanism downstream of Wnt11 in Xenopus controls cellular rearrangements that drive epiboly and axial extension in the cells of the blastocoel roof (BCR, Dzamba 2009). Here, stimulation of noncanonical Wnt/PCP signaling promoted C-cadherin adhesion in BCR cells, resulting in increased traction forces through myosin II contractility and Rac. Wnt-induced, cadherin-dependent mechanical tension in the BCR was shown to be necessary for formation of the FN fibril meshwork that promotes tissue extension (Dzamba 2009, Mardsen 2003). These studies highlighted that Wnt/PCP signal transduction results in propagation of a mechanical signal to orchestrate various types of cell adhesion, both intercellular and to the extracellular matrix.

In both examples, cell polarity acts upstream of ECM metabolism and organization to drive tissue growth, and depends on cytoskeletal mediators for efficient mechanotransduction. Several studies suggest that cartilage may also employ noncanonical Wnt/PCP signaling to affect ECM structure, possibly as a means to maintain cell shape/polarity. For example, the PCP-interacting proteoglycan Gpc4, (also known as *knypek* in zebrafish) is required for convergent extension movements in the gastrulating embryo, and later for chondrocyte stacking in the zebrafish craniofacial cartilage (Dohn 2013, Sisson 2015). Failure of cell intercalation by loss of Gpc4 is associated with loss of the collagen network organization, resulting in shorter, thicker cartilage (Sisson 2015). Since Gpc4 is a glycosylphosphatidylinositol- (GPI) anchored protein, loss of Gpc4 cell surface expression could be one explanation for the polarity-defective phenotype in limb lineage mutants that truncate the GPI biosynthetic pathway (Romereim 2011, Ahrens 2009). As a member of the heparan sulfate proteoglycan family, Gpc4 could have several functions, but in the context of convergent extension appears to specifically interact with non-canonical Wnt signaling, potentially by binding Wnt ligands or receptors to potentiate signaling (Topczewski 2001, Marlow 1998). In vitro studies support this possibility, as in micromass cultures from chicken mandibular cartilage, Wnt5a-conditioned medium greatly stimulated expression of Aggrecanase and matrix metalloproteinase (MMP) 1 and 13, leading to subsequent degradation of Collagen II and Aggrecan (Hosseini-Farahabadi 2013). The matrix-degrading effect of WNT5a occurred through JNK signaling in these chondrocyte cultures, similar to what has been shown in osteosarcoma cell lines. Conversely, silencing of Wnt5a expression in rat articular chondrocytes prevents interleukin 1B-induced collagen degradation (Shi 2016). Thus, much like the highly context dependent mechanisms underlying PCP regulation of cell adhesion, noncanonical Wnt signaling can alter cartilage ECM metabolism in multiple ways, so whether and how Wnt5a signals could shape ECM

patterns in the growth plate should be a top priority towards identifying its contributions in column formation. For example, by studying the matrix development over time in Wnt5a mutant compared to wild type, both *in vivo* and in alginate beads, we may learn which components of the extracellular environment would require Wnt5a signaling for their proper assembly. Future experiments might also ask, would conditional deletion of Wnt5a in mature growth plates still produce growth defects, or is the Wnt5a allele dispensable for column formation given the correct extracellular environment? Conditional Ror2 deletion at E14.5 does produce subtle defects in columnar clonal arrangement (data not shown), but whether this affected column elongation and/or new recruitment from resting to proliferative zone is unknown. Further, whether Ror2 function would depend on Wnt5a ligand binding in this context is unclear, because the extensive feedback reported among transmembrane PCP molecules may maintain cell polarity even in the absence of Wnt5a, and because the proximal-distal expression gradient of Wnt5a observed in limb bud mesenchyme does not appear to last for the entirety of growth. Since the current work suggests either Wnt5a or integrin binding can influence myosin localization, a crucial question is to identify the direct versus indirect consequences of PCP deregulation in early cartilage.

Does PCP signaling dynamically couple cytoskeletal organization and tension?

The literature provides ample reason to suspect there may be a direct connection between disrupted Wnt5a signaling and the observed defects in myosin positioning in Wnt5a null cartilage. Mass tissue movements based on mediolateral intercalation are conserved across many phyla, including cartilage column formation and limb bud outgrowth. In many systems that exhibit these phenomena, Wnt/PCP signaling controls cell organization by directly controlling the production of actin-based force, utilizing Rho-GTPase-mediated actomyosin contractility, as well as JNK signaling-mediated actin

polymerization. For example, in the cnidarian Hydra (the most basic metazoan), noncanonical and canonical Wnt signaling pathways cooperate to control tissue evagination by controlling polarity of actin-cytoskeletal force via JNK signaling activity (Phillip 2009). In Drosophila, Frizzled/Dishevelled function upstream of Rho-GTPase and Rho-associated kinase (Rok, homolog of mammalian ROCK) to stimulate myosin II phosphorylation, thus precisely controlling the location of actin bundles in each cell (Winter 2001). The same signaling hierarchy was demonstrated during planar polarization the drosophila wing epithelium (Chung 2007). Additionally, JNK signaling operates within the WNT5a pathway to control mesoderm convergence-extension in Xenopus gastrulation (Yamanaka 2001). Wnt5a is capable of acting as a positional cue to directly polarize the cytoskeletal reorganization necessary for asymmetric cell divisions needed to form the early endoderm in C. elegans (Goldstein 2006). Interestingly, it was also recently shown that myosin activity regulates localization of Vangl2, strongly indicating a fundamental feedback mechanism among force-generating molecules and polarity proteins in actively organizing cells (Ossipova 2015). This kind of feedback could occur in response to engagement of integrin or cadherin adhesion surfaces, and could play an important role in maintaining cell polarity to enable the process of chondrocyte rotation. Thus, activation of planar cell polarity by Wnt5a gradients could involve direct regulation of actin architecture. However, Wnt5a does not always act in a gradient, but sometimes signals in a permissive manner, exemplified by the finding that Wnt5a permissively acts during cell migration in the presence of pre-existing chemokine gradients by mobilization of adhesion molecules, myosin2b, actin into a contractility complex (Witze 2008). This Wnt-induced receptor actin-myosin polarity promotes directional cell migration along the chemokine gradient.

If Wnt5a is simply acting to modulate an alternative system of positional cues, one potential candidate is the IHH/PTHrP circuit. Chondrocytes lacking Wnt5a signals

are delayed in early stages of chondrocyte differentiation, demonstrated by the loss of early IHH expression in Wnt5a null chondrocytes (Yang 2003). By our current understanding based on the literature and our scRNAseq results, lack of early IHH signaling will disrupt the timely formation of PTHrP-expressing resting domains as well as hypertrophic differentiation (Kronenberg 2006). However at later developmental stages, Wnt5a null cartilage clearly displays hypertrophic and prehypertrophic zones (personal observation by FISH), suggesting chondrocyte maturation is not completely abolished. Additionally, treatment with thyroxine, as well as overexpression of Wnt/PCP signaling components, has been reported to cause column formation in long-term (three weeks) chondrocyte pellet cultures (Ballock 1994, Randall 2012). If IHH expression is an outcome of both conditions, those results are consistent with a model in which polarizing gradients of IHH/PTHrP signaling drive column formation. Thus, a simple explanation would view disrupted columnar architecture in Wnt5a mutants as a consequence of defective zonal arrangement. However, this interpretation is problematic for two reasons. First, strong genetic evidence points against a role for PTHrP and IHH gradients in column formation, namely the partial rescue of column formation phenotypes in a PTHrP null growth plate by constitutive activation of PTH1R, and in IHH null growth plates by deletion of Gli3 (Koziel 2005, Soegiarto 2001). So even if gradients of IHH/PTHrP may be important for patterning zones, the same gradients might be dispensable for the specific process of column formation, leaving the actual identity of the polarizing signals unknown. The second problem is the argument that Wnt5a null chondrocytes simply fail to differentiate into proliferative cells based on aberrant IHH/PTHrP environment, does not quite fit with the data showing differential myosin localization in wild-type resting daughter cells (ubiquitous membrane localization) versus Wnt5a and Ror2 mutant daughter cells (highly cell-cell junctional), suggesting instead that resting cells and Wnt5a null chondrocytes do not form columns for slightly different reasons. Because of

these results, the contributions of a Wnt5a gradient may not be wholly accounted for by its potential actions on IHH/PTHrP signaling.

Transforming tissue-wide spatial information into a template for cell arrangement.

However, the impacts of Wnt5a signaling on early cartilage differentiation cannot be simply discarded. Instead, a hypothetical model is proposed that depends on a dual nature of Wnt5a signaling (Figure 5.6). One function is the inducing IHH expression leading to a functional IHH/PTHrP negative feedback loop that results in the establishment of cartilage zones. The second function involves mobilization of the actin cytoskeleton and/or ECM deposition, resulting in positive feedback between cortical actomyosin-based forces and integrin adhesions. As chondrocytes exit the resting zone and gradually transition towards a proliferative zone, further modifications of the cytoskeleton and/or ECM would occur that could depend on PTH1R activation, but not necessarily rely on a PTHrP gradient. This two-step process would poise chondrocytes to form columns once pro-proliferative signals are received. In this way, the relationship between zonal and columnar polarity may feature a limited set of signaling molecules that interact with local chondrocyte biomechanics to drive daughter cell arrangement and linear tissue elongation.

The results of our alginate cultures, and our mapping of chondrocyte cytoskeletal dynamics, suggest the possibility that chondrocyte properties could be tuned towards large-scale organization with minimal instruction. Future advances towards engineering columnar cartilage architecture will involve investigating how delivery of Wnt5a gradients in alginate culture impact patterns of cytoskeletal and matrix proteins in single and doublet chondrocytes, as well as patterns of zonal maturation. If Wnt5a is required but not sufficient to induce IHH expression, co-treatment of Wnt5a gradients combined with

thyroxine or even simply using IHH protein may provide the dual mechanisms to set up features of the growth plate. However, in a model where positional cues become translated from the signaling environment into the local solid-state environment, later experiments in alginate may demonstrate that the signaling mechanisms that appear to be crucial for polarized rearrangements would ultimately be dispensable as long as local surroundings are correctly arranged. This means that chondrocyte behavior could prove to be flexible enough to generate tissue architecture in the absence of long-range communication. Thus, for tissue engineers, finding either a suitable cocktail to create an impetus for chondrocyte remodeling the mechanical environment may be an equally valid solution compared to specifically providing the detailed nanoscale ECM surroundings that would otherwise be produced by the chondrocyte itself during differentiation. Hopefully, the culture system presented in this dissertation will be applied in synchrony with future *in vivo* and computational systems, to cross-validate predictions and results generated by individual models. Ideally, using this strategy in future studies can hasten progress towards the kind of predictive control over chondrocyte biology that will be required to design self-organizing cartilage tissues with customizable growth properties.

Figure 5.6: Hypothetical model describing the relationship between the global signaling networks that create zonal architecture and local process that effect column formation. This schematic is simplified to highlight the hypothesis that Wnt5a signaling is predicted to initiate both local and global mechanisms, but feedback among the individual components maintains anisotropy at their respective length scales. This model views Wnt5a as an early messenger of positional information from the limb bud mesenchyme, but also recognizes contributions of IHH/PTHrP signaling loop as affecting both differentiation as well as chondrocyte cell dynamics. Correct transcriptional, cytoskeletal, and ECM architectures are all required for columnar arrangement of chondrocytes to emerge.

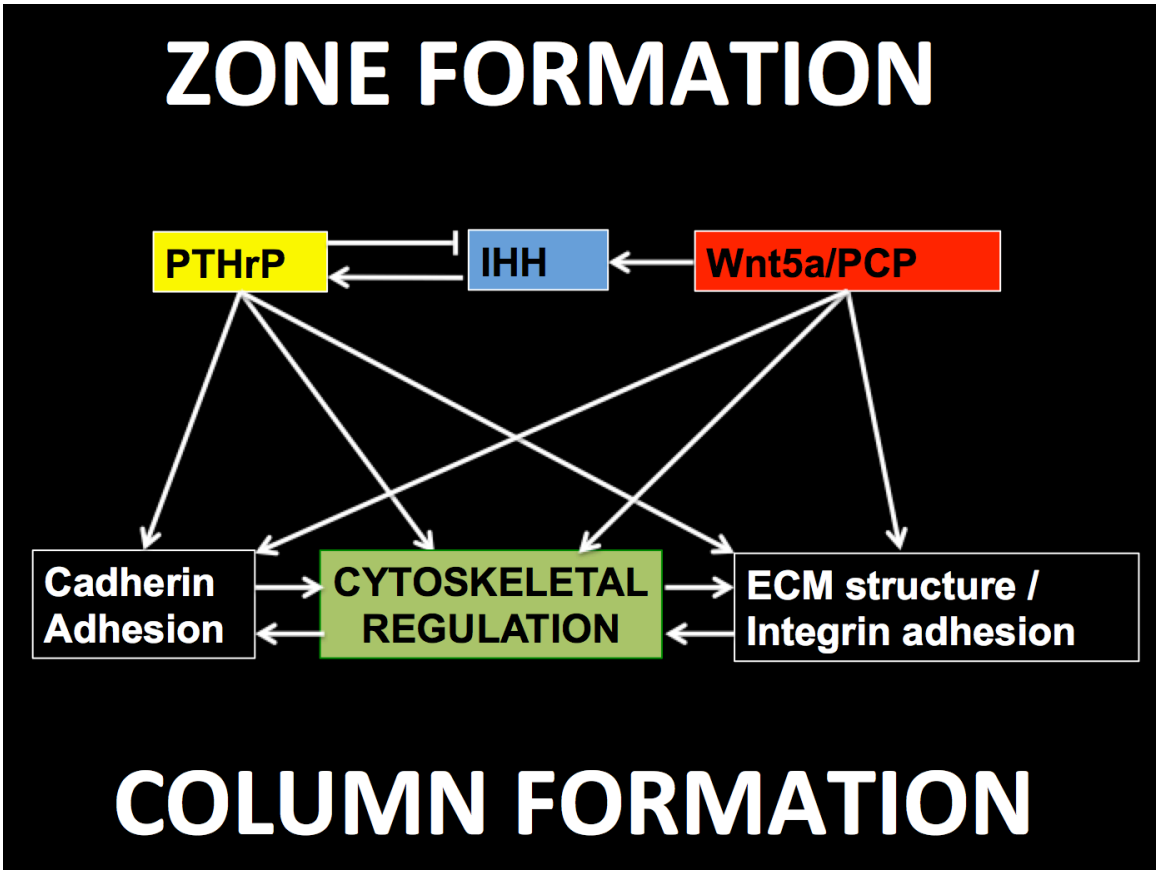
ZONE FORMATION
PTHrP
IHH
Wnt5a/PCP
Cadherin Adhesion
CYTOSKELETAL REGULATION
ECM structure / Integrin adhesion
COLUMN FORMATION

BIBLIOGRAPHY

Abad, V., Meyers, J. L. Weise, M., Gafni, R. I., Barnes, K. M., Nilsson, O., Baron, J. (2002). The role of the resting zone in growth plate chondrogenesis. Endocrinology, 143(5),1851–1857.

Abad, V., Uyeda, J. A., Temple, H. T., De Luca, F., & Baron, J. (1999). Determinants of spatial polarity in the growth plate. Endocrinology, 140(2), 958–962.

Abzhanov, A., & Tabin, C. J. (2004). Shh and Fgf8 act synergistically to drive cartilage outgrowth during cranial development. Developmental Biology, 273(1), 134–148.

Agarwal, A., Farouz, Y., Nesmith, A. P., Deravi, L. F., McCain, M. L., & Parker, K. K. (2013). Micropatterning Alginate Substrates for in vitro Cardiovascular Muscle on a Chip. Advanced Functional Materials, 23(30), 3738–3746.

Ahrens, M. J., & Dudley, A. T. (2011). Chemical Pretreatment of Growth Plate Cartilage Increases Immunofluorescence Sensitivity. Journal of Histochemistry and Cytochemistry, 59(4), 408–418.

Ahrens MJ, Li Y, Jiang H, Dudley AT (2009). Convergent extension movements in growth plate chondrocytes require gpi-anchored cell surface proteins. Development (Cambridge, England) 136(20), 3463-3474.

Ahrens, M. J., Romereim, S., & Dudley, A. T. (2011). A re-evaluation of two key reagents for *in vivo* studies of Wnt signaling. Developmental Dynamics, 240(9), 2060–2068.

Akiyama, R., Kawakami, H., Taketo, M. M., Evans, S. M., Wada, N., Petryk, A., & Kawakami, Y. (2014). Distinct populations within Isl1 lineages contribute to appendicular and facial skeletogenesis through the β-catenin pathway. Developmental Biology, 387(1), 37–48.

Al-Kilani, A., de Freitas, O., Dufour, S., & Gallet, F. (2011). Negative Feedback from Integrins to Cadherins: A Micromechanical Study. Biophysical Journal, 101(2), 336–344.

Alberch P., Gould S.J., Oster G.F., Wake D.B. (1979). Size and Shape in Ontogeny and Phylogeny. Paleobiology, 5(3),296-317.

Albert P.J, Schwarz U.S. (2016). Dynamics of Cell Ensembles on Adhesive Micropatterns: Bridging the Gap between Single Cell Spreading and Collective Cell Migration. PLoS Comput Biol 12(4): e1004863.

Alexopoulos, L. G., Youn, I., Bonaldo, P., & Guilak, F. (2009). Developmental and osteoarthritic changes in Col6a1-knockout mice: Biomechanics of type VI collagen in the cartilage pericellular matrix. Arthritis and Rheumatism, 60(3), 771–779.

Alfandari, D., Cousin, H., & Marsden, M. (2010). Mechanism of Xenopus cranial neural crest cell migration. Cell Adhesion & Migration, 4(4), 553–560.

Alfandari, D., Cousin, H., Gaultier, A., Hoffstrom, B. G., & DeSimone, D. W. (2003). Integrin α5β1 supports the migration of Xenopus cranial neural crest on fibronectin. Developmental Biology, 260(2), 449–464.

Alsberg E., Anderson K.W., Albeiruti A., Rowley J.A., Mooney D.J. (2002). Engineering growing tissues. PNAS, 99(19), 12025-12030.

Alsberg E, Anderson KW, Albeiruti A, Franceschi RT, Mooney DJ (2001). Cell-interactive alginate hydrogels for bone tissue engineering. Journal of Dental Research, 80(11), 2025-2029.

Antoni D, Burckel H, Josset E, Noel G (2015). Three-dimensional cell culture: a breakthrough *in vivo*. Int J Mol Sci 2015, 16(3), 5517-5527.

Anderson, P. W. (1972). More Is Different. Science, 177(4047), 393-396.

Arita, M., Li, S.-W., Kopen, G., Adachi, E., Jimenez, S. A., & Fertala, A. (2002). Skeletal abnormalities and ultrastructural changes of cartilage in transgenic mice expressing a collagen II gene (COL2A1) with a Cys for Arg-α1-519 substitution. Osteoarthritis and Cartilage, 10(10), 808–815.

Arthur W.T., Noren N.K., Burridge K. (2002). Regulation of Rho Family GTPases by Cell-Cell and Cell-Matrix Adhesion. Biological Research, 35(2), 239-246.

Ashe, H. L., & Briscoe, J. (2006). The interpretation of morphogen gradients. Development, 133(3), 385 LP-394.

Aszodi, A., Hunziker, E. B., Brakebusch, C., & Fässler, R. (2003). β1 integrins regulate chondrocyte rotation, G1 progression, and cytokinesis. Genes & Development, 17(19), 2465–2479.

Axelrod, J. D. and Tomlin, C. J. (2011), Modeling the control of planar cell polarity. WIREs Syst Biol Med, 3, 588–605.

Ballock R.T., O'Keefe R.J. (2003): Physiology and pathophysiology of the growth plate. Birth defects research Part C, Embryo today: reviews, 69(2),123-143.

Ballock RT, Reddi AH (1994): Thyroxine is the serum factor that regulates morphogenesis of columnar cartilage from isolated chondrocytes in chemically defined medium. J Cell Biol, 126(5), 1311-1318.

Balzac, F., Avolio, M., Degani, S., Kaverina, I., Torti, M., Silengo, L., Retta, S. F. (2005). Ecadherin endocytosis regulates the activity of Rap1: a traffic light GTPase at the crossroads between cadherin and integrin function. Journal of Cell Science, 118(20), 4765 LP-4783.

Barolo S., Posakony JW. (2002). Three habits of highly effective signaling pathways: principles of transcriptional control by developmental cell signaling. Genes & Dev. 16, 1167-1181

Bashey RI, Iannotti JP, Rao VH, Reginato AM, Jimenez SA (1991). Comparison of morphological and biochemical characteristics of cultured chondrocytes isolated from proliferative and hypertrophic zones of bovine growth plate cartilage. Differentiation; research in biological diversity 46(3), 199-207.

Bengtsson, T., Aszodi, A., Nicolae, C., Hunziker, E. B., Lundgren-Åkerlund, E., & Fässler, R. (2005). Loss of α10β1 integrin expression leads to moderate dysfunction of growth plate chondrocytes. Journal of Cell Science, 118(5), 929-936.

Benham-Pyle, B. W., Pruitt, B. L., & Nelson, W. J. (2015). Mechanical strain induces Ecadherin-dependent Yap1 and β-catenin activation to drive cell cycle entry. Science, 348(6238), 1024–1027.

Benya, P. D., Padilla, S. R., & Nimni, M. E. (1978). Independent regulation of collagen types by chondrocytes during the loss of differentiated function in culture. Cell, 15(4), 1313–21.

Bertet, C., Rauzi, M., & Lecuit, T. (2009). Repression of Wasp by JAK/STAT signalling inhibits medial actomyosin network assembly and apical cell constriction in intercalating epithelial cells. Development, 136(24), 4199 LP-4212.

Bertet, C., Sulak, L., & Lecuit, T. (2004). Myosin-dependent junction remodelling controls planar cell intercalation and axis elongation. Nature, 429(6992), 667–671.

Bian, W., Juhas, M., Pfeiler, T. W., & Bursac, N. (2012). Local Tissue Geometry Determines Contractile Force Generation of Engineered Muscle Networks. Tissue Engineering. Part A, 18(9-10), 957–967.

Bijlsma, M.F., Groot, A.P., Oduro, J.P, Franken, R.J, Schoenmakers S.H.H.F, Peppelenbosch M.P., Spek C.A. (2009) Hypoxia induces a hedgehog response mediated by HIF-1α. J. Cell. Mol. Med. Vol 13, No 8B, pp. 2053-2060

Bleuel J, Zaucke F, Brüggemann GP, Niehoff A. (2015). Effects of cyclic tensile strain on chondrocyte metabolism: A systematic review. PLoS One, 10(3).

Blumbach K, Niehoff A, Paulsson M, Zaucke F. (2008). Ablation of collagen IX and COMP disrupts epiphyseal cartilage architecture. Matrix Biol, 27(4),306-318.

Bökel C, Brand M. (2013) Generation and interpretation of FGF morphogen gradients in vertebrates. Curr Opin Genet Dev, 23(4):415-422.

Bordonaro M, Ogryzko V. (2013) Quantum biology at the cellular level—Elements of the research program. Biosystems, 112(1),11-30.

Borghi N., Sorokina M., Shcherbakova O.G. (2012). E-cadherin is under constitutive actomyosin generated tension that is increased at cell–cell contacts upon externally applied stretch. PNAS,109(31),12568-12573.

Bougault C, Paumier A, Aubert-Foucher E & Mallein-Gerin F. (2008). Molecular analysis of chondrocytes cultured in agarose in response to dynamic compression. BMC Biotechnology 8,71

Brachvogel B, Zaucke F, Dave K, (2013).Comparative Proteomic Analysis of Normal and Collagen IX Null Mouse Cartilage Reveals Altered Extracellular Matrix Composition and Novel components of the Collagen IX Interactome. The Journal of Biological Chemistry, 288(19),13481-13492.

Brama, P. A.J., Holopainen, J., van Weeren, P. R., Firth, E. C., Helminen, H. J. and Hyttinen, M. M. (2009), Effect of loading on the organization of the collagen fibril network in juvenile equine articular cartilage. J. Orthop. Res., 27,1226–1234.

Breur GJ, Vanenkevort BA, Farnum CE, Wilsman NJ. (1991). Linear relationship between the volume of hypertrophic chondrocytes and the rate of longitudinal bone growth in growth plates. J Orthop Res., 9(3):348-359.

Brown, A. C., Muthukrishnan, S. D., & Oxburgh, L. (2015). A Synthetic Niche for Nephron Progenitor Cells. Developmental Cell, 34(2), 229–241.

Brunet T, Arendt T (2016). Animal Evolution: the Hard Problem of Cartilage Origins. Current Biology, 26 (14), 685-688.

Budde, B., Blumbach, K., Ylo, J., Zaucke, F., Ehlen, H. W. A., Wagener, R., Gra, S. (2005). Altered Integration of Matrilin-3 into Cartilage Extracellular Matrix in the Absence of Collagen IX, 25(23), 10465–10478.

Burian, R. M. (Virginia P. I. and S. U. (2005). The Epistemology of Development, Evolution, and Genetics. Science Studies.

Butler, L. C., Blanchard, G. B., Kabla, A. J., Lawrence, N. J., Welchman, D. P., Mahadevan, L.… Sanson, B. (2009). Cell shape changes indicate a role for extrinsic tensile forces in Drosophila germ-band extension. Nature Publishing Group, 11(7), 859–864.

Calderwood, D. A. (2004). Talin controls integrin activation. Biochemical Society Transactions, 32(3), 434 LP-437.

Calisto, J. De, Araya, C., Marchant, L., Riaz, C. F., & Mayor, R. (2005). Essential role of noncanonical Wnt signalling in neural crest migration, 2587–2597.

Canciani, B., Ruggiu, A., Giuliani, A., Panetta, D., Marozzi, K., Tripodi, M.,Tavella, S. (2015). Effects of long time exposure to simulated micro- and hypergravity on skeletal architecture. Journal of the Mechanical Behavior of Biomedical Materials, 51, 1–12.

Cao, X., Xia, H., Li, N., Xiong, K., Wang, Z., & Wu, S. (2015). A mechanical refractory period of chondrocytes after dynamic hydrostatic pressure. Connective Tissue Research, 56(3), 212–218.

Caron M.M.J., P.J. Emans, M.M.E. Coolsen, L. Voss, D.A.M. Surtel, A. Cremers, L.W. van Rhijn, T.J.M. Welting (2012). Redifferentiation of dedifferentiated human articular chondrocytes: comparison of 2D and 3D cultures. Osteoarthritis and Cartilage 20(10), 1170-1178

Cavey, M., Rauzi, M., Lenne, P.F., & Lecuit, T. (2008). A two-tiered mechanism for stabilization and immobilization of E-cadherin. Nature, 453(7196), 751–756.

Chausovsky, A., Bershadsky, A. D., & Borisy, G. G. (2000). Cadherin-mediated regulation of microtubule dynamics. Nat Cell Biol, 2(11), 797–804.

Chen C, Jiang Y, Xu C, Liu X, Hu L, Xiang Y, Chen Q, Chen D, Li H, Xu X, Tang S. (2016). Skeleton Genetics: a comprehensive database for genes and mutations related to genetic skeletal disorders. Database (Oxford) http://101.200.211.232/skeletongenetics/.

Chen, X., Macica, C. M., Ng, K. W., & Broadus, A. E. (2005). Stretch-induced PTH-related protein expression in osteoblasts, JMBR 20(8), 1454–1461.

Chernobelskaya, O. A., Alieva, I. B., & Vorobjev, I. A. (2009). Radial-organized microtubules provide maintenance of the cell shape and more effective intercellular transport than in the case of free microtubules. Tsitologiya, 51(6), 475–483.

Chesterman PJ, Smith AU (1968). Homotransplantation of articular cartilage and isolated chondrocytes. An experimental study in rabbits. The Journal of bone and joint surgery British volume 1968, 50(1), 184-197.

Chiang, C., Litingtung, Y., Harris, M. P., Simandl, B. K., Li, Y., Beachy, P. A., & Fallon, J. F. (2001). Manifestation of the Limb Prepattern: Limb Development in the Absence of Sonic Hedgehog Function, 435, 421–435.

Chu, C., & Sokol, S. Y. (2016). Wnt proteins can direct planar cell polarity in vertebrate ectoderm, 3, 1–13.

Chung, U., Lanske, B., Lee, K., Li, E., & Kronenberg, H. (1998). The parathyroid hormone/parathyroid hormone-related peptide receptor coordinates endochondral bone development by directly controlling chondrocyte differentiation. PNAS, 95(22), 13030–13035.

Chung, S., Kim, S., Yoon, J., Adler, P. N., & Yim, J. (2007). The Balance Between the Novel Protein Target of Wingless and the Drosophila Rho-Associated Kinase Pathway Regulates Planar Cell Polarity in the Drosophila Wing, 903(June), 891–903.

Claes, L. E., & Heigele, C. A. (1999). Magnitudes of local stress and strain along bony surfaces predict the course and type of fracture healing. Journal of Biomechanics, 32(3), 255–266.

Clark, A. G., Wartlick, O., Salbreux, G., & Paluch, E. K. (2014). Stresses at the cell surface during animal cell morphogenesis. Current Biology, 24(10), R484–R494.

Cohen, M., Kam, Z., Addadi, L., Geiger, B., Albersdorfer, A., Sackmann, E., Addadi, L. (2006). Dynamic study of the transition from hyaluronan- to integrin-mediated adhesion in chondrocytes. The EMBO Journal, 25(2), 302–11.

Cole AG, Hall KH (2004). The nature and significance of invertebrate cartilages revisited: distribution and histology of cartilage and cartilage-like tissues within the metazoan. Zoology 107, 261-273

Collinet, C., Rauzi, M., Lenne, P., & Lecuit, T. (2015). Local and tissue-scale forces drive oriented junction growth during tissue extension, 17(10).

Collins, C., & Nelson, W. J. (2015). Running with neighbors : coordinating cell migration and cell – cell adhesion. Current Opinion in Cell Biology, 36, 62–70.

Conte, D., Garaffo, G., Lo Iacono, N., Mantero, S., Piccolo, S., Cordenonsi, M., Merlo, G. R. (2015). The apical ectodermal ridge of the mouse model of ectrodactyly Dlx5;Dlx6-/- shows altered stratification and cell polarity, which are restored by exogenous Wnt5a ligand. Human Molecular Genetics, 25(4), 740–754.

Cooper, KL, Oh, S, Sung, Y., Dasari, RR, Marc, W, & Tabin, CJ (2013). Multiple Phases of Chondrocyte Enlargement Underlie Differences in Skeletal Proportions, Nature 495(7441), 375–378

Cortes, M., Baria, A. T., & Schwartz, N. B. (2009). Sulfation of chondroitin sulfate proteoglycans is necessary for proper Indian hedgehog signaling in the developing growth plate, 1706,1697–1706.

Craig, F. M., Bentley, G., & Archer, C. W. (1987). The spatial and temporal pattern of collagens I and II and keratan sulphate in the developing chick metatarsophalangeal joint, 391, 383–391.

Cruz, E. M. D. La, Roland, J., Mccullough, B. R., & Blanchoin, L. (2010). Origin of twist-bend coupling in actin filaments. Biophysj, 99(6), 1852–1860.

Cytrynbaum, E. N., Rodionov, V., & Mogilner, A. (2006). Nonlocal mechanism of self-organization and centering of microtubule asters. Bulletin of Mathematical Biology, 68(5),1053–1072.

Dallas, S. L., Prideaux, M., & Bonewald, L. F. (2013). The Osteocyte: An Endocrine Cell and More. Endocrine Reviews, 34(5), 658–690.

Damek-Poprawa, M., Golub, E., Otis, L., Harrison, G., Phillips, C., & Boesze-Battaglia, K. (2006). Chondrocytes utilize a cholesterol-dependent lipid translocator to externalize phosphatidylserine. Biochemistry, 45(10), 3325–3336.

Danopoulos, S., Parsa, S., Alam, D. Al, Tabatabai, R., Baptista, S., Tiozzo, C., Bellusci, S. (2013). Transient inhibition of FGFR2b ligands signaling leads to irreversible loss of cellular β-catenin organization and signaling in AER during mouse limb development, 8(10).

Daulat, A. M., Luu, O., Sing, A., Zhang, L., Wrana, J. L., McNeill, H., … Angers, S. (2012). Mink1 regulates β-catenin-independent Wnt signaling via Prickle phosphorylation. Molecular and Cellular Biology, 32(1), 173–85.

Davidson, L. A., Marsden, M., Keller, R., & DeSimone, D. W. (2006). Integrin alpha5beta1 and Fibronectin Regulate Polarized Cell Protrusions Required for Xenopus Convergence and Extension. Current Biology, 16(9), 833–844.

de Andrea, C. E., Wiweger, M., Prins, F., Bovee, J. V. M. G., Romeo, S., & Hogendoorn, P. C.W. (2010). Primary cilia organization reflects polarity in the growth plate and implies loss of polarity and mosaicism in osteochondroma. Lab Invest, 90(7), 1091–1101.

De Ceuninck, F., Lesur, C., Pastoureau, P., Caliez, A., & Sabatini, M. (2004). Culture of chondrocytes in alginate beads. Methods in Molecular Medicine, 100, 15–22.

Delanoë-Ayari, H., Al Kurdi, R., Vallade, M., Gulino-Debrac, D., & Riveline, D. (2004). Membrane and acto-myosin tension promote clustering of adhesion proteins. PNAS, 101(8), 2229–2234.

DeLise, A. M., Fischer, L., & Tuan, R. S. (2000). Cellular interactions and signaling in cartilage development. Osteoarthritis and Cartilage, 8(5), 309–334.

Demali, K. A., Barlow, C. A., & Burridge, K. (2002). Coupling membrane protrusion to matrix adhesion, 159(5), 881–891.

DeMali, K. A., Sun, X., & Bui, G. A. (2014). Force Transmission at Cell–Cell and Cell–Matrix Adhesions. Biochemistry, 53(49), 7706–7717.

Dodds, G. S. (1930). Row formation and other types of arrangement of cartilage cells in endochondral ossification. Anat. Rec. 46, 385-399.

Judge, D. P., & Dietz, H. C. (2005). Marfan's syndrome. Lancet, 366(9501), 1965–1976.
Dohn, M. R., Mundell, N. A., Sawyer, L. M., Dunlap, J. A., & Jessen, J. R. (2013). Planar cell polarity proteins differentially regulate extracellular matrix organization and assembly during zebrafish gastrulation. Developmental Biology, 383(1), 39–51.

Doodhi, H., Katrukha, E. A., Kapitein, L. C., & Akhmanova, A. (2014). Mechanical and geometrical constraints control kinesin-based microtubule guidance. Current Biology, 24(3), 322–328.

Dowling, E. P., Ronan, W., & Mcgarry, J. P. (2013). Acta Biomaterialia Computational investigation of in situ chondrocyte deformation and actin cytoskeleton remodelling under physiological loading. Acta Biomaterialia, 9(4), 5943–5955.

Dreier, R., Opolka, A., Grifka, J., Bruckner, P., & Grässel, S. (2008). Collagen IX-deficiency seriously compromises growth cartilage development in mice. Matrix Biology, 27(4), 319–329.

Du, J., Chen, X., Liang, X., Zhang, G., Xu, J., He, L Yang, C. (2011). Integrin activation and internalization on soft ECM as a mechanism of induction of stem cell differentiation by ECM elasticity. PNAS, 108(23), 9466–9471.

Dudley, A. T., Ros, M. A., & Tabin, C. J. (2002). A re-examination of proximodistal patterning during vertebrate limb development. Nature, 418(6897), 539–544.

Duke, P. J., & Montufar-Solis, D. (1999). Exposure to altered gravity affects all stages of

endochondral cartilage differentiation. Advances in Space Research, 24(6), 821–827.

Duman, J. G., Mulherkar, S., Tu, Y. K., X. Cheng, J., & Tolias, K. F. (2015). Mechanisms for spatiotemporal regulation of Rho-GTPase signaling at synapses. Neuroscience Letters, 601, 4–10.

Dürr, J., Goodman, S., Potocnik, A., von der Mark, H., & von der Mark, K. (1993). Localization of β1-integrins in human cartilage and their role in chondrocyte adhesion to collagen and fibronectin. Experimental Cell Research, 207(2), 235–244.

Dzamba, B. J., Jakab, K. R., Marsden, M., Schwartz, M. A., & DeSimone, D. W. (2009). Cadherin adhesion, tissue tension, and noncanonical Wnt signaling regulate fibronectin matrix organization. Developmental Cell, 16(3), 421–432.

Eames, B. F., Yan, Y.-L., Swartz, M. E., Levic, D. S., Knapik, E. W., Postlethwait, J. H., & Kimmel, C. B. (2011). Mutations in fam20b and xylt1 reveal that cartilage matrix controls timing of endochondral ossification by inhibiting chondrocyte maturation. PLoS Genetics, 7(8), e1002246.

Edwards, J. C., Wilkinson, L. S., Jones, H. M., Soothill, P., Henderson, K. J., Worrall, J. G., & Pitsillides, A. A. (1994). The formation of human synovial joint cavities: a possible role for hyaluronan and CD44 in altered interzone cohesion. Journal of Anatomy, 185(Pt 2), 355–367.

Emerman, A. B., Zhang, Z.-R., Chakrabarti, O., & Hegde, R. S. (2010). Compartment-restricted biotinylation reveals novel features of prion protein metabolism *in vivo*. Molecular Biology of the Cell, 21(24), 4325–4337.

Enomoto-Iwamoto M, Iwamoto M, Nakashima K, Mukudai Y, Boettiger D, Pacifici M, Kurisu K, Suzuki F: Involvement of α5β1 integrin in matrix interactions and proliferation of chondrocytes. Journal of Bone and Mineral Research 1997, 12(7), 1124-1132.

Erdemir, A., Bennetts, C., Davis, S., Reddy, A., & Sibole, S. (2015). Multiscale cartilage biomechanics: technical challenges in realizing a high-throughput modeling and simulation workflow. Interface Focus, 5(2), 20140081.

Everaert B. R., Boulet G. A., Timmermans J. P., Vrints C. J. (2011) Importance of suitable reference gene selection for quantitative real-time PCR: special reference to mouse myocardial infarction studies. PLoS ONE 6:e23793

Eykhoff, P. (1994). Every good regulator of a system must be a model of that system. Modeling, Identification and Control: A Norwegian Research Bulletin, 15(3), 135–139.

Farhadifar, R., Röper, J.C., Aigouy, B., Eaton, S., & Jülicher, F. (2007). The influence of cell mechanics, cell-cell interactions, and proliferation on epithelial packing. Current Biology, 17(24), 2095–2104.

Fässler, R., Pfaff, M., Murphy, J., Noegel, A. A., Johansson, S., Timpl, R., & Albrecht, R. (1995). Lack of beta 1 integrin gene in embryonic stem cells affects morphology, adhesion, and migration but not integration into the inner cell mass of blastocysts. The Journal of Cell Biology, 128(5), 979 LP-988.

Fässler, R., Schnegelsberg, P. N., Dausman, J., Shinya, T., Muragaki, Y., McCarthy, M. T., Jaenisch, R. (1994). Mice lacking alpha 1 (IX) collagen develop noninflammatory degenerative joint disease. PNAS, 91(11), 5070–5074.

Fernandes, R. J., Weis, M., Scott, M. A., Seegmiller, R. E., & Eyre, D. R. (2007). Collagen XI chain misassembly in cartilage of the chondrodysplasia (cho) mouse. Matrix Biology: Journal of the International Society for Matrix Biology, 26(8), 597–603.

Finnøy, A., Olstad, K., Lilledahl, M. B., & Finnøy, A. (2016). Second harmonic generation imaging reveals a distinct organization of collagen fibrils in locations associated with cartilage growth fibrils in locations associated with cartilage growth. Connective Tissue Research, 57(5), 374–387.

Foty RA, Steinberg MS (2005). The differential adhesion hypothesis: a direct evaluation. Dev Biol. Feb 1;278(1), 255-63.

Friedland, J. C., Lee, M. H., & Boettiger, D. (2009). mechanically activated integrin switch controls α5β1 function. Science, 323(5914), 642 LP-644.

Fuller, B. G. (2010). Self-organization of intracellular gradients during mitosis. Cell Division, 5,5.

Gallos, L. K., Song, C., Havlin, S., & Makse, H. A. (2007). Scaling theory of transport in complex biological networks. PNAS, 104(19), 7746–7751.

Gálvez, B. G., Matías-Román, S., Yáñez-Mó, M., Sánchez-Madrid, F., & Arroyo, A. G. (2002). ECM regulates MT1-MMP localization with β1 or αvβ3 integrins at distinct cell compartments modulating its internalization and activity on human endothelial cells. Journal of Cell Biology, 159(3), 509–521.

Gao, B., Hu, J., Stricker, S., Cheung, M., Ma, G., Law, K. F., and Chan, D. (2009). A mutation in Ihh that causes digit abnormalities alters its signalling capacity and range. Nature, 458(7242), 1196–1200.

Gao, B., Song, H., Bishop, K., Elliot, G., Garrett, L., English, M. A., Yang, Y. (2011). Wnt signaling gradients establish planar cell polarity by inducing Vangl2 phosphorylation through Ror2. Developmental Cell, 20(2), 163–176.

Gao, J., Williams, J. L., & Roan, E. (2016). Multi-scale modeling of growth plate cartilage mechanobiology. Biomechanics and Modeling in Mechanobiology.

Garciadiego-Cazares, D. (2004). Coordination of chondrocyte differentiation and joint formation by 5 1 integrin in the developing appendicular skeleton. Development, 131(19), 4735–4742.

Garrison P, Yue S, Hanson J, Baron J, Lui JC . (2017) Spatial regulation of bone morphogenetic proteins (BMPs) in postnatal articular and growth plate cartilage Plos One 12(5): e0176752

Garstang, W. (1922). The Theory of Recapitulation: A Critical Re-statement of the Biogenetic Law. Journal of the Linnean Society of London, Zoology, 35(232), 81–101.

Garvalov, B. K., Higgins, T. E., Sutherland, J. D., Zettl, M., Scaplehorn, N., Köcher, T., Way, M. (2003). The conformational state of Tes regulates its zyxin-dependent recruitment to focal adhesions, 33–39.

Geister, K. A., & Camper, S. A. (2015). Advances in Skeletal Dysplasia Genetics. Ann. Rev Genomics Hum Genet, 16(4), 199–227.

Gkantidis, N., Blumer, S., Katsaros, C., Graf, D., & Chiquet, M. (2012). Site-Specific Expression of Gelatinolytic Activity during Morphogenesis of the Secondary Palate in the Mouse Embryo. PLoS ONE, 7(10).

Godwin, A. R. F., Starborg, T., Sherratt, M. J., Roseman, A. M., & Baldock, C. (2016). Defining the hierarchical organisation of collagen VI microfibrils at nanometre to micrometre length scales. Acta Biomaterialia.

Goehring, N. W., & Grill, S. W. (2013). Cell polarity: Mechanochemical patterning. Trends in Cell Biology, 23(2), 72–80.

Goksoy, E., Ma, Y.-Q., Wang, X., Kong, X., Perera, D., Plow, E. F., & Qin, J. (2008). Structural basis for the autoinhibition of talin in regulating integrin activation. Molecular Cell, 31(1), 124–133.

Goldstein, B., Takeshita, H., Mizumoto, K., & Sawa, H. (2006). Wnt Signals Can Function as Positional Cues in Establishing Cell Polarity. Developmental Cell, 10(3), 391–396.

Gopal, S., Multhaupt, H. A. B., Pocock, R., & Couchman, J. R. (n.d.). Cell-extracellular matrix and cell-cell adhesion are linked by syndecan-4. Matrix Biology.

Gosset M, Berenbaum F, Thirion S, Jacques C: Primary culture and phenotyping of murine chondrocytes. Nat Protocols 2008, 3(8):1253-1260.

Goto, T., Davidson, L., Asashima, M., & Keller, R. (2005). Planar cell polarity genes regulate polarized extracellular matrix deposition during frog gastrulation. Current Biology, 15(8), 787–793.

Gould, R. P., Selwood, L., Day, A., & Wolpert, L. (1974). The mechanism of cellular orientation during early cartilage formation in the chick limb and regenerating amphibian limb. Experimental Cell Research, 83(2), 287–296.

Grant WT, Sussman MD, Balian G (1985). A disulfide-bonded short chain collagen synthesized by degenerative and calcifying zones of bovine growth plate cartilage. The Journal of biological chemistry, 260(6), 3798-3803.

Grashoff, C., Aszódi, A., Sakai, T., Hunziker, E. B., & Fässler, R. (2003). Integrin-linked kinase regulates chondrocyte shape and proliferation. EMBO Reports, 4(4), 432–438.

Gregory, D. E., & Callaghan, J. P. (2012). Medical Engineering & Physics An examination of the mechanical properties of the annulus fibrosus : The effect of vibration on the intra-lamellar matrix strength. Medical Engineering and Physics, 34(4), 472–477.

Grigoriev, I., Borisy, G., & Vorobjev, I. (2006). Regulation of microtubule dynamics in 3T3 fibroblasts by Rho family GTPases. Cell Motility and the Cytoskeleton, 63(1), 29–40.

Grimsrud CD, Romano PR, D'Souza M, Puzas JE, Schwarz EM, Reynolds PR, Roiser RN, O'Keefe RJ BMP signaling stimulates chondrocyte maturation and the expression of Indian hedgehog. J Orthop Res (2000) 19,18–25

Grishchuk, E. L., Molodtsov, M. I., Ataullakhanov, F. I., & McIntosh, J. R. (2005). Force production by disassembling microtubules. Nature, 438(7066), 384–388.

Gros, J., Hu, J. K.-H., Vinegoni, C., Feruglio, P. F., Weissleder, R., & Tabin, C. J. (2010). Wnt5a/Jnk and FGF/Mapk pathways regulate the cellular events shaping the vertebrate limb bud. Current Biology, 20(22),1993–2002.

Gross JB, Hanken J. (2008). Review of fate-mapping studies of osteogenic cranial neural crest in vertebrates. Dev Biol. 317(2),389-400

Guillot, C., & Lecuit, T. (2013). Adhesion disengagement uncouples intrinsic and extrinsic

forces to drive cytokinesis in epithelial tissues. Developmental Cell, 24(3), 227–241.

Guimond, J.-C., Lévesque, M., Michaud, P.-L., Berdugo, J., Finnson, K., Philip, A., & Roy, S. (2010). BMP-2 functions independently of SHH signaling and triggers cell condensation and apoptosis in regenerating axolotl limbs. BMC Developmental Biology, 10, 15.

Guo JF, Jourdian GW, MacCallum DK: Culture and growth characteristics of chondrocytes encapsulated in alginate beads. Connective tissue research 1989, 19(2-4):277-297.

Guo J, Chung U-I, Kondo H, Bringhurst FR, Kronenberg HM (2002). The PTH/PTHrP receptor can delay chondrocyte hypertrophy *in vivo* without activating phospholipase C. Developmental Cell, 3(2), 183-194.

Gupta, M., Sarangi, B. R., Deschamps, J., Nematbakhsh, Y., Callan-Jones, A., Margadant, F., Ladoux, B. (2015). Adaptive rheology and ordering of cell cytoskeleton govern matrix rigidity sensing. Nature Communications, 6, 7525.

Gustafsson, E., & Fa, R. (2000). Insights into extracellular matrix functions from mutant mouse models, 68, 52–68.

Habicher, J., Haitina, T., Eriksson, I., Holmborn, K., Dierker, T., Ahlberg, P. E., & Ledin, J. (2015). Chondroitin / dermatan sulfate modification enzymes in zebrafish development. PLoS ONE, 10(3)

Hadjivasiliou, Z., Hunter, G. L., & Baum, B. (2016). A new mechanism for spatial pattern formation via lateral and protrusion-mediated lateral signalling. Journal of The Royal Society Interface, 13(124).

Haeger, A., Wolf, K., Zegers, M. M., & Friedl, P. (2015). Collective cell migration: Guidance principles and hierarchies. Trends in Cell Biology, 25(9), 556–566.

Hafez, A., Squires, R., Pedracini, A., Joshi, A., Seegmiller, R. E., & Oxford, J. T. (2015). Col11a1 regulates bone microarchitecture during embryonic development. Journal of Developmental Biology, 3(4), 158–176.

Hägg, P., Väisänen, T., Tuomisto, A., Rehn, M., Tu, H., Huhtala, P., Pihlajaniemi, T. (2001). Type XIII collagen: a novel cell adhesion component present in a range of cell–matrix adhesions and in the intercalated discs between cardiac muscle cells. Matrix Biology, 19(8), 727–742.

Hamburger V, Hamilton HL. A series of normal stages in the development of the chick embryo. (1951). Dev Dyn 1992(195), 231-72.

Harrington EK, Coon DJ, Kern MF, Svoboda KKH (2010). PTH Stimulated Growth and Decreased Col-X Deposition are Phosphotidylinositol-3,4,5 Triphosphate Kinase and Mitogen Activating Protein Kinase Dependent in Avian Sterna. The Anatomical Record: Advances in Integrative Anatomy and Evolutionary Biology, 293(2), 225-234.

Häusler, G., Helmreich, M., Marlovits, S., & Egerbacher, M. (2002). Integrins and extracellular matrix proteins in the human childhood and adolescent growth plate. Calcified Tissue International, 71(3), 212–218.

Hayashi T, Carthew RW. Surface mechanics mediate pattern formation in the developing retina. Nature. 2004 Oct 7;431(7009):647-52.

Haycraft, C. J., Zhang, Q., Song, B., Jackson, W. S., Detloff, P. J., Serra, R., & Yoder, B. K. (2007). Intraflagellar transport is essential for endochondral bone formation, 316, 307–316.

Heemskerk, I., Lecuit, T., & LeGoff, L. (2014). Dynamic clonal analysis based on chronic *in vivo* imaging allows multiscale quantification of growth in the Drosophila wing disc. Development, 141(11), 2339-2348.

Helminen, H. J., Säämänen, A. -M., Salminen, H., & Hyttinen, M. M. (2002). Transgenic mouse models for studying the role of cartilage macromolecules in osteoarthritis. Rheumatology , 41(8), 848–856.

Hering, T. M., Wirthlin, L., Ravindran, S., & Mcalinden, A. (2014). Changes in type II procollagen isoform expression during chondrogenesis by disruption of an alternative 5′ splice site within Col2a1 exon 2. Matrix Biology, 36, 51–63.

Herszterg S, Leibfried A, Bosveld F, Martin C, Bellaiche Y (2013). Interplay between the dividing cell and its neighbors regulates adherens junction formation during cytokinesis in epithelial tissue. Dev. Cell. 24(3), 256-70

Herzfeld, J. (2004), Crowding-induced organization in cells: spontaneous alignment and sorting of filaments with physiological control points. J. Mol. Recognit., 17, 376–381.

Hiramatsu K, Sasagawa S, Outani H, Nakagawa K, Yoshikawa H, Tsumaki N. (2011). Generation of hyaline cartilaginous tissue from mouse adult dermal fibroblast culture by defined factors. J Clin Invest 121, 640

Hirasawa T, Nagashima H, Kuratani S. (2013). The endoskeletal origin of the turtle carapace. Nat Commun. 4():2107.

Hirasawa, T., & Kuratani, S. (2015). Evolution of the vertebrate skeleton: morphology, embryology, and development. Zoological Letters, 1, 2.

Hiscock, TW, Megason, SG (2015) Orientation of Turing-like patterns by morphogen gradients and tissue anisotropies. Cell Systems. 1 (6), 408 - 416

Ho, H. H., Susman, M. W., Bikoff, J. B., Kyoung, Y., Jonas, A. M., Hu, L., Eldon, M. (2012). Wnt5a-Ror-Dishevelled signaling constitutes a core developmental pathway that controls tissue morphogenesis, PNAS, 109(11), 4044-51

Holder, N. (1977). An experimental investigation into the early development of the chick elbow joint. Journal of Embryology and Experimental Morphology, 39(1), 115-127.

Holmborn, K., Habicher, J., Kasza, Z., Eriksson, A. S., Filipek-gorniok, B., Gopal, S., Ledin,J. (2012). On the roles and regulation of chondroitin sulfate and heparan sulfate in zebrafish pharyngeal cartilage, 287(40), 33905–33916.

Hojo, H., Mcmahon, A. P., & Ohba, S. (2016). An emerging regulatory landscape for skeletal development. Trends in Genetics, 32(12), 774–787.

Hosseini-farahabadi, S., Geetha-loganathan, P., Fu, K., Nimmagadda, S., Yang, H. J., & Richman, J. M. (2013). Dual functions for WNT5A during cartilage development and in disease. Matrix Biology, 32(5), 252–264.

Hu, K., Ji, L., Applegate, K. T., Danuser, G., & Waterman-Storer, C. M. (2007). Differential transmission of actin motion within focal adhesions. Science, 315(5808), 111-115.

Hu, J. K.-H., McGlinn, E., Harfe, B. D., Kardon, G., & Tabin, C. J. (2012). Autonomous and nonautonomous roles of Hedgehog signaling in regulating limb muscle formation. Genes & Development, 26(18), 2088–2102.

Huang, C., Wang, T.C., Lin, B.-H., Wang, Y.W., Johnson, S. L., & Yu, J. (2009). Collagen IX is required for the integrity of collagen II fibrils and the regulation of vascular plexus formation in Zebrafish caudal fins. Developmental Biology, 332(2), 360–370.

Huang, H., & Kornberg, T. B. (2016). Cells must express components of the planar cell polarity system and extracellular matrix to support cytonemes. eLife, 5, e18979.

Huang, J., Chew, T. G., Gu, Y., Palani, S., Kamnev, A., Martin, D. S., Balasubramanian, M. K. (2016). Curvature-induced expulsion of actomyosin bundles during cytokinetic ring contraction. eLife, 5, e21383.

Huang, S., Brangwynne, C. P., Parker, K. K., & Ingber, D. E. (2005). Symmetry-breaking in mammalian cell cohort migration during tissue pattern formation: role of random- walk persistence. Cell. Motil. Cytoskeleton, 213, 201–213.

Huang, X., Birk, D. E., & Goetinck, P. F. (1999). Mice lacking matrilin-1 (cartilage matrix protein) have alterations in type II collagen fibrillogenesis and fibril organization. Dev. Dyn. 216(4-5), 434–441.

Huang, Z., Yan, D.-P., & Ge, B.-X. (2008). JNK regulates cell migration through promotion of tyrosine phosphorylation of paxillin. Cellular Signaling, 20(11), 2002–2012.

Huber, F. and Käs, J. (2011), Self-regulative organization of the cytoskeleton. Cytoskeleton, 68: 259–265.

Hyams, J. S., & Borisy, G. G. (1978). Nucleation of microtubules in vitro by isolated spindle pole bodies of the yeast Saccharomyces cerevisiae. Journal of Cell Biology, 78(2), 401–414.

Hynes, R. O. (2009). Extracellular matrix: not just pretty fibrils. Science (New York, N.Y.), 326(5957), 1216–1219.

Hyttinen, M. M., Holopainen, J., René van Weeren, P., Firth, E. C., Helminen, H. J., & Brama, P. A. J. (2009). Changes in collagen fibril network organization and proteoglycan distribution in equine articular cartilage during maturation and growth. Journal of Anatomy, 215(5), 584–591.

Inoue T, Hashimoto R, Matsumoto A, Jahan E, Rafiq AM, Udagawa J, Hatta T, Otani H: *In vivo* analysis of Arg-Gly-Asp sequence/integrin α5β1-mediated signal involvement in embryonic enchondral ossification by exo-utero development system. Journal of Bone and Mineral Research 2014, 29(7),1554-1563.

Jeong, C., Lee, J. Y., Kim, J., Chae, H., Park, H., Kim, M., Jung, J. (2014). Novel COL9A3 mutation in a family diagnosed with multiple epiphyseal dysplasia: a case report. BMC Musculoskeletal Disorders, 15(1), 371.

Jülich, D., Cobb, G., Melo, A. M., McMillen, P., Lawton, A. K., Mochrie, S. G. J., Holley, S. A. (2015). Cross-scale Integrin regulation organizes ECM and tissue topology. Developmental Cell, 34(1), 33–44.

Kahn, J., Shwartz, Y., Blitz, E., Krief, S., Sharir, A., Breitel, D. A., Zelzer, E. (2009). Muscle contraction is necessary to maintain joint progenitor cell fate. Developmental Cell, 16(5), 734–743.

Karp SJ, Schipani E, St-Jacques B, Hunzelman J, Kronenberg H, McMahon AP (2000). Indian hedgehog coordinates endochondral bone growth and morphogenesis via Parathyroid Hormone

related-Protein-dependent and -independent pathways. Development (Cambridge, England), 127(3), 543-548.

Kato, K., Bhattaram, P., Penzo-Méndez, A., Gadi, A., & Lefebvre, V. (2015). SOXC transcription factors induce cartilage growth plate formation in mouse embryos by promoting noncanonical WNT signaling. Journal of Bone and Mineral Research: The Official Journal of the American Society for Bone and Mineral Research, 30(9), 1560–1571.

Katsumi, A., Milanini, J., Kiosses, W. B., del Pozo, M. A., Kaunas, R., Chien, S., Schwartz, M. A. (2002). Effects of cell tension on the small GTPase Rac. The Journal of Cell Biology, 158(1), 153–164.

Kaucka, M., Ivashkin, E., Gyllborg, D., Zikmund, T., Tesarova, M., Kaiser, J., Adameyko, I. (2016). Analysis of neural crest–derived clones reveals novel aspects of facial development. Science Advances, 2(8).

Kaufman, MH. The atlas of mouse development, first edition. (1992). Academic press.

Kerridge, S., Munjal, A., Philippe, J.-M., Jha, A., de las Bayonas, A. G., Saurin, A. J., & Lecuit, T. (2016). Modular activation of Rho1 by GPCR signalling imparts polarized myosin II activation during morphogenesis. Nature Cell Biology, 18(3), 261–270.

Kerschnitzki, M., Kollmannsberger, Ã. P., Burghammer, Ã. M., Duda, G. N., Weinkamer, R., Wagermaier, W., & Fratzl, P. (2013). J BMR Architecture of the Osteocyte Network Correlates With Bone Material Quality, 28(8), 1837–1845.

Keung, A. J., Joung, J. K., Khalil, A. S., & Collins, J. J. (2015). Chromatin regulation at the frontier of synthetic biology. Nature Reviews. Genetics, 16(3), 159–171.

Kiecker, C., Graham, A., & Logan, M. (2016). Differential Cellular Responses to Hedgehog Signalling in Vertebrates—What is the Role of Competence? Journal of Developmental Biology.

Klumpers, D. D., Smit, T. H., & Mooney, D. J. (2015). The effect of growth-mimicking continuous strain on the early stages of skeletal development in micromass culture. PLoS ONE, 10(4), 1–11.

Kobayashi, T., Chung, U., Schipani, E., Starbuck, M., Karsenty, G., Katagiri, T., Kronenberg, H. M. (2002). PTHrP and Indian hedgehog control differentiation of growth plate chondrocytes at multiple steps, 2986, 2977–2986.

Kock, L., van Donkelaar C.C., Ito K. (2012) Tissue engineering of functional articular cartilage: the current status. Cell Tissue Res. 347(3), 613-627

Komarova, Y. A., Huang, F., Geyer, M., Daneshjou, N., Garcia, A., Idalino, L., Malik, A. B. (2012). VE-cadherin signaling induces Eb3 phosphorylation to suppress microtubule growth and assemble adherens junctions. Molecular Cell, 48(6), 914–925.

Komarova, Y., De Groot, C. O., Grigoriev, I., Gouveia, S. M., Munteanu, E. L., Schober, J. M., Akhmanova, A. (2009). Mammalian end binding proteins control persistent microtubule growth. Journal of Cell Biology, 184(5), 691–706.

Koo, H., & Yamada, K. M. (2016). Dynamic cell – matrix interactions modulate microbial biofilm and tissue 3D microenvironments. Current Opinion in Cell Biology, 42(1), 102–112. Körkkö, J., Ritvaniemi, P., Haataja, L., Kääriäinen, H., Kivirikko, K. I., Prockop, D. J., & Ala- Kokko, L. (1993). Mutation in type II procollagen (COL2A1) that substitutes aspartate for glycine alpha 1-67 and that causes cataracts and retinal detachment: evidence for molecular heterogeneity in the

Wagner syndrome and the Stickler syndrome (arthroophthalmopathy). American Journal of Human Genetics, 53(1), 55–61.

Korhonen, R. K., & Herzog, W. (2008). Depth-dependent analysis of the role of collagen fibrils, fixed charges and fluid in the pericellular matrix of articular cartilage on chondrocyte mechanics. Journal of Biomechanics, 41(2), 480–485.

Kornberg, T. B. (2014). Cytonemes and the dispersion of morphogens. Wiley Interdisciplinary Reviews. Developmental Biology, 3(6), 445–463.

Koyama, E., Young, B., Nagayama, M., Shibukawa, Y., Enomoto-iwamoto, M., Iwamoto, M., Pacifici, M. (2007). Conditional Kif3a ablation causes abnormal hedgehog signaling topography , growth plate dysfunction , and excessive bone and cartilage formation during mouse skeletogenesis, 2169, 2159–2169.

Kozhemyakina E, Lassar AB, Zelzer E (2015). A pathway to bone: signaling molecules and transcription factors involved in chondrocyte development and maturation. Development (Cambridge, England), 142(5):817-831.

Koziel, L., Kunath, M., Kelly, O. G., & Vortkamp, A. (2004). Ext1-Dependent Heparan Sulfate Regulates the Range of Ihh Signaling during Endochondral Ossification, 6, 801–813.

Koziel, L., Wuelling, M., Schneider, S., & Vortkamp, A. (2005). Gli3 acts as a repressor downstream of Ihh in regulating two distinct steps of chondrocyte differentiation. Development (Cambridge, England), 132(23), 5249–60.

Krakow D, Rimoin D. The skeletal dysplasias. Genetics in Medicine (2010) 12, 327–341

Kreeger P.K., Deck J.W., Woodruff T.K., Shea L.D. (2006). The in vitro regulation of ovarian follicle development using alginate-extracellular matrix gels. Biomaterials, 27(5):714-723.

Krendel, M., Zenke, F. T., & Bokoch, G. M. (2002). Nucleotide exchange factor GEF-H1 mediates cross-talk between microtubules and the actin cytoskeleton. Nature Cell Biology, 4(4), 294–301.

Kronenberg H.M., Lee K., Lanske B., Segre G.V. (1997). Parathyroid hormone-related protein and Indian hedgehog control the pace of cartilage differentiation. J Endocrinol. 154 Suppl:S39-45. PMID: 9379136.

Kronenberg H.M. (2003). Developmental regulation of the growth plate. Nature, 423(6937), 332-336.

Kronenberg H.M. (2006). PTHrP and skeletal development. Annals of the New York Academy of Sciences. 1068(1), 1-13.

Kruger C, Kappen C. (2010). Expression of cartilage developmental genes in Hoxc8 and Hoxd4 transgenic mice. PLoS ONE 5:2 e8978

Kumar, M. E., Bogard, P. E., Espinoza, F. H., Menke, D. B., Kingsley, D. M., & Krasnow, M. A. (2014). Defining a mesenchymal progenitor niche at single cell resolution. Science (New York, N.Y.), 346(6211), 1258810.

Kuss, P., Kraft, K., Stumm, J., Ibrahim, D., Vallecillo-Garcia, P., Mundlos, S., & Stricker, S. (2014). Regulation of cell polarity in the cartilage growth plate and perichondrium of metacarpal elements by HOXD13 and WNT5A. Developmental Biology, 385(1), 83–93.

Kyöstilä, K., Lappalainen, A. K., & Lohi, H. (2013). Canine chondrodysplasia caused by a truncating mutation in collagen-binding integrin alpha subunit 10. PLoS ONE, 8(9), e75621.

Ladoux, B., Anon, E., Lambert, M., Rabodzey, A., Hersen, P., Buguin, A., & Silberzan, P. (2010). Strength Dependence of Cadherin-Mediated Adhesions. Biophysj, 98(4), 534–542.

Laevsky G, Knecht D.A. (2003) Cross-linking of actin filaments by myosin II is a major contributor to cortical integrity and cell motility in restrictive environments. J Cell Sci. 116(18), 3761-70.

Langelier, E., Suetterlin, R., Hoemann, C. D., Aebi, U., & Buschmann, M. D. (2000). The chondrocyte cytoskeleton in mature articular cartilage: structure and distribution of actin, tubulin, and vimentin filaments. Journal of Histochemistry & Cytochemistry, 48(10), 1307–1320.

Langer R, Vacanti JP: Tissue engineering. Science 1993, 260(5110), 920-926.

Lau, K., Tao, H., Liu, H., Wen, J., Sturgeon, K., Sorfazlian, N., Hopyan, S. (2015). Anisotropic stress orients remodelling of mammalian limb bud ectoderm. Nature Cell Biology, 17(5), 569–579.

Lauing, K. L., Cortes, M., Domowicz, M. S., Henry, J. G., Baria, A. T., & Schwartz, N. B. (2014). Aggrecan is required for growth plate cytoarchitecture and differentiation. Developmental Biology, 396(2), 224–236.

Lecuit, T., Lenne, P.-F., & Munro, E. (2011). Force generation, transmission, and integration during cell and tissue morphogenesis. Annual Review of Cell and Developmental Biology, 27(1), 157–184.

Lecuit, T., & Yap, A. S. (2015). E-cadherin junctions as active mechanical integrators in tissue dynamics. Nature Publishing Group, 17(5), 533–539.

Lee, D (2017). A microfluidic platform and atomic force microscopy for a mechanobiology study: dynamic compressive stress reduces growth plate chondrocyte stiffness (doctoral dissertation). ETD collection for University of Nebraska - Lincoln. AAI10637184.

Lee KY, Mooney DJ: Hydrogels for tissue engineering. Chem Rev 2001, 101(7), 1869-1879.

Lee KY, Mooney DJ: Alginate: Properties and biomedical applications. Progress in Polymer Science 2012, 37(1), 106-126.

Lee, S. E., Kamm, R. D., & Mofrad, M. R. K. (2007). Force-induced activation of Talin and its possible role in focal adhesion mechanotransduction. Journal of Biomechanics, 40(9), 2096–2106.

Lefort, C. T., Wojciechowski, K., & Hocking, D. C. (2011). N-cadherin cell-cell adhesion complexes are regulated by fibronectin matrix assembly. Journal of Biological Chemistry, 286(4), 3149–3160.

Leijten J.C., Moreira Teixeira L.S., Landman E.B., van Blitterswijk C.A, Carperien M (2012). Hypoxia inhibits hypertrophic differentiation and endochondral ossification in explanted tibiae. Plos One. 7(11) e49896

Leite-Castro J, Beviano V, Rodrigues PN and Freitas R. (2016). HoxA Genes and the Fin-to-Limb Transition in Vertebrates J. Dev. Biol. 4(1), 10

Levayer, R., & Lecuit, T. (2013). Article Oscillation and Polarity of E-Cadherin Asymmetries Control Actomyosin Flow Patterns during Morphogenesis. Developmental Cell, 26(2), 162–175.

Li, J., Luo, H., Wang, R., Lang, J., Zhu, S., Zhang, Z., Wu, Q. (2016). Systematic Reconstruction of Molecular Cascades Regulating GP Development Using Single-Cell RNA-Seq. Cell Reports, 15(7), 1467–1480.

Li, S.-W., Takanosu, M., Arita, M., Bao, Y., Ren, Z.-X., Maier, A., Prockop, D. J. and Mayne, R. (2001), Targeted disruption of Col11a2 produces a mild cartilage phenotype in transgenic mice: Comparison with the human disorder otospondylomegaepiphyseal dysplasia (OSMED). Dev. Dyn., 222, 141–152.

Li, S., Li, S., Han, Y., Tong, C., Wang, B., Chen, Y., & Jiang, J. (2016). Regulation of Smoothened Phosphorylation and High-Level Hedgehog Signaling Activity by a Plasma Membrane Associated Kinase. PLoS Biology, 14(6), e1002481.

Li, X., Young, N. M., Tropp, S., Hu, D., Xu, Y., Hallgrímsson, B., & Marcucio, R. S. (2013). Quantification of shape and cell polarity reveals a novel mechanism underlying malformations resulting from related FGF mutations during facial morphogenesis. Human Molecular Genetics, 22(25), 5160–5172.

Li, Y., Ahrens, M. J., Wu, A., Liu, J., & Dudley, A. T. (2011). Calcium/calmodulin-dependent protein kinase II activity regulates the proliferative potential of growth plate chondrocytes. Development (Cambridge, England), 138(2), 359–70.

Li, Y., & Dudley, A. T. (2009). Noncanonical frizzled signaling regulates cell polarity of growth plate chondrocytes. Development (Cambridge, England), 136(7), 1083–92.

Lim, J., Tu, X., Choi, K., Akiyama, H., Mishina, Y., & Long, F. (2015). BMP-Smad4 signaling is required for precartilaginous mesenchymal condensation independent of Sox9 in the mouse. Developmental Biology, 400(1), 132–138.

Lin Z, Willers C, Xu JA, Zheng MH (2006). The chondrocyte: Biology and clinical application. Tissue engineering, 12(7),1971-1984.

Liu, C. H., Singh, M., Li, J., Han, Z., Wu, C., Wang, S., Larin, K. V. (2015). Quantitative assessment of hyaline cartilage elasticity during optical clearing using optical coherence elastography. Sovremennye Tehnologii v Medicine, 7(1), 44–51.

Liu, C., Lin, C., Gao, C., May-Simera, H., Swaroop, A., & Li, T. (2014). Null and hypomorph Prickle1 alleles in mice phenocopy human Robinow syndrome and disrupt signaling downstream of Wnt5a. Biology Open, 3(9), 861–70.

Liu H, Lee YW, Dean MF: Re-expression of differentiated proteoglycan phenotype by dedifferentiated human chondrocytes during culture in alginate beads. Biochimica et biophysica acta 1998, 1425(3), 505-515.

Liu, S., Calderwood, D. A., & Ginsberg, M. H. (2000). Integrin cytoplasmic domain-binding proteins. Journal of Cell Science, 113(20), 3563-3571.

Liu, Y., Zhou G., Cao Y., (2017). Recent progress in cartilage tissue engineering – our experience and future directions. Engineering 3, 28-35.

Loganathan, R., Rongish, B. J., Smith, C. M., Filla, M. B., Czirok, A., Bénazéraf, B., & Little, C.D. (2016). Extracellular matrix motion and early morphogenesis. Development, 143(12), 2056-2065.

Lomakin, A. J., Semenova, I., Zaliapin, I., Kraikivski, P., Nadezhdina, E., Slepchenko, B. M., Rodionov, V. (2009). CLIP-170-Dependent Capture of Membrane Organelles by Microtubules Initiates Minus-End Directed Transport. Developmental Cell, 17(3), 323–333.

Long F., Zhang X.M., Karp S., Yang Y., McMahon A.P. (2001). Genetic manipulation of hedgehog signaling in the endochondral skeleton reveals a direct role in the regulation of chondrocyte proliferation. Development (Cambridge, England), 128(24), 5099-5108

Lopez-Rios, J., Speziale, D., Robay, D., Scotti, M., Osterwalder, M., Nusspaumer, G., Zeller, R. (2012). GLI3 constrains digit number by controlling both progenitor proliferation and Bmp-dependent exit to chondrogenesis. Developmental Cell, 22(4), 837–848.

Loty, S., Sautier, J.M., Loty, C., Boulekbache, H., Kokubo, T., and Forest, N. (1998). Cartilage formation by fetal rat chondrocytes cultured in alginate beads: a proposed model for investigating tissue-biomaterial interactions. J Biomed Mater Res 42, 213.

Lui, J. C. K., Andrade, A. C., Forcinito, P., Hegde, A., Chen, W., Baron, J., & Nilsson, O. (2010). Spatial and temporal regulation of gene expression in the mammalian growth plate. Bone, 46(5), 1380–1390.

Lui, J. C., Nilsson, O., & Baron, J. (2014). Recent research on the growth plate: Recent insights into the regulation of the growth plate. Journal of Molecular Endocrinology, 53(1), 1–9.

Luparello, C. (2011). Parathyroid hormone-related protein (PTHrP): A key regulator of life/death decisions by tumor cells with potential clinical applications. Cancers, 3(1), 396–407.

Ma, X., Kovács, M., Conti, M. A., Wang, A., Zhang, Y., Sellers, J. R., & Adelstein, R. S. (2012). Nonmuscle myosin II exerts tension but does not translocate actin in vertebrate cytokinesis. PNAS, 109(12), 4509–4514.

Maaten L.V.D., Hinton G. (2008). Visualizing data using t-SNE. Journal of Machine Learning Research, Vol 9(Nov), pp. 2579—2605.

MacDougald, O. A. (2014). Bone marrow adipose tissue is an endocrine organ that contributes to increased circulating adiponectin during caloric restriction. Cell Metabolism, 20(2), 368–375.

Machado, P. F., Duque, J., Étienne, J., Martinez-Arias, A., Blanchard, G. B., & Gorfinkiel, N. (2015). Emergent material properties of developing epithelial tissues. BMC Biology, 13(1), 98.

Mackie EJ, Tatarczuch L, Mirams M (2011). The skeleton: a multi-functional complex organ. The growth plate chondrocyte and endochondral ossification. J Endocrinology, 211(2),109-121.

Madden, T. L., & Herzfeld, J. (1994). Crowding-induced Organization of Cytoskeletal Elements Dissolution of Spontaneously Formed Filament Bundles by Capping Proteins, 126(1), 169–174.

Maddox, B. K., Garofalo, S., Smith, C., Keene, D. R., & Horton, W. A. (1997). Skeletal development in transgenic mice expressing a mutation at Gly574Ser of type II collagen. Developmental Dynamics, 208, 170–7.

Mains, P. E., Sulston, I. A., & Wood, W. B. (1990). Dominant maternal-effect mutations causing embryonic lethality in Caenorhabditis elegans. Genetics, 125(2), 351–369.

Mak, K. K., Kronenberg, H. M., Chuang, P., Mackem, S., & Yang, Y. (2008). Indian hedgehog signals independently of PTHrP to promote chondrocyte hypertrophy, 1956, 1947–1956.

Mak, K. K., Chen, M., Day, T. F., Chuang, P., & Yang, Y. (2006). Wnt/β-catenin signaling interacts differentially with Ihh signaling in controlling endochondral bone and synovial joint formation, 3707, 3695–3707.

Manning, M. L., Foty, R. A., Steinberg, M. S., & Schoetz, E.-M. (2010). Coaction of intercellular adhesion and cortical tension specifies tissue surface tension. PNAS, 107(28), 12517–22.

Marigo, V., Johnson, R. L., Vortkamp, A., & Tabin, C. J. (1996). Sonic hedgehog Differentially Regulates Expression of GLI and GLI3 during Limb Development. Developmental Biology, 180(1), 273–283.

Marsden, M., & DeSimone, D. W. (2003). Integrin-ecm interactions regulate cadherin-dependent cell adhesion and are required for convergent extension in xenopus. Current Biology, 13(14), 1182–1191.

Martell, J.D., Deerink, T.J., Sancak Y, Poulos T.L, Mootha V.K., Sosinsky G.E., Ellisman M.H., Ting A.Y. (2012). Engineered ascorbate peroxidase as a genetically-encoded reporter for electron microscopy. Nat Biotechnol. 30(11), 1143–1148.

Martin, A. C., Kaschube, M., & Wieschaus, E. F. (2009). Pulsed actin-myosin network contractions drive apical constriction. Nature, 457(7228), 495.

Martin, P. (1990). Tissue patterning in the developing mouse limb. International Journal of Developmental Biology, 34(3), 323–336.

Maruthamuthu, V., Sabass, B., Schwarz, U. S., & Gardel, M. L. (2011). Cell-ECM traction force modulates endogenous tension at cell–cell contacts. PNAS, 108(12), 4708–4713.

Matsumoto, K., Li, Y., Jakuba, C., Sugiyama, Y., Sayo, T., Okuno, M., … Kosher, R. A. (2009). Conditional inactivation of Has2 reveals a crucial role for hyaluronan in skeletal growth, patterning, chondrocyte maturation and joint formation in the developing limb. Development (Cambridge, England), 136(16), 2825–2835.

Matsumoto S, Fumoto K, Okamoto T, Kaibuchi K, Kikuchia A. (2010) Binding of APC and dishevelled mediates Wnt5a-regulated focal adhesion dynamics in migrating cells. EMBO J; 29(7), 1192–1204.

Mau, E., Whetstone, H., Yu, C., Hopyan, S., Wunder, J. S., & Alman, B. A. (2007) PTHrP regulates growth plate chondrocyte differentiation and proliferation in a Gli3 dependent manner utilizing hedgehog ligand dependent and independent mechanisms. Developmental Biology, 305(1), 28–39.

Mavrakis, M., Azou-Gros, Y., Tsai, F.-C., Alvarado, J., Bertin, A., Iv, F., Lecuit, T. (2014). Septins promote F-actin ring formation by crosslinking actin filaments into curved bundles. Nat Cell Biol, 16(4), 322–334.

May, S. R., Ashique, A. M., Karlen, M., Wang, B., Shen, Y., Zarbalis, K., Peterson, A. S. (2005). Loss of the retrograde motor for IFT disrupts localization of Smo to cilia and prevents the expression of both activator and repressor functions of Gli. Developmental Biology, 287(2), 378–389.

Mayer, M., Depken, M., Bois, J. S., Jülicher, F., & Grill, S. W. (2010). Anisotropies in cortical tension reveal the physical basis of polarizing cortical flows. Nature, 467(7315), 617–621.

McCain, M. L., Lee, H., Aratyn-Schaus, Y., Kléber, A. G., & Parker, K. K. (2012). Cooperative coupling of cell-matrix and cell–cell adhesions in cardiac muscle. PNAS, 109(25), 9881–9886.

McGlashan, S. R., Haycraft, C. J., Jensen, C. G., Yoder, B. K., & Poole, C. A. (2007). Articular cartilage and growth plate defects are associated with chondrocyte cytoskeletal abnormalities in Tg737orpk mice lacking the primary cilia protein polaris. Matrix Biology, 26(4), 234–246.

McGowan, K. B., & Sah, R. L. (2005). Treatment of cartilage with beta-aminopropionitrile accelerates subsequent collagen maturation and modulates integrative repair. Journal of Orthopaedic Research, 23(3), 594–601.

Mcmillen, P., & Holley, S. A. (2015). Integration of cell – cell and cell – ECM adhesion in vertebrate morphogenesis. Current Opinion in Cell Biology, 36, 48–53.

van der Meulen, M. C. H., Morey-Holton, E. R. and Carter, D. R. (1995), Hindlimb suspension diminishes femoral cross-sectional growth in the rat. J. Orthop. Res., 13, 700–707.

Miao D, Su H, He B, Gao J, Xia Q, Zhu M, Gu Z, Goltzman D, Karaplis AC. (2008). Severe growth retardation and early lethality in mice lacking the nuclear localization sequence and C-terminus of PTH-related protein. PNAS, 105(51), 20309-14

Michigami, T. (2014). Current understanding on the molecular basis of chondrogenesis. Clinical Pediatric Endocrinology, 23(1), 1–8.

Minina E, Wenzel HM, Kreschel C, Karp S, Gaffield W, McMahon AP, Vortkamp A (2001). BMP and Ihh/PTHrP signaling interact to coordinate chondrocyte proliferation and differentiation. Development (Cambridge, England), 128(22), 4523-4534.

Minina, E., Kreschel, C., Naski, M. C., Ornitz, D. M., & Vortkamp, A. (2002). Interaction of FGF, Ihh/Pthlh, and BMP signaling integrates chondrocyte proliferation and hypertrophic differentiation. Developmental Cell, 3(3), 439–449.

Mirkovic, I., & Mlodzik, M. (2006). Cooperative activities of Drosophila DE-Cadherin and DN-Cadherin regulate the cell motility process of ommatidial rotation. Development, 133(17), 3283-3293.

Mitra, S. K., & Schlaepfer, D. D. (2006). Integrin-regulated FAK–Src signaling in normal and cancer cells. Current Opinion in Cell Biology, 18(5), 516–523.

Montenegro Gouveia, S., Leslie, K., Kapitein, L. C., Buey, R. M., Grigoriev, I., Wagenbach, M., & Akhmanova, A. (2010). In vitro reconstitution of the functional interplay between MCAK and EB3 at microtubule plus ends. Current Biology, 20(19), 1717–1722.

Mook, O. R. F., Overbeek, C. V., Ackema, E. G., Maldegem, F. V., & Frederiks, W. M. (2003). In situ localization of gelatinolytic activity in the extracellular matrix of metastases of colon cancer in rat liver using quenched fluorogenic DQ-gelatin. Journal of Histochemistry & Cytochemistry, 51(6), 821–829.

Morishita, Y., Kuroiwa, A., & Suzuki, T. (2015). Quantitative analysis of tissue deformation dynamics reveals three characteristic growth modes and globally aligned anisotropic tissue deformation during chick limb development. Development (Cambridge, England), 142(9), 1672–1683.

Mork, L., & Crump, G. (2015). Zebrafish craniofacial development: a window into early patterning. Current Topics in Developmental Biology, 115, 235–269.

Mueller, MB., & Tuan, RS. (2008). Functional characterization of hypertrophy in chondrogenesis of human mesenchymal stem cells. Arthritis Rheum. 58(5), 1377-1388.

Munjal, A., Philippe, J.-M., Munro, E., & Lecuit, T. (2015). A self-organized biomechanical network drives shape changes during tissue morphogenesis. Nature, 524(7565), 351–355.

Muñoz, R., Moreno, M., Oliva, C., Orbenes, C., & Larrain, J. (2006). Syndecan-4 regulates noncanonical Wnt signalling and is essential for convergent and extension movements in Xenopus embryos. Nature Cell Biology, 8(5), 492–500.

Muñoz, R., & Larraín, J. (2006). xSyndecan-4 regulates gastrulation and neural tube closure in Xenopus embryos. The Scientific World Journal, 6, 1298–1301.

Murrell, M., Oakes, P. W., Lenz, M., & Gardel, M. L. (2015). Forcing cells into shape : the mechanics of actomyosin contractility. Nature Publishing Group, 16(8), 486–498.

Naganathan, S. R. am, Fürthauer, S., Nishikawa, M., Jülicher, F., & Grill, S. W. (2014). Active torque generation by the actomyosin cell cortex drives left-right symmetry breaking. eLife, 3, e04165.

Nagaoka, T., Ohashi, R., Inutsuka, A., Sakai, S., Fujisawa, N., Yokoyama, M., & Kishi, M. (2014). The Wnt/planar cell polarity pathway component Vangl2 induces synapse formation through direct control of N-cadherin. Cell Reports, 6(5), 916–927.

Nagaoka, T., Inutsuka, A., Begum, K., Hafiz, K. Musabbir B., & Kishi, M. (2014). Vangl2 Regulates E-Cadherin in Epithelial Cells. Scientific Reports, 4, 6940.

Nakashima, E., Kitoh, H., Maeda, K., Haga, N., Kosaki, R., Mabuchi, A., Nishimura, G., Ohashi, H. & Ikegawa, S. (2005), Novel COL9A3 mutation in a family with multiple epiphyseal dysplasia. Am. J. Med. Genet, 132A, 181–184.

Narimatsu, M., Bose, R., Pye, M., Zhang, L., Miller, B., Ching, P., Wrana, J. L. (2009). Regulation of planar cell polarity by smurf ubiquitin ligases. Cell, 137(2), 295–307.

Nelson, J., Allen, W. E., Scott, W. N., Bailie, J. R., Walker, B., McFerran, N. V, & Wilson, D. J. (1995). Murine epidermal growth factor (EGF) fragment (33–42) inhibits both EGF- and laminin-dependent endothelial cell motility and angiogenesis. Cancer Research, 55(17), 3772-3776.

Ng, M. R., Besser, A., Brugge, J. S., & Danuser, G. (2014). Mapping the dynamics of force transduction at cell–cell junctions of epithelial clusters. eLife, 3, e03282.

Ng, M. R., Besser, A., Danuser, G., & Brugge, J. S. (2012). Substrate stiffness regulates cadherin-dependent collective migration through myosin-II contractility. Journal of Cell Biology, 199(3), 545–563.

Nicolae, C., Ko, Y., Miosge, N., Niehoff, A., Studer, D., Enggist, L., Aszodi, A. (2007). Abnormal collagen fibrils in cartilage of matrilin-1 / matrilin-3-deficient mice. The Journal of Biological Chemistry, 282(30), 22163–22175.

Nilsson O, Parker EA, Hegde A, Chau M, Barnes K & Baron J (2007) Gradients in bone morphogenetic protein-related gene expression across the growth plate. Journal of Endocrinology 193 (75-84)

Nishimoto, S., Wilde, S. M., Wood, S., & Logan, M. P. O. (2015). RA Acts in a Coherent Feed-Forward Mechanism with Tbx5 to Control Limb Bud Induction and Initiation. Cell Reports, 12(5), 879–891.

Noonan, K. J., Hunziker, E. B., Nessler, J. & Buckwalter, J. A. (1998), Changes in cell, matrix

compartment, and fibrillar collagen volumes between growth-plate zones. J. Orthop. Res., 16, 500–508.

Nowlan, N. C., Prendergast, P. J., & Murphy, P. (2008). Identification of Mechanosensitive Genes during Embryonic Bone Formation. PLoS Computational Biology, 4(12), e1000250.

Oberlender, S. A., & Tuan, R. S. (1994). Expression and functional involvement of N-cadherin in embryonic limb chondrogenesis. Development, 120(1), 177 LP-187.

Ogawa T, Yamagiwa H, Hayami T, Liu Z, Huang K-Y, Tokunaga K, Murai T, Endo N (2002). Human PTH (1–34) induces longitudinal bone growth in rats. Journal of Bone and Mineral Metabolism, 20(2), 83-90.

Ohashi, N., Robling, A. G., Burr, D. B. & Turner, C. H. (2002), The Effects of Dynamic Axial Loading on the Rat Growth Plate. J Bone Miner Res, 17, 284–292.

Ohira, Y., Kawano, F., Wang, X. D., Sudoh, M., Iwashita, Y., Majima, H. J., & Nonaka, I. (2006). Irreversible morphological changes in leg bone following chronic gravitational unloading of growing rats. Life Sciences, 79(7), 686–694.

Oji GS, Gomez P, Kurriger G, Stevens J, Morcuende JA (2007). Indian hedgehog signaling pathway differences between swarm rat chondrosarcoma and native rat chondrocytes. The Iowa orthopaedic journal, 27, 9-16.

Okubo, N., Minami, Y., Fujiwara, H., Umemura, Y., Tsuchiya, Y., Shirai, T., Yagita, K. (2013). Prolonged bioluminescence monitoring in mouse *ex vivo* bone culture revealed persistent circadian rhythms in articular cartilages and growth plates. PLoS ONE, 8(11), e78306.

Oliva, C. A., Vargas, J. Y., & Inestrosa, N. C. (2013). Wnt signaling: Role in LTP, neural networks and memory. Ageing Research Reviews, 12(3), 78–800.

Onodera, K., Takahashi, I., Sasano, Y., Bae, J.-W., Mitani, H., Kagayama, M., & Mitani, H. (2005). Stepwise mechanical stretching inhibits chondrogenesis through cell–matrix adhesion mediated by integrins in embryonic rat limb-bud mesenchymal cells. European Journal of Cell Biology, 84(1), 45–58.

Ossipova, O., Kim, K., & Sokol, S. Y. (2015). Planar polarization of Vangl2 in the vertebrate neural plate is controlled by Wnt and Myosin II signaling. Biology Open, 4(6), 722–730.

Pacifici M, Golden EB, Oshima O, Shapiro IM, Leboy PS, Adams SL: Hypertrophic chondrocytes. The terminal stage of differentiation in the chondrogenic cell lineage? Annals of the New York Academy of Sciences 1990, 599, 45-57.

Page-McCaw, A., Ewald, A. J., & Werb, Z. (2007). Matrix metalloproteinases and the regulation of tissue remodelling. Nature Reviews. Molecular Cell Biology, 8(3), 221–33.

Paige KT, Cima LG, Yaremchuk MJ, Schloo BL, Vacanti JP, Vacanti CA: De novo cartilage generation using calcium alginate-chondrocyte constructs. Plastic and reconstructive surgery 1996, 97(1),168-178.

Parsons, J. T., Horwitz, A. R., & Schwartz, M. A. (2010). Cell adhesion: integrating cytoskeletal dynamics and cellular tension. Nature Reviews. Molecular Cell Biology, 11(9), 633–643.

Paszek, M. J., Boettiger, D., Weaver, V. M., & Hammer, D. A. (2009). Integrin Clustering Is Driven by Mechanical Resistance from the Glycocalyx and the Substrate. PLoS Computational Biology, 5(12), e1000604.

Patra, D., DeLassus, E., Liang, G., & Sandell, L. J. (2014). Cartilage-specific ablation of site-1 protease in mice results in the endoplasmic reticulum entrapment of type iib procollagen and down-regulation of cholesterol and lipid homeostasis. PLoS ONE, 9(8), e105674.

Pearse, R. V., Scherz, P. J., Campbell, J. K., & Tabin, C. J. (2007). A cellular lineage analysis of the chick limb bud. Developmental Biology, 310(2), 388–400.

Pelosi, M., Lazzarano, S., Thoms, B. L., & Murphy, C. L. (2013). Parathyroid hormone-related protein is induced by hypoxia and promotes expression of the differentiated phenotype of human articular chondrocytes. Clinical Science, 125(10), 461 LP-470.

Peng, Y., & Axelrod, J. (2012). Asymmetric protein localization in planar cell polarity. Current topics in developmental biology (1st ed., Vol. 101). Elsevier Inc.

Peng XX, Zhao RL, Song W, Chu HR, Li M, et al. Selection of suitable reference genes for normalization of quantitative real-time PCR in cartilage tissue injury and repair in rabbits. Int J Mol Sci (2012) 13, 14344–14355.

Pertz, O., Hodgson, L., Klemke, R. L., & Hahn, K. M. (2006). Spatiotemporal dynamics of RhoA activity in migrating cells. Nature, 440(April), 1069–1072.

Peter, B. J., Kent, H. M., Mills, I. G., Vallis, Y., Butler, P. J. G., Evans, P. R., & McMahon, H. T. (2004): BAR Domains as Sensors of Membrane Curvature: The Amphiphysin BAR Structure. Science, 303(5657), 495 LP-499.

Petrosyan, A., Ali, M. F., Verma, S. K., Cheng, H., & Cheng, P.-W. (2012): Non-muscle myosin IIA transports a Golgi glycosyltransferase to the endoplasmic reticulum by binding to its cytoplasmic tail. The International Journal of Biochemistry & Cell Biology, 44(7), 1153–1165.

Philipp, I., Aufschnaiter, R., Özbek, S., Pontasch, S., Jenewein, M., Watanabe, H., & Hobmayer, B. (2009): Wnt/β-Catenin and noncanonical Wnt signaling interact in tissue evagination in the simple eumetazoan Hydra. PNAS, 106(11), 4290–4295.

Pietila, I., Sormunen, R., Naillat, F., Prunskaite-hyyryla, R., Jokela, T., Shan, J., & Vainio, S. J. (2010). Wnt4 / 5a signalling coordinates cell adhesion and entry into meiosis during presumptive ovarian follicle development. Hum. Mol. Genet., 19(8), 1539–1550.

Pilot, F., Philippe, J.-M., Lemmers, C., & Lecuit, T. (2006). Spatial control of actin organization at adherens junctions by a synaptotagmin-like protein. Nature, 442(7102), 580–584.

Piróg KA, Briggs MD. (2010). Skeletal dysplasias associated with mild myopathy—a clinical and molecular review. J Biomed Biotechnol., 2010, 686457.

Plaas, A. H., & Sandy, J. D. (1993). A cartilage explant system for studies on aggrecan structure, biosynthesis and catabolism in discrete zones of the mammalian growth plate. Matrix, 13(2), 135–147.

Plow, E. F., Haas, T. A., Zhang, L., Loftus, J., & Smith, J. W. (2000). Ligand binding to integrins. Journal of Biological Chemistry, 275(29), 21785–21788.

Ponik, S. M., Trier, S. M., Wozniak, M. A., Eliceiri, K. W., & Keely, P. J. (2013). RhoA is downregulated at cell–cell contacts via p190RhoGAP-B in response to tensional homeostasis. Molecular Biology of the Cell, 24(11), 1688–1699.

Porazinski, S., Wang, H., Asaoka, Y., Behrndt, M., Miyamoto, T., Morita, H., Furutani-Seiki, M. (2015). YAP is essential for tissue tension to ensure vertebrate 3D body shape. Nature, 521(7551), 217-221

Posey, K. L., Hankenson, K., Veerisetty, A. C., Bornstein, P., Lawler, J., & Hecht, J. T. (2008). Skeletal abnormalities in mice lacking extracellular matrix proteins, thrombospondin-1, thrombospondin-3, thrombospondin-5, and type IX collagen. The American Journal of Pathology, 172(6), 1664–1674.

Prein, C., Warmbold, N., Farkas, Z., Schieker, M., Aszodi, A., & Clausen-Schaumann, H. (2016). Structural and mechanical properties of the proliferative zone of the developing murine growth plate cartilage assessed by atomic force microscopy. Matrix Biology, 50, 1–15.

Prieto, A. L., Andersson-Fisone, C., & Crossin, K. L. (1992). Characterization of multiple adhesive and counteradhesive domains in the extracellular matrix protein cytotactin. The Journal of Cell Biology, 119(3), 663-678.

Provenzano, P. P., & Keely, P. J. (2011). Mechanical signaling through the cytoskeleton regulates cell proliferation by coordinated focal adhesion and Rho GTPase signaling. Journal of Cell Science, 124(8), 1195–1205.

Provot, S., Zinyk, D., Gunes, Y., Kathri, R., Le, Q., Kronenberg, H. M., Schipani, E. (2007). Hif-1α regulates differentiation of limb bud mesenchyme and joint development. The Journal of Cell Biology, 177(3), 451–464.

Provot S, Schipani E: Molecular mechanisms of endochondral bone development. Biochemical and Biophysical Research Communications 2005, 328(3), 658-665.

Puech, P.-H., Taubenberger, A., Ulrich, F., Krieg, M., Muller, D. J., & Heisenberg, C.-P. (2005). Measuring cell adhesion forces of primary gastrulating cells from zebrafish using atomic force microscopy. Journal of Cell Science, 118(18), 4199-4206.

Radhakrishnan, P., Lewis, N. T., & Mao, J. J. (2004). Zone-Specific Micromechanical Properties of the Extracellular Matrices of Growth Plate Cartilage. Annals of Biomedical Engineering, 32(2), 284–291.

Rais, Y., Reich, A., Simsa-Maziel, S., Moshe, M., Idelevich, A., Kfir, T., & Monsonego-Ornan, E. (2015). The growth plate's response to load is partially mediated by mechano-sensing via the chondrocytic primary cilium. Cellular and Molecular Life Sciences, 72(3), 597–615.

Randall RM, Shao YY, Wang L, & Ballock RT (2012). Activation of Wnt Planar Cell Polarity (PCP) signaling promotes growth plate column formation in vitro. Journal of Orthopaedic Research: official publication of the Orthopaedic Research Society 30(12), 1906-1914.

Rauzi, M., Lenne, P., & Lecuit, T (2010). Planar polarized actomyosin contractile flows control epithelial junction remodelling. Nature, 468(7327), 1110–1114.

Ravasio, A., Cheddadi, I., Chen, T., Pereira, T., Ong, H. T., Bertocchi, C., & Ladoux, B (2015). Gap geometry dictates epithelial closure efficiency. Nature Communications, 6, 7683.

Ravasio, A., Vaishnavi, S., Ladoux, B., & Viasnoff, V (2015). High-resolution imaging of cellular processes across textured surfaces using an indexed-matched elastomer. Acta Biomaterialia, 14, 53–60.

Reilly, G. C., & Engler, A. J. (2010). Intrinsic extracellular matrix properties regulate stem cell differentiation. Journal of Biomechanics, 43(1), 55–62.

Ren, X. D., Kiosses, W. B., Sieg, D. J., Otey, C. A., Schlaepfer, D. D., & Schwartz, M. A. (2000). Focal adhesion kinase suppresses Rho activity to promote focal adhesion turnover. Journal of Cell Science, 113(20), 3673-3678.

del Rio, A., Perez-Jimenez, R., Liu, R., Roca-Cusachs, P., Fernandez, J. M., & Sheetz, M. P. (2009). Stretching single talin rod molecules activates vinculin binding. Science, 323(5914), 638 641.

Robinson, E. E., Foty, R. A., & Corbett, S. A. (2004). Fibronectin Matrix Assembly Regulates α5β1-mediated Cell Cohesion. Molecular Biology of the Cell, 15(3), 973–981.

Robinson, E. E., Zazzali, K. M., Corbett, S. A., & Foty, R. A. (2002). α5β1 integrin mediates strong tissue cohesion. Journal of Cell Science, 116(2), 377-386.

Robson H, Siebler T, Stevens DA, Shalet SM, & Willlams GR: Thyroid hormone acts directly on growth plate chondrocytes to promote hypertrophic differentiation and inhibit clonal expansion and cell proliferation. Endocrinology 2000, 141(10), 3887-3897.

Roddy, K. A., Kelly, G. M., Es, M. H. Van, Murphy, P., & Prendergast, P. J. (2011). Dynamic patterns of mechanical stimulation co-localise with growth and cell proliferation during morphogenesis in the avian embryonic knee joint. Journal of Biomechanics, 44(1), 143–149.

Roddy, K. A., Prendergast, P. J., & Murphy, P. (2011). Mechanical Influences on Morphogenesis of the Knee Joint Revealed through Morphological, Molecular and Computational Analysis of Immobilised Embryos. PLoS ONE, 6(2), e17526. http://doi.org/10.1371/journal.pone.0017526

Rodgers, K. D., Sasaki, T., Aszodi, A., & Jacenko, O. (2007). Reduced perlecan in mice results in chondrodysplasia resembling Schwartz–Jampel syndrome. Human Molecular Genetics,16(5), 515–528.

Roer R, Abehsera S, Sagi A. (2015) Exoskeletons across the Pancrustacea: Comparative Morphology, Physiology, Biochemistry and Genetics. Integr Comp Biol. 55(5), 771-91

Romereim, S. M., Conoan, N. H., Chen, B., & Dudley, A. T. (2014). A dynamic cell adhesion surface regulates tissue architecture in growth plate cartilage. Development (Cambridge, England), 141(10), 2085–2095.

Romereim, S.M. (2014). The polarized reorganization crucial to growth plate cartilage architecture depends on the interplay of morphogens, adhesion, and cytoskeletal dynamics (doctoral dissertation). Northwestern university, UMI Number: 3669308

Romereim, S. M., & Dudley, A. T. (2011). Cell polarity: The missing link in skeletal morphogenesis? Organogenesis, 7(3), 217–228.

Römgens, A. M., van Donkelaar, C. C., & Ito, K. (2013). Contribution of collagen fibers to the compressive stiffness of cartilaginous tissues. Biomechanics and Modeling in Mechanobiology, 12(6), 1221–1231.

Ritvaniemi, P., Körkkö, J., Bonaventure, J., Vikkula, M., Hyland, J., Paassilta, P., Kaitila, I., Kääriäinen, H., Sokolov, B. P., Hakala, M., Mannismäki, P., Meerson, E. M., Klemola, T., Roselló-Díez, A., & Joyner, A. L. (2015). Regulation of long bone growth in vertebrates; it is time to catch up. Endocrine Reviews, 36(6), 646–680.

Rosenblueth, A., & Wiener, N. (1945). The role of models in science. Philosophy of Science, 12(4), 316-321.

Ross, A. J., May-Simera, H., Eichers, E. R., Kai, M., Hill, J., Jagger, D. J., & Beales, P. L. (2005). Disruption of Bardet-Biedl syndrome ciliary proteins perturbs planar cell polarity in vertebrates. Nat Genet, 37(10), 1135–1140.

Roszko, I., S. Sepich, D., Jessen, J. R., Chandrasekhar, A., & Solnica-Krezel, L. (2015). A dynamic intracellular distribution of Vangl2 accompanies cell polarization during zebrafish gastrulation. Development (Cambridge, England), 142(14), 2508–2520.

Rot, C., Stern, T., Blecher, R., Friesem, B., & Zelzer, E. (2014). A Mechanical Jack-like Mechanism Drives Spontaneous Fracture Healing in Neonatal Mice. Developmental Cell, 31(2), 159–170.

Rowley J.A., Mooney D.J. (2002). Alginate type and RGD density control myoblast phenotype. J Biomed Mater Res 2002, 60(2), 217-223.

Rowley J.A., Madlambayan G., Mooney D.J. (1999). Alginate hydrogels as synthetic extracellular matrix materials. Biomaterials, 20(1), 45-53.

Rozenblatt-Rosen O., Mosonego-Ornan E., Sadot E., Madar-Shapiro L., Sheinin Y., Ginsberg D., & Yayon A. (2002). Induction of chondrocyte growth arrest by FGF: transcriptional and cytoskeletal alterations. Journal of cell science, 115(3), 553-562.

Saetzler, K., Sonnenschein, C., & Soto, A. M. (2011). Systems biology beyond networks: Generating order from disorder through self-organization. Seminars in Cancer Biology, 21(3), 165–174.

Saez, A., Ghibaudo, M., Buguin, A., Silberzan, P., & Ladoux, B. (2007). Rigidity-driven growth and migration of epithelial cells on microstructured anisotropic substrates. PNAS, 104(20), 8281–8286.

Saha, A., Nishikawa, M., Behrndt, M., Heisenberg, C.-P., Jülicher, F., & Grill, S. W. (2016). Determining Physical Properties of the Cell Cortex. Biophysical Journal, 110(6), 1421–1429.

Sahar D, Longmaker M, & Quarto N. Sox9 neural crest determinant gene controls patterning and closure of the posterior frontal cranial suture. Dev. Bio (2005) 280:2 344–361

Samsa, W. E., Zhou, X., & Zhou, G. (2016). Signaling pathways regulating cartilage growth plate formation and activity. Seminars in Cell and Developmental Biology. 62, 3-15

Samuel, M. S., Lopez, J. I., McGhee, E. J., Croft, D. R., Strachan, D., Timpson, P., & Olson, M. F. (2011). Actomyosin-mediated cellular tension drives increased tissue stiffness and β-catenin activation to induce interfollicular epidermal hyperplasia and tumor growth. Cancer Cell, 19(6), 776–791.

Sanders, T. A., Llagostera, E., & Barna, M. (2013). Specialized filopodia direct long-range transport of Shh during vertebrate tissue patterning. Nature, 497(7451), 628–632.

Sant S, Hancock MJ, Donnelly JP, Iyer D, Khademhosseini A (2010). Biomimetic Gradient Hydrogels for Tissue Engineering. Canadian Journal of Chemical Engineering, 88(6), 899-911.

Sargus-Patino C.N., Wright E.C., Plautz S.A., Miles J.R., Vallet J.L., & Pannier A.K. (2014). In vitro development of preimplantation porcine embryos using alginate hydrogels as a three-dimensional extracellular matrix. Reproduction, fertility, and development, 26(7), 943-953.

Sasai, Y. (2013). Cytosystems dynamics in self-organization of tissue architecture. Nature, 493(7432), 318–26.

Satir, P., Pedersen, L. B., & Christensen, S. T. (2010). The primary cilium at a glance. Journal of Cell Science, 123(4), 499–503.

Sato, K., Koizumi, Y., Takahashi, M., Kuroiwa, A., & Tamura, K. (2007). Specification of cell fate along the proximal-distal axis in the developing chick limb bud. Development, 134(7), 1397 LP-1406.

Sawada, Y., Tamada, M., Dubin-Thaler, B. J., Cherniavskaya, O., Sakai, R., Tanaka, S., & Sheetz, M. P. (2006). Force Sensing by Extension of the Src Family Kinase Substrate, p130Cas. Cell, 127(5), 1015–1026.

Scarpa, E., & Mayor, R. (2016). Collective cell migration in development. Journal of Cell Biology, 212(2), 143–155.

Scheller, E. L., Troiano, N., VanHoutan, J. N., Bouxsein, M. A., Fretz, J. A., Xi, Y., Horowitz, M. C. (2014). Use of osmium tetroxide staining with microcomputerized tomography to visualize and quantify bone marrow adipose tissue *in vivo*. Methods in Enzymology, 537, 123–139.

Schilling, T. F., & Kimmel, C. B. (1994). Segment and cell type lineage restrictions during pharyngeal arch development in the zebrafish embryo. Development, 120(3), 483 LP-494.

Schnabel, M., Marlovits, S., Eckhoff, G., Fichtel, I., Gotzen, L., Vécsei, V., & Schlegel, J. (2002). Dedifferentiation associated changes in morphology and gene expression in primary human articular chondrocytes in cell culture. Osteoarthritis and Cartilage, 10(1), 62–70.

Schwabe, G. C., Trepczik, B., Süring, K., Brieske, N., Tucker, A. S., Sharpe, P. T., Minami, Y. and Mundlos, S. (2004). Ror2 knockout mouse as a model for the developmental pathology of autosomal recessive Robinow syndrome. Dev. Dyn., 229, 400–410.

Shwartz, Y., Farkas, Z., Stern, T., Aszódi, A., & Zelzer, E. (2012). Muscle contraction controls skeletal morphogenesis through regulation of chondrocyte convergent extension. Developmental Biology, 370(1), 154–163.

Selmi TA1, Verdonk P, Chambat P, Dubrana F, Potel JF, Barnouin L, Neyret P. (2008) Autologous chondrocyte implantation in a novel alginate-agarose hydrogel: outcome at two years. J Bone Joint Surg Br. 90(5), 597-604

Serra, R. (2008), Role of Intraflagellar Transport and Primary Cilia in Skeletal Development. Anat Rec, 291, 1049–1061.

Sharir, A., Stern, T., Rot, C., Shahar, R., & Zelzer, E. (2011). Muscle force regulates bone shaping for optimal load-bearing capacity during embryogenesis. Development, 138(15), 3247-3259.

Shao, Y, Y. Y., Wang, L., Welter, J, J. F., & Ballock, R. T. (2012). Primary cilia modulate Ihh signal transduction in response to hydrostatic loading of growth plate chondrocytes. Bone, 50(1), 79–84.

Sharov, A. A. (2016). Evolution of Natural Agents: Preservation, Advance, and Emergence of Functional Information. Biosemiotics, 9(1), 103–120.

Shea, C. A., Rolfe, R. A., & Murphy, P. (2015). The importance of foetal movement for coordinated cartilage and bone development in utero: clinical consequences and potential for therapy. Bone & Joint Research, 4(7), 105–116.

Sheth R., Marcon L., Félix B.M., Junco M., Quintana L., Dahn R., Kmita M., Sharpe J, Ros M.A. (2012). Hox Genes Regulate Digit Patterning by Controlling the Wavelength of a Turing-Type Mechanism. Science, 338(6113), 1476-1480.

Shi Q, Chien YH, and Leckband D (2008) Biophysical Properties of Cadherin Bonds Do Not Predict Cell Sorting. The Journal of Biological Chemistry, 283, 28454-28463.

Shi, S., Man, Z., Li, W., Sun, S., & Zhang, W. (2016). Silencing of Wnt5a prevents interleukin-1β-induced collagen type II degradation in rat chondrocytes. Experimental and Therapeutic Medicine, 12(5), 3161–3166.

Shin H, Lee MN, Choung JS, Kim S, Choi BH, Noh M, Shin JH (2016). Focal Adhesion Assembly Induces Phenotypic Changes and Dedifferentiation in Chondrocytes. J Cell Physiol, 231(8), 1822-1831.

Shutova, M. S., Alexandrova, A. Y., & Vasiliev, J. M. (2008). Regulation of polarity in cells devoid of actin bundle system after treatment with inhibitors of myosin II activity. Cell Motility and the Cytoskeleton, 65(9), 734–746.

Sim, J. Y., Moeller, J., Hart, K. C., Ramallo, D., Vogel, V., Dunn, A. R., & Pruitt, B. L. (2015). Spatial distribution of cell-cell and cell-ECM adhesions regulates force balance while maintaining E-cadherin molecular tension in cell pairs. Molecular Biology of the Cell, 26(13), 2456–2465.

Simons, M., & Mlodzik, M. (2008). Planar Cell Polarity Signaling: From Fly Development to Human Disease. Annual Review of Genetics, 42, 517.

Singh, D. & Pohl, C. (2014). Coupling of Rotational Cortical Flow, Asymmetric Midbody Positioning, and Spindle Rotation Mediates Dorsoventral Axis Formation in C. elegans. Dev. Cell, 28, pp. 253-267

Singh, P., & Schwarzbauer, J. E. (2014). Fibronectin matrix assembly is essential for cell condensation during chondrogenesis. Journal of Cell Science, 127(20), 4420–4428.

Sinha S, Chen J. (2006). Purmorphamine activates the Hedgehog pathway by targeting Smoothened Nature Chemical Biology 2,29-30

Sisson, B. E., Dale, R. M., Mui, S. R., Topczewska, J. M., & Topczewski, J. (2015). A role of glypican4 and wnt5b in chondrocyte stacking underlying craniofacial cartilage morphogenesis. Mechanisms of Development, 138, 279–290.

Smits, P., Dy, P., Mitra, S., & Lefebvre, V. (2004). Sox5 and Sox6 are needed to develop and maintain source, columnar, and hypertrophic chondrocytes in the cartilage growth plate. The Journal of Cell Biology, 164(5), 747–758.

Snoek-van Beurden, P. A., & Von den Hoff, J. W. (2005). Zymographic techniques for the analysis of matrix metalloproteinases and their inhibitors. BioTechniques, 38(1), 73–83.

Soegiarto DW, Kiachopoulos S, Schipani E, Jüppner H, Erben RG, Lanske B. (2001). Partial rescue of PTH/PTHrP receptor knockout mice by targeted expression of the Jansen transgene. Endocrinology. 142(12):5303-10.

Soll, D., Soll, D., Wessels, Lusche, Kuhl, & Scherer. (2011). Role of extracellular cations in cell

motility, polarity, and chemotaxis. Research and Reports in Biology, 2 69-88.

Sommer, R. J., & Mayer, M. G. (2015). Toward a Synthesis of Developmental Biology with Evolutionary Theory and Ecology. Annual Review of Cell and Developmental Biology, 31(1), 453–71.

Song, B., Haycraft, C. J., Seo, H., Yoder, B. K., & Serra, R. (2007). Development of the postnatal growth plate requires intraflagellar transport proteins. Developmental Biology, 305(1), 202–216.

Spiegelberg B., Parratt T., Dheerendra S.K., Khan W.S., Jennings R, Marsh DR (2010). Ilizarov principles of deformity correction. Ann R Coll Surg Engl. 92(2),101-5.

Spranger J.W., Brill P., Superti-Furga A., Unger S., Nishimura G (2012) Bone Dysplasias: An Atlas of Genetic Disorders of Skeletal Development, 3rd Edition. Oxford University Press.

St-Jacques B., Hammerschmidt M., McMahon A.P. (1999). Indian hedgehog signaling regulates proliferation and differentiation of chondrocytes and is essential for bone formation. Genes & Development, 13(16), 2072-2086.

Stanganello, E., Hagemann, A. I. H., Mattes, B., Sinner, C., Meyen, D., Weber, S.,Scholpp, S. (2015). Filopodia-based Wnt transport during vertebrate tissue patterning. Nature Communications, 6, 5846.

Stehbens, S. J., Paterson, A. D., Crampton, M. S., Shewan, A. M., Ferguson, C., Akhmanova, A., & Yap, A. S. (2006). Dynamic microtubules regulate the local concentration of E-cadherin at cell-cell contacts. Journal of Cell Science, 119(9), 1801-1811.

Stokes, I. A. F., Aronsson, D. D., Dimock, A. N., Cortright, V., & Beck., S. (2006). Endochondral Growth in Growth Plates of Three Species at Two Anatomical Locations Modulated by Mechanical Compression and Tension. Journal of Orthopaedic Research, 24(6), 1327–1334.

Summerbell D. (1981) Evidence for regulation of growth, size and pattern in the developing chick limb bud. J Embryol Exp Morphol, 65,129-50.

Swartz, M. E., Nguyen, V., McCarthy, N. Q., & Eberhart, J. K. (2012). Hh signaling regulates patterning and morphogenesis of the pharyngeal arch-derived skeleton. Developmental Biology, 369(1), 65–75.

Swindle, C. S., Tran, K. T., Johnson, T. D., Banerjee, P., Mayes, A. M., Griffith, L., & Wells, A. (2001). Epidermal growth factor (EGF)-like repeats of human tenascin-C as ligands for EGF receptor. The Journal of Cell Biology, 154(2), 459–468.

Tamamura, Y., Otani, T., Kanatani, N., Koyama, E., Kitagaki, J., Komori, T., Enomotoiwamoto, M. (2005). Developmental regulation of Wnt / β-catenin signals is required for growth plate assembly, cartilage integrity, and endochondral ossification. The Journal of Biological Chemistry, 280(19), 19185–19195.

Tanaka H, Matsumura M, Veliky IA (1984). Diffusion Characteristics of Substrates in Ca-alginate gel beads. Biotechnol Bioeng, 26(1), 53-58.

Tarazona, O.A., Slota, L.A., Lopez, D.H., Zhang, G., and Cohn, M.J. (2016). The genetic program for cartilage development has deep homology within Bilateria. Nature. 533, 86–89

Tatin, F., Taddei, A., Weston, A., Fuchs, E., Devenport, D., Tissir, F., & Makinen, T. (2013). Article Planar Cell Polarity Protein Celsr1 Regulates Endothelial Adherens Junctions and Directed Cell Rearrangements during Valve Morphogenesis. Developmental Cell, 26(1), 31–44.

Taubenberger, A., Cisneros, D. A., Friedrichs, J., Puech, P.-H., Muller, D. J., & Franz, C. M. (2007). Revealing Early Steps of α2β1 Integrin-mediated adhesion to collagen type I by using single-cell force spectroscopy. Molecular Biology of the Cell, 18(5), 1634–1644.

Tavella S, Biticchi R, Schito A, Minina E, Di Martino D, Pagano A, Vortkamp A, Horton WA, Cancedda R, Garofalo S (2004). Targeted expression of SHH affects chondrocyte differentiation, growth plate organization, and Sox9 expression. Journal of bone and mineral research, 19(10), 1678-1688.

Tchetina EV, Mwale F, Poole AR (2014): Changes in gene expression associated with matrix turnover, chondrocyte proliferation and hypertrophy in the bovine growth plate. Acta Naturae, 6(3), 89-97.

Terpstra, L., Prud'Homme, J., Arabian, A., Takeda, S., Karsenty, G., Dedhar, S., & St-Arnaud, R. (2003). Reduced chondrocyte proliferation and chondrodysplasia in mice lacking the integrin-linked kinase in chondrocytes. Journal of Cell Biology, 162(1), 139–148.

Théry, M., Racine, V., Pépin, A., Piel, M., Chen, Y., Sibarita, J.-B., & Bornens, M. (2005). The extracellular matrix guides the orientation of the cell division axis. Nature Cell Biology, 7(10), 947–953.

Thomopoulos, S., Das, R., Birman, V., Smith, L., Ku, K., Elson, E. L., & Genin, G. M. (2011). Fibrocartilage tissue engineering: the role of the stress environment on cell morphology and matrix expression. Tissue Engineering. Part A, 17(7-8), 1039–1053.

Thur, J., Rosenberg, K., Nitsche, D. P., Pihlajamaa, T., Ala-kokko, L., Heinegård, D., & Maurer, P. (2001). Mutations in cartilage oligomeric matrix protein causing pseudoachondroplasia and multiple epiphyseal dysplasia affect binding of calcium and collagen I, II, and IX. The Journal of Biological Chemistry, 276(9), 6083–6092.

Tickle, C. and Barker, H. (2013), The Sonic hedgehog gradient in the developing limb. WIREs Dev Biol, 2, 275–290.

Torday, J. S., & Rehan, V. K. (2002). Stretch-stimulated surfactant synthesis is coordinated by the paracrine actions of PTHrP and leptin. American Journal of Physiology - Lung Cellular and Molecular Physiology, 283(1), L130 LP-L135.

Torday, J. S. (2016). The Emergence of Physiology and Form: Natural Selection Revisited. Biology, 5(2), 15.

Totsukawa, G., Yamakita, Y., Yamashiro, S., Hartshorne, D. J., Sasaki, Y., & Matsumura, F. (2000). Distinct roles of ROCK (Rho-kinase) and MLCK in spatial regulation of MLC phosphorylation for assembly of stress fibers and focal adhesions in 3T3 fibroblasts. The Journal of Cell Biology, 150(4), 797–806.

Tsang KY, Chan D, Cheah KS. (2015). Fate of growth plate hypertrophic chondrocytes: Death or lineage extension? Development, growth & differentiation, 57(2),179-192.

Tsubouchi, A., Sakakura, J., Yagi, R., Mazaki, Y., Schaefer, E., Yano, H., & Sabe, H. (2002). Localized suppression of RhoA activity by Tyr31/118-phosphorylated paxillin in cell adhesion and migration. The Journal of Cell Biology, 159(4), 673–683.

Tsvetkov, A. S., Samsonov, A., Akhmanova, A., Galjart, N., & Popov, S. V. (2007). Microtubule-binding proteins CLASP1 and CLASP2 interact with actin filaments. Cell Motility and the Cytoskeleton, 64(7), 519–530.

Tufan, A. C., Daumer, K. M. and Tuan, R. S. (2002). Frizzled-7 and limb mesenchymal chondrogenesis, Effect of misexpression and involvement of N-cadherin. Dev. Dyn., 223, 241–253.

Turing, A. M. (1952). The chemical basis of morphogenesis. Bulletin of Mathematical Biology, 52(1–2), 153–197.

Tveita, A., Rekvig, O. P., & Zykova, S. N. (2008). Glomerular matrix metalloproteinases and their regulators in the pathogenesis of lupus nephritis. Arthritis Research & Therapy, 10(6), 229.

Ueki, M., Tanaka, N., Tanimoto, K., Nishio, C., Honda, K., Lin, Y.-Y., Tanne, K. (2008). The effect of mechanical loading on the metabolism of growth plate chondrocytes. Annals of Biomedical Engineering, 36(5), 793–800.

Umulis, D. M., & Othmer, H. G. (2013). Mechanisms of scaling in pattern formation. Development, 140(24), 4830 LP-4843.

Uriu, K., & Morelli, L. G. (2014). Article Collective Cell Movement Promotes Synchronization of Coupled Genetic Oscillators. Biophysj, 107(2), 514–526.

van der Eerden BCJ, Karperien M, & Wit JM (2003). Systemic and local regulation of the growth plate. Endocr Rev, 24(6), 782-801.

van der Vaart, B., van Riel, W. E., Doodhi, H., Kevenaar, J. T., Katrukha, E. A., Gumy, L., & Akhmanova, A. (2013). CFEOM1-associated kinesin KIF21A is a cortical microtubule growth inhibitor. Developmental Cell, 27(2), 145–160.

Vandooren, J., Geurts, N., Martens, E., Van den Steen, P. E., & Opdenakker, G. (2013). Zymography methods for visualizing hydrolytic enzymes. Nature Methods, 10(3), 211–220.

Vasiliev, J. M., Gelfand, I. M., Domnina, L. V, Ivanova, O. Y., Komm, S. G., & Olshevskaja, L. V. (1970). Effect of colcemid on the locomotory behaviour of fibroblasts. Journal of Embryology and Experimental Morphology, 24(3), 625–640.

Verma, S., Shewan, A. M., Scott, J. A., Helwani, F. M., Elzen, N. R. Den, Miki, H., Yap, A. S. (2004). Arp2 / 3 Activity Is Necessary for Efficient Formation of E-cadherin Adhesive Contacts. The Journal of Biological Chemistry, 279(32), 34062–34070.

Vico L., Barou O., Laroche N., Alexandre C., Lafage-Proust M.H. (1999). Effects of centrifuging at 2g on rat long bone metaphyses. Eur J Appl Physiol Occup Physiol, 80(4), 360-366.

Villemure, I., & Stokes, I. A. F. (2009). Growth Plate Mechanics and Mechanobiology. A Survey of Present Understanding. Journal of Biomechanics, 42(12), 1793–1803.

Mao, Q., & Lecuit, T. (2017). Evo–Devo: Universal Toll Pass for the Extension Highway? Current Biology, 26(14), R680–R683.

Vinatier C, Guicheux J. (2016): Cartilage tissue engineering: From biomaterials and stem cells to osteoarthritis treatments. Annals of physical and rehabilitation medicine 2016, 59(3),139-144.

Vincourt, J. B., Etienne, S., Grossin, L., Cottet, J., Bantsimba-Malanda, C., Netter, P., Magdalou, J. (2012). Matrilin-3 switches from anti- to pro-anabolic upon integration to the extracellular matrix. Matrix Biology, 31(5), 290–298.

Vortkamp, A., Lee, K., Lanske, B., Segre, G. V, Kronenberg, H. M., & Tabin, C. J. (1996). Regulation of Rate of Cartilage Differentiation by Indian Hedgehog and PTH-Related Protein. Science, 273(5275), 613 LP-622.

Vuong-Brender, T. T. K., Ben Amar, M., Pontabry, J., & Labouesse, M. (2016). The interplay of stiffness and force anisotropies drive embryo elongation. bioRxiv.

Wada, N., Javidan, Y., Nelson, S., Carney, T. J., Kelsh, R. N., & Schilling, T. F. (2005). Hedgehog signaling is required for cranial neural crest morphogenesis and chondrogenesis at the midline in the zebrafish skull. Development, 132(17), 3977 LP-3988.

Wang, B., Sinha, T., Jiao, K., Serra, R., & Wang, J. (2011). Disruption of PCP signaling causes limb morphogenesis and skeletal defects and may underlie Robinow syndrome and brachydactyly type B. Human Molecular Genetics, 20(2), 271–285.

Wang, D., Taboas, J. M., & Tuan, R. S. (2011). PTHrP Overexpression Partially Inhibits a mechanical strain-induced arthritic phenotype in chondrocytes. Osteoarthritis and Cartilage / OARS, Osteoarthritis Research Society, 19(2), 213–221.

Wang, Y., Meng, F., Sachs, F., (2011). Genetically encoded force sensors for measuring mechanical forces in proteins. Commun. Integ. Biol. July-Aug 4(4). 395-390.

Wardale, R. J., & Duance, V. C. (1994). Characterisation of articular and growth plate cartilage collagens in porcine osteochondrosis. Journal of Cell Science, 107(1), 47 LP-59.

Wardale, R. J., & Duance, V. C. (1993). Quantification and immunolocalisation of porcine articular and growth plate cartilage collagens. Journal of Cell Science, 105(4), 975 LP-984.

Warrell, E., & Taylor, J. F. (1979). The role of periosteal tension in the growth of long bones. Journal of Anatomy, 128(Pt 1), 179–184.

Weir, E. C., Philbrick, W. M., Amling, M., Neff, L. A., Baron, R., & Broadus, A. E. (1996). Targeted overexpression of parathyroid hormone-related peptide in chondrocytes causes chondrodysplasia and delayed endochondral bone formation. PNAS, 93(19), 10240–5.

Whittaker, M., & Ayscough, A. (2001). Matrix metalloproteinases and their inhibitors—current status and future challenges. Cell transmissions, 17(1), 3–12.

Von Wichert, G., Jiang, G., Kostic, A., De Vos, K., Sap, J., & Sheetz, M. P. (2003). RPTP-α acts as a transducer of mechanical force on αv/β3-integrin–cytoskeleton linkages. The Journal of Cell Biology, 161(1), 143–153.

Widelitz, R. B., Jiang, T.X., Murray, B. A. and Chuong, C.-M. (1993), Adhesion molecules in skeletogenesis: II. Neural cell adhesion molecules mediate precartilaginous mesenchymal condensations and enhance chondrogenesis. J. Cell. Physiol., 156, 399–411.

Williams BB, Cantrell VA, Mundell NA, Bennett AC, Quick RE, Jessen JR. (2012) Vangl2 regulates membrane trafficking of MMP14 to control cell polarity and migration. J Cell Sci., 125(9), 2141-7.

Williams, C., Peltonen, L., Kivirikko, K. I., Prockop, D. J. and Ala-kokko, L. (1995). Identification of col2a1 gene mutations in patients with chondrodysplasias and familial osteoarthritis. Arthritis & Rheumatism, 38, 999–1004.

Williams G. Thyroid hormone actions in cartilage and bone. Eur Thyroid J. 2013 Mar; 2(1), 3–13.

Winter, C. G., Wang, B., Ballew, A., Royou, A., Karess, R., Axelrod, J. D., & Luo, L. (2011). Drosophila Rho-associated kinase (Drok) links frizzled-mediated planar cell polarity signaling to the actin cytoskeleton. Cell, 105(1), 81–91.

Witze, E. S., Litman, E. S., Argast, G. M., Moon, R. T., & Ahn, N. G. (2008). Wnt5a control of cell polarity and directional movement by polarized redistribution of adhesion receptors. Science (New York, N.Y.), 320(5874), 365–369.

Wiweger, M. I., Avramut, C. M., De Andrea, C. E., Prins, F. A., Koster, A. J., Ravelli, R. B. G., & Hogendoorn, P. C. W. (2011). Cartilage ultrastructure in proteoglycan-deficient zebrafish mutants brings to light new candidate genes for human skeletal disorders. Journal of Pathology, 223(4), 531–542.

Woods, A., Wang, G., & Beier, F. (2005). RhoA / ROCK signaling regulates Sox9 expression and actin organization during chondrogenesis. The Journal of Biological Chemistry, 280(12), 11626–11634.

Wosu, R., Sergerie, K., Lévesque, M., & Villemure, I. (2012). Mechanical properties of the porcine growth plate vary with developmental stage. Biomechanics and Modeling in Mechanobiology, 11(3), 303–312.

Wyngaarden, L. A., Vogeli, K. M., Ciruna, B. G., Wells, M., Hadjantonakis, A.-K., & Hopyan, S. (2010). Oriented cell motility and division underlie early limb bud morphogenesis. Development (Cambridge, England), 137(15), 2551–2558.

Ghibaudo, M., Saez, A., Trichet, L., Xayaphoummine, A., Browaeys, J., Silberzan, P., Ladoux, B. (2008). Traction forces and rigidity sensing regulate cell functions. Soft Matter, 4(9), 1836–1843.

Yamanaka, H., Moriguchi, T., Masuyama, N., Kusakabe, M., Hanafusa, H., Takada, R., Nishida, E. (2002). JNK functions in the non-canonical Wnt pathway to regulate convergent extension movements in vertebrates. EMBO Reports, 3(1), 69–75.

Yan, D., & Lin, X. (2009). Shaping Morphogen Gradients by Proteoglycans. Cold Spring Harbor Perspectives in Biology, 1(3), a002493.

Yang, C., Zhang, X., Guo, Y., Meng, F., Sachs, F., & Guo, J. (2015). Mechanical dynamics in live cells and fluorescence-based force/tension sensors. Biochimica et Biophysica Acta, 1853(8), 1889–1904.

Yang, Y. (2003). Wnt5a and Wnt5b exhibit distinct activities in coordinating chondrocyte proliferation and differentiation. Development, 130(5), 1003–1015.

Yang, Y., & Mlodzik, M. (2015). Wnt-Frizzled/Planar Cell Polarity Signaling: Cellular Orientation by Facing the Wind (Wnt). Annual Review of Cell and Developmental Biology, 31(1), 623–646.

Yasuda T, Shimizu K, Nakagawa Y, Ishikawa H, Nishihara H, Nakamura T. (1996) Possible involvement of RGD (arg-gly-asp)-containing extracellular matrix proteins in rat growth plate chondrocyte differentiation in culture. Journal of Bone and Mineral Research, 11(10),1430-1437.

Ye, K., Wang, X., Cao, L., Li, S., Li, Z., Yu, L., & Ding, J. (2015). Matrix Stiffness and Nanoscale Spatial Organization of Cell-Adhesive Ligands Direct Stem Cell Fate. Nano Letters, 15(7), 4720–4729.

Yodmuang, S., Gadjanski, I., Chao, P. G., & Vunjak-Novakovic, G. (2013). Transient Hypoxia Improves Matrix Properties in Tissue Engineered Cartilage. Journal of Orthopaedic Research : Official Publication of the Orthopaedic Research Society, 31(4), 544–553.

Yang, T., Bassuk, A. G., & Fritzsch, B. (2013). Prickle1 stunts limb growth through alteration of cell polarity and gene expression. Developmental Dynamics: An Official Publication of the American Association of Anatomists, 242(11), 1293–1306.

Yang W, Garrett L, Feng D, Elliott G, Liu X, Wang N, Wong M, Choi T, Yang Y & Gao B (2017) Wnt-induced Vangl2 phosphorylation is dose-dependently required for planar cell polarity in mammalian development. Cell Research volume 27, pages 1466–1484

Yu, F. X., Zhao, B., & Guan, K. L. (2015). Hippo Pathway in Organ Size Control, Tissue Homeostasis, and Cancer. Cell, 163(4), 811–828.

Yuan, X., & Yang, S. (2016). Primary Cilia and Intraflagellar Transport Proteins in Bone and Cartilage. Journal of Dental Research, 95(12), 1341–1349.

Yuasa, T., Kondo, N., Yasuhara, R., Shimono, K., Mackem, S., Pacifici, M., & Iwamoto, M. (2009). Transient activation of Wnt/β-Catenin signaling induces abnormal growth plate closure and articular cartilage thickening in postnatal mice. The American Journal of Pathology, 175(5), 1993–2003.

Zaidel-Bar, R., Itzkovitz, S., Ma'ayan, A., Iyengar, R., & Geiger, B. (2007). Functional atlas of the integrin adhesome. Nature Cell Biology, 9(8), 858–867.

Zaidel-Bar, R., Kam, Z., & Geiger, B. (2005). Polarized downregulation of the paxillin-p130CAS Rac1 pathway induced by shear flow. Journal of Cell Science, 118(17), 3997-4007.

Zamir, E., & Zamir, E. (2017). Integrative systems and synthetic biology of cell- matrix adhesion sites. Cell Adhesion & Migration, 10(5), 451–460.

Zanetti, N. C., & Solursh, M. (1986). Epithelial effects on limb chondrogenesis involve extracellular matrix and cell shape. Developmental Biology, 113(1), 110–118.

Zaucke, F., & Grässel, S. (2009). Genetic mouse models for the functional analysis of the perifibrillar components collagen IX, COMP and matrilin-3: Implications for growth cartilage differentiation and endochondral ossification. Histology and Histopathology, 24(8), 1067–1079.

Zeller, R., Ríos, J. L., & Zuniga, A. (2009). Vertebrate limb bud development : moving towards integrative analysis of organogenesis. Nature Reviews Genetics, 10(12), 845–858.

Zelzer, E., & Olsen, B. R. (2003). The genetic basis for skeletal diseases. Nature, 423(6937), 343–348.

Zhai Z., Yao Y. & Wang Y. Importance of Suitable Reference Gene Selection for Quantitative RT-PCR during ATDC5 Cells Chondrocyte Differentiation. PLoS ONE (2013) 8, e64786

Zhang, J., Tan, X., Li, W., Wang, Y., Wang, J., Cheng, X., & Yang, X. (2005). Smad4 is required for the normal organization of the cartilage growth plate. Developmental Biology, 284(2), 311–322.

Zhang, Y., Lin, Z., Foolen, J., Schoen, I., Santoro, A., Zenobi-Wong, M., & Vogel, V. (2014). Disentangling the multifactorial contributions of fibronectin, collagen and cyclic strain on MMP expression and extracellular matrix remodeling by fibroblasts. Matrix Biology, 40, 62–72.

Zhang M, Xie R, Hou W, Wang BL, Shen R, Wang XM, Wang Q, Zhu TH, Jonason JH, Chen D (2009) PTHrP prevents chondrocyte premature hypertrophy by inducing cyclin-D1-dependent

Runx2 and Runx3 phosphorylation, ubiquitylation and proteasomal degradation. Journal of cell science, 122(9),1382-1389.

Zheng L, Yamashiro T, Fukunaga T, Balam TA, Takano-Yamamoto T (2005). Bone morphogenetic protein 3 expression pattern in rat condylar cartilage, femoral cartilage and mandibular fracture callus. European J Oral Sci. Aug;113(4), 318-25.

Appendix 2.1: Chondrocytes undergoing rotation exhibit protrusions at the periphery of the daughter cell junction (from Romereim 2014b).

A) Electron micrograph of rotating daughter chondrocytes in cranial base cartilage. B) Magnified region from the boxed region. Nanoscale protrusions are evident at the daughter cell junction periphery that resembles leading edge of migrating cells.


A
2µm
B
500nm

Appendix 2.2: ARP2/3 inhibition disrupts column formation and blunts protrusions at the daughter cell junction (from Romereim 2014b).

(A-E) Treatment with 1.5μM ARP2/3 inhibitor caused inhibition chondrocyte rotation. During this treatment, cell division was not disrupted (B) but morphology at daughter cell interface was disorganized (C). After 6 hours, when untreated cells would have completed rotation, treated cells did not finish rotating (D). However, slowly over the course of several hours, most of these cells continued to rotate until they were in line with the local columns (E). (F-I) Using TEM, there were a variety of previously unobserved phenotypes at the junction periphery. These blunted (F, I) and collapsed (G, H) protrusive elements are consistent with an inhibition of actin branching. (J-M) A higher dose of the ARP2/3 inhibitor, 2μM, was sufficient to cause premature rotation termination where chondrocytes did not complete rearrangement for the course of the experiment. (N-P) TEM at the 2μM dose also reveals blunted and collapsed protrusions.

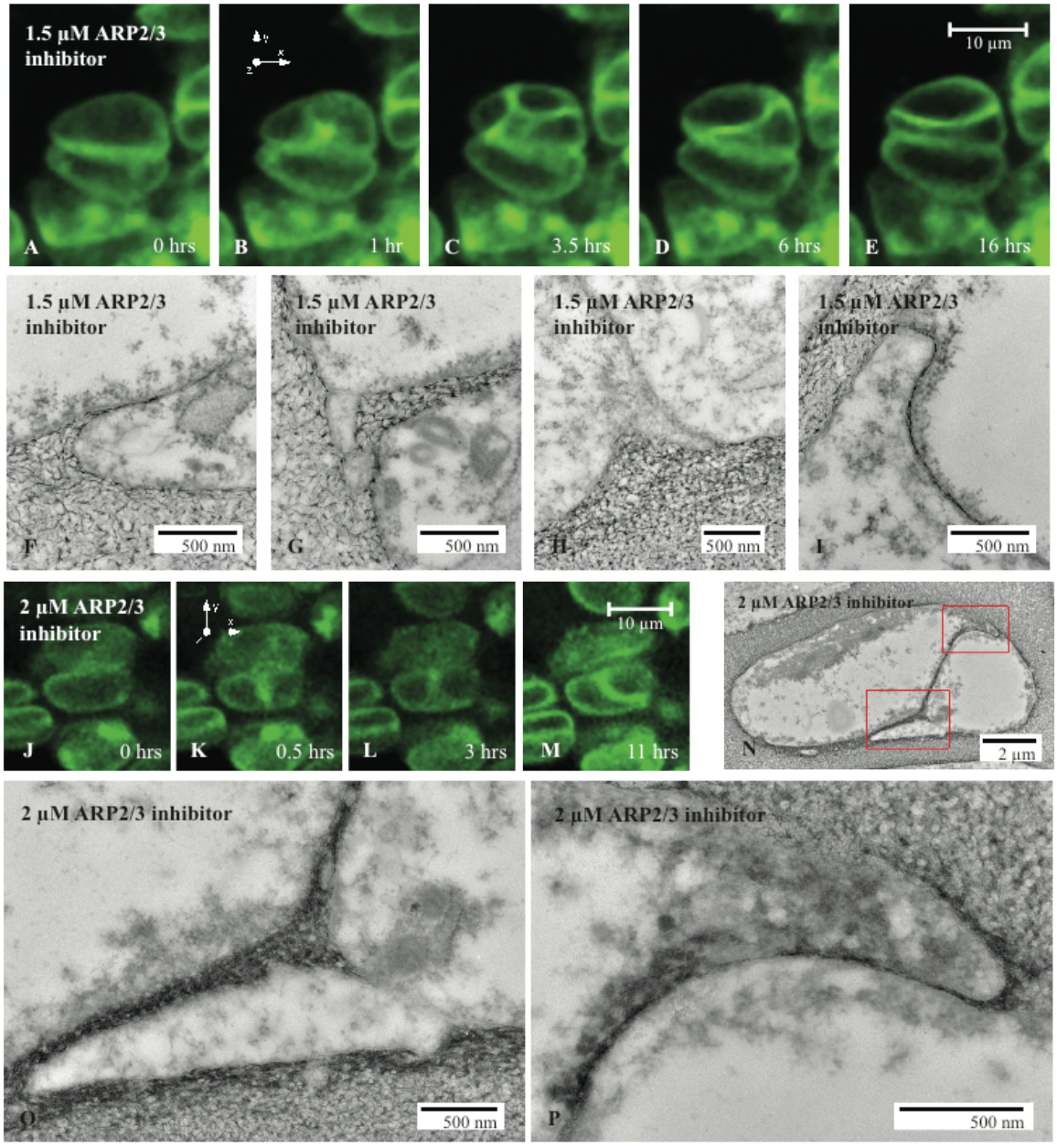
1.5 µM ARP2/3 inhibitor
A 0 hrs
B 1 hr
C 3.5 hrs
D 6 hrs
E 16 hrs
10 µm
1.5 µM ARP2/3 inhibitor
F
500 nm
1.5 µM ARP2/3 inhibitor
G
500 nm
1.5 µM ARP2/3 inhibitor
H
500 nm
1.5 µM ARP2/3 inhibitor
I
500 nm
2 µM ARP2/3 inhibitor
J 0 hrs
K 0.5 hrs
L 3 hrs
M 11 hrs
10 µm
2 µM ARP2/3 inhibitor
N
2 µm
2 µM ARP2/3 inhibitor
O
500 nm
2 µM ARP2/3 inhibitor
P
500 nm

Appendix 2.3: Beta catenin is reliable readout for the dynamic cellular events that occur during chondrocyte column formation. A schematic illustrates the process of column formation from cytokinesis (A), active rotation (E), completing rotation (I), early separation (M) and late separation (N). Dotted green lines represent the path used to quantify membrane-targeted GFP and beta catenin immunofluorescence intensity as a function of position. Immunolocalization of GFP (B, F, J, N, R, shown in green) and beta catenin (C, G, K, O, S, shown in red) during each stage is shown for the same double-labeled daughter chondrocyte pairs in tamoxifen-injected Col2CreER-TDTomato mice. Fluorescent pixel intensity of both membrane-targeted GFP (green line) and beta catenin (red line) quantified as a function of position along the path of the daughter cell adhesion interface shown in (D, H, L, P, T). Nuclear staining by DAPI is shown in blue. Scale bar = 5 um.

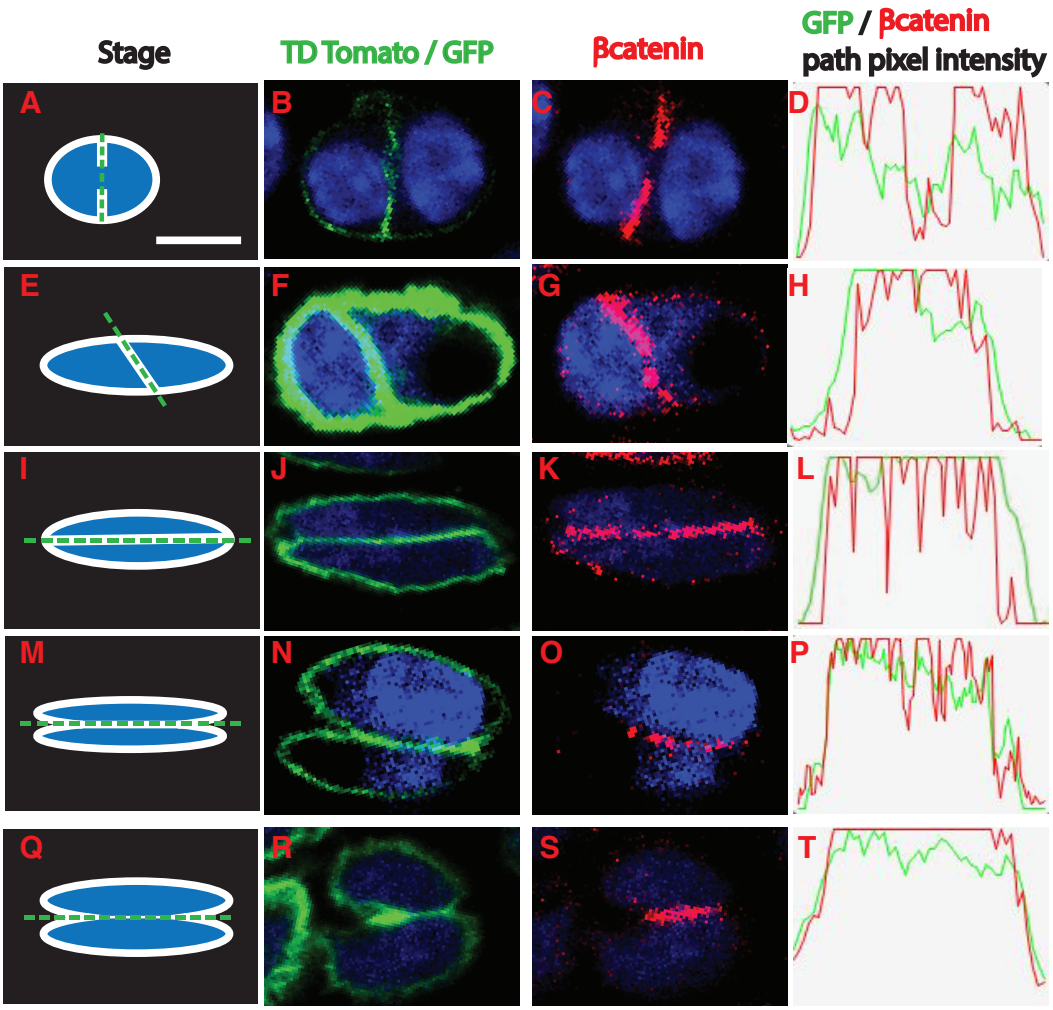
Stage
TD Tomato / GFP
βcatenin
GFP / βcatenin
path pixel intensity
A
B
C
D
E
F
G
H
I
J
K
L
M
N
O
P
Q
R
S
T

Appendix 2.4: Myosin protein localizes to nascent cell separations.

Immunolocalization of Myosin 2B (Myo2B, yellow arrowheads) in proliferative zone (D-F) and resting zone (J-L) daughter cells that are disengaging, detected by apparent shortening (A, G) and eventual loss (E, H) of the beta-catenin-rich adhesion interface (red arrows). Myosin localization for actively separating cell pairs is summed over the entire population and represented as a stacked bar chart. As chondrocytes become more distant from sister cells, myosin activity becomes redistributed away from the prior cadherin interface (F, L). Nuclear staining by DAPI is shown in blue. Scale bar = 5 um.

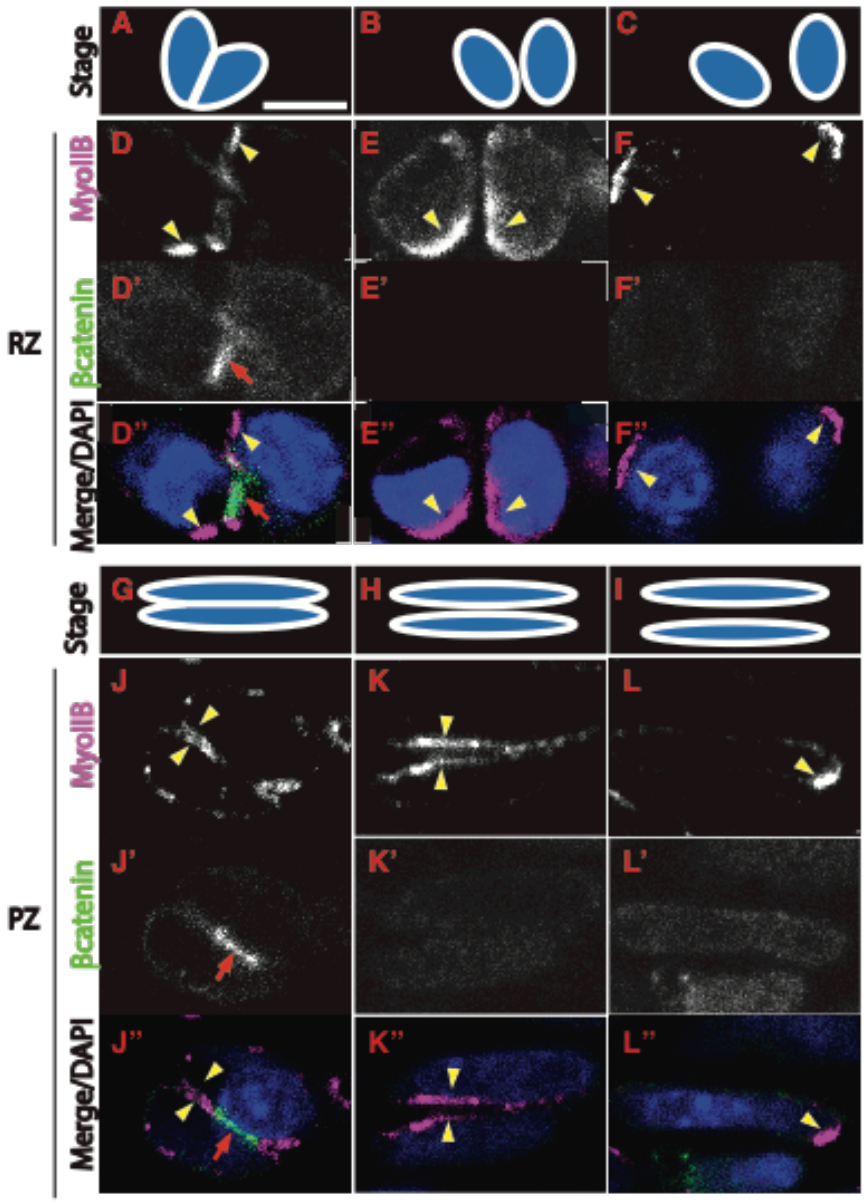
Stage
A
B
C
RZ
MyoIIB
D
E
F
βcatenin
D'
E'
F'
Merge/DAPI
D''
E''
F''
Stage
G
H
I
PZ
MyoIIB
J
K
L
βcatenin
J'
K'
L'
Merge/DAPI
J''
K''
L''

Appendix 2.5. Myosin protein is mislocalized in planar cell polarity signaling deficient cartilage. Immunolocalization of myosin 2B (Myo2B, yellow arrowheads) in daughter cell pairs during cytokinesis (E, I) after the cell-cell adhesion interface has matured (F, J), during separation (G, K) and after complete separation (H, L) in embryonic growth plate cartilage from Wnt5a (E-H) and Ror2 (I-L) mutant mice. Cadherin adhesions are labeled using antibody specific to beta catenin (red arrows). Percentage of cells observed expressing myosin activity at cell-matrix associations versus cell-cell associations is tabulated in the stacked bar chart below. Nuclear staining by DAPI is shown in blue. Scale bar = 5 um.

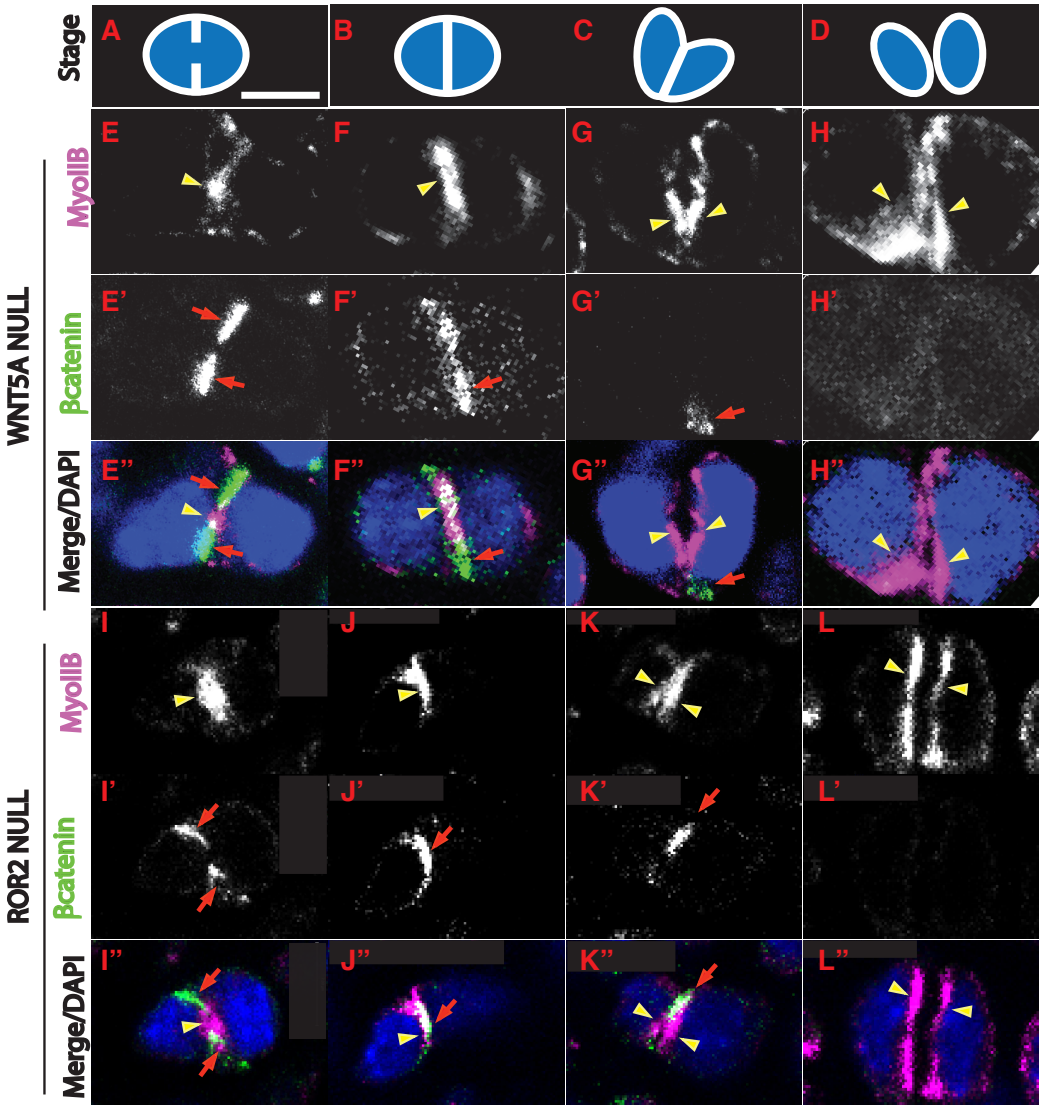
Stage
A
B
C
D
WNT5A NULL
MyoIIB
E
F
G
H
βcatenin
E'
F'
G'
H'
Merge/DAPI
E''
F''
G''
H''
ROR2 NULL
MyoIIB
I
J
K
L
βcatenin
I'
J'
K'
L'
Merge/DAPI
I''
J''
K''
L''

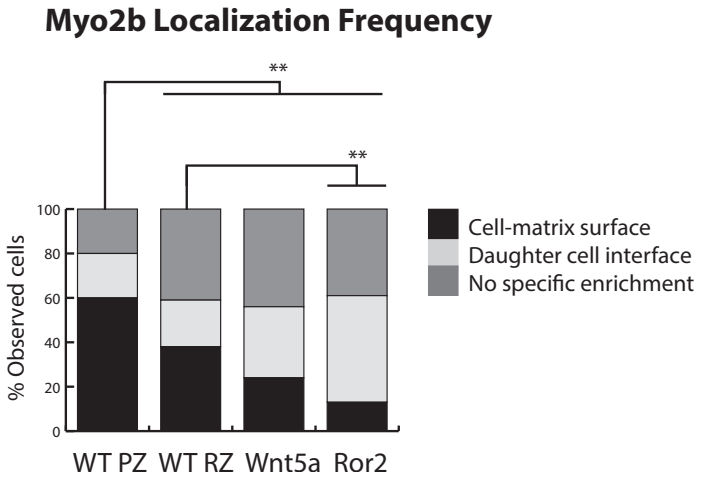
Myo2b Localization Frequency
**
**
% Observed cells
100
80
60
40
20
0
WT PZ
WT RZ
Wnt5a
Ror2
Cell-matrix surface
Daughter cell interface
No specific enrichment

Appendix 3.1: Two distinct populations of chondrocytes isolated from growth plate cartilage and cultured alginate beads. (A-B) Example scatterplots generated in ModFit LTE software showing distributions of cell area with respect to cell width (left) and forward scatter with respect to side scatter (right) of Propidium iodide stained chondrocytes isolated from alginate bead culture. Rectangles show the gating strategy used to separate FACS data pertaining to smaller (A) versus larger (B) chondrocytes.

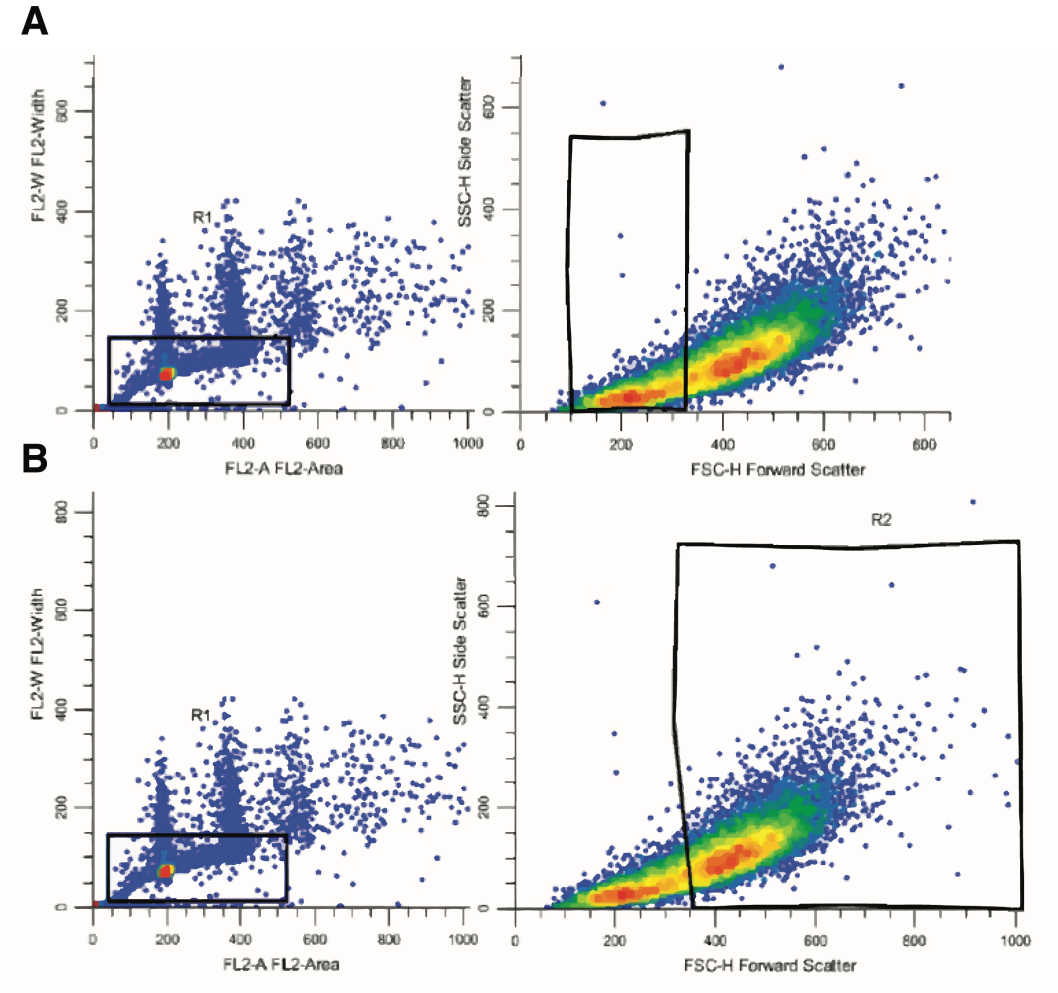
A
FL2-W FL2-Width
R1
FL2-A FL2-Area
SSC-H Side Scatter
FSC-H Forward Scatter
B
FL2-W FL2-Width
R1
FL2-A FL2-Area
SSC-H Side Scatter
R2
FSC-H Forward Scatter

Appendix 3.2. Cell size distribution modulated by exogenously activating IHH signaling. For all panels, counts of large, small, and total cell populations derived from Propidium iodide S-phase analysis and used to calculate the fraction of total cells that were in the larger cell population. (A) Large cell fraction of chondrocytes cultured for 1 (left) and 4 (days) in the presence or absence of PTH1-34 or IHH (n=3). (B-C) Large cell fraction of chondrocytes cultured in the presence or absence of IHH-stimulating factors for 1 day (B) and 4 days (C) in culture.

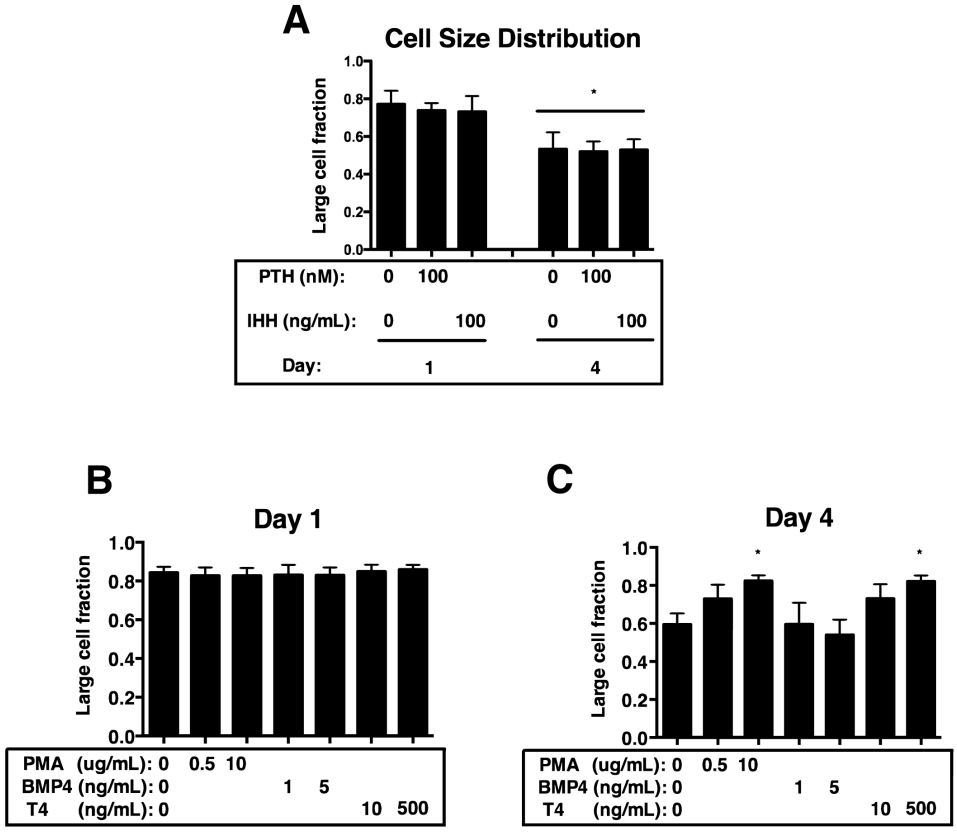
A
Cell Size Distribution
Large cell fraction
1.0
0.8
0.6
0.4
0.2
0.0
*
PTH (nM): 0 100 0 100
IHH (ng/mL): 0 100 0 100
Day: 1 4
B
Day 1
Large cell fraction
1.0
0.8
0.6
0.4
0.2
0.0
PMA (ug/mL): 0 0.5 10
BMP4 (ng/mL): 0 1 5
T4 (ng/mL): 0 10 500
C
Day 4
Large cell fraction
1.0
0.8
0.6
0.4
0.2
0.0
*
*
PMA (ug/mL): 0 0.5 10
BMP4 (ng/mL): 0 1 5
T4 (ng/mL): 0 10 500

Appendix: 3.3: Supplemental ImageJ macro

```
title = getTitle;
dotIndex = indexOf(title, ".");
Name = substring(title, 0, dotIndex);
run("Stack to Images");

selectWindow(Name+"-0001");
setOption("BlackBackground", false);
run("Make Binary", "thresholded remaining black");
run("Analyze Particles...", "size=50-1000 clear summarize");

selectWindow(Name+"-0002");
setOption("BlackBackground", false);
run("Make Binary", "thresholded remaining black");
run("Analyze Particles...", "size=50-1000 clear summarize");

selectWindow(Name+"-0003");
setOption("BlackBackground", false);
run("Make Binary", "thresholded remaining black");
run("Analyze Particles...", "size=50-1000 clear summarize");

selectWindow(Name+"-0004");
setOption("BlackBackground", false);
run("Make Binary", "thresholded remaining black");
run("Analyze Particles...", "size=50-1000 clear summarize");

selectWindow(Name+"-0005");
setOption("BlackBackground", false);
run("Make Binary", "thresholded remaining black");
run("Analyze Particles...", "size=50-1000 clear summarize");

selectWindow(Name+"-0006");
setOption("BlackBackground", false);
run("Make Binary", "thresholded remaining black");
run("Analyze Particles...", "size=50-1000 clear summarize");

close("*")
```

Time point	Live count	Dead count	Total cells	Live / total	Percent Viability
Day 0	100	9	109	0.917431193	91.74311927
Day 1	143	11	154	0.928571429	92.85714286
Day 4	314	10	324	0.969135802	96.91358025
Day 7	258	13	271	0.95202952	95.20295203

Appendix Table 3.1. Quantification of the live-dead stains from Figure 1A.

Fluorescence images resulting from our viability assay were input to our automated ImageJ object-counting macro. Results from all time points analyzed are shown in each row. Counts in the green channel (live cells), and red channel (dead cells) were summed to calculate total cells. The ratio of living and total cells was multiplied by 100 in order to calculate percent viability (rightmost column).

Sequence of primers used for ddPCR amplification.

Gene	Forward Sequence	Reverse Sequence
Actin NM_007393.3 [42-44]	AAATCGTGCGTGACATCAAAGA	GCCATCTCCTGCTCGAAGTC
HPRT NM_013556.2 [42-44]	GACCTCTCGAAGTGTTGGATAC	TCAACAGGACTCGTATTTG
RPL13-a NM_009438.4 [45]	ATCCCTCCACCCTATGACAA	GCCCCAGGTAAGCAAACTT
Col1 NM_007742.4 [46]	GCAACAGTCGCTTCACCTAC	GTGGGAGGGAACCAGATTG
Col2 NM_031163 [47]	CGAGTGGAAGAGCGGAGACTAC	CCAGTTTTTCCGAGGGACAGT
ColX NM_009925 [46]	TTCTGCTGCTAATGTTCTTGACC	GGGATGAAGTATTGTGTCTTGGG
PTHrP NM_008970	GAAACGCAGAGAACAGGAGAA	AATTTCAATGCGTCCTTAAGCTG
IHH NM_010544 [48]	CCCCAACTACAATCCCGACA	TCATGAGGCGGTCGG

Appendix Table 3.2. Primers used for ddPCR gene expression analysis. The above table lists the name of all genes analyzed by ddPCR in the current study, the gene accession numbers that were used to generate each set of primers, and the publications that guided the selection of primers, where applicable (left column). Full sequences for each primer used in the current study (forward and reverse) are shown to the right.

Appendix Table 4.1: Differentially expressed genes in PTH(1-34) treated alginate cultures.

Genes are condensed into multiple columns to conserve space, and are ordered by L(FC), or log2 fold change value. Significance is shown as the Benjamini-Hochberg-corrected p-value (BH-p).

Gene	L(FC)	BH-p	Gene	L(FC)	BH-p	Gene	L(FC)	BH-p	Gene	L(FC)	BH-p
Cmtm5	-0.56	0.03	2510009E07	-0.36	0.008	Smc3	0.1	0.044	Tgfbi	0.31	0.024
3632451O	-0.55	0.02	Crim1	-0.36	0.024	Hsp90ab1	0.13	0.047	Hmgn2	0.31	0.032
Trim47	-0.55	0.022	Sort1	-0.35	0.031	Atp1a1	0.13	0.024	Sertad4	0.32	0.024
Col5a2	-0.54	0.026	Pink1	-0.35	0.05	Arf1	0.13	0.047	Esyt2	0.32	0.035
Gm5617	-0.54	0.024	Bod1	-0.35	0.031	Prrc2a	0.14	0.048	Paics	0.32	0.024
Srpx	-0.53	0.034	Fam46a	-0.35	0.02	Golph3	0.14	0.04	Ptpn13	0.32	0.036
Osbpl1a	-0.53	0.024	Prelp	-0.34	0.02	Nomo1	0.15	0.023	Hif1a	0.32	0.028
Il10rb	-0.53	0.039	Map1lc3b	-0.34	0.033	Rpl13	0.15	0.037	Dlc1	0.32	0.048
Tns2	-0.53	0.032	Cbr1	-0.33	0.047	Spire1	0.17	0.022	Nucks1	0.33	0.044
Islr	-0.51	0.038	Col12a1	-0.33	0.042	Cacfd1	0.17	0.048	Asap3	0.34	0.045
Tspan4	-0.51	0.01	Mvp	-0.32	0.039	Rps10	0.17	0.033	Rpa1	0.34	0.02
Smad3	-0.48	0.044	Tbcel	-0.31	0.04	Pofut2	0.18	0.048	Serpina3c	0.34	0.008
Itih5l-ps	-0.48	0.048	Cab39	-0.31	0.042	Pabpn1	0.18	0.04	Fosl2	0.35	0.043
Capn6	-0.48	0.023	Dennd5a	-0.31	0.048	Rps11	0.18	0.049	Tnpo1	0.35	0.024
Ctsz	-0.48	0.048	2310022B05	-0.3	0.047	Ppp6r3	0.18	0.036	Csgalnact2	0.37	0.024
Itm2b	-0.48	0.024	Adcy2	-0.3	0.022	Rpl27a	0.18	0.035	Prune2	0.37	0.04
Comp	-0.47	0.019	Ccpg1	-0.29	0.008	Hspe1	0.18	0.02	Npm3	0.37	0.024
Gsn	-0.47	0.024	Arhgef1	-0.29	0.04	Xpo7	0.18	0.04	Rfc2	0.38	0.035
Itpkb	-0.46	0.037	Ivns1abp	-0.29	0.039	Asna1	0.2	0.026	Fen1	0.39	0.024
Pmp22	-0.46	0.023	Rin2	-0.28	0.042	Baz1b	0.2	0.027	Anxa2	0.39	0.018
Gper1	-0.46	0.037	Obsl1	-0.28	0.024	Smc5	0.2	0.018	Itga5	0.39	0.037
Cpe	-0.46	0.008	Susd5	-0.28	0.029	Mgea5	0.21	0.046	Nudt4	0.39	0.047
Smim14	-0.45	0.018	Cdv3	-0.28	0.044	Ybx1	0.21	0.036	Nxt1	0.39	0.028
Fam180a	-0.45	0.02	Ctdsp2	-0.27	0.017	Rcor1	0.22	0.048	Tubb4b	0.4	0.028
Map7d3	-0.45	0.011	Ccdc8	-0.27	0.032	Odc1	0.23	0.008	Tubb5	0.4	0.023
Erbb2	-0.43	0.02	Nrk	-0.27	0.018	Chsy3	0.23	0.038	Pcna	0.4	0.024
Ezh1	-0.43	0.024	Klf16	-0.27	0.02	Tmem64	0.24	0.031	Tsc22d3	0.4	0.013
Eid1	-0.42	0.024	Sobp	-0.26	0.023	Dhx9	0.25	0.04	Ctsl	0.4	0.028
Prkar2b	-0.42	0.024	Wipi1	-0.25	0.048	Snrpf	0.25	0.02	Cars2	0.41	0.043
Pcsk6	-0.42	0.023	Tiam2	-0.23	0.039	Snrnp40	0.26	0.015	Rad18	0.41	0.04
E130308A1	-0.41	0.048	Fam129b	-0.22	0.047	Rif1	0.27	0.024	Rps13-ps1	0.42	0.046
Anxa5	-0.4	0.024	Ctnnb1	-0.21	0.036	Stat3	0.27	0.039	Tubg1	0.45	0.042
Agpat4	-0.39	0.039	Stk11ip	-0.21	0.023	Ipo5	0.28	0.024	Serpine2	0.45	0.014
Plagl1	-0.39	0.037	Cul7	-0.2	0.027	H2afv	0.28	0.04	Dnmt1	0.46	0.018
F13a1	-0.38	0.018	Tmem176b	-0.18	0.023	Ubp1	0.29	0.036	Chsy1	0.47	0.048
Anxa8	-0.38	0.048	Peg3	-0.17	0.019	Ahsa2	0.29	0.029	Rhno1	0.47	0.033
Zcchc5	-0.37	0.039	Gnas	-0.17	0.032	Actg1	0.3	0.02	Rangap1	0.48	0.043
Ndn	-0.37	0.024	Dap	-0.15	0.024	Adpgk	0.3	0.046	Wdr60	0.48	0.048
Dcn	-0.36	0.024	Fam53c	-0.11	0.044	Rad21	0.3	0.024	Dnajc9	0.48	0.023

Appendix Table 4.1 cont'd

Gene	L(FC)	BH-p	Gene	L(FC)	BH-p	Gene	L(FC)	BH-p	Gene	L(FC)	BH-p
Lifr	0.48	0.041	Cdc25b	0.67	0.048	Rell1	0.82	0.024	Cdca2	1.03	0.023
Gm10053	0.49	0.034	Chst3	0.67	0.024	Gtse1	0.82	0.022	Shisa5	1.05	0.022
Topbp1	0.49	0.03	Mcm5	0.68	0.02	Fancd2	0.82	0.033	Cpm	1.08	0.015
Zmiz1	0.49	0.049	Camk4	0.68	0.034	Top2a	0.82	0.031	Kank4	1.08	0.02
Plekhg3	0.51	0.048	Bin3	0.68	0.022	Ints6l	0.83	0.024	Gja1	1.09	0.02
Gxylt1	0.51	0.035	Matn2	0.69	0.01	Knl1	0.83	0.035	Kif18b	1.1	0.035
Tuba1b	0.52	0.015	Sgol2a	0.69	0.02	Prc1	0.83	0.048	Hopx	1.12	0.024
Senp1	0.52	0.02	Mad2l1	0.69	0.024	Pxylp1	0.83	0.035	Lef1	1.13	0.04
Mcm2	0.53	0.022	Lmnb1	0.69	0.008	Cenpn	0.84	0.036	Pcdhga2	1.14	0.05
H2afz	0.53	0.036	Racgap1	0.7	0.012	Aurka	0.84	0.024	Gpm6b	1.15	0.018
Ncapd3	0.53	0.023	Smc2	0.71	0.025	Vdr	0.84	0.015	Dusp1	1.16	0.01
Tcf19	0.54	0.034	Kif20b	0.71	0.048	Plk1	0.85	0.023	Col8a2	1.17	0.02
Gm14150	0.54	0.02	Prss53	0.71	0.034	Agtr2	0.85	0.029	Mybpc1	1.17	0.039
G2e3	0.54	0.029	Srebf1	0.72	0.04	Kif11	0.86	0.047	Gem	1.19	0.036
C1qtnf3	0.54	0.034	Ptgfrn	0.72	0.013	Tpx2	0.86	0.02	Plk2	1.19	0.026
Dhfr	0.54	0.048	Ncaph	0.72	0.024	Ccsap	0.86	0.04	Flrt2	1.19	0.022
Skp2	0.55	0.048	Cdk1	0.73	0.021	Cep55	0.87	0.048	Pdgfd	1.26	0.048
Kcnk5	0.55	0.039	Kif18a	0.74	0.01	Mybl1	0.87	0.034	Pde4d	1.29	0.004
Hat1	0.56	0.048	Nusap1	0.74	0.039	Ccna2	0.88	0.032	Fam198a	1.32	0.025
Brip1os	0.58	0.017	Cdca3	0.74	0.048	Kif20a	0.88	0.005	Tnfaip8l3	1.35	0.024
Igsf3	0.58	0.008	Incenp	0.75	0.02	Dhrs3	0.88	0.008	Il22ra2	1.37	0.036
Sytl2	0.58	0.04	Uhrf1	0.75	0.048	Tk1	0.88	0.035	Itih5	1.4	0.025
Pola1	0.58	0.04	Rrm1	0.75	0.024	Tyms	0.89	0.02	Podnl1	1.42	0.02
Iqgap3	0.58	0.034	Ifi30	0.77	0.024	Sat1	0.89	0.008	Gdf5	1.43	0.024
1190002N	0.59	0.018	Nt5c3	0.78	0.044	Ckb	0.9	0.024	Pappa	1.44	0.008
Tmem2	0.59	0.02	Clmn	0.78	0.015	Impa1	0.91	0.01	Pnpla3	1.49	0.039
Tacc3	0.59	0.04	Fzd9	0.79	0.008	Mgat4a	0.92	0.018	Hdac4	1.55	0.025
Sgk1	0.6	0.036	Ckap2l	0.79	0.02	Aurkb	0.92	0.049	Enpp2	1.59	0.008
Sdc1	0.6	0.026	Man2a1	0.79	0.036	Grem1	0.94	0.026	Sema3c	1.61	6E-04
Ets2	0.6	0.041	Spon1	0.79	9E-04	Fmo1	0.95	0.039	Sik1	1.62	0.034
Emb	0.61	0.034	Hmmr	0.79	0.036	Ect2	0.97	0.037	Sema4f	1.65	0.028
Tenm3	0.63	0.019	Ncapg	0.8	0.041	Gas1	0.97	0.023	Srgn	1.66	0.044
Tipin	0.63	0.028	Pde8a	0.8	0.003	Nuf2	0.98	0.031	Csdc2	1.7	0.04
Pde7b	0.65	0.04	Ube2c	0.8	0.012	Kif14	0.99	0.008	Gm43684	1.72	0.048
Tubb6	0.65	0.024	Ccnf	0.8	0.04	Pde3a	0.99	0.008	Aim1	1.73	0.008
Frs2	0.66	0.024	Ncapg2	0.8	0.04	Nr4a1	1	0.027	Dhh	1.89	0.048
Kcne4	0.66	0.026	Slc25a48	0.8	0.03	Fabp5	1	0.038	Tnfsf11	1.92	0.024
Ucp2	0.67	0.048	Mki67	0.81	0.01	Ndc80	1.02	0.04	Gm44791	2.15	0.048
Calml3	0.67	0.02	Adamts3	0.81	0.019	Gadd45	1.03	0.031	Olfml2b	2.28	0.008
									Cmklr1	2.46	0.02
									Gm12840	3.08	0.048
									Nap1l5	3.1	0.022

Appendix Table 4.2: Principal component genes of IHH- and untreated samples.

SHARED PC GENES			UNIQUE TO NT		UNIQUE TO IHH		
Tspan13	Abi3bp	Il17b	Lgals3	Nfib	Gna12	Fbn1	Mef2c
Wnt4	Boc	Mllt4	Psmb3	Frzb	Saa3	Glul	Cdc42ep3
Cxcl1	Clu	Smoc1	Thbs3	Nim1k	Chchd10	Igfbp4	Lpar4
Ddit3	Col12a1	Tgfbr3	Cdca3	Plac1	Casc5	Phlda1	Nav2
Aspm	Col3a1	Tspan7	Cenpe	Serpine2	Ccnb1	Slc20a1	Sema6a
Birc5	Col5a2	Scd1	Cenpf	Hp	Cdc20	Mfap2	Aen
Ccna2	Dlk1	Chrdl2	Nuf2	Angptl4	Ckap2	Timp1	Dnaja1
Ckap2l	Efemp1	Cytl1	Prc1	Glmp	Fam64a	C1qtnf3	Syce2
Depdc1a	Grem1	Map2	Spc25	Lcn2	Neil3	Lum	Txnrd1
Hmmr	Igfbp5	Timp4	Tk1	Clic3	Sesn3	M1ap	Runx3
Kif23	Omd	Cldn11	Tpx2	Fam213b	Ero1l	Scrg1	Mgst2
Mki67	Penk	Sh2b2	Tmsb4x	Rps12-ps3	Hspa1a	Papss2	Dnajb1
Nusap1	Ptgis	Col6a3	Cited2	C4b	Plet1	Serpine1	Nrk
Pbk	Pthlh	Prkg2	Psma7	Agt	F3	Rpl22l1	
Top2a	Rbp4	Sgms2	Rasl11b	Asns	Hspb1	C4b	
Barx1	Sfrp5	Tgm2	Rps26	Fxyd3	Atf3	Gapdh	
Gas1	Slc40a1	Fxyd5	Rps26-ps1	Htatip2	Cxcl14	Stbd1	
Mest	Spp1	H2-D1	Rps10	Lgmn	Cdsn	Espn	
Pcp4	Slc6a6	Col10a1	Zfos1	Naga	Mmp13	Gbe1	
Ramp1	Cgref1	Slc44a2	Srxn1	P4ha2	Tmem140	Gja1	
Tmem213	Tshz2	Slpi	Dhcr24	Ldlr	Aurkb	Plaur	
Tnni2	Cpm	Smpd3	Ibsp	Phgdh	Mxd3	Slc2a1	
Bmp3	Serpina3n	Unc5b	Pcolce	Psmc4	Nek2	Uck2	
Calml3	Arsi	Fxyd2	Pdia4	Ctsl	Fxyd6	Egln1	
Anxa8	Comp	Hmox1	Psmc2	Socs2	Apoe	Tnfrsf12a	
Cxcl2	Ihh	Ccdc80	Sqstm1	Vdr	Chil1	Trib3	
Ddit4l	Ppa1						

Appendix Table 4.3: PC genes that separate BMP3 from PTHrP-expressing resting cells.

GENE	FOLD CHANGE
Bmp3	1.98
Spp1	1.86
Tspan13	1.72
Angptl4	1.42
F13a1	1.36
Mef2c	1.28
Slc40a1	1.28
Tmsb4x	1.23
Tnni2	1.21
Agl	1.2
Penk	1.15
Cdkn1c	1.12
Pcp4	1.11
Ube2e3	1.07
Kctd4	1.05
Fam46a	1.05
Map2	1.02
Efemp1	0.99
Bhlhe41	0.99
Marcks	0.94
Dhx58os	-0.75
Mt2	-0.78
Trim47	-0.79
Timp4	-0.84
Crip1	-0.85
Klf3	-0.88
Cxcl14	-0.88
Emp1	-0.9
Timp1	-0.91
Klf2	-0.97
Pthlh	-1.03
Insig1	-1.05
Lcn2	-1.12
Chrdl2	-1.22
Crip2	-1.26
S100a6	-1.35
Calml3	-1.57
Cytl1	-1.62
Tgm2	-1.76

Appendix Table 4.4: PC genes of proliferative chondrocytes with gene expression outputs that match a response to PTHrP signaling

GENE
Vdr
Tnni2
Efemp1
Col12a1
Ramp1
Nim1k
Omd
Ptgis
Frzb
Col10a1
Tk1
Nusap1
Tpx2
Cdca3
Ccna2
Top2a
Smpd3
Unc5b
Ibsp
Anxa8
Comp
Ccdc80
Col5a2
Pthlh
Nuf2
Ckap2l
Prc1
Hmmr
Mki67

Appendix 4.1: Analysis of PTHrP/IHH signaling mediator gene expression in t-SNE space. Expression of single genes in each single cell is displayed as a heat map where darker color indicates higher levels of expression. Ligands PTHrP/IHH, receptors Smo/PTH1R, and collagens Col2a1/Col10a1 are shown below in untreated and IHH-treated populations. Cells expressing PTHrP ligand also express Smoothened. Cells expressing IHH also express PTH1r, indicating the potential for long-range signaling. Analysis of collagen 2 shows uniform gene expression across all clusters, confirming chondrocyte identity. Sox9 shows similar patterns as Col2a1 (data not shown).

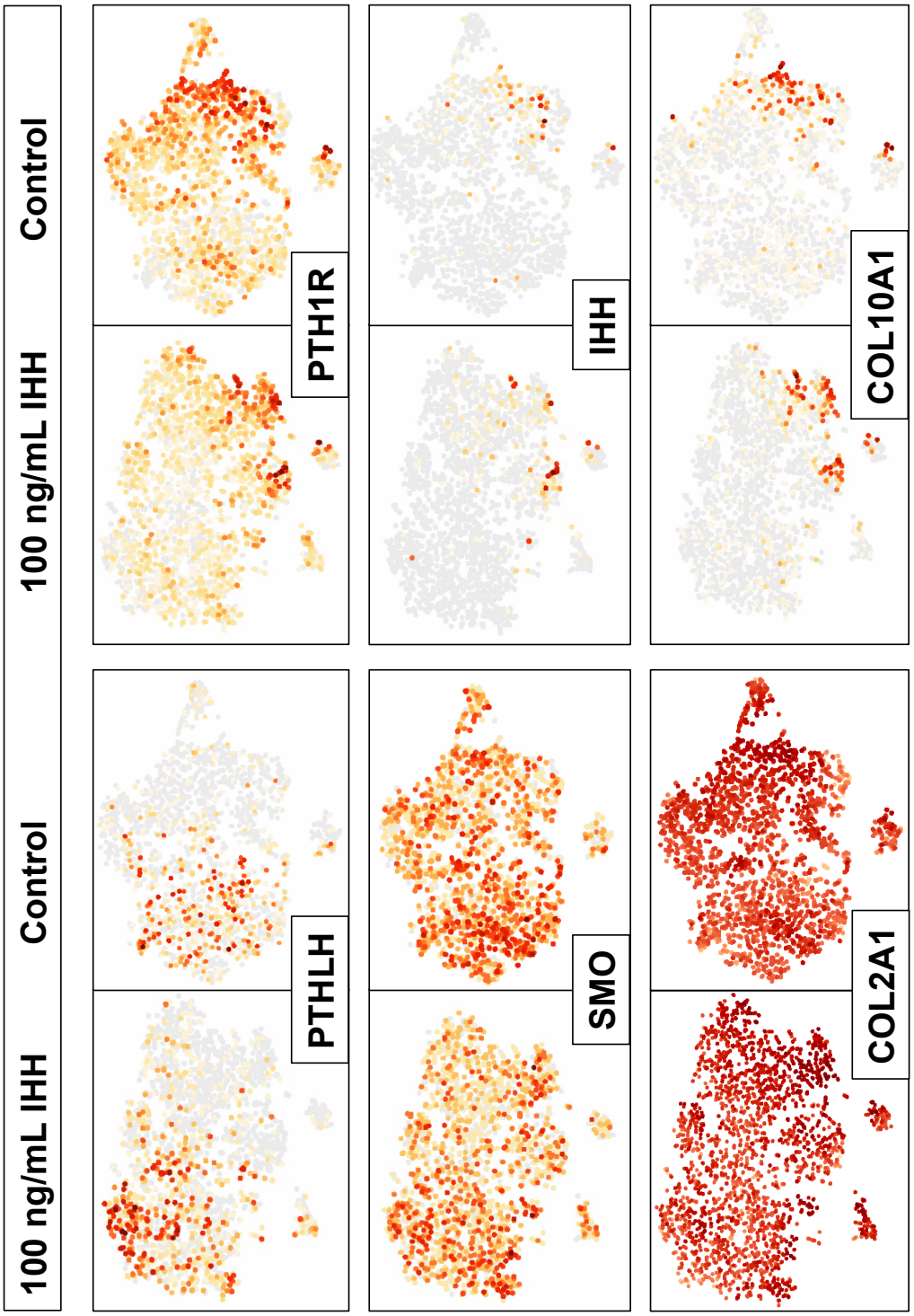
100 ng/mL IHH
Control
100 ng/mL IHH
Control
PTHLH
PTH1R
SMO
IHH
COL2A1
COL10A1

Appendix 4.2: MATLAB Script for ISH pattern analysis

```
%% Quantifying the number and the location of cells in the gel sphere
%% Written by Donghee Lee, Jan 2018
%% Clear unnecessary items
clear all
close all
clc
%% Initial input
% Image scale
length_um=3137.71; % um
length_pixel=6836; % pixel
dxy=length_um/length_pixel; % x- and y-resolution of image (in um/pixel)
%% Load image stacks
imdata = 'type the file name.tif'; % input the file name
information=imfinfo(imdata); % file information
final=size(information,1); % the number of image
k=0;
for i=1:2
%     for i=1:final
data.image{1,i}=imread(imdata, 'index', i);
%% Image processing
Image = imadjust(data.image{1,i});                % Level adjust
Image_filtered = wiener2(Image, [5,5]);  % Use Wiener filter to reduce noise
level=graythresh(Image_filtered);      % Otsu's thresholding method
BW = im2bw(Image_filtered,level);

%% Counting cells
[data.centers{1,i}, data.radii{1,i}] = imfindcircles(data.image{1,i},[9 25],'ObjectPolarity','bright', ...
    'Sensitivity',0.85); % best
data.number{1,i}=length(data.radii{1,i})
%% Finding the center of a bead
% B = bwboundaries(Open_BW, 'noholes');
[xvals_1, xindex_1] = sort(data.centers{1,i}(:,1), 'descend'); % x-coordinate: H -> L
[xvals_2, xindex_2] = sort(data.centers{1,i}(:,1), 'ascend'); % x-coordinate: L -> H
[yvals_1, yindex_1] = sort(data.centers{1,i}(:,2), 'descend'); % y-coordinate: H -> L
[yvals_2, yindex_2] = sort(data.centers{1,i}(:,2), 'ascend'); % y-coordinate: L -> H
x_largest5 = xvals_1(1:5); % 5 largest x values
x_smallest5 = xvals_2(1:5); % 5 smallest x values
y_largest5 = yvals_1(1:5); % 5 largest y values
y_smallest5 = yvals_2(1:5); % 5 smallest y values
x_index_of_largest5 = xindex_1(1:5);
x_index_of_smallest5 = xindex_2(1:5);
y_index_of_largest5 = yindex_1(1:5);
y_index_of_smallest5 = yindex_2(1:5);
data.B_center_x{1,i}=mean((x_largest5+x_smallest5)/2); % center of bead - x coordinate
data.B_center_y{1,i}=mean((y_largest5+y_smallest5)/2); % center of bead - y coordinate
end

%% Calculating the distance between the cell and the bead center
data.distance{1,1} = sqrt((data.centers{1,1}(:,1)-data.B_center_x{1,2}).^2+((data.centers{1,1}(:,2)-
data.B_center_y{1,2}).^2));
data.distance_um{1,1} = sqrt((data.centers{1,1}(:,1)-
data.B_center_x{1,2}).^2+((data.centers{1,1}(:,2)-data.B_center_y{1,2}).^2))*dxy;
data.distance{1,2} = sqrt((data.centers{1,2}(:,1)-data.B_center_x{1,2}).^2+((data.centers{1,2}(:,2)-
```

```
data.B_center_y{1,2}).^2));
data.distance_um{1,2} = sqrt((data.centers{1,2}(:,1)-
data.B_center_x{1,2}).^2+((data.centers{1,2}(:,2)-data.B_center_y{1,2}).^2))*dxy;
[dist_vals, dist_index] = sort(data.distance{1,2}, 'descend'); % distance: H -> L
dist_largest10 = dist_vals(1:10);
data.B_radius{1,1}=mean(dist_largest10);
data.B_radius_um{1,1}=mean(dist_largest10)*dxy;
data.B_radius{1,2}=mean(dist_largest10);
data.B_radius_um{1,2}=mean(dist_largest10)*dxy;
Cell_number1=data.number{1,1}
Cell_number2=data.number{1,2}
Ratio=Cell_number1/Cell_number2
Radius_of_the_bead=data.B_radius{1,2};
Radius_of_the_bead_um=data.B_radius{1,2}*dxy
Average_distance = mean(data.distance_um{1,1})
Std_distance=std(data.distance_um{1,1})

%% Plot
figure
imshow(data.image{1,1})
title('Raw image')
h1 = viscircles(data.centers{1,1},data.radii{1,1});
hold on
plot(data.B_center_x{1,2},data.B_center_y{1,2},'c*', 'markersize', 10)
viscircles([data.B_center_x{1,2},data.B_center_y{1,2}],data.B_radius{1,2},'color', 'c');
hold off
figure
imshow(data.image{1,2})
title('Raw image')
h2 = viscircles(data.centers{1,2},data.radii{1,2});
hold on
plot(data.B_center_x{1,2},data.B_center_y{1,2},'c*', 'markersize', 10)
viscircles([data.B_center_x{1,2},data.B_center_y{1,2}],data.B_radius{1,2}, 'color','c');
hold off
```

Appendix 5.1: Observed asymmetries in myosin phosphorylation among daughter chondrocytes in culture. N=1 experiment. Primary chondrocytes were fixed and immunostained for DAPI, myosin, and β–catenin after 1 day of monolayer culture. All cell pairs (100% of 10 observed daughter cell pairs) that stained positive for both β-catenin (green) and pMLC (magenta) only labeled one of the two daughter cells.

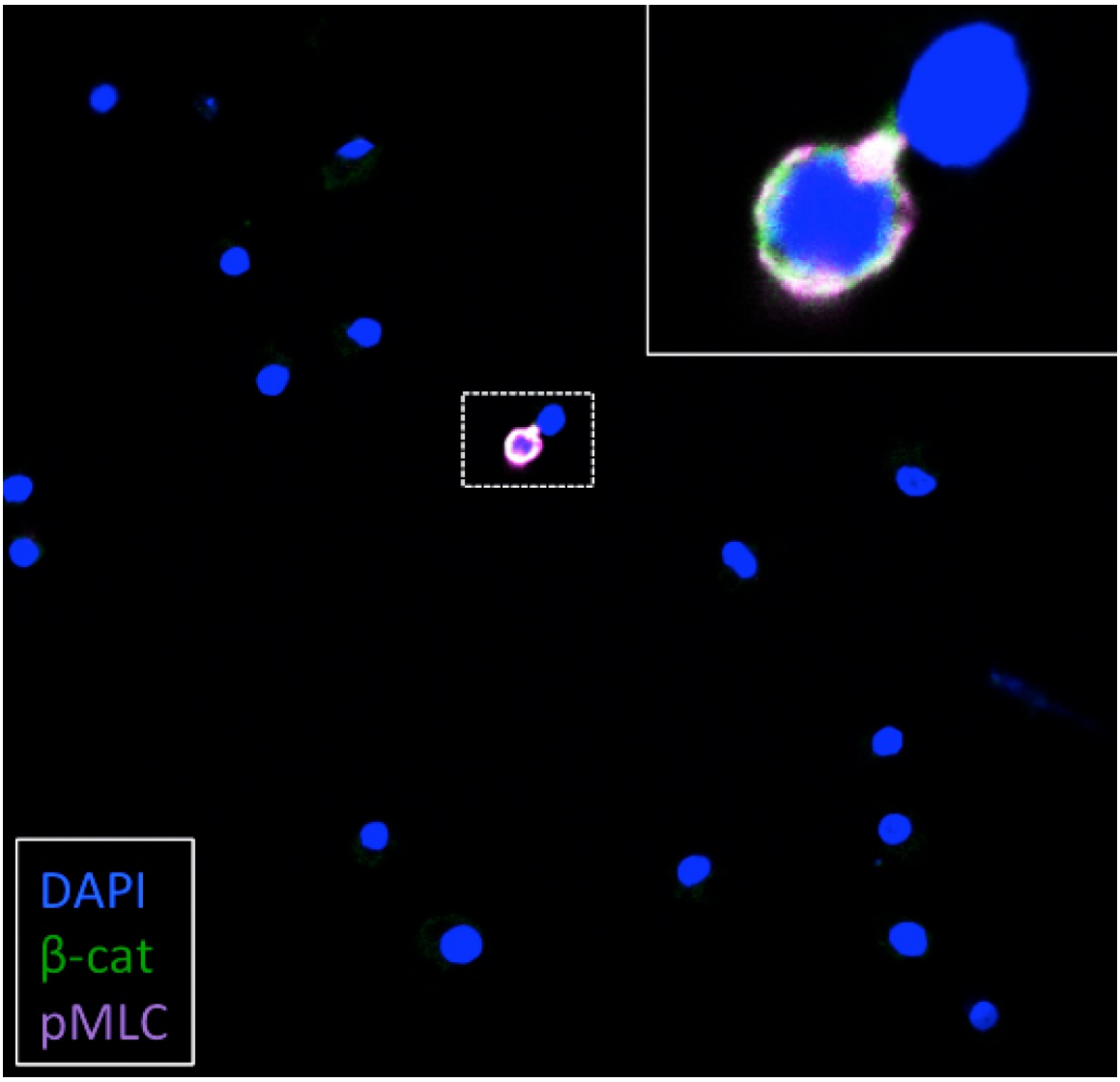
DAPI
β-cat
pMLC